Modern Aspects of Superconductivity

Theory of Superconductivity

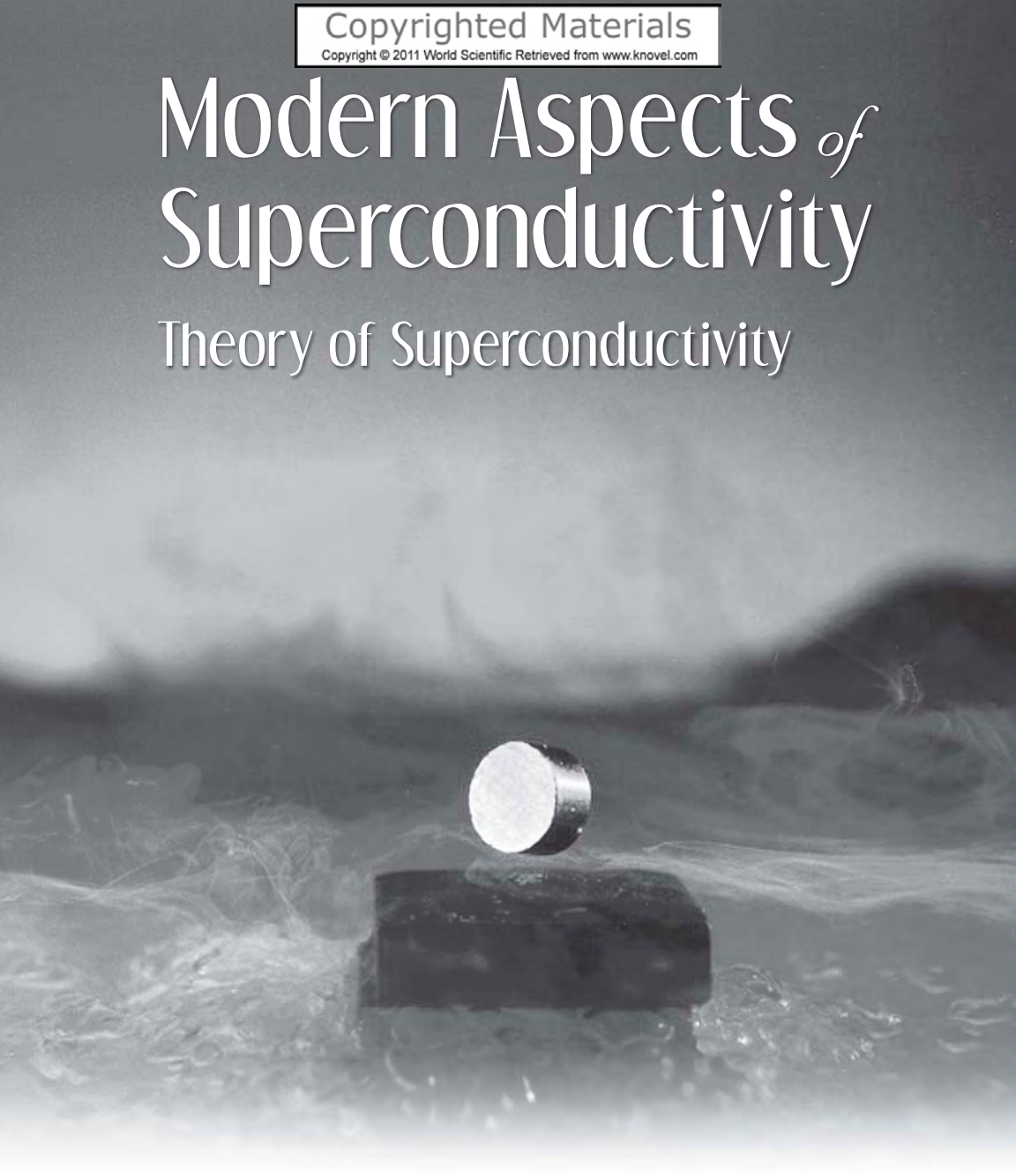

Sergei Kruchinin
Bogolyubov Institute for Theoretical Physics, Kiev, Ukraine

Hidemi Nagao & Shigeyuki Aono
Kanazawa University, Japan

NEW JERSEY • LONDON • SINGAPORE • BEIJING • SHANGHAI • HONG KONG • TAIPEI • CHENNAI

Published by

World Scientific Publishing Co. Pte. Ltd.

5 Toh Tuck Link, Singapore 596224

USA office: 27 Warren Street, Suite 401-402, Hackensack, NJ 07601

UK office: 57 Shelton Street, Covent Garden, London WC2H 9HE

British Library Cataloguing-in-Publication Data
A catalogue record for this book is available from the British Library.

MODERN ASPECTS OF SUPERCONDUCTIVITY
Theory of Superconductivity

ISBN-13 978-981-4261-60-9
ISBN-10 981-4261-60-2

Typeset by Stallion Press
Email: enquiries@stallionpress.com

Printed in Singapore.

"The single reason for our inability to treat the problems of superconductivity consists in the absence of a sufficient imagination."

— Richard P. Feynman

Preface

Studies of superconductivity theory are among the most fruitful and promising trends in the theoretical physics of condensed matter, since superconductivity remains one of the most interesting research areas in physics.

The goal of this book is to give a representation of certain modern aspects of superconductivity. We discuss important aspects of the theory of superconductivity, such as the nature of high-T_c superconductivity, two-gap superconductivity, room-temperature superconductivity, mesoscopic superconductivity, the pairing state and the mechanism of cuprate high-T_c superconductivity.

In Chap. 1, we consider the field-theoretical method of superconductivity and discuss the basic idea of superconductivity and the elaboration of the Ginzburg–Landau and Bardeen–Cooper–Schrieffer theories in the frame of many-particle quantum field theory.

In Chap. 2, we consider the structures of high-T_c superconductors, phase diagrams and the problem of pseudogaps, and analyze the mechanisms of superconductivity. We present general arguments regarding the pairing symmetry in cuprate superconductors and investigate their thermodynamical properties within the spin-fluctuation mechanism of superconductivity, by using the method of functional integrals.

Chapter 3 concentrates on two-band and multiband superconductivity. We consider the physical properties of the superconductor MgB_2 and use our two-band model to explain the two coupled superconductor gaps of MgB_2. To study the effect of the increasing T_c in MgB_2, we use the renormalization-group approach and phase diagrams. In the field of superconductivity we meet the problem-maximum, which consists in the creation of room-temperature superconductors. We consider this problem in our book and make some recommendations on the search for these superconductors.

Chapter 4 deals with the problem of mesoscopic superconductivity. We consider the two-band superconductivity in ultrasmall grains, by extending the Richardson exact solution to two-band systems, and develop the theory of interactions between nanoscale ferromagnetic particles and superconductors. The properties of nanosize two-gap superconductors and the Kondo effect in superconducting ultrasmall grains are investigated as well.

We also consider the ideas of quantum computing and quantum information in mesoscopic circuits. The theory of the Josephson effect is presented, and its applications to quantum computing are analyzed.

This book deals with a wide scope of theoretical and experimental topics in superconductivity, and has been written for advanced students and researchers in that field.

S. Kruchinin, H. Nagao and S. Aono
Kiev, Kanazawa, July 2009

Contents

CHAPTER 1

Theory of Superconductivity

1.1 Introduction

In the preface to the book *Superconductivity*, edited by Parks,[1] one of the editors says: "During the preparation of this treatise one of the authors commented that it would be the last nail in the coffin [of superconductivity]." Some specialists in superconductivity told us that we would hardly be able to find articles useful for our future investigations, except for Anderson's comments at the end of that book. Further, we learned that Anderson was pessimistic about further advance of superconductivity; for example, high-temperature or room-temperature superconductivity was most unlikely. However, against his expectation, the discovery of high-temperature superconductivity, due to Bednorz and Müller,[2] is astonishing. The traditional Bardeen–Cooper–Schrieffer (BCS) theory[3] has failed to explain the mechanism of such superconductivity. Anderson[5] proposed a new idea called the resonating valence bond (RVB) theory or the $t-J$ model (the term t implies the transfer integral, and J the electron correlation). We have never known his theory to be successful.

A comment by Feynman, found in his book *Statistical Mechanics*,[4] says that it will take almost 50 years for the problem of superconductivity to be reduced to that of explaining the gap. Following the BCS theory, we will explain the gap, and the theory is essentially correct, but we believe that it needs to be made obviously correct. As it stands now, there are a few seemingly loose ends to tie up.

The theory of superconductivity seems to be founded on the London postulate.[7] Associated with the gauge transformation, the conserved current is

$$\mathbf{j} = -\frac{i}{2}(\phi^*\nabla\phi - \phi\nabla\phi^*) - e|\phi|^2\mathbf{A}. \tag{1.1}$$

The current due to the first term is called the paramagnetic current; and that due to the second, the diamagnetic current. In the superconducting state, the first term on the right-hand side changes very slightly, and sometimes the wave function is quite rigid, that only the diamagnetic current survives. In this respect, the superconductor is the perfect diamagnetic substance. The current is dominated by

$$\mathbf{j} = -k^2\mathbf{A}, \tag{1.2}$$

where k is a properly chosen positive constant. The Meissner effect is easily derived from Ampére's equation:

$$\nabla \times \mathbf{B} = \mathbf{j}. \tag{1.3}$$

Taking rotation gives

$$\nabla^2\mathbf{B} = k^2\mathbf{B} \tag{1.4}$$

or

$$B_x = B_0 e^{-kx}. \tag{1.5}$$

It is important to note that $|\phi|^2$ in Eq. (1.1) is very large, i.e. it is the classic scale quantity, so that the magnetic field in Eq. (1.5) damps very rapidly. This is the Meissner effect. On the book cover, we see the very spectacular experiment demonstrating the Meissner effect — a permanent magnet hovers above a superconducting plate. We know of similar phenomena — the screening of the Coulomb interaction, or quark confinement.

The boson model of Cooper pairs is considerably successful. Equation (1.3) yields $\nabla^2\mathbf{A} = k^2\mathbf{A}$, which is

$$\partial^\mu A_\mu = -k^2 A_\mu \tag{1.6}$$

in the covariant form, suggesting that a photon is massive, which is a fundamental aspect of superconductivity.[8]

An essentially similar treatment has been presented by Ginzburg and Landau (GL).[9] The superconducting state is the macroscopic state; in other words, a thermodynamic phase. They characterized this phase by introducing the order parameter, Ψ. This looks like the Schrödinger function Ψ, and then the primitive quantum theorists got confused, saying that behind the Iron Curtain the quantum theory was different in features from that of the Western countries.

The theory is handled as the phase transition. The Lagrangian for the superconducting state is postulated as

$$F_s = F_0 + a|\Psi|^2 + \frac{1}{2}b|\Psi|^4 + \frac{1}{2m^*}\left|\left(-i\hbar\nabla + \frac{e^*\mathbf{A}}{c}\right)\right|^2 + \frac{h^2}{8\pi}, \tag{1.7}$$

where * indicates the quantities in question referred to the superconductor ($\times 2$). Note that there are $|\Psi|^2$ and $|\Psi|^4$ terms in the potential parts. These drive the system to spontaneous symmetry breaking and lead to a phase transition for the suitable choice of constants a and b. This is now called the Higgs mechanism.[8] Certainly, the GL treatment is a few years ahead of the Nambu–Goldstone suggestion.

The GL theory is known as the macroscopic quantum mechanism, and in this sense, the big Ψ is sometimes amusingly called the cat's Ψ.

A very instructive presentation of the macroscopic quantum theory is found in *The Feynman Lectures on Physics*. Vol. III, Chap. 21. Various topics there, such as the Josephson junction, are quite readable.

The microscopic theory was prepared by Bardeen, Cooper and Schrieffer.[3] However, as a preliminary discussion, we present the Bogoliubov treatment. The superconductivity is a kind of many-electron problems. The most general Hamiltonian should be

$$H = \int dx\psi^+(x)h(x)\psi(x) + \frac{1}{2}\int dx\,dx'\psi^+(x)\psi(x)v(x,x')\psi^+(x')\psi(x'). \tag{1.8}$$

Since the algebra of electrons is the spinor, the terms other than the above identically vanish. In other words, the three- or four-body interactions are useless. First, we specify the spin indices, and next the plane-wave representation for the spatial parts. Equation (1.8) is simply written as

$$H = \epsilon_k(a_k^+ + a_k) + v_{k,-k}a_k^*a_{-k}^*a_{-k}a_k. \tag{1.9}$$

The simplification or the mean-field approximation for the two-body part is twofold — say,

$$\begin{aligned}&\Delta_{k,-k}a_{k\alpha}a_{k\alpha}\langle a_{-k\beta}^+a_{-k\beta}^+\rangle\\ &\Delta'_{k,-k}a_{k\alpha}^+a_{k\beta}^+\langle a_{k\alpha}a_{-k\beta}\rangle + \text{c.c.}\end{aligned} \tag{1.10}$$

The latter looks curious, since such an expectation value, $\langle a_{k\alpha}a_{-k\beta}\rangle$, vanishes identically. Against this common sense, Bogoliubov put the Hamiltonian

$$H = \epsilon_k(a_k^+ + a_k) + \Delta_k a_k^*a_{-k}^* + \Delta_k^*a_{-k}a_k. \tag{1.11}$$

We understand that Bogoliubov presumed the Cooper pair, and provided the effective Hamiltonian for pairs. His theory may be a shorthand treatment of the BCS theory. This Hamiltonian is diagonalized by the so-called Bogoliubov transformation which defines the quasiparticle responsible for the superconductivity as

$$\begin{pmatrix} \gamma_{k\uparrow} \\ \gamma^{+}_{-k\downarrow} \end{pmatrix} = \begin{pmatrix} u_k & -v_k \\ v_k & u_k \end{pmatrix} \begin{pmatrix} c_{k\uparrow} \\ c^{+}_{-k\downarrow} \end{pmatrix}, \tag{1.12}$$

with

$$u_k^2 - v_k^2 = 1. \tag{1.13}$$

The spirit of the Bogoliubov transformation is to mix operators $c_{k\uparrow}$ and $c^{+}_{-k\downarrow}$, which are different in spin. The quasiparticle yields the new ground state, so that the particle pair or the hole pair arises near the chemical potential. The stabilization energy thus obtained is called the gap energy Δ_k.[3,10]

We now follow the BCS microscopic treatment. The Green function has been effectively used by employing the Nambu spinor. This makes the unified treatment of normal and superconducting states possible. However, the temperature Green function (Matsubara function) is used from the beginning.

1.2 Spinors

We start with the general many-electron Hamiltonian not restricted to the BCS Hamiltonian. The BCS state responsible for the superconducting state is easily recognized from the formal description. The simplest method of the quantum chemistry should be the Hückel theory. This consists of the single energy matrix,

$$\beta_{rs} = \int dx\, h(x) \rho_{rs}(x), \tag{1.14}$$

where $h(x)$ is the single-particle quantum-mechanical Hamiltonian, and the electron density $\rho_{rs}(x)$ is given by the product of the single-particle (atomic) orbitals χ_r and χ_s. Note that this is the spinless theory.

We then extend the treatment into the spin space:

$$\beta_{rs} = \begin{pmatrix} \beta_{rs}^{\uparrow\uparrow} & \beta_{rs}^{\uparrow\downarrow} \\ \beta_{rs}^{\downarrow\uparrow} & \beta_{rs}^{\downarrow\downarrow} \end{pmatrix}. \tag{1.15}$$

Any 2×2 matrix is expanded in the Pauli spin matrices together with the unit matrix:

$$\sigma^0 = \begin{pmatrix} 1 & 0 \\ 0 & 1 \end{pmatrix}, \quad \sigma^3 = \begin{pmatrix} 1 & 0 \\ 0 & -1 \end{pmatrix}, \quad \sigma^1 = \begin{pmatrix} 0 & 1 \\ 1 & 0 \end{pmatrix}, \quad \sigma^2 = \begin{pmatrix} 0 & -i \\ i & 0 \end{pmatrix}. \tag{1.16}$$

However, we employ other combinations:

$$\begin{aligned} \sigma^{\uparrow} &= \frac{1}{2}(\sigma^0 + \sigma^3) = \begin{pmatrix} 1 & 0 \\ 0 & 0 \end{pmatrix}, \\ \sigma^{\downarrow} &= \frac{1}{2}(\sigma^0 - \sigma^3) = \begin{pmatrix} 0 & 0 \\ 0 & 1 \end{pmatrix}, \\ \sigma^{+} &= \frac{1}{2}(\sigma^1 + i\sigma^2) = \begin{pmatrix} 0 & 1 \\ 1 & 0 \end{pmatrix}, \\ \sigma^{-} &= \frac{1}{2i}(\sigma^1 - i\sigma^2) = \begin{pmatrix} 0 & 0 \\ 1 & 0 \end{pmatrix}. \end{aligned} \tag{1.17}$$

In Eq. (1.24), we then have

$$\begin{aligned} \beta_{rs} &= \beta_{rs}^{\mu}\sigma^{\mu}, \\ \beta_{rs}^{\mu} &= \mathrm{Tr}(\sigma^{\mu}\beta_{rs}), \end{aligned} \tag{1.18}$$

in detail:

$$\begin{aligned} \beta_{rs}^{\uparrow} = \beta_{rs}^{\uparrow\uparrow} \quad \beta_{rs}^{\downarrow} = \beta_{rs}^{\downarrow\downarrow}, \\ \beta_{rs}^{+} = \beta_{rs}^{\downarrow\uparrow} \quad \beta_{rs}^{-} = \beta_{rs}^{\uparrow\downarrow}. \end{aligned} \tag{1.19}$$

As to the Pauli matrices, the ordinary commutators are

$$\left.\begin{aligned} &[\sigma^i, \sigma^j] = 2i\epsilon_{ijk}\sigma^k \\ &[\sigma^3, \sigma^+] = 2\sigma^+ \\ &[\sigma^3, \sigma^-] = -2\sigma^- \\ &[\sigma^+, \sigma^-] = \sigma^3 \end{aligned}\right\}, \tag{1.20}$$

$$\left.\begin{aligned} &[\sigma^{\uparrow}, \sigma^{\downarrow}] = 0 \\ &[\sigma^{\uparrow}, \sigma^{+}] = \sigma^{+} \\ &[\sigma^{\uparrow}, \sigma^{-}] = -\sigma- \\ &[\sigma^{\downarrow}, \sigma^{+}] = -\sigma^{+} \\ &[\sigma^{\downarrow}, \sigma^{-}] = \sigma- \\ &[\sigma^{+}, \sigma^{-}] = \sigma^3 \end{aligned}\right\}, \tag{1.21}$$

and the anticommutators are

$$\left.\begin{aligned}[\sigma^i, \sigma^j]_+ &= 2i\delta_{ij} \\ [\sigma^+, \sigma^-]_+ &= 1\end{aligned}\right\}. \tag{1.22}$$

We then express the matrix in Eq. (1.15) as

$$\begin{aligned}\beta_{rs} &= \beta_{rs}^{\mu}\sigma^{\mu}, \\ \beta_{rs}^{\mu} &= \mathrm{Tr}(\sigma^{\mu}\beta_{rs}),\end{aligned} \tag{1.23}$$

in detail:

$$\begin{aligned}\beta_{rs}^{\uparrow} = \beta_{rs}^{\uparrow\uparrow} \quad \beta_{rs}^{\downarrow} = \beta_{rs}^{\downarrow\downarrow}, \\ \beta_{rs}^{+} = \beta_{rs}^{\downarrow\uparrow} \quad \beta_{rs}^{-} = \beta_{rs}^{\uparrow\downarrow}.\end{aligned} \tag{1.24}$$

Here, if the quantum-mechanical Hamiltonian has the single-particle character without the external field causing a rotation in the spin space, the off-diagonal elements are meaningless. The Hückel theory involves the spin diagonal terms.

However, if we take the electron–electron interaction into account, even in the mean-field approximation, the off-diagonal elements become meaningful and responsible for the superconductivity. This is what we investigate here.

1.2.1 *Spinor*

The algebra representing electrons is the spinor. The Dirac relativistic (special relativity) function describes this property well. However, the relativity seems not so important for the present problem. We now concentrate on the spinor character of the electron. The field operator has two components in the spin space:

$$\begin{aligned}\phi(x) &= \begin{pmatrix}\phi_{\uparrow}(x) \\ \phi_{\downarrow}^{+}(x)\end{pmatrix}, \\ \bar{\phi}(x) &= \phi^{+}(x)\sigma^3 = (\phi_{\uparrow}^{+}(x) \quad \phi_{\downarrow}(x))\begin{pmatrix}1 & 0 \\ 0 & -1\end{pmatrix} \\ &= (\phi_{\uparrow}^{+}(x) \quad -\phi_{\downarrow}(x)).\end{aligned} \tag{1.25}$$

This is called the Nambu representation.[11] The negative sign in front of $\phi_{\downarrow}$ is seen in the Dirac conjugate $\phi^{+} \to \bar{\phi}$.

The field operators satisfy, of course, the anticommutators

$$[\phi_{\alpha}(x), \phi_{\beta}^{+}(s')]_{+} = \delta_{\alpha,\beta}\delta(x - x'), \tag{1.26}$$

where $(\alpha, \beta) = (\uparrow, \downarrow)$ and $x = (\mathbf{r}, t)$. Then, for the spinors (1.25), the matrix commutator holds:

$$\begin{aligned}
[\phi(x), \bar{\phi}(x')]_+ &= \left[\begin{pmatrix} \phi_\uparrow(x) \\ \phi_\downarrow^+(x) \end{pmatrix}, \begin{pmatrix} \phi_\uparrow^+(x') & -\phi_\downarrow(x') \end{pmatrix} \right]_+ \\
&= \begin{pmatrix} \left[\phi_\uparrow(x), \phi_\uparrow^+(x')\right]_+ & \left[\phi_\downarrow(x'), \phi_\uparrow(x)\right]_+ \\ \left[\phi_\downarrow^+(x), \phi_\uparrow^+(x')\right]_+ & \left[\phi_\downarrow(x'), \phi_\downarrow^+(x)\right]_+ \end{pmatrix} \\
&= \begin{pmatrix} \delta(x - x') & 0 \\ 0 & \delta(x - x') \end{pmatrix}.
\end{aligned} \tag{1.27}$$

1.2.2 *Noether theorem and Nambu–Goldstone theorem*

We seek for the meaning of the Nambu spinor.[12] Consider a global transformation of fields with the constant Λ:

$$\begin{aligned}
\phi_\alpha(x) &\to \phi_\alpha(x) e^{i\Lambda}, \\
\phi_\alpha^+(x) &\to \phi_\alpha(x) e^{-i\Lambda}.
\end{aligned} \tag{1.28}$$

It is recognized that the Hamiltonian and the equation of motion are invariant under this transformation. We can see that this transformation is a rotation around the σ^3 axis with Λ,

$$\phi(x) \to e^{i\sigma^3\Lambda} \phi(x), \tag{1.29}$$

since

$$\begin{aligned}
e^{i\sigma^3\Lambda} &= \cos(\sigma^3\Lambda) + i \sin(\sigma^3\Lambda) \\
&= 1 - \frac{(\sigma^3\Lambda)^2}{2!} + \frac{(\sigma^3\Lambda)^4}{4!} + \cdots + i\left(1 - \frac{(\sigma^3\Lambda)^3}{3!} + \frac{(\sigma^3\Lambda)^5}{5!} + \cdots\right) \\
&= 1 - \frac{\Lambda^2}{2!} + \frac{\Lambda^4}{4!} + \cdots + i\sigma^3\left(1 - \frac{\Lambda^3}{3!} + \frac{\Lambda^5}{5!} + \cdots\right) \\
&= \sigma^0 \cos\Lambda + i\sigma^3 \sin\Lambda = \begin{pmatrix} e^{i\Lambda} & 0 \\ 0 & e^{-i\Lambda} \end{pmatrix}.
\end{aligned}$$

Here, we discuss briefly the Noether theorem and the Nambu–Goldstone theorem. The latter makes a profound investigation possible. If the Lagrangian of the system in question is invariant under some transformation which is just the present case, we have the continuity relation. Notice that

the density and the current are, in terms of the Nambu spinor,

$$\begin{aligned} j^0 &= \phi^+(x)\sigma^3\phi(x), \\ \mathbf{j} &= -i\frac{\hbar}{2m}(\phi^+(x)\nabla\phi(x) + \nabla\phi^+(x)\phi(x)). \end{aligned} \tag{1.30}$$

Then the continuity relation is

$$\partial_t j_0(x) + \nabla \cdot \mathbf{j} = 0. \tag{1.31}$$

If the system is static, the density must be conserved:

$$\partial_t j^0 = 0. \tag{1.32}$$

Put

$$G = \int dx j^0(x), \tag{1.33}$$

and if it is found that

$$[G, \Psi'(x)] = \Psi(x), \tag{1.34}$$

and the expectation value of $\Psi(x)$ over the ground state does not vanish,

$$\langle 0|\Psi|0\rangle \neq 0, \tag{1.35}$$

i.e. if the ground state satisfying the relation (1.33) does not vanish, we can expect the appearance of a boson $\Psi(x)$, whose mass is zero. This boson is called a Goldstone boson, and the symmetry breaking takes place in the system. This is what the Goldstone theorem insists on. The details are in the standard book on the field theory.[8]

Now we apply this theorem to the superconductivity. The invariant charge is

$$Q = \int d^3x \phi_\alpha^+(x)\phi_\alpha(x) = \int d^3x \phi^+(x)\sigma^3\phi(x). \tag{1.36}$$

In terms of the Nambu spinor, here σ^3 is crucial. In the commutator (1.33), we seek for the spin operators which do not commute with σ^3 and find, say, $\sigma^\pm$. We then have the Goldstone commutator as

$$\begin{aligned} &\int d^3x' \langle [\phi^+(x')\sigma^3\phi(x'), \phi^+(x)\sigma^\pm\phi(x)]\rangle_{t=t'} \\ &\quad = \int d^3x (\pm 2)\langle 0|\phi^+(x)\sigma^\pm\phi(x')|0\rangle\delta(\mathbf{r}-\mathbf{r}'). \end{aligned} \tag{1.37}$$

In detail,

$$\begin{aligned} \phi^+(x)\sigma^+\phi(x) &= \begin{pmatrix} \phi_\uparrow^+(x) & \phi_\downarrow(x) \end{pmatrix} \begin{pmatrix} 0 & 1 \\ 0 & 0 \end{pmatrix} \begin{pmatrix} \phi_\uparrow(x) \\ \phi_\downarrow^+(x) \end{pmatrix} \\ &= \phi_\uparrow^+(x)\phi_\downarrow^+(x), \\ \phi^+(x)\sigma^-\phi(x) &= \phi_\uparrow(x)\phi_\downarrow(x). \end{aligned} \tag{1.38}$$

Notice that here the same symbol ϕ is used for the ordinary field with spin and the Nambu spinor. The above are nothing but the Cooper pairs, and we now find the Goldstone bosons Ψ^* and Ψ. In literature, it is noted that

$$\langle 0|\phi^+(x)\sigma^{\pm}\phi(x)|0\rangle = \pm\frac{\Delta_{\pm}}{g} \neq 0, \tag{1.39}$$

where Δ and g are the gap and the coupling parameter, respectively. We expect the estimate

$$\Delta_+ \sim \Delta_- = \Delta$$

to be reasonable.

The Cooper pairs are now the Goldstone bosons. A comment about the Goldstone boson or the massless elementary excitation with $k = 0$ is required. Using Eq. (1.33), we write the Goldstone commutator (1.34) as

$$\begin{aligned}\int d^3y[&\langle 0|j_0(y)|n\rangle\langle n|\phi'(x)|0\rangle \\ &- \langle 0|\phi'(x)|n\rangle\langle n|j_0(y)|0\rangle]_{x_0=y_0} \neq 0,\end{aligned} \tag{1.40}$$

where $|n\rangle$ is the intermediate state, and $x_0 = y_0$ implies that this is the equal time commutator.

Since

$$j_0(y) = e^{-ipy}j_0(0)e^{ipy}, \tag{1.41}$$

it is seen that

$$\begin{aligned}&\int d^3y[\langle 0|J_0(0)|n\rangle\langle n|\phi'(x)|0\rangle e^{ip_n y} \\ &\quad - \langle 0|\phi'(x)|n\rangle\langle n|J_0(0)|0\rangle e^{-ip_n y}]_{x_0=y_0} \quad (p|n\rangle = p_n|n\rangle) \\ &= \delta(\mathbf{p}_n)[\langle 0|J_0(0)|n\rangle\langle n|\phi'(0)|0\rangle e^{ip_{n0}y} \\ &\quad - \langle 0|\phi'(x)|n\rangle\langle n|J_0(0)|0\rangle e^{-ip_{n0}y}]_{x_0=y_0} \\ &= \delta(\mathbf{p}_n)[\langle 0|J_0(0)|n\rangle\langle n|\phi'(0)|0\rangle e^{iM_n y_0} \\ &\quad - \langle 0|\phi'(0)|n\rangle\langle n|J_0(0)|0\rangle e^{-iM_n y_0}]_{x_0=y_0} \neq 0.\end{aligned} \tag{1.42}$$

In order to obtain the first equality, spatial integration is carried out. Then, considering $p^\mu = (\mathbf{p}, M)$, we retain the fourth component. In the last equation, when $M_n \neq 0$, cancellations will arise for the summation over n. We thus obtain, only for $M_n = 0$, the finite result

$$\begin{aligned}&\langle 0|j_0(0)|n\rangle\langle n|\phi'(0)|0\rangle - \langle 0|\phi'(0)|n\rangle\langle n|j_0(0)|0\rangle \\ &\quad = \text{Im } \langle 0|j_0(0)|n\rangle\langle n|\phi'(x)|0\rangle,\end{aligned} \tag{1.43}$$

which is met with the requirement (1.34). The excitation with $M_n = 0$ needs no excitation energy, suggesting the Goldstone boson.

We further note that the mass-zero excitation is the imaginary quantity. This suggests the current to be the phase current, as is seen in the Josephson effect.

Before closing this preliminary discussion, we want to make a few remarks. At the beginning, we mentioned London's postulate that the superconducting state is characterized by a statement that the wave function is rigid, so that the current is entirely the diamagnetic current due to only the vector potential $\mathbf{A}$. "Rigid" is not really rigid, but it is understood that the spatial derivative is vanishing, or the current flows along the entirely flat path, which is described in a textbook as the path going around the top of a Mexican hat. Boldly speaking, the electron in the superconducting state is massless. Also, we have pointed out that the vector potential $\mathbf{A}$, which leads to the Meissner effect, satisfies the covariant relation (1.6),

$$\partial_\mu A_\mu = -k^2, \tag{1.44}$$

so that a photon is massive in the superconductor.

In the following chapters, we develop a substantial microscopic explanation of the above assertions.

1.3 Propagator

In the previous section, we have found that, as is seen in Eq. (1.41), the superconducting state strongly concerns the gap function or the anomalous Green function. We want to deal with the solid-state substances. However, the infinite crystals described by the single band have already been fully investigated in literature, and the recent investigations were carried out on objects with multiband structure.[13,14] The infinite system with many bands is constructed from the unit cell, which is really a chemical molecule. The atoms in this molecule give the band index of the real crystal. In this respect, we first investigate the Green function of a unit cell. The Green function is now shown in the site representation.

Corresponding to the spinors (1.24), we define the spinor in the site representation as

$$\mathbf{a}_r = \begin{pmatrix} a_{r\uparrow} \\ a^+_{r\downarrow} \end{pmatrix}, \quad \bar{\mathbf{a}}_r = (a^+_{r\uparrow} \quad -a_{r\downarrow}). \tag{1.45}$$

Due to this definition, it is unnecessary to insert σ^3 in the matrix $\mathbf{G}$, as is seen in Schrieffer's book.[3] The commutator is

$$[\mathbf{a}_r, \bar{\mathbf{a}}_s]_+ = \begin{pmatrix} [a_{r\uparrow}, a^+_{s\uparrow}]_+ & [a_{s\downarrow}, a_{r\uparrow}]_+ \\ [a^+_{r\downarrow}, a^+_{s\uparrow}]_+ & [a_{s\downarrow}, a^+_{r\downarrow}]_+ \end{pmatrix} = \begin{pmatrix} \delta_{rs} & 0 \\ 0 & \delta_{rs} \end{pmatrix} = \delta_{rs}\mathbf{1}_{2\times 2}. \quad (1.46)$$

The matrix propagator is defined by

$$\begin{aligned} \mathbf{G}_{rs}(\tau) &= -\langle\langle \mathbf{a}_r(\tau_1), \bar{\mathbf{a}}_s(\tau_2)\rangle\rangle \\ &= -\begin{pmatrix} \langle\langle a_{r\uparrow}(\tau_1), a^+_{s\uparrow}(\tau_2)\rangle\rangle & -\langle\langle a_{r\uparrow}(\tau_1), a_{s\downarrow}(\tau_2)\rangle\rangle \\ \langle\langle a^+_{r\downarrow}(\tau_1), a^+_{s\uparrow}(\tau_2)\rangle\rangle & -\langle\langle a^+_{r\downarrow}(\tau_1), a_{s\downarrow}(\tau_2)\rangle\rangle \end{pmatrix} \\ &= -\langle \theta(\tau_1-\tau_2)\mathbf{a}_r(\tau_1)\bar{\mathbf{a}}_s(\tau_2) + \theta(\tau_2-\tau_1)\bar{\mathbf{a}}_s(\tau_2)\mathbf{a}_r(\tau_1)\rangle, \end{aligned} \quad (1.47)$$

where τ is the imaginary time, so that the propagator is the temperature Green function or the Matsubara function. In what follows, we put

$$\tau = \tau_1 - \tau_2, \quad (1.48)$$

and the system depends on $\tau_1 - \tau_2$. If we want to obtain the gap function, we consider

$$\mathrm{Tr}(\sigma^+ \mathbf{G}_{rs}(\tau)) = \langle\langle a^+_{r\downarrow}(\tau_1), a^+_{s\uparrow}(\tau_2)\rangle\rangle, \quad (1.49)$$

and the standard procedure will be followed.

1.3.1 *Hamiltonian*

Various Hamiltonians can be written by using the charge density matrix,

$$\rho_{rs}(x) = \begin{pmatrix} \rho_{r\uparrow s\uparrow}(x) & \rho_{r\uparrow s\downarrow}(x) \\ \rho_{r\downarrow s\uparrow}(x) & \rho_{r\downarrow s\downarrow}(x) \end{pmatrix} = \sigma^\mu \rho^\mu_{rs}, \quad (1.50)$$

where the basis orbitals are put to be real, so that we do not need the conjugation procedure for field operators.

The Hückel Hamiltonian or the single-particle Hamiltonian has the structure

$$H^0 = h^\mu_{rs} \bar{\mathbf{a}}_r \sigma^\mu \mathbf{a}_r, \quad (1.51)$$

where h includes the chemical potential and can be explicitly written as

$$h_{rs} = \int \rho_{rs} h(x) = \int dx h(x) \begin{pmatrix} \rho_{r\uparrow s\uparrow}(x) & \rho_{r\uparrow s\downarrow}(x) \\ \rho_{r\downarrow s\uparrow}(x) & \rho_{r\downarrow s\downarrow}(x) \end{pmatrix} = \sigma^\mu h^\mu_{rs}. \quad (1.52)$$

Hereafter, we use the summation convention that repeated indices imply that the summation is carried out to facilitate manipulations. Other two-particle Hamiltonians are given in a similar way. Noting that

$$v^{\mu\upsilon}_{rs;tu} = \int dx\, dx' \rho^{\mu}_{rs}(x) v(x - x') \rho^{\upsilon}_{tu}(x'), \tag{1.53}$$

we have[17]

$$\begin{aligned} H^{\mathrm{dir}} &= \frac{1}{2}(\bar{\mathbf{a}}_r \sigma^a \mathbf{a}_s) v^{ab}_{rs;tu} (\bar{\mathbf{a}}_t \sigma^b \mathbf{a}_u) \quad (a, b = \uparrow, \downarrow), \\ H^{\mathrm{ex}} &= -\frac{1}{2}(\bar{\mathbf{a}}_r \sigma^a \mathbf{a}_s) v^{aa}_{rs;ut} (\bar{\mathbf{a}}_t \sigma^a \mathbf{a}_u) \quad (a = \uparrow, \downarrow), \\ H^{\mathrm{super}} &= \frac{1}{2}\{(\bar{\mathbf{a}}_r \sigma^+ \mathbf{a}_s) v^{+-}_{rs;tu} (\bar{\mathbf{a}}_t \sigma^- \mathbf{a}_u) \\ &\qquad + (\bar{\mathbf{a}}_r \sigma^- \mathbf{a}_s) v^{-+}_{rs;tu} (\bar{\mathbf{a}}_t \sigma^+ \mathbf{a}_u)\}. \end{aligned} \tag{1.54}$$

For the direct interaction, the quantum-mechanical Hamiltonian is

$$H^{\mathrm{dir}} = \int dx\, dx' \chi^*_{r\uparrow}(r) \chi_{s\uparrow}(r) (x) v(x - x') \chi^*_{\downarrow}(x') \chi^*_{u\downarrow}(x').$$

For the field-theoretical Hamiltonian, the wave functions are replaced by the creation–annihilation operators $a^+_{r\uparrow}$, $a_{r\uparrow}$, and so on. These are written in the spinor notation; for example,

$$\begin{aligned} a^+_{r\uparrow} a_{s\uparrow} &= \begin{pmatrix} a^+_{r\uparrow} & a_{r\downarrow} \end{pmatrix} \begin{pmatrix} 1 \\ 0 \end{pmatrix} \begin{pmatrix} 1 & 0 \end{pmatrix} \begin{pmatrix} a_{s\uparrow} \\ a^+_{s\downarrow} \end{pmatrix} \\ &= \mathbf{a}^+_r \begin{pmatrix} 1 & 0 \\ 0 & 0 \end{pmatrix} \mathbf{a}_s = \mathbf{a}^+_r \sigma^{\uparrow} \mathbf{a}_s. \end{aligned}$$

Note that H^{ex} is obtained by reversing indices ($u \leftrightarrow t$) in $v_{rs;tu}$.

1.4 Noninteracting

"Noninteracting" implies that the Hamiltonian is bilinear with respect to operators so that diagonalization is always possible. It should be instructive to begin with the single-particle case, since even if we manipulate the complicated two-particle case, the procedures are almost the same when the mean-field approximation is employed.

The energy for the Hamiltonian (1.52) is

$$E^0 = \mathrm{Tr}(\hat{\rho} H^0) = h_{rs} \langle \bar{\mathbf{a}}_r \mathbf{a}_s \rangle, \tag{1.55}$$

where $\hat{\rho}$ is the statistical operator,

$$\hat{\rho} = e^{\beta(H^0 - \Omega)}, \tag{1.56}$$

with the normalization factor Ω. We now define the temperature Green function, in which τ is the imaginary time, $\tau = it$,[15,16]

$$\begin{aligned} G_{rs}(\tau) &= -\mathrm{Tr}\hat{\rho}[(\theta(\tau_1)\mathbf{a}_r(\tau_1)\mathbf{a}_s^+(\tau_2) - \theta(-\tau)\mathbf{a}_s^+(\tau_2)\mathbf{a}_r(\tau_1)] \\ &= \langle\langle \mathbf{a}_r(\tau_1)\mathbf{a}_s^+(\tau_2)\rangle\rangle, \end{aligned} \tag{1.57}$$

where

$$\tau = \tau_1 - \tau_2, \tag{1.58}$$

and it is assumed that the system is dependent only on the relative time τ. Then we can write E^0 in terms of the temperature Green function:

$$E^0 = \mathrm{Tr}[h_{rs}G_{sr}(\tau = 0^-)]. \tag{1.59}$$

Note that h_{rs} and G_{sr} are matrices.

The equation of motion (1.57) for the noninteracting Hamiltonian (1.51) can be read as

$$\begin{aligned} &\partial_{\tau_1}\langle\langle \mathbf{a}_s(\tau_1)\bar{\mathbf{a}}_r(\tau_2)\rangle\rangle \\ &\quad = \delta(\tau_1 - \tau_2)\langle[\mathbf{a}_s(\tau_1), \bar{\mathbf{a}}_r(\tau_2)]_+\rangle + \langle[\mathbf{a}_s(\tau_1), \bar{\mathbf{a}}_{s'}\mathbf{a}_{r'}h_{s'r'}(\tau_1)]_-, \bar{\mathbf{a}}_r(\tau_2)\rangle \\ &\quad = \delta(\tau_1 - \tau_2)\delta_{sr} + \langle\delta_{ss'}h_{r's'}(\tau_1)\mathbf{a}_{r'}(\tau_1), \bar{\mathbf{a}}_r(\tau_2)\rangle \\ &\quad = \delta(\tau_1 - \tau_2)\delta_{sr} + \{h_{sr'}\}\langle\langle \mathbf{a}_{r'}(\tau_1), \bar{\mathbf{a}}_r(\tau_2)\rangle\rangle. \end{aligned} \tag{1.60}$$

It can be solved using the Fourier transformation[15]

$$\langle\langle \mathbf{a}_s(\tau_1)\bar{\mathbf{a}}_r(\tau_2)\rangle\rangle = \frac{1}{\beta}\sum_n e^{i\omega_n\tau}\langle\langle \mathbf{a}_s\bar{\mathbf{a}}_r; \omega_n\rangle\rangle, \tag{1.61}$$

with

$$\omega_n = \frac{(2n+1)\pi}{\beta}, \tag{1.62}$$

where the odd number indicates that particles are fermions. Then Eq. (1.50) becomes

$$(i\omega_n\delta_{sr'} - h_{sr'})\langle\langle \mathbf{a}_{r'}\bar{\mathbf{a}}_r; \omega_n\rangle\rangle = \delta_{sr}. \tag{1.63}$$

In this step, the matrix structure of the above should be carefully investigated. Let us assume that the single-particle Hamiltonian is spin-diagonal:

$$h_{sr} = \begin{pmatrix} h_{sr}^{\uparrow} & 0 \\ 0 & h_{sr}^{\downarrow} \end{pmatrix}. \tag{1.64}$$

It is preferable to introduce the flame diagonalizing each element:

$$h_{sr}^{\uparrow} = (\langle s|i\rangle\langle i|h|i\rangle|i\rangle\langle ir\rangle)^{\uparrow} = \langle s|i\rangle^{\uparrow}\epsilon_{i\uparrow}\langle i|r\rangle^{\uparrow}. \tag{1.65}$$

Then we have

$$\langle\langle \mathbf{a}_s \bar{\mathbf{a}}_r \rangle\rangle = \frac{1}{\beta}\sum_n \frac{1}{\begin{pmatrix} \frac{(\langle s|i\rangle\langle i|r\rangle)^\uparrow}{i\omega_n - \epsilon_{i\uparrow}} & 0 \\ 0 & \frac{(\langle s|i\rangle\langle i|r\rangle)^\downarrow}{i\omega_n - \epsilon_{i\downarrow}} \end{pmatrix}}$$

$$= \frac{1}{\beta}\sum_n \begin{pmatrix} \frac{(\langle s|i\rangle\langle i|r\rangle)^\uparrow}{i\omega_n - \epsilon_{i\uparrow}} & 0 \\ 0 & \frac{(\langle s|i\rangle\langle i|r\rangle)^\downarrow}{i\omega_n - \epsilon_{i\downarrow}} \end{pmatrix}$$

$$= \begin{pmatrix} (\langle s|i\rangle n(\epsilon_i)\langle i|r\rangle)^\uparrow & 0 \\ 0 & (\langle s|i\rangle n(\epsilon_i)\langle i|r\rangle)^\downarrow \end{pmatrix}, \tag{1.66}$$

where

$$n(\epsilon_{i\uparrow}) = \frac{1}{1 + e^{\epsilon_{i\uparrow}/k_B T}}. \tag{1.67}$$

Another sophisticated way starts from the decomposed Hamiltonian

$$H^0 = \bar{\mathbf{a}}_r \sigma^\mu h^\mu_{rs} \mathbf{a}_s. \tag{1.68}$$

The commutator is evaluated as

$$[\mathbf{a}_s, \bar{\mathbf{a}}_{r'} \sigma^\mu h^\mu_{r's'} \mathbf{a}_{s'}] = \delta_{sr'} \sigma^0 \sigma^\mu h^\mu_{r's'} \mathbf{a}_{s'} = \sigma^\mu h^\mu_{ss'} \mathbf{a}_{s'}. \tag{1.69}$$

The equation of motion

$$(i\omega_n \delta_{ss'} - \sigma^\mu h^\mu_{ss'}) \langle\langle \mathbf{a}_{s'}, \bar{\mathbf{a}}_r; \omega_n \rangle\rangle = \sigma^0 \delta_{sr}. \tag{1.70}$$

In the matrix notation,

$$(i\omega_n - \sigma^\mu h^\mu) \langle\langle \mathbf{a}, \bar{\mathbf{a}}; \omega_n \rangle\rangle = \sigma^0$$

or

$$\langle\langle \mathbf{a}, \bar{\mathbf{a}}; \omega_n \rangle\rangle = \frac{\sigma^0}{i\omega_n - \sigma^\mu h^\mu}. \tag{1.71}$$

In the representation where h is diagonal,

$$\langle r|h|s\rangle = \langle r|i\rangle\langle i|h|i\rangle\langle i|s\rangle = \epsilon_i \langle r|i\rangle\langle i|s\rangle, \tag{1.72}$$

the relation (1.71) becomes

$$\langle\langle \mathbf{a}, \bar{\mathbf{a}}; \omega_n \rangle\rangle = \frac{(|i\rangle\langle i|)(i\omega_n + \sigma^\mu \epsilon^\mu_i)}{(i\omega_n - \sigma^\mu \epsilon^\mu_i)(i\omega_n + \sigma^\mu \epsilon^\mu_i)}$$

$$= \frac{(|i\rangle\langle i|)(i\omega_n + \sigma^\mu \epsilon^\mu_i)}{(i\omega_n)^2 - (\epsilon^\mu_i)^2}. \tag{1.73}$$

Now

$$\begin{aligned}\frac{i\omega_n+\sigma^\mu\epsilon_i^\mu}{(i\omega_n)^2-(\epsilon_i^\mu)^2} &= \frac{i\omega_n}{(i\omega_n)^2-(\epsilon_i^\mu)^2}+\frac{\sigma^\mu\epsilon_i^\mu}{(i\omega_n)^2-(\epsilon_i^\mu)^2}\\ &= \frac{1}{2}\left(\frac{1}{i\omega_n-\epsilon_i^\mu}+\frac{1}{i\omega_n+\epsilon_i^\mu}\right)+\frac{\sigma^\mu}{2}\left(\frac{1}{i\omega_n-\epsilon_i^\mu}-\frac{1}{i\omega_n+\epsilon_i^\mu}\right)\\ &= \frac{1}{2}\left(\frac{1}{i\omega_n+\epsilon_i^\mu}+\frac{1}{i\omega_n+\epsilon_i^\mu}\right)\quad(\text{summing }\omega_n)\\ &\to \frac{1}{2}(n(\epsilon_i^\mu)+n(-\epsilon_i^\mu))+\frac{\sigma^\mu}{2}(n(\epsilon_i^\mu)-n(-\epsilon_i^\mu)).\end{aligned}\tag{1.74}$$

We evaluate

$$\begin{aligned}G_{rs}^{\uparrow} &= \mathrm{Tr}\sigma^{\uparrow}\left\{\langle r|i\rangle\langle i|s\rangle\frac{\sigma^0}{2}(n(\epsilon_i^\mu)+n(-\epsilon_i^\mu))+\frac{\sigma^\mu}{2}(n(\epsilon_i^\mu)-n(-\epsilon_i^\mu))\right\}\\ &= [\langle r|i\rangle\langle i|s\rangle]^{\uparrow}n(\epsilon_i^{\uparrow}).\end{aligned}\tag{1.75}$$

We then have

$$\frac{1}{\beta}\sum_n G_{rs}^{\uparrow}(0^-)=\frac{1}{\beta}\sum_n\frac{\langle r|i\rangle\langle i|s\rangle}{i\omega_n-\epsilon_i^{\uparrow}}=\langle r|i\rangle n(\epsilon_i^{\uparrow})\langle i|s\rangle.\tag{1.76}$$

This relation holds for both $\uparrow$ and $\uparrow$, and we recover the result (1.66).

Along the way, we give the energy expression for Eq. (1.51):

$$\begin{aligned}E^0 &= \mathrm{Tr}(h_{rs}G_{sr})\\ &= \mathrm{Tr}\begin{pmatrix}h_{rs}^{\uparrow} & 0\\ 0 & h_{rs}^{\downarrow}\end{pmatrix}\begin{pmatrix}\langle s|i\rangle n(\epsilon_i^{\uparrow})\langle i|r\rangle & 0\\ 0 & \langle s|i\rangle n(\epsilon_i^{\downarrow})\langle i|r\rangle\end{pmatrix}.\end{aligned}\tag{1.77}$$

It may be needless to present another illustration:

$$E^0=\mathrm{Tr}(h_{rs}G_{sr})=\mathrm{Tr}(\sigma^\mu h_{rs}^\mu)(\sigma^\upsilon G_{sr}^\upsilon).\tag{1.78}$$

The result is meaningful if $\sigma^\mu\sigma^\upsilon=\sigma^0$, which leads to, in the present case,

$$\sigma^\mu=\sigma^\upsilon=\sigma^{\uparrow},\quad\text{or}\quad\sigma^\mu=\sigma^\upsilon=\sigma^{\downarrow}.$$

Such manipulations will be used in the later investigation.

1.5 Interacting

In this chapter, the electron–electron interactions are taken into account, and we will discuss how they lead to the superconducting state. The

Hamiltonians given in Eq. (1.54) are

$$
\begin{aligned}
H^{\mathrm{dir}} &= \frac{1}{2}(\bar{\mathbf{a}}_r\sigma^a\mathbf{a}_s)v^{ab}_{rs;tu}(\bar{\mathbf{a}}_t\sigma^b\mathbf{a}_u) \quad (a,b=\uparrow,\downarrow),\\
H^{\mathrm{ex}} &= -\frac{1}{2}(\bar{\mathbf{a}}_r\sigma^a\mathbf{a}_s)v^{aa}_{rs;ut}(\bar{\mathbf{a}}_t\sigma^a\mathbf{a}_u) \quad (a=\uparrow,\downarrow),\\
H^{\mathrm{sup}} &= \frac{1}{2}\{(\bar{\mathbf{a}}_r\sigma^+\mathbf{a}_s)v^{+-}_{rs;tu}(\bar{\mathbf{a}}_t\sigma^-\mathbf{a}_u)+(\bar{\mathbf{a}}_r\sigma^-\mathbf{a}_s)v^{-+}_{rs;tu}(\bar{\mathbf{a}}_t\sigma^+\mathbf{a}_u)\}.
\end{aligned}
$$

These are written in the mean-field approximation. The estimate beyond this approximation is not the case of the present consideration. We have

$$
\begin{aligned}
H^0 &= h^a_{rs}\bar{\mathbf{a}}_r\sigma^a\mathbf{a}_r \quad (a=\uparrow,\downarrow),\\
H^{\mathrm{dir}} &= (\bar{\mathbf{a}}_r\sigma^a\mathbf{a}_s)v^{ab}_{rs;tu}\langle\bar{\mathbf{a}}_t\sigma^b\mathbf{a}_u\rangle = (\bar{\mathbf{a}}_r\sigma^a\mathbf{a}_s)D^{a:\mathrm{dir}}_{rs} \quad (a,b=\uparrow,\downarrow),\\
H^{\mathrm{ex}} &= -(\bar{\mathbf{a}}_r\sigma^a\mathbf{a}_s)v^{aa}_{rs;ut}\langle\bar{\mathbf{a}}_t\sigma^b\mathbf{a}_u\rangle = (\bar{\mathbf{a}}_r\sigma^a\mathbf{a}_s)D^{a:\mathrm{ex}}_{rs} \quad (a=\uparrow,\downarrow),\\
H^{\mathrm{sup}} &= (\bar{\mathbf{a}}_r\sigma^+\mathbf{a}_s)v^{+-}_{rs;ut}\langle\bar{\mathbf{a}}_t\sigma^-\mathbf{a}_u\rangle + (\bar{\mathbf{a}}_r\sigma^-\mathbf{a}_s)v^{-+}_{rs;ut}\langle\bar{\mathbf{a}}_t\sigma^+\mathbf{a}_u\rangle\\
&= (\bar{\mathbf{a}}_r\sigma^+\mathbf{a}_s)D^{-:\mathrm{sup}}_{rs} + \bar{\mathbf{a}}_r\sigma^-\mathbf{a}_s)D^{+:\mathrm{sup}}_{rs},
\end{aligned}
\tag{1.79}
$$

where

$$
\begin{aligned}
D^{a:\mathrm{dir}}_{rs} &= v^{ab}_{rs;tu}\langle\bar{\mathbf{a}}_t\sigma^b\mathbf{a}_u\rangle,\\
D^{a:\mathrm{ex}}_{rs} &= -v^{ab}_{rs;ut}\langle\bar{\mathbf{a}}_t\sigma^b\mathbf{a}_u\rangle\delta_{ab},\\
D^{+:\mathrm{sup}}_{rs} &= v^{+-}_{rs;tu}\langle\bar{\mathbf{a}}_t\sigma^-\mathbf{a}_u\rangle,
\end{aligned}
\tag{1.80}
$$

where $\langle\cdots\rangle$ implies the ground-state average, which was actually obtained with wave functions in the previous step during the self-consistent field (SCF) calculations.

These Hamiltonians are classified into two kinds called modes — the normal many-electron problem and that for the superconductivity:

$$
H = H^{\mathrm{norm}} + H^{\mathrm{sup}}, \tag{1.81}
$$

where

$$
\begin{aligned}
H^{\mathrm{norm}} &= (\bar{\mathbf{a}}_r\sigma^a\mathbf{a}_s)(h^a_{rs}\delta_{rs} + D^{a:\mathrm{dir}}_{rs} + D^{a:\mathrm{ex}}_{rs}),\\
H^{\mathrm{sup}} &= \bar{\mathbf{a}}_r\sigma^{\pm}\mathbf{a}_s D^{\mp:\mathrm{sup}}_{rs}.
\end{aligned}
\tag{1.82}
$$

The main difference between the two is that in the former we have the single-particle Hamiltonian, and in the latter we do not. Various D_{rs} are complicated, but they are merely the c-numbers in this treatment. The propagator in question in Eq. (1.57) is presented here again:

$$
\begin{aligned}
G_{rs}(\tau) &= -\mathrm{Tr}\hat{\rho}\big[(\theta(\tau)\mathbf{a}_r(\tau_1)\mathbf{a}^+_s(\tau_2) - \theta(-\tau)\mathbf{a}^+_s(\tau_2)\mathbf{a}_r(\tau_1)\big]\\
&= \langle\langle\mathbf{a}_r(\tau_1)\mathbf{a}^+_s(\tau_2)\rangle\rangle.
\end{aligned}
$$

The equation of motion can be read as

$$\begin{aligned}
&\partial_{\tau_1}\langle\langle \mathbf{a}_s(\tau_1)\bar{\mathbf{a}}_r(\tau_2)\rangle\rangle \\
&\quad = \delta(\tau_1-\tau_2)\langle[\mathbf{a}_s(\tau_1),\bar{\mathbf{a}}_r(\tau_2)]_+\rangle + \langle[\mathbf{a}_s(\tau_1),\bar{\mathbf{a}}_{s'}\mathbf{a}_{r'}H^a_{s'r'}(\tau_1)]_-,\bar{\mathbf{a}}_r(\tau_2)\rangle \\
&\qquad (a;\text{norm, sup}) \\
&\quad = \delta(\tau_1-\tau_2)\delta_{sr} + D^a_{sr'}\sigma^a\langle\langle \mathbf{a}_{r'}(\tau_1),\bar{\mathbf{a}}_r(\tau_2)\rangle\rangle. \qquad (1.83)
\end{aligned}$$

Making the Fourier transformation with respect to $\tau=\tau_2-\tau_2$ gives

$$(i\omega_n - D^a_{rs'}\sigma^a)G_{s'r} = \delta_{sr} \qquad (1.84)$$

or, in the matrix form,

$$G(\omega_n) = \frac{1}{i\omega_n - D^a\sigma^a} = \frac{i\omega_n + D^a\sigma^a}{(i\omega_n)^2-(D^a)^2}. \qquad (1.85)$$

Note that D^a consists of the single-electron part and the two-electron interaction term which involves another mate ρ^a_{tu} combined with the propagator $\langle\bar{\mathbf{a}}_t\sigma^a\mathbf{a}_u\rangle$:

$$D^a(x) = h^a(x) + \int dx' v(x-x')\rho^b_{tu}(x')\sigma^b\langle\bar{\mathbf{a}}_\mathbf{t}\mathbf{a}_\mathbf{t}\rangle. \qquad (1.86)$$

However, the mean-field approximation makes this as if it were the single-electron interaction. A few comments will be given about the matrix character of G. This is a big matrix with site indices, and each element is a 2×2 matrix in the spin space. The index a characterizes the mode of the mean-field potential. All the modes are independent of each other and are individually diagonalized. We now introduce a flame, in which these are diagonal:

$$\langle i^a|D^a|i^a\rangle = \eta^a_i. \qquad (1.87)$$

Look at the right-hand side of Eq. (1.85) and remember the Einstein convention that repeated indices imply summation:

$$(D^a)^2 = (\eta^\uparrow)^2 + (\eta^\downarrow)^2 + (\eta^+)^2 + (\eta^-)^2 = (\eta^{\text{norm}})^2 + (\eta^{\text{sup}})^2, \qquad (1.88)$$

where the second line is in a simple notation. Then we have

$$\begin{aligned}
G(\omega_n) &= \frac{|i^a\rangle(i\omega_n + \langle i^a|D^a|i^a\rangle\sigma^a)\langle i^a|}{\{i\omega_n - (\eta^{\text{norm}}_i + \eta^{\text{sup}}_i)\}\{i\omega_n + (\eta^{\text{norm}}_i + \eta^{\text{sup}}_i)\}}. \\
&= |i^a\rangle\frac{1}{2}\left(\frac{1}{i\omega_n - (\eta^{\text{norm}}_i + \eta^{\text{sup}}_i)} + \frac{1}{i\omega_n + (\eta^{\text{norm}}_i + \eta^{\text{sup}}_i)}\right)\langle i^a| \\
&\quad + |i^a\rangle\frac{D^a_{ii}\sigma^a}{2(\eta^{\text{norm}}_i + \eta^{\text{sup}}_i)} \\
&\quad \times\left(\frac{1}{i\omega_n - (\eta^{\text{norm}}_i + \eta^{\text{sup}}_i)} - \frac{1}{i\omega_n - (\eta^{\text{norm}}_i + \eta^{\text{sup}}_i)}\right)\langle i^a|. \qquad (1.89)
\end{aligned}$$

Taking the (r, s) matrix elements and the mode c which is achieved by the operation,

$$\mathrm{Tr}\sigma^c G_{rs} = G^c rs, \tag{1.90}$$

we select the terms on the right-hand side with the mode c satisfying

$$\mathrm{Tr}\sigma^c\sigma^a = 1. \tag{1.91}$$

Otherwise, the Tr operation leads to the vanishing result.

Carrying out the summation over ω_n, we get

$$\begin{aligned}
G^c_{rs}(0^-) &= \frac{1}{\beta}\sum_n G^c_{rs}(\omega_n) \\
&= \frac{1}{\beta}\sum_n \langle r^c|i^a\rangle \frac{1}{2}\left(\frac{1}{i\omega_n - (\eta_i^{\mathrm{norm}} + \eta_i^{\mathrm{sup}})} + \frac{1}{i\omega_n + (\eta_i^{\mathrm{norm}} + \eta_i^{\mathrm{sup}})}\right) \\
&\quad \times \langle i^a|s^c\rangle + \frac{1}{\beta}\sum_n \langle r^c|i^a\rangle \frac{D^a_{ii}}{2(\eta_i^{\mathrm{norm}} + \eta_i^{\mathrm{sup}})} \\
&\quad \times \left(\frac{1}{i\omega_n - (\eta_i^{\mathrm{norm}} + \eta_i^{\mathrm{sup}})} - \frac{1}{i\omega_n + (\eta_i^{\mathrm{norm}} + \eta_i^{\mathrm{sup}})}\right)\langle i^a|s^c\rangle \\
&= \langle r^c|i^a\rangle \frac{1}{2}(n(\eta_i^{\mathrm{norm}} + \eta_i^{\mathrm{sup}}) + n(-\eta_i^{\mathrm{norm}} - \eta_i^{\mathrm{sup}}))\langle i^a|s^c\rangle \\
&\quad + \langle r^c|i^a\rangle \frac{D^a_{ii}}{2(\eta_i^{\mathrm{norm}} + \eta_i^{\mathrm{sup}})} \\
&\quad \times (n(\eta_i^{\mathrm{norm}} + \eta_i^{\mathrm{sup}}) - n(-\eta_i^{\mathrm{norm}} - \eta_i^{\mathrm{sup}}))\,\langle i^a|s^c\rangle \\
&= \frac{1}{2}\delta_{rs} - \langle r^c|i^a\rangle \frac{D^a_{ii}}{2(\eta_i^{\mathrm{norm}} + \eta_i^{\mathrm{sup}})}\tanh\left(\frac{\eta_i}{2k_BT}\right)\langle i^a|s^c\rangle,
\end{aligned} \tag{1.92}$$

where

$$n(\eta_i^a) = \frac{1}{1 + e^{\eta_i^a/kBT}} \tag{1.93}$$

and

$$\begin{aligned}
&n(\eta) + n(-\eta) = 1, \\
&n(\eta) - n(-\eta) = -\tanh\left(\frac{\eta}{2k_BT}\right).
\end{aligned}$$

In the estimation of matrix elements, the chemical potential which has been disregarded up to now is taken into account. Namely, the Hamiltonian has an additive term $-\mu\bar{\mathbf{a}}_r\mathbf{a}_r$, which causes

$$\eta_i^a \to \eta_i^a - \mu < 0, \quad \text{while } -\eta_i^a \to -(\eta_i^a - \mu) > 0.$$

The mean-field potentials are carefully treated. In modes with ↑ and ↓, we have the nonvanishing single-particle parts, $h^{\uparrow}_{rs}\delta_{rs}$ and $h^{\downarrow}_{rs}\delta_{rs}$, which are usually negative. However, for superconducting modes, $h^{\pm}_{rs}=0$, and the chemical potential is lost for the same reason. The latter may be closely related to the fact that the number of particles is not conserved in a superconductor. These circumstances are crucial for the superconducting mode.

1.5.1 *Unrestricted Hartree–Fock (HF)*

Let us review the SCF procedure. We now discuss the ordinary many-electron system. As an example, the propagator with the up spin, Eq. (1.89), is

$$G^{\uparrow}_{rs}(0^{-}) = \frac{1}{2}\langle r^{\uparrow}|s^{\uparrow}\rangle - \langle r^{\uparrow}|i^{a}\rangle \frac{D^{a}_{ii}}{2(\eta^{\mathrm{norm}}_{i}+\eta^{\mathrm{sup}}_{i})}\tanh\left(\frac{\eta^{a}_{i}}{2k_{B}T}\right)\langle i^{a}|s^{\uparrow}\rangle, \tag{1.94}$$

where $\langle r^{\uparrow}|s^{\uparrow}\rangle$ is the overlap integral between the sites r and s and approximately vanishes, and

$$D^{a}_{ii} = h^{\uparrow}_{ii} + v^{\uparrow a}_{ii;tu}G^{a}_{tu} - v^{\uparrow\uparrow}_{ii;tu}G^{\uparrow}_{tu}. \qquad (a:\uparrow,\downarrow) \tag{1.95}$$

Note that

$$\tan\mathrm{h}\left(\frac{\eta^{a}_{i}}{2k_{B}T}\right) < 0, \text{ since } \eta^{a}_{i} < 0. \tag{1.96}$$

Look at the potential of the mode ↑:

$$D^{\uparrow}(x) = h^{\uparrow}(x) + \int dx' v(x-x')\rho^{b}_{tu}(x')\sigma^{b}\langle \bar{\mathbf{a}}_{\mathbf{t}}\mathbf{a}_{\mathbf{t}}\rangle. \tag{1.97}$$

In this case, there is $h^{\uparrow}(x)$, whose matrix element should be negative, so that even if the matrix elements of the second terms are positive, the (r,s) matrix element of $D^{\uparrow}(x)$ is probably negative. This is usually the case in atoms, molecules and solids. In evaluating $D^{\uparrow}(x)$, the propagators (wave functions) of all other modes are required. In this respect, Eq. (1.94) is the self-consistent relation between propagators. Usually, the self-consistent relation between wave functions is given in a such a way that, at the beginning, the total energy is given by the potentials given in terms of tentatively approximated wave functions, and the new approximate wave functions in the next step are obtained by optimizing the total energy. This procedure is lacking in the present consideration.

1.5.2 *Gap equation for superconductivity*

In the case of superconductivity, since $\sigma^+(\sigma^-)$ is traceless, the first term of Eq. (1.92) vanishes, and also $h^+ = 0$. Now Eq. (1.92) can be read as

$$G^+_{rs}(0^-) = -\left\{\langle r^+|i^+\rangle \frac{v^{+-}_{ii;tu}\langle \bar{\mathbf{a}}_\mathbf{t}\mathbf{a}_\mathbf{u}\rangle^-)}{2(\eta^{\text{norm}}_i + \eta^{\text{sup}}_i)}\langle i^+|s^+\rangle\right\}\tanh\left(\frac{\eta^+_i}{2k_BT}\right)$$

$$= -\left\{\langle r^+|i^+\rangle \frac{v^{+-}_{ii;tu}G^-_{tu}}{2(\eta^{\text{norm}}_i + \eta^{\text{sup}}_i)}\langle i^+|s^+\rangle\right\}\tanh\left(\frac{\eta^+_i}{2k_BT}\right). \quad (1.98)$$

This complicated equation gives the relation between G^+_{rs} and G^-_{rs}, both referring to the superconductivity, and is called the gap equation. A few points should be presented. While selecting the superconducting mode, we used

$$\text{Tr}(\sigma^+\sigma^-) = \text{Tr}\begin{pmatrix}0 & 1\\ 0 & 0\end{pmatrix}\begin{pmatrix}0 & 0\\ 1 & 0\end{pmatrix} = \text{Tr}\begin{pmatrix}1 & 0\\ 0 & 0\end{pmatrix} = 1, \quad (1.99)$$

so that

$$\text{Tr}(\sigma^+ v^{+a}\sigma^a) = v^{+-}_{ii;tu}. \quad (1.100)$$

The relation (1.98) yields

$$-\left\{\langle r^+|i^+\rangle \frac{v^{+-}_{ii;tu}}{2(\eta^{\text{norm}}_i + \eta^{\text{sup}}_i)}\langle i^+|s^+\rangle\right\} > 0. \quad (1.101)$$

As has been mentioned previously, we have no chemical potential in the superconducting state, so that η^+_i is positive, the same as $v^{+-}_{ii;tu}$ is. Therefore, it is required that $\langle r^+|i^+\rangle\langle i^+|s^+\rangle$ be negative so that Eq. (1.101) can hold. This is really possible, as will be mentioned below. Thus, we are not at all concerned with the electron–phonon coupling. Let us perform the successive approximations as

$$\langle r^+|i^+\rangle v^{+-}_{ii;tu}\langle i^+|s^+\rangle \tan\text{h}(\eta^+_i/2k_BT) \approx \sum_i^{\text{occ}}\langle r^+|i^+\rangle v^{+-}_{ii;tu}\langle i^+|s^+\rangle \quad (T\to 0)$$

$$= q_{rs}v^{+-}_{ii;tu} \quad (<0). \quad (1.102)$$

Here, $v^{+-}_{ii;tu}$ is the electron–electron interaction between two electron densities and is certainly positive (repulsive). However, the bond order is not necessarily so, but $q_{14} < 0$ in the following example. The last relation was usually assumed at the beginning of the superconductivity theory.

We thus obtain the condition for the superconducting state to appear; it is purely electronic and is apart from the electron–phonon coupling mechanism. Actually, for the chain molecule of four carbon atoms, called butadiene, the matrix $q_{rs}(r,s) = 1 - 4$ is

$$\{q_{rs}\} = \begin{pmatrix} 1.000 & 0.894 & 0.000 & -0.447 \\ & 1.000 & 0.447 & 0.000 \\ & & 1.000 & 0.894 \\ & & & 1.000 \end{pmatrix}. \tag{1.103}$$

We can clearly see that

$$v^{+-}_{11;14} q_{14} < 0. \tag{1.104}$$

1.6 Illustrative Example, Critical Temperature

The gap equation (1.98) is, in appearance, considerably different from the usual one. We rewrite this equation in a form similar to the usual one. To this end, we adopt, as an example, a polyacene high polymer. Benzene, naphthalene, anthracene, etc. are a series of polyacene, shown in Fig 1.1. Here, the unit cell which is the butadiene molecule is in the dotted rectangle numbered by n. The interactions t_1 and t_2 are given for the corresponding bonds.

1.6.1 *Bond alternation*

At the beginning, we discuss the bond alternation or the Peierls instability of these molecules. The infinite chain of acetylene, the so-called polyacetylene, has the bond alternation, i.e., the long and short bonds do not lose their memories in the limit where an infinite chain has been formed. This is popular with chemists,[19] but physicists call it Peierls distortion.[20] The bond alternation causes the gap between the conduction and valence bands. It has

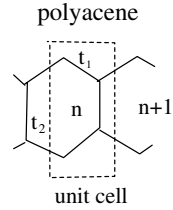

Fig. 1.1 Polyacene.

been said that this discontinuity prevents the superconducting phase from arising. However, this is an old-fashioned assertion and now seems sceptical.

In the Hückel theory, the interaction matrix elements are put as t_1 for the shorter bond and t_2 for the longer bond:

$$H^0 = -t_1(a_{2n}^+ a_{1n} + a_{1n}^+ a_{2n}) - t_2(a_{1n+1}^+ a_{2n} + a_{2n}^+ a_{n+1}), \tag{1.105}$$

where we consider the neighboring unit cells numbered n and $n+1$, and each cell has two kinds of bonds. The transfer integrals are parametrized as

$$t_1 = t - \delta, \quad t_2 = t + \delta \quad \left(\delta > 0, \frac{\delta}{t} \ll 1\right), \tag{1.106}$$

and then the Hamiltonian is easily diagonalized as

$$\epsilon_k = \pm[t^2(1+\cos k) + \delta^2(1-\cos k)]^{1/2}, \tag{1.107}$$

where $+$ and $-$ correspond to the conduction and valence bands, respectively. We are interested in the features at the zone boundary, $k = \pi$:

$$\epsilon_\pi^c = 2\delta, \quad \epsilon_\pi^v = -2\delta. \tag{1.108}$$

Here, the superscripts c and v indicate the conduction and valence bands, respectively. When $\delta \neq 0$, certainly we have the gap, and if $\delta = 0$, the two bands continuously join into a single band called the half-filled band.

Next, we turn to the polyacene, whose unit cell is the butadiene molecule. In this case, we obtain four bands:

$$\begin{aligned} \epsilon_k^{c'} &= \frac{1}{2}[t_3 + (t_3^2 + 4|\tilde{t}_k|^2)^{1/2}] = -\epsilon_k^v, \\ \epsilon_k^c &= \frac{1}{2}[-t_3 + (t_3^2 + 4|\tilde{t}_k|^2)^{1/2}] = -\epsilon_k^v, \end{aligned} \tag{1.109}$$

where

$$\tilde{t}_k = t_1 + t_2 e^{ik}. \tag{1.110}$$

The usual pairing property in alternant hydrocarbons is also seen in this case. Employing the parametrization (1.106) gives, at $k = \pi$,

$$\epsilon_\pi^v = \frac{1}{2}[t_3 + (t_3^2 + 16\delta^2)^{1/2}] \approx 4t_3 \left(\frac{\delta}{t_1}\right)^2. \tag{1.111}$$

When $\delta = 0$ (without bond alternation), we have

$$\epsilon_k^v = \frac{1}{2}\{t_3 - [t_3^2 + 8t^2(1+\cos k)]^{1/2}\}. \tag{1.112}$$

Consider single-particle states. If $\delta = 0$ and $k = \pi$ we have, from Eq. (1.110), $\tilde{t} = 0$, so that the amplitudes at sites 2 and 5 vanish. Therefore, when $\delta = 0$, we get at $k = \pi$

$$\begin{aligned} |\psi_k^v\rangle &= \frac{1}{2}(a_{1k}^+ - a_{4k}^+)|0\rangle, \\ |\psi_k^c\rangle &= \frac{1}{2}(a_{1k}^+ + a_{4k}^+)|0\rangle. \end{aligned} \tag{1.113}$$

It is seen that $|\psi_k^v\rangle$ is antisymmetric about the C_{2v} symmetry axis, and $|\psi_k^v\rangle$ is symmetric. Thus, v and c bands are not continuous at $k = \pi$.

1.6.2 *Deformation energy*

For these systems, let us study whether the bond alternation is energetically favorable or not. We assume that the energy gain due to the bond alternation mainly contributes to the highest valence band energy, ϵ_k^v.

The case of polyacetylene. The energy gain ΔE is

$$\Delta E = \int_0^{2\pi} \frac{dk}{2\pi}(\epsilon_k^v - \epsilon_k^v(0)), \tag{1.114}$$

where the second term refers to the case without bond alternation ($\delta = 0$). In Eq. (1.107), we shift the integration origin from 0 to π, then approximate

$$\cos k = \cos(\pi + p) \approx -1 + \frac{p^2}{2}.$$

For small p, we obtain

$$\begin{aligned}\Delta E &= -\int_0^{2\pi} \frac{dk}{2\pi}\left\{\sqrt{(tp)^2 + 4\delta^2} - tp\right\} \\ &= \frac{2t}{\pi}\left(\frac{\delta}{t}\right)^2 \ln\left(\frac{\delta}{\pi t}\right) \quad (<0).\end{aligned} \tag{1.115}$$

For polyacene, similar treatment of ϵ_k^v of Eq. (1.109) leads to

$$\epsilon_k^v = \frac{1}{2}\left(1 - \left\{1 + 16\left(\frac{\delta}{t}\right)^2 + 4p^2\left[1 - \left(\frac{\delta}{t}\right)^2\right]\right\}^{1/2}\right), \tag{1.116}$$

and then the deformation energy becomes

$$\Delta E = t\left(\frac{\delta}{t}\right)^2\left(\frac{\pi}{4} - \frac{2}{\pi}\ln 4\pi\right) \approx -0.83t\left(\frac{\delta}{t}\right)^2. \tag{1.117}$$

The bond alternation looks favorable for both cases. However, when the effect of the σ bond is taken into account, this almost cancels out the stabilization energy of the π system in the case of polyacene. On the other hand, this is not the case for polyacetylene due to the singular term in the relation (1.117).

Therefore, in what follows, by concentrating on polyacene, we are free from the bond alternation.

1.6.3 *Polyacene, gap equation, critical temperature*

The unit cell of polyacene is a butadiene molecule composed of four $2p\pi$ carbon atoms. The Hamiltonian in the tight-binding approximation is given as

$$\begin{aligned} H^0 = {} & t(a_{n1}^+ a_{n2} + a_{n2}^+ a_{n3} + a_{n4}^+ a_{n3}^+ + \text{H.c.}) \\ & + t(a_{n+1,1}^+ a_{n2} + a_{n+1,4}^+ a_{n3}^+ + \text{H.c.}), \end{aligned} \tag{1.118}$$

where the second line connects the unit cells n and $n+1$.[21]

The band structure of levels and the linear combination of atomic orbitals (LCAO) coefficients U are

$$\begin{aligned} \epsilon_1(k) &= \frac{t}{2}\{1 + s(k)\}, \\ \epsilon_2(k) &= -\frac{t}{2}\{1 - s(k)\}, \\ \epsilon_3(k) &= \frac{t}{2}\{1 - s(k)\}, \\ \epsilon_4(k) &= -\frac{t}{2}\{1 + s(k)\}, \end{aligned} \tag{1.119}$$

with

$$s(k) = \sqrt{9 + 8\cos\, k}, \tag{1.120}$$

$$U = \begin{pmatrix} N_4 & N_3 & N_2 & N_1 \\ -N_4\epsilon_4/\tilde{t}_k & -N_3\epsilon_3/\tilde{t}_k & -N_2\epsilon_2/\tilde{t}_k & -N_1\epsilon_1/\tilde{t}_k \\ N_4\epsilon_4/\tilde{t}_k & -N_3\epsilon_3/\tilde{t}_k & N_2\epsilon_2/\tilde{t}_k & -N_1\epsilon_1/\tilde{t}_k \\ -N_4 & N_3 & -N_2 & N_1 \end{pmatrix}, \tag{1.121}$$

where, for example,

$$N_1^2 = \frac{|\tilde{t}_k|^2}{2(|\tilde{t}_k|^2 + \epsilon_1^2)}, \quad \frac{1}{\tilde{t}_k} = \frac{e^{ik/2}}{2t\cos(k/2)}. \tag{1.122}$$

At this stage, we have completed, in principle, the usual many-electron problem. The mean-field approximation makes the interaction problem a one-particle problem even though the SCF treatment is required at each step. In other words, from the viewpoint of the Hückel theory, the spin-diagonal parts provide the answer. On the other hand, the spin-off diagonal part, which means less in the case without electron–electron interactions, is responsible for the superconductivity.

Up to the previous chapter, the problem had been investigated in the site representation. That is to say, the system is considered to be composed

of N sites. However, the real substance is formed from unit cells, so that the system is a repetition of the unit cell. The usual band theory of polyacene has thus been completed at this stage.

We turn to the onset of superconductivity. In this case, the single-particle approach is almost meaningless, but the pair state — say, the wave function of a Cooper pair — should be investigated. For this purpose, the Green function of a Cooper pair is most preferable. The gap equation (1.98) is nothing but the SCF equation for a Cooper pair.

The electronic structure of the single butadiene molecule referring to $k = 0$ is suggestive. Let the total number of sites of high polymer polyacene be N. The number of sites in the unit cell is four. Then $N = 4n$, with the number of unit cells n. The numbers 1–4 are the band indices; then we have the chemical potential between the $2n$ level and $3n$ level. The Cooper pair should be the hole pair of the $2n$ level indicated by mode $(-)$ or the particle pair of the $3n$ level. The discussion is confined to these levels in solid-state physics, even if the interaction with other bands is taken into account.

The $2n$ and $2n + 1$ levels are called highest occupied molecular orbital (HOMO) and lowest unoccupied molecular orbital (LUMO). These features and behaviors are not so far or qualitatively the same as those for $k = 0$.

The electronic structure of a single butadiene molecule is suggestive. The levels and the bond orders are (the unit $= t$)

$$\begin{array}{l|r} \epsilon_1 & -1.618 \\ \epsilon_2 & -0.618 \\ \epsilon_3 & 0.618 \\ \epsilon_4 & 1.618. \end{array} \tag{1.123}$$

Here, ϵ_1 and ϵ_2 are occupied (valence) levels, while ϵ_3 and ϵ_4 are unoccupied (conduction) ones. Let the probability amplitude, with which the electron on level i is found at the site r, be $\langle r|i\rangle$, then the bond order q_{rs} is defined as (at the zero temperature)

$$q_{rs} = \sum_{i}^{\text{occ}} \langle r|i\rangle\langle i|s\rangle, \tag{1.124}$$

where the summation includes the spin state. In the determination of the attractive electron–electron interaction, the bond order is of crucial importance.

The bond orders are

Site				
1	1.000	0.894	0.000	−0.447
2	0.894	1.000	0.447	0.000
3	0.000	0.447	1.000	0.894
4	−0.447	0.000	0.894	1.000.

(1.125)

We indicate the negative value of q_{14}. In solid-state physics, the discussion is concentrated on the highest valence band or the lowest conduction band. In the quantum-chemical language, the partial bond orders referring only to level 2, q_{rs}^{H}, which seem not so far from those with k, are listed as

Site				
1	0.362	0.224	−0.224	−0.362
2	0.224	0.138	−0.138	−0.224
3	−0.224	−0.138	0.138	0.224
4	−0.362	−0.224	0.224	0.362.

(1.126)

We indicate the negative value of q_{14}^{H}.

If we want to look at the band structure, such as q_{rs}^{H}, it is multiplied by the third column of Eq. (1.121).

Based on these results, we may perform successive approximations or simplifications:

(1) The denominator of Eq. (1.98) is the sum of the ordinary Hartree–Fock energy and that of the superconducting state, and the latter is

$$\eta_i^{\mathrm{sup}} = -v_{ii;tu}^{+-} G_{tu}^{-}. \tag{1.127}$$

The total energy is obtained by summing

$$\eta_i = \eta_i^{\mathrm{norm}} + \eta_i^{\mathrm{sup}} \tag{1.128}$$

with respect to the chemical potential.

(2) Each level with η_i has really a band structure and is then written as $\eta_{i;k}$, by stressing the band structure by k with the band index i. Then i is put to be the highest occupied level, and the integration over k is carried out. The bond orders thus obtained are approximated by the partial bond orders q_{rs}^{H}.

(3) The electron–electron interaction, which is effectively negative due to the chemical structure of species, can be simply written for $g < 0$:

$$g = q_{rs} v_{rs;tu}^{-+}. \tag{1.129}$$

(4) The energy interval establishing the superconductivity in the BCS theory is related to the electron–phonon interaction, $\hbar\omega_D$ (Debye frequency). In the present theory, it is replaced by the band width nearly equal to $|g|$.

(5) Assuming that

$$G^+_{s\uparrow,r\downarrow}(0^-) = G^+_{t\uparrow,u\downarrow}(0^-) \tag{1.130}$$

in Eq. (1.98), we have

$$1 = gN(0)\int_0^{|g|} \frac{d\xi}{\xi + \eta^{\sup}} \tanh\left(\frac{\xi + \eta^{\sup}}{2k_BT}\right), \tag{1.131}$$

where $\xi = \eta^{\text{norm}}$. The critical temperature T_C is determined by the condition that $\eta^{\sup}$ vanishes at this temperature. The integration in Eq. (1.131) is carried out as usual. Approximating

$$\int \frac{d^3k}{(2\pi)^3} = N(0)\int d\xi$$

gives

$$\begin{aligned}\int_0^{|g|} \frac{d\xi}{\xi} \tanh\left(\frac{\xi}{2k_BT}\right) &= \int_0^Z \frac{dz}{z}\tanh\, z, \quad z = \frac{|g|}{2k_BT} \\ &= [\ln z\, \tanh\, z]_0^Z - \int_0^\infty dz \ln z\, \operatorname{sech}^2 z, \end{aligned} \tag{1.132}$$

where the upper limit in the second integration is replaced by ∞, which makes it integrable[15]:

$$\int_0^\infty dz \ln z\, \operatorname{sec\,h}^2 z = -\ln\frac{4e^\gamma}{\pi}; \quad \gamma \text{ is the Euler constant.}$$

A simple rearrangement of the result gives

$$k_BT_C = \frac{2e^\gamma}{\pi}|g|e^{-1/N(0)g} \sim 1.13|g|e^{-/N(0)g}. \tag{1.133}$$

The result is entirely the same as the current one. However, since it is probable that

$$\frac{|g|}{k_BT} \sim 100, \tag{1.134}$$

the critical temperature is, at most, enhanced by this value, even though it is considerably reduced by the factor $e^{-1/N(0)g}$.

1.6.4 *Conclusion*

As has been presented, superconductivity is not a too-complicated phenomenon. If we employ the spinor representation, superconductivity is

described in parallel with the normal electronic processes. If we find, in the copper oxide complex, the four-site unit as a butadiene molecule, it might be the origin of the superconductivity of this material. We think that it is not so difficult a problem for quantum chemists.

1.7 Linear Response Magnetic Resonance in Normal and Superconducting Species; Spin–lattice Relaxation Time

1.7.1 *Introduction*

The theory of linear response is one of the main topics in solid-state physics, and its application to superconductivity is also a fundamental problem. Perhaps the most important problem is the Meissner effect. However, we are now interested in the magnetic resonance, whose main theme should concern the relaxation time. Let us discuss the spin–lattice relaxation time T_1 in the nuclear magnetic resonance. An elegant theory has been provided by Kubo and Tomita,[22] and revised by us with the temperature Green function.[23]

The spin–lattice relaxation time T_1 increases remarkably in a superconductor just below the critical temperature. This is explained by the BCS pairing theory and is said to be its brilliant triumph.[3,24,25] The external perturbation acting on the electron is written as

$$H' = B_{k\sigma,k'\sigma'} c^+_{k\sigma} c_{k'\sigma'}, \tag{1.135}$$

where $c^+_{k\sigma}$, $c_{k\sigma}$, etc. are the creation and annihilation operators of an electron in the normal phase, and $B_{k\sigma,k'\sigma'}$ is the matrix element of the perturbation operator between the ordinary one-electron states in the normal phase. The problem is as follows: If we rewrite it in terms of operators of a quasiparticle in the superconducting phase, what will arise?

The time reversal to the above, $B_{-k'-\sigma',-k-\sigma}$, has the same absolute value, but the phase is the same or the reverse.

It is possible to classify as follows:

$1_\pm$. The spin flip-flop does not arise:

$$B_{k\sigma,k'\sigma}(c^+_{k\sigma} c_{k'\sigma} \pm c^+_{-k'-\sigma} c_{-k-\sigma}).$$

$2_\pm$. The spin flip-flop does arise:

$$B_{k\sigma,k'-\sigma}(c^+_{k\sigma} c_{k'-\sigma} \pm c^+_{-k'\sigma} c_{-k-\sigma}).$$

As seen above, the theory implicitly assumes that the system is a perfect crystal and is described by the single wave vector k. The positive and negative signs of k indicate waves propagating from the vertex or off the vertex. Before entering into the discussion about the relaxation time of the magnetic resonance, we briefly review the Bogoliubov theory.[3,10,15] The Bogoliubov transformation defines a quasiparticle responsible for the superconductivity as

$$\begin{pmatrix} \gamma_{k\uparrow} \\ \gamma^+_{-k\downarrow} \end{pmatrix} = \begin{pmatrix} u_k & -v_k \\ v_k & u_k \end{pmatrix} \begin{pmatrix} c_{k\uparrow} \\ c^+_{-k\downarrow} \end{pmatrix} \tag{1.136}$$

with

$$u_k^2 - v_k^2 = 1.$$

The spirit of the Bogoliubov transformation is to mix the operators $c_{k\uparrow}$ and $c^+_{-k\downarrow}$, which are different in spin (as to the wave number, this mixing is not so serious) and not mixed in the normal situation. The quasiparticle yields the new ground state near the chemical potential. The stabilization energy thus obtained is called the gap energy, Δ_k. What we have done in Sec. 1.3 is a substantial understanding of this reason. However, if we want to make the $\pm k$ distinction meaningful, it is natural to adopt the four-component spinor — say, the extended Nambu spinor (perhaps spurious).[26] For ordinary states,

$$\mathbf{c}_k^+ = \left(c^+_{k\uparrow}\ c_{-k\downarrow}\ c_{-k\uparrow}\ c^+_{k\downarrow}\right), \quad \mathbf{c}_k = \begin{pmatrix} c_{k\uparrow} \\ c^+_{-k\downarrow} \\ c^+_{-k\uparrow} \\ c_{k\downarrow} \end{pmatrix}, \tag{1.137}$$

and, for the superconducting state,

$$\gamma_k^+ = \left(\gamma^+_{k\uparrow}\ \gamma_{-k\downarrow}\ \gamma_{-k\uparrow}\ \gamma^+_{k\downarrow}\right), \quad \gamma_k = \begin{pmatrix} \gamma_{k\uparrow} \\ \gamma^+_{-k\downarrow} \\ \gamma^+_{-k\uparrow} \\ \gamma_{k\downarrow} \end{pmatrix}. \tag{1.138}$$

These are connected with each other by the Bogoliubov transformation as

$$\gamma_k = U_k \mathbf{c}_k, \quad \gamma_k^+ = \mathbf{c}_k U_k^+, \tag{1.139}$$

where

$$U_k = \begin{pmatrix} \mathbf{u}_k & 0 \\ 0 & \mathbf{u}_k^+ \end{pmatrix}, \quad \text{with } \mathbf{u}_k = \begin{pmatrix} u_k & v_k \\ -v_k & u_k^+ \end{pmatrix}. \tag{1.140}$$

Careful manipulation is instructive.

Case 1_+:

$$(c^+_{k\sigma}c_{k'\sigma} + c^+_{-k'-\sigma}c_{-k-\sigma}) = \mathbf{c}^+_k \boldsymbol{\Sigma}^3 \mathbf{c}_{k'} = \boldsymbol{\gamma}^+_k U_k \boldsymbol{\Sigma}^3 U^+_{k'} \boldsymbol{\gamma}_{k'}, \tag{1.141}$$

where

$$\boldsymbol{\Sigma}^3 = \begin{pmatrix} \sigma^3 & \\ & -\sigma^3 \end{pmatrix}. \tag{1.142}$$

This is the 4×4 matrix manipulation; however, it is enough to note the upper half of the result.

The upper half of Eq. (1.139) is

$$\begin{aligned} &(c^+_{k\uparrow} \quad c_{-k\downarrow}) \begin{pmatrix} 1 & 0 \\ 0 & -1 \end{pmatrix} \begin{pmatrix} c_{k'\uparrow} \\ c^+_{-k'\downarrow} \end{pmatrix} \\ &\quad = (\gamma^+_{k\uparrow} \quad \gamma_{-k\downarrow}) \begin{pmatrix} u & v \\ -v & u \end{pmatrix} \begin{pmatrix} 1 & 0 \\ 0 & -1 \end{pmatrix} \begin{pmatrix} u' & -v' \\ v' & u' \end{pmatrix} \begin{pmatrix} \gamma_{k'\uparrow} \\ \gamma^+_{-k'\downarrow} \end{pmatrix} \\ &\quad = (\gamma^+_{k\uparrow} \quad \gamma_{-k\downarrow}) \begin{pmatrix} uu' - vv' & -uv' - vu' \\ -vu' - uv' & vv' - uu' \end{pmatrix} \begin{pmatrix} \gamma_{k'\uparrow} \\ \gamma^+_{-k'\downarrow} \end{pmatrix}, \end{aligned} \tag{1.143}$$

where u and v are the abbreviations of u_k and v_k, respectively, while u' and v' are those of $u_{k'}$ and $v_{k'}$.

Case 1_-:

$$\sum_\sigma (c^+_{k\sigma}c_{k'\sigma} - c^+_{-k'-\sigma}c_{-k-\sigma}) = \mathbf{c}^+_k \mathbf{1} \mathbf{c}_{k'} = \boldsymbol{\gamma}^+_k U_k \mathbf{1} U^+_{k'} \boldsymbol{\gamma}_{k'}. \tag{1.144}$$

The upper half of the above is

$$\begin{pmatrix} \gamma^+_{k\uparrow} & \gamma_{-k\downarrow} \end{pmatrix} \begin{pmatrix} uu' + vv' & -uv' + vu' \\ -vu' + uv' & vv' + uu' \end{pmatrix} \begin{pmatrix} \gamma_{k'\uparrow} \\ \gamma^+_{-k'\downarrow} \end{pmatrix}. \tag{1.145}$$

As is shown clearly, the original term is transformed in the quasiparticle representation into a combination of the scattering term with the diagonal element in the $\mathbf{u}_k$ matrix and the creation or annihilation of a pair with the off-diagonal element of $\mathbf{u}$. These matrix elements are called the coherent factors.

Let us turn to the case where the spin flip-flop is allowed.

Case 2_+:

$$c^+_{k\sigma}c_{k'-\sigma} + c^+_{-k'\sigma}c_{-k-\sigma} = \mathbf{c}^+_k \boldsymbol{\Sigma}^J \mathbf{c}_{k'} = \boldsymbol{\gamma}^+_k U_k \boldsymbol{\Sigma}^J U^+_{k'} \boldsymbol{\gamma}_{k'} \tag{1.146}$$

with

$$\boldsymbol{\Sigma}^J = \begin{pmatrix} & & & 1 \\ & & -1 & \\ & -1 & & \\ 1 & & & \end{pmatrix}. \tag{1.147}$$

This relation connects the left half of γ_k^+ and the lower half of $\gamma_{k'}$, by giving

$$\text{Eq. (1.147)} = \begin{pmatrix} \gamma_{k\uparrow}^+ & \gamma_{-k\downarrow} \end{pmatrix} \begin{pmatrix} uu' + vv' & uv' - vu' \\ -vu' + uv' & -vv' - uu' \end{pmatrix} \begin{pmatrix} \gamma_{-k'\uparrow} \\ \gamma_{k'\downarrow}^+ \end{pmatrix}. \tag{1.148}$$

Case 2_-:

$$c_{k\sigma}^+ c_{k'-\sigma} - c_{-k'\sigma}^+ c_{-k-\sigma} = \mathbf{c}_k^+ \mathbf{J} \mathbf{c}_{k'} = \gamma_k^+ U_k \mathbf{J} U_{k'}^+ \gamma_{k'}, \tag{1.149}$$

with

$$\mathbf{J} = \begin{pmatrix} & & & 1 \\ & & 1 & \\ & 1 & & \\ 1 & & & \end{pmatrix}. \tag{1.150}$$

This relation also connects the left half of γ_k^+ and the lower half of $\gamma_{k'}$, and we have

$$\text{Eq. (1.150)} = (\gamma_{k\uparrow}^+ \quad \gamma_{-k\downarrow}) \begin{pmatrix} uu' - vv' & uv' + vu' \\ -vu' - uv' & -vv' + uu' \end{pmatrix} \begin{pmatrix} \gamma_{-k'\uparrow} \\ \gamma_{k'\downarrow}^+ \end{pmatrix}. \tag{1.151}$$

Note that, at present, the scattering terms are off-diagonal, and the creation and annihilation terms are diagonal.

By the use of the relations[3, 10, 15]

$$\begin{gathered} u_k^2 = \frac{1}{2}\left(1 + \frac{\epsilon_k}{E_k}\right) \quad v_k^2 = \frac{1}{2}\left(1 - \frac{\epsilon_k}{E_k}\right), \\ E_k^2 = \epsilon_k^2 + \triangle_k^2 \end{gathered} \tag{1.152}$$

($\triangle_k$ is the gap energy), the coherent factors are expressed substantially as

$$\begin{aligned} 1_\pm: \quad & (uu' \mp vv')^2 = \frac{1}{2}\left(1 + \frac{\epsilon_k \epsilon_{k'}}{E_k E_{k'}} \mp \frac{\triangle_k \triangle_{k'}}{E_k E_{k'}}\right); \\ 2_\pm: \quad & (uv' \mp vu')^2 = \frac{1}{2}\left(1 \mp \frac{\triangle_k \triangle_{k'}}{E_k E_{k'}}\right). \end{aligned} \tag{1.153}$$

In case 1_+, we have the ultrasonic attenuation, while the electromagnetic interaction is in case 2_+ and the magnetic resonances are in case 2_-.

1.7.2 T_1 *in NMR*

A detailed analysis of the spin–lattice relaxation time T_1 in the nuclear magnetic resonance will be presented in the next section. Here, the results

are given briefly.

$$T_1 \sim \sum_{kk'} |B_{kk'}|^2 \frac{1}{2}\left(1 + \frac{\triangle_k \triangle_{k'}}{E_k E_{k'}}\right) n_k(1 - n_{k'})\delta(E_k - E_{k'} - \omega), \qquad (1.154)$$

where ω is the applied radio frequency. By converting the summation (explicitly shown) to the integration, and further by using the relation of state densities,

$$N(E)\,dE = N(\epsilon)\,d\epsilon, \quad \text{then}$$
$$\frac{N(E)}{N(\epsilon)} = \frac{d\epsilon}{dE} = \begin{cases} \dfrac{E}{(E^2 - \triangle^2)^{1/2}} & (E > \triangle), \\ 0 & (E < \triangle), \end{cases} \qquad (1.155)$$

we rewrite Eq. (1.152) for $\omega \ll \triangle$ as

$$T_1 \sim |B|^2 N^2(0) \int_{\triangle}^{\infty} \frac{1}{2}\left(1 + \frac{\triangle^2}{E(E+\omega)}\right) \times \frac{E(E+\omega)k_B T(-\partial n/\partial E)\,dE}{(E^2 - \triangle^2)^{1/2}[(E+\omega)^2 - \triangle^2]^{1/2}}, \qquad (1.156)$$

where the coupling constant and the state density are replaced by their suitable averages. This integral is divergent. Therefore, T_1 of a superconductor is strongly enhanced just below the critical temperature. This phenomenon was observed and explained by Slichter *et al.*[24,25] This was said to be one of the brilliant victories of the BCS theory. However, it has been found, in the recent experiments on the high-temperature superconductors or the copper-oxide superconductors, that the T_1 enhancement is lost. This phenomenon is considered deeply connected with the mechanism of the high-temperature superconductivity of these species, and it attracted the interest of many investigators.[27,29] However, as far as we know, the theory of magnetic resonance of a superconductor has been done almost entirely under the scheme mentioned in this introduction. Then it will be preferable to develop the theory of magnetic resonance in accordance with the sophisticated recent theory of superconductivity.

1.7.3 *Theory with Green's function*

Our idea is as follows: the algebra of electrons is related to their field operators. In the same way, we assume the field for nuclei. For example, the creation operator for a nucleus a^+_{KM} yields the nuclear motion with K and M, which are spatial and spin quantum numbers, respectively. The energy

spectrum of the propagator $\mathcal{G}_{KM}(\tau) = \langle\langle a_{KM}(\tau) a^{+}_{KM} \rangle\rangle$ gives the line shape of the magnetic resonance.

The nuclear propagator $\mathcal{G}_{KM}(\tau)$ sees the electron sea, followed by the electron excitation in the spin space. This gives the additional line width of the nuclear magnetic resonance. The phenomenon looks like the vacuum polarization in quantum electrodynamics. The self-energy part that has thus arisen in the nuclear energy is the source of the line shape of the nuclear magnetic resonance.[23]

The spin–lattice relaxation time of the nuclear spin I^z is given by the imaginary part of the magnetic susceptibility χ_{zz}, which is equal to $(\chi_{+-} + \chi_{-+})/2$ in the spatially homogeneous system. Here, $\pm$ correspond to $(I^x \pm iI^y)/2$, respectively. The ensemble average of a change, $\delta\langle I^+(t)\rangle$, is given by the linear response theory as

$$\delta\langle I^+(t)\rangle = i\int_{-\infty}^{t} dt' \mathrm{Tr}\{\rho_G [H^{\mathrm{ex}}(t'), I^+(t)]_-\}, \tag{1.157}$$

where ρ_G is the grand canonical statistical operator. However, the chemical potential is not given explicitly, unless otherwise stated. The rotating magnetic field causing the magnetic transition is, assuming a single mode for simplicity,

$$H^{\mathrm{ex}}(t) = H_R(I^+(t)e^{i\omega t} + I^-(t)e^{-i\omega t}). \tag{1.158}$$

As has been said, the spin–lattice relaxation arises from the interaction between the nuclear spin and the electron spin. In other words, the electron spins play the role of a lattice system.

$$H' = \hbar\gamma g\beta_B F(R, r)\mathbf{I}\cdot\mathbf{S}, \tag{1.159}$$

where $F(R, r)$ is a function of spatial coordinates of the nucleus, R, and that of the electron, r. The term γ is the gyromagnetic ratio of the nucleus, and g and β_B are the g factor and the Bohr magneton of the electron, respectively.

Now the second quantization of the above is carried out. First of all, the orthonormalized wave function describing the nuclear behavior, $|\xi_K(R)M\rangle$, is introduced as

$$\begin{aligned}(H_N + H_M)|\xi_K(R)M\rangle &= (\epsilon_K + M)|\xi_K(R), M\rangle \\ &= \epsilon_{KM}|\xi_K(R,)M\rangle,\end{aligned} \tag{1.160}$$

with

$$\epsilon_{KM} = \epsilon_K + M,$$

where H_N is the spatial part and H_M is the Zeeman part. Then we have

$$\begin{aligned} I^\alpha &\to \langle \xi_K(R) M | I^\alpha | \xi_{K'}(R) M' \rangle a^+_{KM} a_{K'M'} \\ &= \langle M | I^\alpha | M' \rangle a^+_{KM} a_{K'M'} \delta_{KK'}. \end{aligned} \tag{1.161}$$

A similar equation is given for electrons,

$$(H_S + H_m)\phi_k(r)|m\rangle = (\epsilon_k + m)|\phi_k(r), m\rangle = \epsilon_{km}|\phi_k(r), m\rangle, \tag{1.162}$$

where

$$\epsilon_{km} = \epsilon_k + m,$$

so that

$$\begin{aligned} H' \to\ & h\gamma g \beta_B \langle M | I^\beta | M' \rangle \langle m | S^\alpha | m' \rangle \langle \xi_K(R)\phi_k(r) | F(R,r) | \xi_{K'}(R)\phi_{k'}(r) \rangle \\ & \times (a^+_{KM} a_{K'M'})(c^+_{km} c_{k'm'}). \end{aligned} \tag{1.163}$$

If the nuclear motion is assumed to be that of a harmonic oscillator, a^+_{KM} and a_{KM} are the creation and annihilation operators of vibrational excitations. When the nuclei carry noninteger spins, these are considered to obey the Fermi statistics or satisfy the anticommutation relation

$$[a^+_{KM}, a_{K'M'}]_+ = \delta_{KK'}\delta_{MM'}. \tag{1.164}$$

However, as will be seen in the following, this selection of the statistics is not fatal for the theory. Needless to say, the operators for electrons satisfy the anticommutation relations.

The change of I^+ in Eq. (1.157) can be written, in the interaction representation, as (we retain the I^- term in Eq. (1.158))

$$\begin{aligned} \delta\langle I^+(t)\rangle &= i\gamma H_R \int_{-\infty}^{t} dt' e^{-i\omega t'} \\ &\quad \times \mathrm{Tr}\{\rho_G \langle M-1|I^-|M\rangle\langle M|I^+|M-1\rangle \\ &\quad \times [a^+_{K,M-1}(t')a_{K,M}(t'), a^+_{K,M}(t)a_{K,M-1}(t)]_-\} \\ &= -\gamma H_R \int_{-\infty}^{t} dt' e^{-i\omega t'} D_{K,M-1,M}(t'-t) \\ &= -\frac{1}{2}\gamma H_R e^{-i\omega t} \int_{-\infty}^{\infty} ds e^{-i\omega s} \sum_{KM} D_{K,M-1,M}(s) \\ &= -\frac{1}{2}\gamma H_R e^{-i\omega t} D_{K,M-1,M}(\omega). \end{aligned} \tag{1.165}$$

From this result, the magnetic susceptibility of the present system is

$$\chi_{+-}(\omega) = -\frac{\gamma}{2} D_{K,M-1,M}(\omega). \tag{1.166}$$

In the course of derivation, the matrix elements of spin operators are put to be equal to 1, and then the Tr operation is carried out. Here, $D_{K,M-1,M}(s)$ is a retarded Green function,

$$D_{K,M-1,M}(s) = -i\theta(s)\mathrm{Tr}\{\rho_G[a^+_{KM-1}(s)a_{KM}(s), a^+_{KM}a_{KM-1}]_-\}, \quad (1.167)$$

and $D_{K,M-1,M}(\omega)$ is its Fourier transform. Now our problem is to estimate this retarded function.

The retarded Green function is easily obtained by analytical continuation from the Matsubara function (or the temperature Green function with imaginary time τ) which is causal in τ,

$$\mathcal{D}_{K,M-1,M}(\tau) = -\mathrm{Tr}\left\{\rho_G T\tau\left[a^+_{K,M-1}(\tau)a_{K,M}(\tau)a^+_{K,M}a_{K,M-1}\right]\right\}, \quad (1.168)$$

for which the Feynman diagram analysis is available.[15]

1.7.4 *Noninteracting*

Here, we deal with the case without the spin–lattice interaction. It might be trivial; however, it seems instructive for the later investigation. By the use of the simplified notation, $\langle\cdots\rangle = \mathrm{Tr}(\rho_G\cdots)$, the Green function in this case is written as

$$\begin{aligned}\mathcal{D}^0_{K,M-1,M}(\tau) &= \langle T\tau[a^+_{KM-1}(\tau)a_{K,M}(\tau)a^+_{KM}a_{KM-1}]\rangle \\ &= \mathcal{G}^0_{KM}(\tau)\mathcal{G}^0_{KM-1}(-\tau),\end{aligned} \quad (1.169)$$

where

$$\mathcal{G}^0_{KM}(\tau) = -\langle T\tau[a_{KM}(\tau)a^+_{KM}]\rangle, \quad (1.170)$$

and the corresponding Fourier transform of Eq. (1.169) is

$$\mathcal{D}^0_{K,M-1,M}(\omega_n) = \frac{1}{\beta}\sum_{\upsilon_n}\mathcal{G}^0_{KM}(\upsilon_n)\mathcal{G}^0_{KM-1}(\upsilon_n - \omega_n), \quad (1.171)$$

where

$$\mathcal{G}^0_{KM}(\upsilon_n) = \frac{1}{i\upsilon_n - \epsilon_{KM}}. \quad (1.172)$$

Therefore,

$$\begin{aligned}\mathcal{D}^0_{K,M-1,M}(\omega_n) &= \frac{1}{\beta}\sum_{\upsilon_n}\frac{1}{i\upsilon_n - i\omega_n - \epsilon_{KM-1}}\cdot\frac{1}{i\upsilon_n - \epsilon_{KM}} \\ &= \frac{1}{\beta}\sum_{\upsilon_n}\left(\frac{1}{i\upsilon_n - i\omega_n - \epsilon_{KM-1}} - \frac{1}{i\upsilon_n - \epsilon_{KM}}\right)\frac{1}{i\omega_n + \epsilon_{KM-1} - \epsilon_{KM}} \\ &= [n(\epsilon_{KM-1}) - n(\epsilon_{KM})]\frac{1}{i\omega_n - \epsilon_{KI}},\end{aligned} \quad (1.173)$$

where

$$\epsilon_{KI} = \epsilon_{KM} - \epsilon_{KM-1},$$

and it is noted that ω_n is even, and that it does not matter in obtaining the particle number. The retarded Green function is obtained simply by replacing $i\omega_n$ with $\omega + i\eta$ (η is a positive infinitesimal). Thus, we obtain

$$\delta\langle I^+(t)\rangle = e^{-i\omega t} H_R (n(\epsilon_{K-}) - n(\epsilon_{K+})) \frac{1}{\omega - \epsilon_{KI} + i\eta}, \tag{1.174}$$

where the radio frequency stimulating the resonance is rewritten by ω^0. The magnetic susceptibility χ_{+-} thus becomes

$$\chi_{+-}(\omega) = \gamma (n(\epsilon_{K-}) - n(\epsilon_{K+})) \frac{1}{\omega - \epsilon_{KI} + i\eta},$$

$$\gamma = e^{-i\omega t} H_R, \tag{1.175}$$

whose imaginary part is

$$\chi''_{+-}(\omega) = -\pi\gamma (n(\epsilon_{K-}) - n(\epsilon_{K+}))\delta(\omega - \epsilon_{KI}). \tag{1.176}$$

This gives the sharp δ function-type energy spectrum. We have no line width or the relaxation time, and states are stationary.

1.7.5 *Interacting; normal*

In the interacting system, $\mathcal{G}^0$ in Eq. (1.169) has to be replaced by $\mathcal{G}$, including the interaction, which in the present case is the spin–spin interaction between nuclei and electrons, as has been given in Eq. (1.157),

$$\mathcal{D}_{KM-1,M}(\omega_n) = \frac{1}{\beta} \sum_{\upsilon_n} \mathcal{G}_{KM}(\upsilon_n) \mathcal{G}_{KM-1}(\upsilon_n - \omega_n), \tag{1.177}$$

where, for instance,

$$\mathcal{G}_{KM}(\upsilon_n) = [(\mathcal{G}^0_{KM}(\upsilon_n))^{-1} - \Sigma_{KM}(\omega)]^{-1}, \tag{1.178}$$

ω being the interaction energy.

Our procedure is as follows. The two Green functions with the self-energy part are evaluated. Combining them gives the retarded Green function $\mathcal{D}$ for estimating the magnetic susceptibility.

The most important (divergent) self-energy part of this self-energy is due to the ring diagram shown in Fig. 1.2. The problem is to examine how the

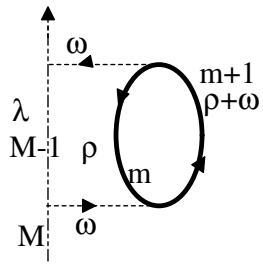

Fig. 1.2 Self-energy part $\mathcal{G}(\upsilon_n)$.

energy of the nucleus propagator (unequal-dashed line) is changed by the ring diagram of the electron (full line). That is to say,

$$\begin{aligned} \mathcal{G}(\upsilon_n)^{-1} &= \mathcal{G}(\upsilon_n)^0 + \Sigma(\omega), \\ \Sigma(\omega) &= -|K|^2 \mathcal{S}(\rho_n)\mathcal{S}(\rho_n + \omega), \end{aligned} \tag{1.179}$$

where $\mathcal{S}$ is the electron propagator, and the minus sign is due to the fermion loop. The self-energy part includes the coupling terms, where

$$\begin{aligned} |K|^2 = {} & \langle M|I^+|M-1\rangle\langle m-1|S^-|m\rangle|^2 \\ & \times |\langle \chi_K(R)\phi_k(r)|F(R,r)|\phi_{k'}(r)\chi_{K'}(R)\rangle|^2, \end{aligned} \tag{1.180}$$

and the minus sign is due to a Fermion loop. The ring diagram is calculated as follows:

$$\begin{aligned} & \mathcal{S}_{km}(\rho_n)\mathcal{S}_{km-1}(\rho_n + \omega) \\ & = \sum_{\rho_n} \frac{1}{i\rho_n - \epsilon_{km}} \cdot \frac{1}{i\rho_n + \omega - \epsilon_{km+1}} \\ & = \sum_{\rho_n} \left(\frac{1}{i\rho_n - \epsilon_{km}} - \frac{1}{i\rho_n + \omega - \epsilon_{km+1}} \right) \frac{1}{\omega - \epsilon_{km+1} + \epsilon_{km}} \\ & = (n(\epsilon_{km}) - n(\epsilon_{km+1})) \frac{1}{\omega - \epsilon_{km+1} + \epsilon_{km}}. \end{aligned} \tag{1.181}$$

The lattice (electron) gets ω from a nucleus to lift the electron spin from m to $m+1$, and at the other vertex, the inverse process occurs. This looks like the radiation process in the photochemistry. We thus have the self-energy part of $\mathcal{G}_{K;M-1,M}$,

$$\Sigma_{K;M-1,M}(\upsilon_n) = |K|^2 (n(\epsilon_{km}) - n(\epsilon_{km+1})) \frac{1}{\omega - \epsilon_{ks}}, \tag{1.182}$$

where

$$\epsilon_{ks} = \epsilon_{km+1} - \epsilon_{km}.$$

Another propagator $\mathcal{G}_{K;M}$, has the self-energy part $\Sigma_{K;M,M-1}(\upsilon_n)$. This is built by replacing $\rho_n + \omega$ with $\rho_n - \omega$ in Eq. (1.181).

$$\begin{aligned}\Sigma_{K;M,M-1}(\upsilon_n) &= |K|^2(n(\epsilon_{km}) - n(\epsilon_{km-1}))\frac{1}{\omega - \epsilon_{km-1} + \epsilon_{km}} \\ &= |K|^2(n(\epsilon_{km}) - n(\epsilon_{km-1}))\frac{1}{\omega - \epsilon_{ks}}, \\ &\approx |K|^2(n(\epsilon_{km+1}) - n(\epsilon_{km}))\frac{1}{\omega - \epsilon_{ks}}. \end{aligned} \tag{1.183}$$

We now turn to the evaluation of the propagator $\mathcal{D}_{K;M-1,M}(\tau)$:

$$\begin{aligned}&\mathcal{D}_{K;M-1,M}(\omega_n) \\ &= \frac{1}{\beta}\sum_{\upsilon_n}\mathcal{G}_{KM}(\upsilon_n)\mathcal{G}_{KM-1}(\upsilon_n - \omega_n) \\ &= \frac{1}{\beta}\sum_{\upsilon_n}(i\upsilon_n - \epsilon_{KM} - \Sigma_{KM-})^{-1}(i\upsilon_n - i\omega_n - \epsilon_{KM-1} - \Sigma_{K;M,M-1})^{-1} \\ &= \frac{1}{\beta}\sum_{\upsilon_n}\left\{\frac{1}{i\upsilon_n - i\omega_n - \epsilon_{KM-1} - \Sigma_{KM-1}} - \frac{1}{i\upsilon_n - \epsilon_{KM} - \Sigma_{KM}}\right\} \\ &\quad\times\left\{\frac{1}{i\omega_n - \epsilon_{KM-1} - \Sigma_{KM-1} + \epsilon_{KM} + \Sigma_{KM}}\right\} \\ &= (N(\epsilon_{KM}) - N(\epsilon_{KM-1}))\left\{\frac{1}{i\omega_n - \epsilon_{KI} + \Sigma_{KM} - \Sigma_{KM-1}}\right\}. \end{aligned} \tag{1.184}$$

Here,

$$\epsilon_{KI} = \epsilon_{KM} - \epsilon_{KM-1},$$

and the self-energy parts are disregarded in obtaining the particle density. We can see that the additional terms in the denominator modify the line shape.

If we put $i\omega_n \to \omega + i\eta$, we can obtain the retarded Green function, whose imaginary part gives the line shape:

$$\begin{aligned}D(\omega) &\sim \left\{\frac{1}{\omega + i\eta - \epsilon_{KI} + \Sigma_{KM} - \Sigma_{KM-1}}\right\} \\ &= \left\{\mathrm{P}\left(\frac{1}{\omega - -\Sigma_{KM-1}\epsilon_{KI}}\right) - i\pi\delta(\omega - \epsilon_{KI} + \Sigma_{KM} - \Sigma_{KM-1})\right\} \\ &= \frac{i(\mathrm{Im})}{(\mathrm{Re})^2 + (\mathrm{Im})^2} \quad \text{(at the resonance point).} \end{aligned} \tag{1.185}$$

The line shape is now changed from the δ function type to the Lorentz type, as expected.

1.8 Interacting; Superconductor

1.8.1 *The extended Nambu spinor*

Now, we investigate how the line shape obtained above is further modified in a superconductor. The electron propagators in the previous section are replaced by those in a superconductor. They have already been studied in Sec. 1.3 and are presented here in a new fashion adequate for the following investigation. As has been done by BCS, let us consider the attractive two-body potential g, which is assumed constant for simplicity, and further keep in mind the Cooper pair. The Hamiltonian

$$H_{\rm el} = \left\{ \epsilon_{k\alpha} c^+_{k\alpha} c_{k\alpha} + \frac{1}{2} g c^+_{k\alpha} c^+_{-k\beta} c_{-k\beta} c_{k\alpha} \right\}, \tag{1.186}$$

where $\epsilon_{k\alpha}$ is the orbital energy, includes the Zeeman energy in the present case.

Now we use the extended Nambu representation of Eq. (1.137),

$$\mathbf{c}_k = \begin{pmatrix} c_{k\alpha} \\ c^+_{-k\beta} \\ c^+_{-k\alpha} \\ c_{k\beta} \end{pmatrix}, \quad \mathbf{c}^+_k = \begin{pmatrix} c^+_{k\alpha} & c_{-k\beta} & c_{-k\alpha} & c^+_{k\beta} \end{pmatrix} \tag{1.187}$$

with the equal-time commutator:

$$[\mathbf{c}_k, \mathbf{c}^+_{k'}]_+ = \mathbf{1}\delta_{kk'}. \tag{1.188}$$

In these terms, the Hamiltonian is rewritten as

$$H_{\rm el} = \epsilon_k \mathbf{c}^+_k \Sigma^3 \mathbf{c}_k + \frac{1}{2} g (\mathbf{c}^+_k \Sigma^+ \mathbf{c}_k)(\mathbf{c}^+_{k'} \Sigma^- \mathbf{c}_{k'}), \tag{1.189}$$

where ϵ_k is the diagonal matrix of ϵ_γ:

$$\epsilon_k = \begin{pmatrix} \epsilon_{k\alpha} & & & \\ & \epsilon_{-k\beta} & & \\ & & \epsilon_{-k\alpha} & \\ & & & \epsilon_{k\beta} \end{pmatrix}. \tag{1.190}$$

Let us define

$$\Sigma^3 = \begin{pmatrix} \sigma^3 & 0 \\ 0 & -\sigma^3 \end{pmatrix}, \quad \Sigma^+ = \begin{pmatrix} \sigma^+ & 0 \\ 0 & -\sigma^- \end{pmatrix},$$

$$\Sigma^- = \begin{pmatrix} \sigma^- & 0 \\ 0 & -\sigma^+ \end{pmatrix}, \tag{1.191}$$

with

$$\sigma^3 = \begin{pmatrix} 1 & 0 \\ 0 & -1 \end{pmatrix}, \quad \sigma^1 = \begin{pmatrix} 0 & 1 \\ 1 & 0 \end{pmatrix}, \quad \sigma^2 = \begin{pmatrix} 0 & -i \\ i & 0 \end{pmatrix},$$

$$\sigma^+ = \frac{1}{2}(\sigma^1 + i\sigma^2), \quad \sigma^- = \frac{1}{2}(\sigma^1 - i\sigma^2). \tag{1.192}$$

As for the electron–electron interaction, only those for the Cooper pairs are selected; namely, Σ^+ selects a Cooper pair in the particle state, and Σ^- in the hole state.

1.8.2 *Green's function*

Here, the discussions done in Sec. 1.4 are repeated briefly. The above Hamiltonian is invariant under the scale transformation. Then we have a current conservation, especially the charge conservation in the static state (Noether's theorem). If we have any quantity which does not commute with this invariant charge, we can expect a phase transition (the Goldstone theorem).

The charge proportional to

$$\langle c^+_{k\gamma} c_{k\gamma} \rangle = \sum_{k>0} \langle \mathbf{c}^+_k \Sigma^3 \mathbf{c}_k \rangle \tag{1.193}$$

is invariant under the rotation about the Σ^3 axis in the space spanned by Σ^3, Σ^+ and Σ^-. Observing that

$$[\Sigma^3, \Sigma^\pm] = \pm 2\Sigma^\pm \tag{1.194}$$

suggests the phase transitions along the $\Sigma^\pm$ directions.

If we define

$$\bar{\mathbf{c}} = \mathbf{c}^+ \Sigma^3,$$

as has been done in Sec. 1.43, the discussions parallel to those there will be possible in the following. However, this is not employed in this case.

The phase transition cannot be achieved by the perturbational approach, but the effective Hamiltonian giving the phase transition should be included at the beginning. For example, the modified Hamiltonian

$$\begin{aligned} H^0 &= \mathbf{c}^+_k (\epsilon_k \Sigma^3 + \rho\Sigma^+ + \eta\Sigma^-)\mathbf{c}_k, \\ H^{\text{int}} &= \frac{1}{2} g \sum_{kk'} \{(\mathbf{c}^+_k \Sigma^+ \mathbf{c}_k) \cdot (\mathbf{c}^+_{k'} \Sigma^- \mathbf{c}_{k'}) - \mathbf{c}^+_k (\rho\Sigma^+ + \eta\Sigma^-)\mathbf{c}_k\}, \end{aligned} \tag{1.195}$$

where ρ and η are the so-called gap energies which are assumed to be independent of k for simplicity. Note that the Hamiltonian H^0 is already symmetry-broken. Here, we adopt a conventional method. In what follows, $H^{\rm int}$ is neglected, i.e. we start from the Green function due to the effective Hamiltonian and then take the interaction (1.158) into account. At this stage, we may expect the result that will be obtained in such a manner that the normal and superconducting states contribute additively.

The temperature Green function with the imaginary time τ is defined as

$$G^0_{kk'}(\tau) = -\langle T_\tau[\mathbf{c}_k(\tau)\mathbf{c}^+_{k'}]\rangle, \tag{1.196}$$

where $\langle\cdots\rangle = {\rm Tr}\{\rho_G\cdots\}$. The equation of motion of $G^0_{kk'}$ is

$$\begin{aligned}\partial_\tau G^0_{kk'}(\tau) &= -\partial_\tau[\theta(\tau)\langle\mathbf{c}_k(\tau)\mathbf{c}^+_{k'}(0)\rangle - \theta(-\tau)\langle\mathbf{c}^+_{k'}(0)\mathbf{c}_k(\tau)\rangle] \\ &= \delta(\tau)\langle[\mathbf{c}_k(\tau),\mathbf{c}^+_{k'}(0)]_+\rangle + \langle T\tau[\mathbf{c}_k(\tau),H^0]_-,\mathbf{c}^+_k(0)\rangle \\ &= \delta_{kk'} + (\epsilon_k\Sigma^3 + \rho\Sigma^+ + \eta\Sigma^-)G^0_{kk'} \end{aligned}\tag{1.197}$$

In the course of the above derivation, the commutator in Eq. (6.65) was used.

We make the Fourier transformation,

$$G^0_{kk'}(\tau) = \frac{1}{\beta}\sum_{\omega_n} e^{-i\omega_n\tau}G^0_{kk'}(\omega_n), \tag{1.198}$$

where $\beta = k_BT$ and k_B is the Boltzmann constant. Then the equation of motion becomes

$$(i\omega_n + \epsilon_k\Sigma^3 + \rho\Sigma^+ + \eta\Sigma^-)G^0_{kk'}(\omega_n) = \delta_{kk'}. \tag{1.199}$$

Namely,

$$\begin{aligned}G^0_{kk'}(\omega_n) &= \frac{1}{i\omega_n - \epsilon_k\Sigma^3 - \rho\Sigma^+ - \eta\Sigma^-} \\ &= \delta_{kk'}\left\{\frac{i\omega_n + \epsilon_k\Sigma^3 + \rho\Sigma^+ + \eta\Sigma^-}{(i\omega_n)^2 - E_k^2}\right\},\end{aligned}\tag{1.200}$$

where

$$E_k^2 = \epsilon_k^2 + \rho\eta. \tag{1.201}$$

1.8.3 *Spin dynamics*

The propagator in Eq. (1.200) is the 4×4 matrix. If we ignore ρ and η, this is reduced to the normal propagator. We have already tried this simple case.

Now we assume the terms responsible for the superconductivity as a perturbation. Namely ($\mathcal{S}$ is the electron propagator),

$$\mathcal{S}(\upsilon_n) = \frac{i\upsilon_n + \epsilon_k \Sigma^3 + \rho\Sigma^+ + \eta\Sigma^-}{(i\upsilon_n)^2 - E_k^2}$$
$$= \frac{i\upsilon_n + \epsilon_k \Sigma^3}{(i\upsilon_n)^2 + \epsilon_k^2} + \frac{\rho\Sigma^+ + \eta\Sigma^-}{(i\upsilon_n)^2 + \epsilon_k^2} + \cdots . \tag{1.202}$$

It is helpful to separate this relation into components and to manipulate each one individually. Noticing that

$$\sigma^0 + \sigma^3 = \sigma^\uparrow + \sigma^\downarrow,$$

we have, for example by operating $\sigma^\uparrow$ followed by Tr,

$$\mathcal{S}^\uparrow(\upsilon_n) = \frac{i\upsilon_n + \epsilon_k \Sigma^3 + \rho\Sigma^+ + \eta\Sigma^-}{(i\upsilon_n)^2 - E_k^2} = \frac{1}{i\upsilon_n - \epsilon_{k\uparrow}} + \frac{\rho + \eta}{(i\upsilon_n)^2 + \epsilon_k^2} + \cdots$$
$$= \frac{1}{i\upsilon_n - \epsilon_{k\uparrow}} + \frac{\rho + \eta}{2\epsilon_{k\uparrow}} \left(\frac{1}{i\upsilon_n - \epsilon_{k\uparrow}} - \frac{1}{i\upsilon_n + \epsilon_{k\uparrow}} \right) + \cdots \tag{1.203}$$

In order to get the self-energy part of the nuclear propagator, we have to evaluate

$$\Sigma_{k;M-1,M}(\omega) = K^2 \frac{1}{\beta} \sum_{\upsilon_n} \mathcal{S}(\upsilon_n)\mathcal{S}(\upsilon_n + \omega). \tag{1.204}$$

The first-order term has already been evaluated in Eq. (1.181). Then we have to carry out the complicated manipulation due to the second term of the last line in Eq. (1.203). However, the combinations other than those satisfying the resonance condition $\omega \sim \epsilon_{ks}$ [see Eq. (1.182)] should give a small effect which is to be neglected.

We then consider that the procedures of the previous section need not be repeated, and we are allowed to multiply the results there by the factor $(\rho + \eta)/2\epsilon_{k\uparrow}$ as the perturbing correction or the superconducting effect.

1.8.4 *Conclusion*

If we review the present investigations from the viewpoints of the line shape problem in the magnetic resonance, three cases are clearly distinguished. In the noninteracting case, the line shape is written in terms of the delta function. In the interacting case of the normal phase, it is presented by the Lorentz-like function, and in the superconducting phase it is further multiplied by a coherent factor; whereas the statistical factors referring to the nuclear states never change throughout.

For a superconductor, the present theory has almost nothing to give more than the current one has done. However, the theory is not merely to reproduce the experimental result, but to predict the mechanism hidden in observations, in such a way that the manipulations reveal step by step the working mechanism inside the matter. We might be satisfied with a slightly deeper understanding of the superconductivity.

Among various opinions we give, as an example, Scalpino's.[29] He pointed out three possibilities regarding the loss of the T_1 enhancement in the copper oxide superconductor:

(1) The d-wave single-particle density of states has logarithmic singularities, rather than the square-root singularity for the s wave gap.
(2) The coherent factor for the quasiparticle scattering vanishes for $k \sim (\pi, \pi)$ for a $d_{x^2-y^2}$ gap.
(3) The inelastic scattering acts to suppress the peak just as for an s wave.

Scalpino had the opinion that the theory of superconductivity is already so well furnished that other fundamental ideas beyond the original BCS one are almost needless, except for some smart equipment. As the phenomena observed in the copper oxide superconductor are rather qualitative and fairly clear-cut, the explanation for them must be simple. It is expected that a quantum-chemical speculation could make this possible.

Let us address scalpino's opinion. The divergent character of Eq. (1.154) seems a merely mathematical problem. The difference between Eq. (1.185) and that (which will be obtained) for the superconducting case is the coherent factor, (1.203). In the case of a BCS superconductor, it holds that $E_k \gg \rho$ so that the enhancement of the spin–lattice relaxation time T_1 is observed due to this factor, which leads to the superconductivity. However, in the case of a high-temperature superconductor, $\rho, \eta \sim E_k$, as has been seen in the previous chapter, we cannot observe the sharp onset of superconductivity. Then we miss the coherent effect.

There is presumably a simpler reason why the T_1 enhancement is not observed. In copper oxide, electrons responsible for superconductivity are probably the d electrons; then we have the vanishing interaction term if it is the Fermi contact term between a nucleus and an electron — say, $F(R, r) \sim \delta(R - r)$ in Eq. (1.159).

1.9 Ginzburg–Landau Theory from the BCS Hamiltonian

The macroscopic quantum theory of superconductivity has been given by Ginzburg and Landau.[9] This looks rather phenomenological; however, since

a microscopic justification has been provided by Gorkov and others,[16,30] it has a substantial foundation. We also reviewed the GL theory, in the introduction of Sec. 1.4, from the viewpoint of Landau's general theory of phase transitions. It is crucial that the Lagrangian of the system is written as the fourth-order function of the order parameter Ψ, which is the electron field. If the coefficients of the second- and fourth-order terms are suitably chosen, the new ground state shapes a champagne bottle, or a Mexican hat is built. If electrons moves on this flat route around the top, the derivative of the orbital vanishes or the kinetic energy vanishes, which implies that the wave function is rigid. We may say that the electron mass is effectively zero. We thus have the current only due to the vector potential, i.e. the diamagnetic current. This causes the Meissner effect.

The GL theory is quite useful for applications, since the microscopic theory by itself is too complicated for manipulating large-scale problems. If we can solve the GL equation for a real problem under an appropriate boundary condition, various information on this system can be obtained.[10] The macroscopic wave function or GL order parameter Ψ is related to the gap function and is understood as the field of Cooper pairs. The parameters in the GL equation are also written in the microscopic terms or by the experimental values. In Ref. 28, the GL function Ψ is derived directly from the BCS Hamiltonian, not via the gap function or the anomalous Green function related to the gap function. The electron–electron interaction composed of the four fermion operators is changed by the Hubbard–Stratonovitch transformation to an auxiliary complex boson field ϕ, in which electrons behave as if they were free. Using the path-integral method, we can carry out the integration up to the quadratic terms of the electron operators. If we carefully analyze the resulting effective Lagrangian for the boson field, we will find that this boson field, which is described by a complex function, suggests a phase transition; the condensation arises in particles described by the real part of the boson field, while particles in the imaginary (or phase) part turn out to be massless Goldstone bosons. It is then clear that the boson field is to be the GL order parameter. In the course of analysis, the concept of supersymmetry is effectively used.

1.9.1 *BCS theory*

We assume the classical field of an electron is described by the Grassmann algebra or the anticommuting c-number; namely, the creation and annihilation operators a_k^* and a_k are treated as anticommuting c-numbers. The

BCS Hamiltonian is written as

$$
\begin{aligned}
H &= H_0 + H_{\text{int}}, \\
H_0 &= \sum_{k\sigma} \epsilon_{k\sigma} a^*_{k\sigma} a_{k\sigma}, \\
H_{\text{int}} &= \sum_{kk'} -g_{k-k,-k'k'} (a^*_{k\uparrow} a^*_{-k\downarrow})(a_{-k'\downarrow} a_{k'\uparrow}), \quad g_{k-k,k'-k'} > 0,
\end{aligned}
\tag{1.205}
$$

and

$$
-g_{k-k,-k'k'} = \int d\mathbf{r}_1 d\mathbf{r}_2 \, \chi^*_{k\uparrow}(\mathbf{r}_1) \chi^*_{-k\downarrow}(\mathbf{r}_2) v(\mathbf{r}_1, \mathbf{r}_2) \chi_{-k'\downarrow}(\mathbf{r}_2) \chi_{k'\uparrow}(\mathbf{r}_1),
\tag{1.206}
$$

where $v(\mathbf{r}_1, \mathbf{r}_2)$ is the effective coupling giving an attractive character for the electron–electron interaction. Here, the summation convention that repeated indices imply summation is used. This is helpful in facilitating the manipulation. We would consider that the BCS Hamiltonian is an attractive interaction between Cooper pairs rather than an attractive interaction between electrons, (Figs. 1.3 and 1.4). In the following, it is assumed that $\epsilon_{k\sigma}$ is independent of spin and $g_{k-k,k'-k'}$ is independent not only of spin but also, finally, of k and k'.

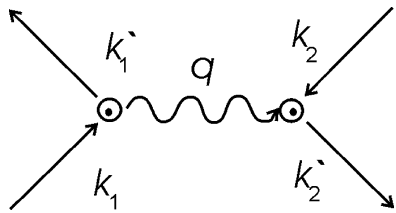

Fig. 1.3 In the BCS model, superconductivity arises due to the attractive electron–electron interaction which appears owing to the scattering by phonons.

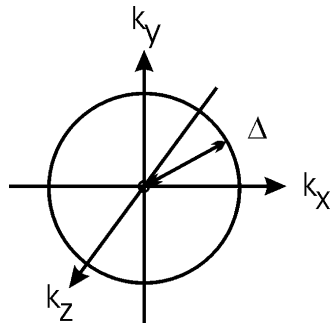

Fig. 1.4 Excitation of the ground state of a Cooper pair demonstrates the presence of the energy gap Δ, which is (very approximately) isotropic in the momentum space.

Let us investigate the partition function

$$Z = \mathrm{Tr} e^{-\beta(H_0+H_{\mathrm{int}})}. \tag{1.207}$$

This is expressed by the use of the path-integral method.[31,32] The spirit of the Feynman path-integral is sometimes written as follows: the (imaginary) time interval $0 \to \beta$ is sliced into numerous pieces, each being labeled by τ_p. Since each slice is made arbitrarily small, the quantum effect arising from the commutation relation can be neglected, so that the operators are regarded as c-numbers in each slice. Instead, this c-number function can take any value even in the small time slice. Connecting these precise values from $0 \to \beta$, we can draw all of the paths in this interval. If we count the effects from all of these paths, the quantum-mechanical result of the subject can be obtained. However, this statement seems rather misleading.

Feynman's path-integral is the third method of quantization.[33] We begin with the classical treatment, and then if we apply the path-integral procedure to it, the quantum effect is certainly taken into account. This corresponds to the conceptual development from the geometric optics to the physical optics. The Bose system (in the quantum-mechanical sense) is written by an ordinary c-number, but the Fermi system should be described by a Grassmann number. Thus, we do not worry about the commutation relations of field operators and obtain

$$\begin{aligned} Z &= \mathrm{Tr}\ e^{-\beta\hat{H}} \\ &= \lim_{N\to\infty} \int \prod_{p=1}^{N} da^*(\tau_p)\, da(\tau_p) \exp \sum_p [\epsilon(\dot{a}^*(\tau_p)a(\tau_p) - H(\tau_p)], \quad \epsilon = \frac{\beta}{N} \\ &= \int \mathcal{D}a^*(\tau)\mathcal{D}a(\tau) \exp \int_0^\beta d\tau \{a^*_{k\sigma}(\tau)(-\partial_\tau - \epsilon_{k\sigma})a_{k\sigma}(\tau) \\ &\quad + g_{k-k,-k'k'} a^*_{k\uparrow}(\tau) a^*_{-k\downarrow}(\tau) a_{-k'\downarrow}(\tau) a_{k'\uparrow}(\tau)\}, \end{aligned} \tag{1.208}$$

where

$$\mathcal{D}a^*(\tau)\mathcal{D}a(\tau) = \prod_{p=1}^{\infty} da^*_{k\sigma}(\tau_p)\, da_{k\sigma}(\tau_p). \tag{1.209}$$

1.9.2 *Hubbard–Stratonovitch transformation*

Difficulty lies in the quartic term of the electron–electron interaction. Let us define

$$B^*_\alpha = a^*_{k\uparrow} a^*_{-k\downarrow}, \quad B_{\alpha'} = a_{-k'\downarrow} a_{k'\uparrow} \tag{1.210}$$

so as to write, in each time slice,

$$g_{k-k,-k'k'}a^*_{k\uparrow}a^*_{-k\downarrow}a_{-k'\downarrow}a_{k'\uparrow} = g_{\alpha\alpha'}B^*_\alpha B_{\alpha'}. \tag{1.211}$$

This is simplified by using the identity called the Hubbard–Stratonovitch transformation.[34] We introduce a complex boson field ϕ, since $(B_\alpha)^* \neq B_\alpha$:

$$\begin{aligned} 1 &= \int_{-\infty}^{\infty} d\phi^*\, d\phi e^{-\pi\phi^*\phi} = \int_{-\infty}^{\infty} d\phi^*\, d\phi e^{-\pi(\phi^* - i\sqrt{g/\pi}B^*)(\phi + i\sqrt{g/\pi}B)} \\ &= \int_{-\infty}^{\infty} d\phi^*\, d\phi e^{-\pi\phi^*\phi + i\sqrt{g\pi}(B^*\phi - B\phi^*)} e^{-gB^*B}, \end{aligned}$$

namely

$$\int_{-\infty}^{\infty} d\phi^*\, d\phi e^{-\pi\phi^*\phi + i\sqrt{g\pi}(B^*\phi - B\phi^*)} = e^{gB^*B}, \tag{1.212}$$

where we have the definition

$$d\phi^*\, d\phi = d(\text{Re }\phi)\, d(\text{Im }\phi).^{\text{a}} \tag{1.213}$$

We cannot apply this identity for the quantum-mechanical partition function because of the noncommutativity of the operators involved, but now we have no trouble since, in the present path-integral treatment, operators turn out to be c-numbers. Then Eq. (1.208) becomes

$$\begin{aligned} Z = \int\!\!\int \mathcal{D}a^*(\tau)\mathcal{D}a(\tau)\, d\phi^*(\tau)\, d\phi(\tau) \\ \times \exp \int_0^\beta d\tau \{ -a^*_{k\sigma}(\tau)\triangle^{-1}_{k\sigma}(\tau)a_{k\sigma}(\tau) - \pi\phi^*_\alpha(\tau)\phi_{\alpha'}(\tau) \\ + i\sqrt{\pi g_{k-k,\alpha'}}a^*_{k\uparrow}(\tau)a^*_{-k\downarrow}(\tau)\phi_{\alpha'}(\tau) - i\sqrt{\pi g_{\alpha,-k'k'}}a_{-k'\downarrow}(\tau)a_{k'\uparrow}(\tau)\phi^*_\alpha(\tau)\}, \end{aligned} \tag{1.214}$$

with

$$\Delta^{-1}_{k\sigma}(\tau) = -\partial_\tau - \epsilon_{k\sigma}.$$

The essential feature of this expression is that the operator appearing in the exponent in Eq. (1.214) is quadratic only in a_k and a^*_k, so that the evaluation with respect to the fermion variables is similar to the evaluation for the noninteracting system, in which particles are moving in an effective boson field ϕ_k. Equation (1.214) shows that, inside the exponent, Z is a weighted average of the second and third terms over the field ϕ_α.

[a] Actually, $d\phi^R\, d\phi^I = \frac{1}{2i} d\phi^*\, d\phi$. The constants are adsorbed in the normalization factor.

1.9.3 *Fourier transform*

The Fourier transformation with respect to τ is performed as

$$a_k(\tau) = \sum_{\omega_n} e^{i\omega_n \tau} a_k(\omega_n), \quad \phi_\alpha(\tau) = \sum_{\upsilon_n} e^{i\upsilon_n \tau} \phi_\alpha(\upsilon_n),$$
$$\omega_n = \frac{(2n+1)\pi}{\beta}, \quad \upsilon_n = \frac{2n\pi}{\beta}. \tag{1.215}$$

Note that ω_n refers to a fermion, and υ_n to a boson.

Using the above and the relation

$$\int_0^\beta d\tau e^{i(\omega_n - \omega_m)\tau} = \beta\delta_{nm}, \tag{1.216}$$

we have

$$\begin{aligned} Z = \int & \mathcal{D}a^*(\omega_n)\mathcal{D}a(\omega_n)\mathcal{D}\phi^*(\upsilon_n)\mathcal{D}\phi(\upsilon_n) \\ & \times \exp \sum_{\omega_n \upsilon_n} \{-\beta a^*_{k\sigma}(\omega_n) \triangle_{k\sigma}(i\omega_n)^{-1} a_{k\sigma}(\omega_n) - \beta\pi\phi^*_\alpha(\upsilon_n)\phi_{\alpha'}(\upsilon_n) \\ & + i\sqrt{\pi g_{k-k,\alpha'}}\, a^*_{k\uparrow}(\omega_n + \upsilon_n) a^*_{-k\downarrow}(\omega)\phi_{\alpha'}(\upsilon_n) \\ & - i\sqrt{\pi g_{\alpha,-k'k'}}\, a_{k'\downarrow}(\omega_n) a_{-k'\uparrow}(\omega_n + \upsilon_n)\phi^*_\alpha(\upsilon_n)\}, \end{aligned} \tag{1.217}$$

where $\triangle_{k\sigma}(i\omega_n)$ is Green's function, given as

$$\triangle_{k\sigma}(i\omega_n) = \frac{1}{i\omega_n - \epsilon_{k\sigma}}. \tag{1.218}$$

We can observe the following in Eq. (1.217): the third line tells us that, at the vertex indicated by the coupling $g_{k-k,\alpha'}$, the boson field $\phi_{\alpha'}$ sinks, and then the particle pair $a^*_{k\uparrow}a^*_{-k\downarrow}$ arises. The last line displays the reverse phenomenon. Note the energy conservations at vertices.

1.9.4 *Nambu spinor*

At this stage, we would rather use a spinor notation due to Nambu[11] that is very useful for investigating the superconductivity:

$$\mathbf{a}_k = \begin{pmatrix} a_{k\uparrow} \\ a^*_{-k\downarrow} \end{pmatrix}, \quad \mathbf{a}^*_k = (a^*_{k\uparrow} \quad a_{-k\downarrow}),$$
$$\mathbf{a}_{-k} = \begin{pmatrix} a_{-k\downarrow} \\ a^*_{k\uparrow} \end{pmatrix}, \quad \mathbf{a}^*_{-k} = (a^*_{-k\downarrow} \quad a_{k\uparrow}). \tag{1.219}$$

It is instructive to manipulate the complicated last line in (1.217) in the present language: it has a structure such that

$$\begin{aligned}\phi_{\alpha'}\ a^*_{k\uparrow}a^*_{-k\downarrow} - \phi^*_\alpha\ a_{-k'\downarrow}a_{k'\uparrow} &= \phi_{\alpha'}(a^*_{k\uparrow} \quad a_{-k\downarrow})\begin{pmatrix}1\\0\end{pmatrix}(0 \quad 1)\begin{pmatrix}a_{k\uparrow}\\a^*_{-k\downarrow}\end{pmatrix}\\ &\quad - \phi^*_\alpha(a^*_{-k'\downarrow} \quad a_{k'\uparrow})\begin{pmatrix}0\\1\end{pmatrix}(1 \quad 0)\begin{pmatrix}a_{-k'\downarrow}\\a^*_{k'\uparrow}\end{pmatrix}\\ &= \phi_{\alpha'}\ \mathbf{a}^*_k\sigma^+\ \mathbf{a}_k + \phi^*_\alpha\ \mathbf{a}^*_{-k'}\sigma^-\mathbf{a}_{-k'}.\end{aligned}$$

The positive sign in the second term is due to the Grassmann character of $a_{k\uparrow}$ and $a_{-k\downarrow}$. Also,

$$a^*_{k\sigma}\epsilon_k a_{k\sigma} = \mathbf{a}^*\sigma^3_k\epsilon_k\mathbf{a}_k, \tag{1.220}$$

since $\epsilon_k = \epsilon_{-k}$.

In the above, the Pauli matrices and related ones are rewritten as

$$\begin{aligned}&\sigma^1 = \begin{pmatrix}0 & 1\\1 & 0\end{pmatrix}, \quad \sigma^2 = \begin{pmatrix}0 & -i\\i & 0\end{pmatrix}, \quad \sigma^3 = \begin{pmatrix}1 & 0\\0 & -1\end{pmatrix},\\ &\sigma^+ = \frac{1}{2}(\sigma^1 + i\sigma^2) = \begin{pmatrix}0 & 1\\0 & 0\end{pmatrix}, \quad \sigma^- = \frac{1}{2}(\sigma^1 - i\sigma^2) = \begin{pmatrix}0 & 0\\1 & 0\end{pmatrix}.\end{aligned} \tag{1.221}$$

Equation (1.217) is now written as

$$\begin{aligned}Z = \int\int \mathcal{D}\mathbf{a}^*\mathcal{D}\mathbf{a}\mathcal{D}\phi^*\mathcal{D}\phi\exp\sum_{\omega_n\upsilon_n}\{&-\beta\pi\phi^*_\alpha(\upsilon)\phi_\alpha(\upsilon)\\ &+\beta\mathbf{a}^*_k(\omega_n)(i\omega_n - \epsilon_k\sigma^3)\mathbf{a}_k(\omega_n)\\ &+i\beta\sqrt{\pi g_{\alpha,k'-k'}}\phi_\alpha(\upsilon_n)\mathbf{a}^*_{k'}(\omega_n+\upsilon_n)\sigma^+\mathbf{a}_{k'}(\omega_n)\\ &+i\beta\sqrt{\pi g_{\alpha',k-k}}\phi^*_{\alpha'}(\upsilon_n)\mathbf{a}^*_{-k}(\omega_n)\sigma^-\mathbf{a}_{-k}(\omega_n+\upsilon_n)\}.\end{aligned} \tag{1.222}$$

We can integrate with respect to fermion variables: note that[31]

$$\begin{aligned}&\int dz^*\,dz e^{(z^*Az)} = \det A \quad \text{for a fermion,}\\ &\int dz^*\,dz e^{(z^*Az)} = (\det A)^{-1} \quad \text{for a boson.}\end{aligned} \tag{1.223}$$

Using the upper one, we can immediately obtain

$$\begin{aligned}Z = \int \mathcal{D}\phi^*\mathcal{D}\phi\exp\sum_{\upsilon_n}\Bigg\{&-\beta\pi\phi^*_\alpha(\upsilon)\phi_\alpha(\upsilon) + \det\Big\|\sum_{\omega_n}\beta(i\omega_n - \epsilon_k\sigma^3)\\ &+i\beta\sqrt{\pi g_{\alpha,k'-k'}}(\phi_\alpha(\upsilon_n)\sigma^+ + \phi^*_{\alpha'}(\upsilon_n)\sigma^-)\Big\|\Bigg\},\end{aligned} \tag{1.224}$$

where we have made use of a symmetry property, $g_{\alpha,k'-k'} = g_{\alpha',k-k}$, and $\|\cdots\|$ stands for a matrix. This can be also rewritten as

$$Z = \int \mathcal{D}\phi^* \mathcal{D}\phi \exp^{-\beta W(\phi)}, \tag{1.225}$$

with the effective action for the boson field

$$W(\phi) = \pi \sum_{\upsilon_n} \phi^*_\alpha(\upsilon_n)\phi_\alpha(\upsilon_n) - \frac{1}{\beta}\sum_{\omega_n} \mathrm{Tr}\log\beta$$
$$\times \left\{ (i\omega_n - \epsilon_k\sigma^3) + i\sum_{\upsilon_n} \sqrt{u_{\alpha,k}}(\phi_\alpha(\upsilon_n)\sigma^+ + \phi^*_\alpha(\upsilon_n)\sigma^-) \right\}, \tag{1.226}$$

where the relation $\log\cdot\det = \mathrm{Tr}\cdot\log$ and the simplified notation

$$u_{\alpha,k} = \pi g_{\alpha,k'-k'} = \pi g_{\alpha',k-k} \tag{1.227}$$

have been used.

By employing the steepest descent method, we can obtain a particular ϕ, by optimizing $W(\phi)$, which will be denoted as $\bar{\phi}$. For example, by differentiating $W(\phi)$ with respect to $\phi^*_\delta(\upsilon_n)$, we have

$$\frac{\partial W(\phi)}{\partial \phi^*_\delta} = \pi\phi_\alpha - \frac{1}{\beta}\sum_{\omega_n} \mathrm{Tr}\frac{i\sqrt{u_{\delta,k}}\sigma^-}{(i\omega_n - \epsilon_k\sigma^3) + i\sqrt{u_{\alpha,k}}(\phi_\alpha(\upsilon_n)\sigma^+ + \phi^*_\alpha(\upsilon_n)\sigma^-)}$$
$$= 0. \tag{1.228}$$

We thus obtain

$$\pi\bar{\phi}_\delta(\upsilon_n) = \frac{1}{\beta}\sum_{i\omega_n} \frac{\sqrt{(u_{\delta,k}u_{\alpha,k})}\cdot\bar{\phi}_\alpha}{(i\omega_n)^2 - E_k^2}, \tag{1.229}$$

where

$$E_k^2(\upsilon) = \epsilon_k^2 + \sqrt{(u_{\alpha,k}u_{\alpha',k})}\bar{\phi}^*_\alpha(\upsilon_n)\bar{\phi}_{\alpha'}(\upsilon_n). \tag{1.230}$$

Note that the field strength $\phi^*_\alpha(\upsilon_n)\phi_{\alpha'}(\upsilon_n)$ has the dimension of energy. In obtaining Eq. (1.229), we first rationalize the denominator, and then the Tr operation on σ's is carried out. The numerator that remains is the coefficient of $\mathrm{Tr}\,\sigma^+\sigma^- = 1$. A similar equation is obtained for ϕ^*. Equation (1.229) corresponds to the gap equation.

Now we employ an approximation in the rest of this study where, as was mentioned at the beginning, $u_{\alpha,k} = u$ (a positive constant). Thus, to the first approximation, ϕ is nearly constant:

$$\frac{\pi}{u} = \frac{1}{\beta}\sum_{\omega_n} \frac{1}{(i\omega_n)^2 - E_k^2}. \tag{1.231}$$

Doing the frequency sum, we get

$$\frac{1}{\beta}\sum_{\omega_n}\frac{1}{i\omega_n - x} = \pm n(x), \tag{1.232}$$

where $n(x)$ is the Fermi or Bose function according to whether ω_n is odd or even, respectively, and we obtain (for fermions)

$$\frac{\pi}{u} = \frac{n(E_k) - n(-E_k)}{2E_k} = \frac{\tan h(\beta E_k/2)}{2E_k}. \tag{1.233}$$

From the above relation combined with Eq. (1.229), we can estimate $\bar{\phi}$, which corresponds to the gap energy.

1.9.5 *Critical temperature*

It is straightforward to obtain the critical temperature, T_c, for the superconductivity from Eq. (1.233).[15] Here, it is repeated for completeness. In the limit $T \to T_c$, the gap, or ϕ_α in the present case, disappears. The summation over k is approximately replaced by the integration

$$\frac{2\pi}{uN(0)} = \int_0^{\omega_D}\frac{d\epsilon}{\epsilon}\tanh\frac{\epsilon}{2k_BT_c}, \tag{1.234}$$

where $N(0)$ is the state density at the Fermi surface, and the cutoff parameter ω_D is, in the case of the BCS theory, the Debye frequency of phonons associated with the attractive interaction between electrons.

The integration in Eq. (1.241) proceeds as follows:

$$\begin{aligned}
\int_0^{\omega_D}\frac{d\epsilon}{\epsilon}\tanh\frac{\epsilon}{2k_BT_c} &= \int_0^{\beta_C\omega_D/2}\frac{dz}{z}\tanh\, z \quad \left(z = \frac{\epsilon\beta_c}{2}\right) \\
&= \log z\tanh\, z]_0^{\beta_c\omega_D/2} - \int_0^{\beta_c\omega_D/2} dz\log z\,\mathrm{sech}^2 z \\
&\approx \log\frac{\beta_c\omega_D}{2} - \int_0^{\infty} dz\log z\,\mathrm{sech}^2 z \quad \left(\tanh\frac{\beta_c\omega_D}{2}\approx 1\right) \\
&= \log\frac{\beta_c\omega_D}{2} + \log\frac{4e^\gamma}{\pi}.
\end{aligned} \tag{1.235}$$

Combined with (1.233), this yields

$$\log\frac{\beta_c\omega_D}{2} = \frac{2\pi}{uN(0)} - \log\frac{4e^\gamma}{\pi}, \tag{1.236}$$

where $\gamma = 0.5772$ is Euler's constant. This relation will be used in the next section. Simple rearrangements yield

$$T_c \approx 1.13\omega_D e^{-2\pi/N(0)u}. \tag{1.237}$$

1.9.6 *Temperature dependence of* ϕ

For the later investigation, we derive a temperature dependence of ϕ_α near the critical temperature.[16] Coming back to (1.231) and restoring the hidden summation with respect to k, we can rewrite this as

$$\frac{2\pi}{uN(0)} = \frac{1}{\beta}\sum_{\omega_n}\int_0^{\omega_D} d\epsilon \frac{1}{(i\omega_n)^2 - (\epsilon^2 + u|\phi_\alpha|^2)}. \tag{1.238}$$

Considering that $|\phi_\alpha|^2 \ll 1$ near the critical temperature, we expand the above as

$$\frac{2\pi}{uN(0)} = \frac{1}{\beta}\sum_{\omega_n}\int_0^{\omega_D} d\epsilon \left\{ \frac{1}{(i\omega_n)^2 - \epsilon^2} + \frac{u|\phi_\alpha|^2}{((i\omega_n)^2 - \epsilon^2)^2} + \frac{(u|\phi_\alpha|^2))^2}{((i\omega_n)^2 - \epsilon^2)^3} + \cdots \right\}. \tag{1.239}$$

For the convergent integrals which are the second and third terms, the integration limit is extended to infinity, and then we obtain (putting $\epsilon = \omega \tan\,\theta$)

$$\frac{2\pi}{uN(0)} = \int_0^{\omega_D} \frac{d\epsilon}{\epsilon}\tanh\frac{\beta\epsilon}{2} + \frac{1}{\beta}\frac{\pi}{4}u|\phi_\alpha|^2\sum\frac{1}{\omega_n^3} + \frac{1}{\beta}\frac{3\pi}{16}(u|\phi_\alpha|^2)^2\sum\frac{1}{\omega_n^5} + \cdots. \tag{1.240}$$

The integration of the first term on the right-hand side, which is similar to (1.235), has β instead of β_c. Then, using (1.236), we have, in the lowest approximation,

$$\log\frac{\beta_c}{\beta} = \frac{1}{\beta}\frac{\pi}{4}u|\phi_\alpha|^2\sum\frac{1}{\omega_n^3} + \cdots. \tag{1.241}$$

Using

$$\sum_0^\infty \frac{1}{(2n+1)^p} = \frac{2^p - 1}{2^p}\zeta(p) \tag{1.242}$$

in (1.241), we have the temperature dependence of ϕ_α,

$$\sqrt{u|\phi_\alpha|^2} = \pi k_B T_c\sqrt{\frac{16}{7\zeta(3)}}\sqrt{1 - \frac{T}{T_c}}, \quad \zeta(3) = 1.202, \tag{1.243}$$

which is the same as that of the energy gap.[15]

1.9.7 *Dynamics of the boson field; symmetry breaking*

The boson field $\phi_\alpha(\upsilon_n)$, which satisfies (1.227), is written as $\bar{\phi}_\alpha$, so that

$$\phi_\alpha(\upsilon_n) = \bar{\phi}_\alpha + (\phi_\alpha - \bar{\phi}_\alpha) = \bar{\phi}_\alpha + \Phi_\alpha(\upsilon_n). \tag{1.244}$$

Now $\Phi_\alpha(\upsilon_n)$ becomes a physical or fluctuation component in solid-state physics. Our aim is to find the effective Lagrangian or Hamiltonian for it.

In order to find the terms proportional to $\Phi_\alpha(\upsilon_n)$ in (1.244), we first observe that

$$\begin{aligned}\phi_\alpha(\upsilon_n)\tau^+ + \phi^*_\alpha(\upsilon_n)\tau^- \equiv \phi_\alpha(\upsilon_n)\cdot\tau &= \phi^{(a)}_\alpha(\upsilon_n)\tau^{(a)}, \quad a = 1,2 \\ &= \bar{\phi}_\alpha(\upsilon_n)\cdot\tau + \Phi_\alpha(\upsilon_n)\cdot\tau. \end{aligned} \tag{1.245}$$

Expanding $W(\phi)$ in (1.226) in $\Phi_\alpha(\upsilon_n)$ and noticing that, upon the Tr operation, the odd terms with respect to τ will vanish. We have

$$\begin{aligned} W(\phi^*,\phi) = \pi\sum_{\upsilon_n}\phi^*_\alpha\phi_\alpha - \frac{1}{\beta}\sum_{\omega_n}\mathrm{Tr}\log\ \beta(i\omega_n - \epsilon\tau^3 - i\sqrt{u}(\bar{\phi}_\alpha\cdot\tau) \\ - \frac{1}{\beta}\sum_{\omega_n\upsilon_n}\sum_{n}^{\text{even}}\frac{1}{n}\mathrm{Tr}\ [\triangle(\omega_n)i\sqrt{u}(\Phi_\alpha(\upsilon_n)\cdot\tau)]^n, \end{aligned} \tag{1.246}$$

where

$$\triangle_k(\omega_n) = \frac{i\omega_n + \epsilon_k\tau^3 + i\sqrt{u}(\bar{\phi}_\alpha\cdot\tau)}{(i\omega_n)^2 - E_k^2}. \tag{1.247}$$

Note that now the propagator includes the mean-field effect. What we are interested in is the second line of Eq. (1.246).

The term with $n = 2$ is precisely written as

$$\begin{aligned}&\frac{-1}{2\beta}\sum_{\omega_n\upsilon_n}\mathrm{Tr}\ u\triangle_k(\omega_n)\left(\Phi^{(a)}_\alpha(\upsilon_n)\tau^{(a)}\right)\triangle_{k+\alpha}(\omega_n+\upsilon_n)\left(\Phi^{*(a')}_\alpha(\upsilon_n)\tau^{(a')}\right) \\ &\quad = \sum_{\upsilon_n} u|\Phi_\alpha(\upsilon_n)|^2 P_\alpha(\upsilon_n), \end{aligned} \tag{1.248}$$

where careful manipulations about τ's are required. Except for the explicit ones combined with Φ's, we have τ's inside $\triangle$'s. Let us call the terms with $a = a' = 1$ and $a = a' = 2$ the direct interactions, and the terms with $a = 1,\ a' = 2$ and $a = 2,\ a' = 1$ the cross interactions. We then have

$$P_\alpha(\upsilon_n) = \frac{-2}{\beta}\sum_{\omega_n}\frac{i\omega_n(i\omega_n + i\upsilon_n) - \epsilon_k\epsilon_{k+\alpha} + u\bar{\phi}^*\cdot\bar{\phi}}{[(i\omega_n)^2 - E_k^2][(i\omega_n+i\upsilon_n)^2 - E^2_{k+\alpha}]}, \tag{1.249}$$

where the first two terms in the numerator arise from the direct interaction and the third from the cross interaction. Here, use has been made of the

fact that Tr $\tau^3\tau^+\tau^3\tau^- = -1$. Employing (1.231), we can carry out a lengthy but not difficult calculation of $P_\alpha(\upsilon_n)$. Note that an even frequency υ_n has nothing to do with obtaining the Fermi functions. The result is

$$P_\alpha(\upsilon_n) = -n(E_k)(1-n(E_{k+\alpha}))\frac{E_{k+\alpha}-E_k}{(i\upsilon)^2-(E_{k+\alpha}-E_k)^2} \times\left[\frac{E_{k+\alpha}E_k-\epsilon_{k+\alpha}\epsilon_k+u(\bar{\phi}^*\cdot\bar{\phi})}{E_{k+\alpha}E_k}\right]. \tag{1.250}$$

Here, we again note that, in the square brackets, the first two terms are obtained from the direct interaction and the third term from the cross interaction.

It might be convenient, for the later investigation, to do the frequency sum for $P_\alpha(\upsilon_n)$:

$$\begin{aligned}
&\sum_{\upsilon_n}\frac{E_{k+\alpha}-E_k}{(i\upsilon_n)^2-(E_{k+\alpha}-E_k)^2}\\
&\quad=\beta\frac{1}{\beta}\sum_{\upsilon_n}\frac{1}{2}\left[\frac{1}{i\upsilon_n-(E_{k+\alpha}-E_k)}-\frac{1}{i\upsilon_n+(E_{k+\alpha}-E_k)}\right]\\
&\quad=\frac{\beta}{2}[-n_B(E_{k+\alpha}-E_k)+n_B(-E_{k+\alpha}+E_k)],\\
&\quad=\frac{-\beta}{2}\cot\mathrm{h}\left[\frac{\beta(E_{k+\alpha}-E_k)}{2}\right],
\end{aligned}$$

where n_B is the Bose function, and use of Eq. (1.232) has been made for the even frequency υ_n. Then Eq. (1.250) becomes

$$\sum_{\upsilon_n}P_\gamma(\upsilon_n) = n(E_\alpha)(1-n(E_{\alpha+\gamma}))\frac{\beta}{2}\cot\mathrm{h}\left[\frac{\beta(E_{\alpha+\gamma}-E_\alpha)}{2}\right] \times\left[\frac{E_{\alpha+\gamma}E_\alpha-\epsilon_{\alpha+\gamma}\epsilon_\alpha+u(\bar{\phi}^*\cdot\phi)}{E_{\alpha+\gamma}E_\alpha}\right]. \tag{1.251}$$

We then obtain the effective action for ϕ up to the second order in Φ, as follows:

$$\begin{aligned}
W_\alpha(\phi^*,\phi) &= \pi\sum_{\upsilon_n}\phi^*_\alpha(\upsilon_n)\phi_\alpha(\upsilon_n)-\frac{1}{\beta}\sum_{\omega_n\upsilon_n}\mathrm{Tr}\\
&\quad\times\log\{-\beta(i\omega_n-\epsilon_k\tau^3-\sqrt{u}\bar{\phi}_\alpha(\upsilon_n)\cdot\tau)\}\\
&\quad-n(E_\alpha)(1-n(E_{\alpha+\gamma}))\sum_{\upsilon_n}\frac{E_{k+\alpha}-E_k}{(i\upsilon)^2-(E_{k+\alpha}-E_k)^2}\\
&\quad\times\left[\frac{E_{k+\alpha}E_k-\epsilon_{k+\alpha}\epsilon_k+u(\bar{\phi}^*\cdot\bar{\phi})}{E_{k+\alpha}E_k}\right].
\end{aligned} \tag{1.252}$$

1.9.8 *Instability*

In order to discuss the dynamics of $\Phi_\alpha(\upsilon_n)$, we must obtain an expression for the action of $\Phi_\alpha(\upsilon_n)$ similar to that for $a_\alpha(\omega_n)$ given in the exponent of Eq. (1.208). Since we are interested in the energy region much lower than that for the electronic excitation $(E_{\alpha+\gamma} - E_\alpha)$, the denominator of $P_\alpha(\upsilon_n)$ in Eq. (1.250) is expanded as

$$\frac{1}{(i\upsilon)^2 - (E_{k+\alpha} - E_k)^2} = \frac{-1}{(E_{k+\alpha} - E_k)^2}\left[1 + \frac{(i\upsilon_n)^2}{(E_{k+\alpha} - E_k)^2} + \cdots\right]. \tag{1.253}$$

Substituting this into $P_\alpha(\upsilon_n)$ in Eq. (1.250) and taking up the terms of the order of $(i\upsilon)^2$ in the above, we have

$$(i\upsilon_n)^2 + u(\bar{\phi}^*\bar{\phi})\frac{(E_{k+\alpha} - E_\gamma)^2}{E_{k+\alpha}E_k} + \cdots . \tag{1.254}$$

The second term is a small and complicated, but positive quantity. We thus obtain the effective Lagrangian for Φ up to the second order of $\Phi^*\Phi$:

$$\mathcal{L}_B \sim \Phi^*(i\upsilon_n)^2\Phi + \eta\Phi^*\Phi + \cdots , \quad \eta > 0. \tag{1.255}$$

In the above, $i\upsilon_n$ is replaced by $\partial/\partial\tau$ in the future. At this stage, the details of η are immaterial except that this is positive.

To put forward the problem, we need the term proportional to $\Phi^*\Phi^*\Phi\Phi$. This is obtainable from the term with $n = 4$ in Eq. (1.246). Without any detailed calculation, we may presume a positive quantity for this, noted by Λ^2. Then the total Lagrangian of the boson field becomes

$$\mathcal{L}_B \sim \Phi^*(i\upsilon_n)^2\Phi + \eta\Phi^*\Phi - \Lambda^2\Phi^*\Phi^*\Phi\Phi. \tag{1.256}$$

This looks like the Lagrangian that Ginzburg and Landau have used for investigating the superconductivity. We thus expect a kind of phase transition. Let us optimize, with respect to Φ^*, the potential part of Eq. (1.256):

$$\mathcal{V} = -\eta\Phi^*\Phi + \Lambda^2\Phi^*\Phi^*\Phi\Phi, \tag{1.257}$$

$$\frac{\partial\mathcal{V}}{\partial\Phi^*} = -\eta\Phi + 2\Lambda^2\Phi^*\Phi\Phi = (-\eta + 2\Lambda^2\Phi^*\Phi)\Phi = 0. \tag{1.258}$$

If $\Phi = 0$, nothing happens; while, in the case of $\Phi \neq 0$, it is possible that

$$\overline{\Phi^*\Phi} = \frac{\eta}{2\Lambda^2} \equiv \bar{a}^2. \tag{1.259}$$

We now put

$$\Phi = (\rho + \bar{a})e^{i\theta}. \tag{1.260}$$

Namely, only the radial part is affected. This choice is allowed in the spirit of the unitary gauge. If we insert this into (1.257), it follows that

$$\mathcal{V} = \Lambda^2[(\rho + \bar{a})^2 - \bar{a}^2]^2 - \Lambda^2\bar{a}^4 = \Lambda^2[\Phi^*\Phi - \bar{a}^2]^2 - \Lambda^2\bar{a}^4. \tag{1.261}$$

Observing the final result, we realize that the potential becomes minimum at $|\Phi| = \bar{a}$; namely, at this position apart from the origin, $|\Phi| = 0$, which corresponds to the HF state. The mass of the field Φ is given by the coefficient of $\Phi^*\Phi$, which is $4\Lambda^2\bar{a}^2$ for a particle of the ρ field, while the term involving θ is completely lost. That is to say, the particle in the θ field is massless, and it is called the Goldstone boson. This is due to the occurrence of the infinite degeneracies along the direction perpendicular to the ρ coordinate.

1.9.9 *Supersymmetry*

The total Lagrangian of the system is

$$\mathcal{L}_{\rm tot} = \mathcal{L}_e + \mathcal{L}_B + \mathcal{L}_{\rm int}, \tag{1.262}$$

where

$$\begin{aligned} \mathcal{L}_e &= \mathbf{a}_i^*(i\omega_n - \epsilon_i\tau^3)\mathbf{a}_i, \\ \mathcal{L}_B &= -\dot{\Phi}^*\dot{\Phi} - \Lambda^2[\Phi^*\Phi - \bar{a}^2]^2, \\ \mathcal{L}_{\rm int} &= -i\sqrt{u}(\Phi\mathbf{a}^*\tau^+\mathbf{a} + \Phi^*\mathbf{a}^*\tau^-\mathbf{a}). \end{aligned} \tag{1.263}$$

In the above, the second line is obtained from Eqs. (1.256) and (1.261), and then the third line from Eq. (1.245) supplied by necessary terms, and a compact notation is used, and the immaterial constant terms are omitted. The $\mathcal{L}$ in the above is, strictly speaking, the Lagrangian density, and the action which we are interested in is the space–time integral of the Lagrangian density, so that the partial integration with respect to τ (after the replacement $i\upsilon_n \to \partial_\tau$) gives the first term with the minus sign. If we define the momentum conjugate to Φ,

$$\Pi = \frac{\partial\mathcal{L}_{\rm tot}}{\partial\dot{\Phi}} = -\dot{\Phi}^*, \quad \Pi^* = \frac{\partial\mathcal{L}_{\rm tot}}{\partial\dot{\Phi}^*} = -\dot{\Phi}, \tag{1.264}$$

the total Hamiltonian for the boson field is obtained as

$$\begin{aligned} \mathcal{H}_{\rm tot} &= \Pi^*\dot{\Phi} + \Pi\dot{\Phi}^* - \mathcal{L} \\ &= \Pi^*\Pi + i\sqrt{u}(\mathbf{a}^*\Phi\tau^+\mathbf{a} + \mathbf{a}^*\Phi^*\tau^-\mathbf{a}) + \Lambda^2[\Phi^*\Phi - \bar{a}^2]^2. \end{aligned} \tag{1.265}$$

The momenta, Π^* and Π conjugate to Φ^* and Φ respectively, have the properties

$$[\Pi, f(\Phi^*, \Phi)]_- = \frac{\partial}{\partial \Phi} f(\Phi^*, \Phi), \quad [\Pi^*, f(\Phi^*, \Phi)]_- = \frac{\partial}{\partial \Phi^*} f(\Phi^*, \Phi), \tag{1.266}$$

since we are now dealing with the classical operators in the framework of the path-integral formalism.

Let us turn to a supersymmetric treatment.[35–37] The fermionic composite charge operators are defined as

$$\begin{aligned} Q^* &= \Pi^* \mathbf{a}^* - i\sqrt{u}(\Phi^*\Phi - \bar{a}^2)\mathbf{a}^*\tau^-, \\ Q &= \Pi \mathbf{a} + i\sqrt{u}(\Phi^*\Phi - \bar{a}^2)\tau^+\mathbf{a}. \end{aligned} \tag{1.267}$$

First of all, we have to manipulate the commutator

$$[Q^*, Q]_+ = [\Pi^*\mathbf{a}^* - i\sqrt{u}(\Phi^*\Phi - \bar{a}^2)\mathbf{a}^*\tau^-, \Pi\mathbf{a} + i\sqrt{u}(\Phi^*\Phi - \bar{a}^2)\tau^+\mathbf{a}]_+. \tag{1.268}$$

Straightforward calculations give

$$\begin{aligned} [\Pi^*\mathbf{a}^*, \Pi\mathbf{a}]_+ &= [\Pi^*\mathbf{a}^*, \mathbf{a}]_+\Pi - \mathbf{a}[\Pi, \Pi^*\mathbf{a}^*]_+ \\ &= \Pi^*[\mathbf{a}^*, \mathbf{a}]_+\Pi - \mathbf{a}[\Pi, \Pi^*]_+\mathbf{a}^* \\ &= \Pi^*\Pi. \end{aligned}$$

Here, for the Grassmann numbers, use has been made of the relation

$$[\mathbf{a}^*, \mathbf{a}]_+ = \frac{\partial}{\partial \mathbf{a}}\mathbf{a} - \mathbf{a}\frac{\partial}{\partial \mathbf{a}} = \frac{\partial \mathbf{a}}{\partial \mathbf{a}} + \mathbf{a}\frac{\partial}{\partial \mathbf{a}} - \mathbf{a}\frac{\partial}{\partial \mathbf{a}} = 1.$$

Further,

$$\begin{aligned} &[\Pi^*\mathbf{a}^*, i\sqrt{u}(\Phi^*\Phi - \bar{a}^2)\tau^+\mathbf{a}]_+ \\ &\quad = [\Pi^*\mathbf{a}^*, i\sqrt{u}(\Phi^*\Phi - \bar{a}^2)]_-\tau^+\mathbf{a} - i\sqrt{u}(\Phi^*\Phi - \bar{a}^2)[\tau^+\mathbf{a}, \Pi^*\mathbf{a}^*]_+ \\ &\quad = [\Pi^*, i\sqrt{u}(\Phi^*\Phi - \bar{a}^2)]_-\mathbf{a}^*\tau^+\mathbf{a} - i\sqrt{u}(\Phi^*\Phi - \bar{a}^2)\tau^-\Pi^*[\mathbf{a}, \mathbf{a}^*]_+ \\ &\quad = i\sqrt{u}\Phi\mathbf{a}^*\tau^+\mathbf{a} \end{aligned}$$

and

$$\begin{aligned} &[i\sqrt{u}(\Phi^*\Phi - \bar{a}^2)\mathbf{a}^*\tau^-, \Pi\mathbf{a}]_+ \\ &\quad = [\Pi\mathbf{a}, i\sqrt{u}(\Phi^*\Phi - \bar{a}^2)]_-\mathbf{a}^*\tau^- - i\sqrt{u}(\Phi^*\Phi - \bar{a}^2)[\mathbf{a}^*\tau^-, \Pi\mathbf{a}]_+ \\ &\quad = [\Pi, i\sqrt{u}(\Phi^*\Phi - \bar{a}^2)]_-\mathbf{a}\mathbf{a}^*\tau^- - i\sqrt{u}(\Phi^*\Phi - \bar{a}^2)\tau^-\Pi[\mathbf{a}^*, \mathbf{a}]_+ \\ &\quad = i\sqrt{u}\Phi^*\mathbf{a}\mathbf{a}^*\tau^- \\ &\quad = -i\sqrt{u}\Phi^*\mathbf{a}^*\tau^-\mathbf{a}. \end{aligned}$$

The final term must be symmetrized:

$$[\mathbf{a}^*\boldsymbol{\tau}^+, \boldsymbol{\tau}^-\mathbf{a}]_+ \to \frac{1}{2}\{[\mathbf{a}^*\boldsymbol{\tau}^+, \boldsymbol{\tau}^-\mathbf{a}]_+ + [\mathbf{a}^*\boldsymbol{\tau}^-, \boldsymbol{\tau}^+\mathbf{a}]_+\} \tag{1.269}$$

$$= \frac{1}{2}\{[(0, a^*), (0, a)]_+ + [(b, 0), (b^*, 0)]_+\}$$

$$= \frac{1}{2}\begin{pmatrix} [b, b^*]_+ & 0 \\ 0 & [a^*, a]_+ \end{pmatrix} \tag{1.270}$$

$$= \frac{1}{2}\mathbf{1}. \tag{1.271}$$

In the second line, b and b^*, which are used in literature, are defined.

We thus obtain the fundamental relation in the supersymmetric quantum mechanics,

$$\mathcal{H} = [Q, Q^*]_+, \tag{1.272}$$

if we endow, to the constant Λ^2 in (1.264), a specified value,

$$\Lambda^2 = 2u, \tag{1.273}$$

which is reasonable.[37] However, as mentioned before, this had to be obtained analytically from the term with $n = 4$ in Eq. (1.252). If it is assumed that the present system is the case of supersymmetry, we can avoid this tedious calculation.

The nilpotency of the charge operators,

$$Q^2 = 0, \quad (Q^*)^2 = 0, \tag{1.274}$$

is clearly preserved from $\mathbf{a}^2 = 0$ and $(\mathbf{a}^*)^2 = 0$. We have thus completed a supersymmetric analysis.

1.9.10 *Towards the Ginzburg–Landau equation*

Now we can think about the GL equation. Since it concerns only the static part of the condensed boson field, we keep the first and third terms of Eq. (1.265). The first term is the kinetic part, while the last term is the potential part:

$$\mathcal{H}_{\mathrm{GL}} = \Pi^*\Pi - \eta\Phi^*\Phi + \Lambda^2(\Phi^*\Phi)^2, \tag{1.275}$$

with

$$\eta = u(\bar{\phi}^*\bar{\phi})\frac{(E_{k+\alpha} - E_\gamma)^2}{E_{k+\alpha}E_k}.$$

As usual, the coefficients of $\Phi^*\Phi$ and $(\Phi^*\Phi)^2$ in the GL equation are a and b, respectively. It is crucial that a is negative, which is given by $-\eta$ in the present consideration. The temperature dependence of η is found through $u(\bar{\phi}^*\bar{\phi})$, as in Eq. (1.265). This is exactly the same as that obtained by Gorkov.[30]

1.9.11 *Discussion*

Some people seemed to be puzzled by the curious look of the GL equation when it was published: the superconductivity being a macroscopic, thermodynamically stable phase — why is it predicted by a Schrödinger-like wave function, to which the microscopic phenomena are subjected? Several years later, the microscopic theory was established by BCS, and soon Abrikosov had successfully correlated these two treatments. He made clear that the GL function is deeply concerned with the gap function characteristic of the superconductivity and is a wave function describing the condensed Cooper pairs.

The superconducting state is certainly a stable thermodynamical state, and a phase transition from the normal state to the superconducting state is interpreted as a long-distance correlation between the Cooper pairs. Yang[38] developed a unified treatment of the phase transition in terms of the density matrix. According to his treatment, the onset of the superconductivity is understood in such a way that the off-diagonal long-range order (ODLRO) of the second-order density matrix has a nonvanishing value. This concept is clearly related to London's rigid function, the quasiboson condensation being widely seen as a powerful model of superconductivity and the variational wave function tried by BCS.[3] Recently, Dunne *et al.*[39] applied the concept of ODLRO to argue the high-temperature superconductivity in copper oxide, where the attractive interaction between electrons is assumed to have originated from Friedel oscillations in the screened potential.

However, the previous presentation of Abrikosov looks to be a detour; a complicated and tedious procedure in which the condensed pair is characterized by an anomalous temperature Green function which is difficult to manipulate for beginners. Therefore, the direct way to reach the GL theory from the BCS Hamiltonian should be preferable. What we have done in the present investigation is the following: the auxiliary boson field driven by the Hubbard–Stratonovitch transformation to eliminate the quartic term of electron operators is just the GL function.

In conclusion, from the treatments used so far, the conditions which are necessary for the occurrence of superconductivity are:

(1) The wave function which means the ground-state average of operators of a Cooper pair must be complex or two-dimensional. If one of these two degrees of freedom gets a new stable structure, the other degree of freedom, whose direction is perpendicular to the former, offers the infinite degeneracy. In the Nambu theory, the first refers to the σ^1 direction, and the second to σ^2 in the fictitious spin space.

(2) The electron–electron interaction should be attractive, otherwise the negative coefficient of $\Phi^*\Phi$ in Eq. (1.275) cannot be obtained. In the present consideration, we have observed that this condition is established in the effective electron–electron interaction of the system involving the multiband structure.

However, we will discuss a little more the normal state under the usual condition. In the normal species, the coupling constant between electrons is intrinsically positive. However, if we are interested in the exchange interaction, i.e. the so-called Fock term with negative coupling, this is met by condition 2. This is a short range interaction, while the direct coupling is so strong as to overwhelm the exchange interaction.

Let us turn to the behavior of the quartic electron operators. It is unexpected that these are grouped into the pair operators of particle–particle and hole–hole, which do not conserve the particle number. Thus, it is natural to group them into a couple of particle–hole pairs. This choice makes the auxiliary boson function real.

The Hamiltonian which satisfies the above two conditions, looking like the BCS Hamiltonian, is the one with the dipole–dipole interaction. The simplest case is that of the intermolecular interaction due to the induced dipole–dipole interaction with a coupling constant $-d$:

$$H_d = -d a_r^* b_r^* b_s a_s, \tag{1.276}$$

where, for example, a_r^* and b_r^* are the creation operators for a particle and a hole, respectively. If the electron–electron interaction is screened sufficiently, this may be another possibility for the superconductivity of a molecular complex.

CHAPTER 2

Physics of High-T_c Superconductors

2.1 Introduction

In 1986, K. A. Müller and J. G. Bednorz discovered the phenomenon of superconductivity in Cu-oxide compounds of lanthanum and barium at the temperature $T_c = 35\,\mathrm{K}$,[2] and they were awarded the Nobel Prize in 1987. This discovery gave an additional push to the intensification of the scientific activity in the field of superconductivity. Over the last 23 years, the superconducting transition temperature has been increased to 140 K. Moreover, one may expect the discovery of new superconductors with higher critical temperatures. Recently, the high critical temperatures of new, Mg-containing superconductors ($MgBr_2$) ($T_c = 39\,\mathrm{K}$) and superconducting oxypnictides $LnO_{(1-x)}F_xFeAs$ ($T_c = 50\,\mathrm{K}$) were registered.

The main purpose of solid-state physics is the development and fabrication of substances which possess superconductivity at room temperature. At present, there is an intensive search for such high-temperature superconductors (HTSCs). Especially promising is the method of producing superconducting materials with the help of laser spraying of layers.

After the discovery of HTSCs, the following problems became urgent:

(1) Conceptual–theoretic: the problem of clarifying mechanisms of high-temperature superconductivity.
(2) Engineering and technical: the problem of practical applications of HTSCs.
(3) Research: the problem of the search for materials with higher T_c.

The great interest in the phenomenon of superconductivity is caused by the basic possibility of using it in the future for electric power transfer without losses and for the construction of quantum high-power generators. This

phenomenon could be applied to superconductive electronics and computer techniques (superconducting elements of memory). At present, a new trend in technology, namely the construction of quantum computers on the basis of HTSCs with d pairing, can be seen.

HTSCs have unique physical properties in both the normal state and the superconducting one. To comprehend the physics of these complex compounds is one of the main tasks of the theory of superconductivity, whose solution will allow one to explain the mechanism ensuring high-temperature superconductivity.

The disappearance of resistance on the cooling of superconductors down to a certain critical temperature is one of the most characteristic effects in superconductors. But, in order to understand the reason for the occurrence of superconductivity, it is necessary to study the other effects which accompany this phenomenon.

Consider briefly the main properties of HTSCs:

(1) New HTSCs have a great anisotropy across the axis **c** and possess a multilayer structure. The main block defining the metallic and superconductive properties is the plane with CuO_2, which form the square lattices of Cu ions.
(2) HTSCs are superconductors of the second kind ($l/\varkappa \ll 1$, where l is the coherence length and $\varkappa$ the penetration depth of a magnetic field).
(3) They have high critical temperatures T_c.
(4) They have antiferromagnetic ordering of spins of Cu in the CuO_2 planes and powerful spin fluctuations with a wide spectrum of excitations.

At present, there exists no theoretical approach which would explain the totality of the thermodynamical, magnetic and superconductive properties of HTSCs from a single viewpoint.

The electron–phonon mechanism of pairing, being the principal one in standard superconductors, makes a considerable contribution to the establishment of the superconducting state in HTSCs. But, in order to obtain a proper description, it is necessary to consider the other mechanisms inherent in HTSCs.

Among such mechanisms is the spin-fluctuation one proposed by D. Pines (USA). The reason for the pairing of electrons can be the scattering of electrons on spin fluctuations. This model of pairing is one of the most real models of high-temperature superconductivity.

The thermodynamics of superconductors at low temperatures is determined by the excitation of two quasiparticles. In the traditional

superconductors with pairing of the BCS type, the energy gap is isotropic (s pairing), and the temperature dependence of the heat capacity has an exponential form $\sim \exp^{-\Delta/k_BT}$, where Δ is the superconductor's gap. In superconductors with anisotropic pairing, the temperature dependence of the heat capacity has a power character, namely T^n. The appearance of such temperature dependences is related to the fact that the superconductor's gap is zero on the Fermi surface. The development of the thermodynamics of this model is the actual problem of HTSCs.

In the following section, we consider the history of the development of studies on the phenomenon of superconductivity. The structure of HTSCs and their physical properties are analyzed. We make a survey of the mechanisms of superconductivity and discuss the problem on the symmetry of the order parameter.

We draw the conclusion that, on the whole, the most probable is the "synergetic" mechanism of pairing which includes, as components, the electron–phonon and spin-fluctuation interactions in cuprate planes.

Only if the interaction of all the degrees of freedom (lattice, electronic and spin ones) is taken into account can a number of contradictory properties observed in the superconducting and normal phases be explained. Moreover, one needs to consider the complicated structure of HTSCs. It will be emphasized that new experiments should be executed in order to explain the available experimental data.

In this section, we also consider the thermodynamics of the spin-fluctuation mechanism of pairing, present the method of functional integration for the calculation of thermodynamical properties on the basis of the Pines spin-fluctuation Hamiltonian, and deduce the Schwinger–Dyson equations for Green functions and equations for the thermodynamic potential. Based on the Schwinger–Dyson equation, we obtain equations for the superconductor gap, which are used in numerical calculations of the thermodynamics of HTSCs. We present analytic formulas for the thermodynamic potential and its jump. The numerical calculations of the temperature dependence of the electron heat capacity indicate that the temperature dependence of the heat capacity is proportional to the square of the temperature. We emphasize that such temperature dependence is related to the d pairing. It is shown that the measurement of the temperature dependence of the heat capacity can be a supplementary test for the establishment of a type of the symmetry of pairing in HTSCs. The jump of the heat capacity of cuprate superconductors near the critical temperature is evaluated as well.

2.2 History of the Development of Superconductivity

The phenomenon of superconductivity was discovered by the physicist H. Kamerlingh-Onnes at the Leiden Laboratory (the Netherlands) in 1911, in the same year when Rutherford discovered the atom. Kamerlingh-Onnes registered the disappearance of resistance of Hg at the temperature $T = 4.5\,\mathrm{K}$. This state was called superconducting. Being cooled down to a temperature less than the above-mentioned critical temperature, many conductors can be transferred in the superconducting state, in which electrical resistance is absent. The disappearance of resistance is the most dramatic effect in superconductors. But, in order to comprehend the reason for the origin of superconductivity, we need to study the other effects accompanying this phenomenon. The dissipationless current states in superconductors were a puzzle for a long period.

The phenomenon of superconductivity is an excellent example of the manifestation of quantum effects on the macroscopic scale. At present, it occupies the place of the most enigmatic phenomenon in condensed-state physics, namely the physics of metals.

The main purpose of solid-state physics is the creation of superconductors which have the superconductive property at room temperature. At present, researchers are continuing the wide-scale search for such HTSCs by testing a variety of substances.

A number of phenomenological models were proposed to clarify the phenomenon of superconductivity, namely the models advanced by London and Ginzburg–Landau.[9,40] The essence of these theories which have played an important role in the development of ideas of superconductivity was presented in Chap. 1.

The success of the GL theory was related to the circumstance that it is placed in the mainstream of the general theory of phase transitions.

Among the first microscopic theories devoted to the consideration of the electron–phonon interaction, the work by H. Fröhlich[41] is of the greatest importance. The following stage in the development of superconductivity started from the universal theory of BCS published in 1957,[104] which strongly promoted the subsequent study of superconductivity.[42] The authors of this theory were awarded by the Nobel Prize.

The BCS theory gave the possibility of elucidating a lot of experiments on the superconductivity of metals and alloys. However, during the development of the theory, some grounded assumptions and approximations were

accepted. Therefore, the BCS theory was needed in substantiation with the help of stricter arguments. This was made by academician N. N. Bogoliubov in Ref. 42. He developed a microscopic theory of the phenomena of superconductivity and superfluidity. By using the Fröhlich effective Hamiltonian, Bogoliubov calculated the spectrum of excitations of a superconductor within the method of canonical transformations proposed by him in 1947.

In 1962, B. D. Josephson advanced the theory of tunnel effects in superconductors (the Josephson effect), which was marked by the Nobel Prize in 1973.[43] This discovery strongly intensified the experimental studies of superconductivity and was applied to electronics and computer technologies.

In 1986, K. A. Müller and J. G. Bednorz discovered HTSCs,[2] which initiated the huge "boom" manifested in numerous publications. The principal thought of Müller was the following: by selecting the suitable chemical composition, one can enhance the electron–phonon interaction and thus increase the critical temperature T_c. Müller and Bednorz found a new class of HTSCs, the so-called cuprate superconductors.

HTSCs have been studied for 23 years by making significant efforts, but the pattern is still not completely clear. This is related to the complicated structure of cuprates, difficulties in the production of perfect single crystals, and difficult control over the degree of doping. The comprehension of HTSCs will be attained if our knowledge about them approaches a critical level sufficient for the understanding of a great amount of experimental data from a single viewpoint. In Fig. 2.1, we present a plot of the critical temperatures of superconductivity over years.[44,45]

2.3 Structural Properties of High-Temperature Superconductors

The properties of new HTSCs differ essentially from those of traditional superconductors, which are described by the BCS theory. Let us briefly consider the main properties of HTSCs. As is known, the atomic structure defines the character of chemical bonds in solids and a number of relevant physical properties. Even small changes of the structure frequently lead to significant changes of their electron properties — for example, at the metal–dielectric phase transitions. Therefore, the study of a crystal structure with long-range atomic order and its dependence on the temperature, pressure and composition is of great importance for HTSCs. Such investigations are

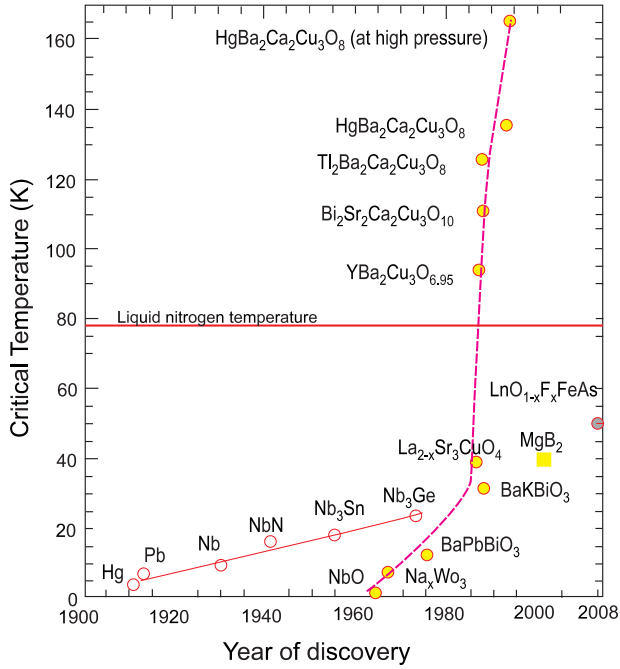

Fig. 2.1 The evolution of critical temperatures since the discovery of superconductivity.

significant for the comprehension of mechanisms of high-temperature superconductivity.

At present, we have several families of HTSCs: thermodynamically stable copper oxides containing lanthanum, yttrium, bismuth, thallium and mercury.[45]

We note that the structure of all copper-oxide superconductors has a block character. The main block defining the metallic and superconductive properties of a compound is the plane with CuO_2 which forms the square lattice of copper ions coupled with one another through oxygen ions. Depending on the composition, the elementary cell of a high-temperature compound can have one, two or more cuprate layers. In this case, the critical temperature of the superconducting transition increases with the number of cuprate layers. In Fig. 2.2, we present an elementary cell of the orthorhombic structure of yttrium ceramics $YBa_2Cu_3O_{7-\delta}$, $\delta \approx 0.1 - 0.3$. The maximum $T_c \approx 90\,\mathrm{K}$. The size of the cell is characterized by the following parameters: $a = 3.81\,\text{Å}$, $b = 3.89\,\text{Å}$, $c = 11.7\,\text{Å}$.

Thus, HTSCs are characterized both by large volumes of elementary cells and by a clearly manifested anisotropy of layers.

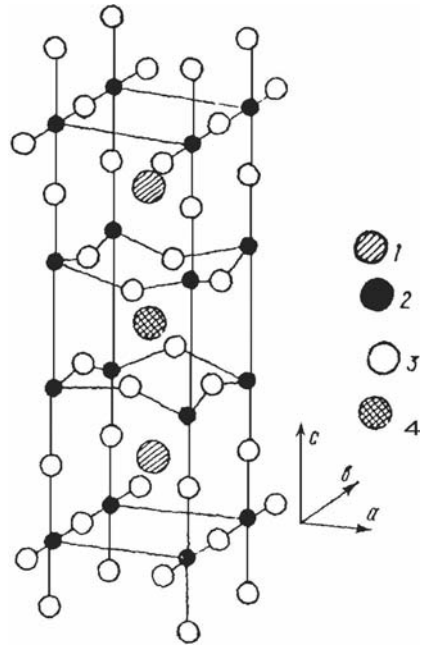

Fig. 2.2 Elementary cell of yttrium ceramics YBa_2CuO_7: 1–yttrium; 2–barium; 3–oxygen; 4–copper.

Of significant interest is the discovery of the compounds $Bi_2CaSr_2Cu_2O_8$ (Bi/2-1-2-2) and $Tl_2CaBa_2Cu_2O_8$ (Tl/2-1-2-2) with the temperature of the superconducting transition $T_c > 100\,\mathrm{K}$. These compounds can have different numbers of cuprate layers and are described by the general formula $A_2Ca_nY_2Cu_nO_{2n4}$, where $A = \mathrm{Bi(Tl)}$ and $Y = \mathrm{Sr(Ba)}$. Their temperature T_c depends on the number of cuprate layers and takes values of 10, 85 and 110 K for the compounds with Bi, and 85, 105 and 125 K for the compounds with Tl for $n = 1, 2, 3$, respectively. For the compounds with Tl with the single layer Tl-O and the general formula $TlCa_{n-1}Ba_2Cu_nO_{2n+3}$(Tl/1...), the number of cuprate layers reaches $n = 5$.

We present the structures of the family of Tl-based superconductors in Figs. 2.3 and 2.4. In Table 2.1, we show the dependences of T_c and the interplane distance (Å) on the number of layers in the unit cell N. The explanation for the dependence of the critical temperature on the number of cuprate layers is an urgent problem.[46,47] All HTSCs have a complicated multiband structure,[98] shown in Fig. 2.5.

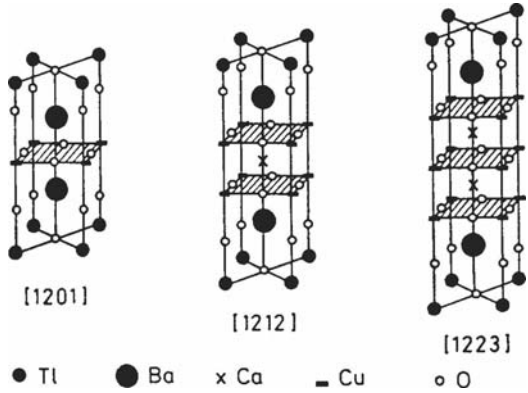

Fig. 2.3 Schematic distribution of ions in the unit cell of superconductors $Tl_1Ba_2Ca_{N-1}Cu_NO_{2N+4}$ or, in the brief notation, $Tl(1:2:N-1:N)$ at $N = 1, 2, \ldots, 5$.

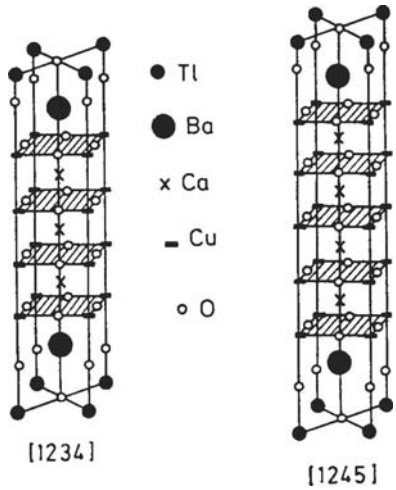

Fig. 2.4 Schematic distribution of ions in the unit cell of superconductors $Tl_1Ba_2Ca_{N-1}Cu_NO_{2N+4}$ or, in the brief notation, $Tl(1:2:N-1:N)$ at $N = 1, 2, \ldots, 5$.

Table 2.1 Tl-based systems $Tl_1Ba_2Ca_{N-1}Cu_NO_{2N+3}$.

N	1	2	3	4	5	6
a (Å)	—	3.8500	3.8493	3.8153	3.8469	—
T_c (K)	13–15	78–91	116–120	122	106	102

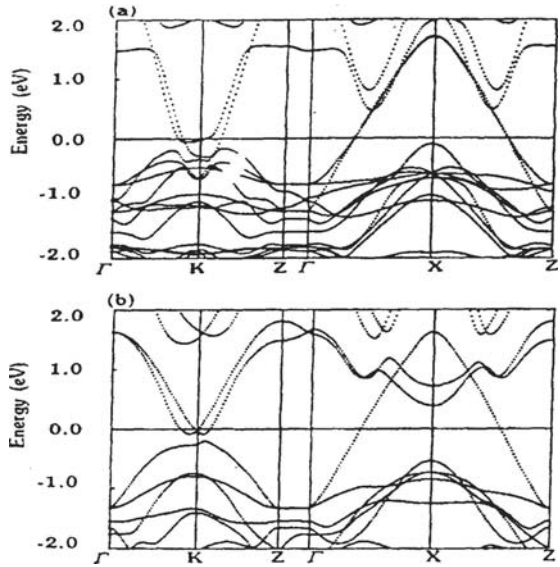

Fig. 2.5 Structure of energy bands near the Fermi energy for (a) high-temperature superconductor $Bi_2Sr_2CaCu_2O_8$ and (b) low-temperature superconductor $Bi_2Sr_2CaCuO_6$.

We note the importance of the structure of zones near the Fermi level. For example, the structures of the bands of two superconductors (high-temperature $Bi_2Sr_2CaCu_2O_8$ and low-temperature $Bi_2Sr_2CaCuO_6$) are significantly different at point K. The energy interval from the band bottom to the Fermi surface is equal to 0.7 eV at point K for the high-temperature superconductor and 0.1 eV for the low-temperature one. The explanation for the influence of the multiband structure on T_c is given in Chap. 3.

It is worth noting that all copper-oxide superconductors have a block character in their structure. The main block defining the metallic and superconductive properties of a compound is the plane with CuO_2 which contains the square lattice of copper ions coupled with one another through oxygen ions. Depending on the composition, the elementary cell of a high-temperature compound can have one, two, three or more cuprate layers. Moreover, the critical temperature of the superconducting transition has a nonmonotonous dependence on the number of cuprate layers.[46]

2.3.1 *Phase diagram of cuprate superconductors*

All electron properties of HTSCs depend strongly on the doping. HTSCs without doping are dielectrics and antiferromagnetics. As the concentration

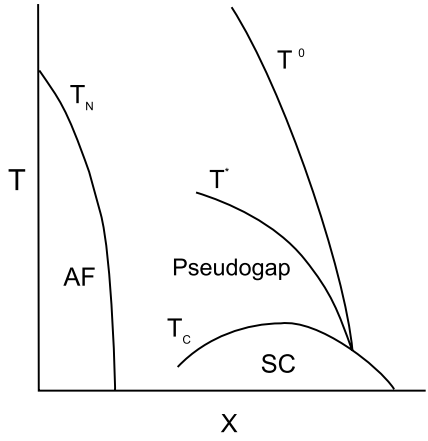

Fig. 2.6 Phase diagram of cuprate superconductors in the temperature-doping variables. T_N — the Néel temperature; T_c — the critical temperature of the superconducting transition; T^* — the characteristic temperature of a pseudogap; T^0 — the upper crossover temperature.

x increases, these materials become metals. Superconductivity arises at large x, behind the limits of the magnetically ordered phase. The experiments showed that the charge carriers have the hole character for all classes of HTSCs.

It has become clear recently that the high-temperature superconductivity is related to peculiarities of the behavior of these compounds in the normal phase. As seen from the phase diagram (Fig. 2.6), the superconducting states arise near the antiferromagnetic phase. In yttrium-containing systems, the antiferromagnetic and superconducting regions adjoin one another.

The experiments on the inelastic magnetic scattering of neutrons indicate the existence of strong magnetic fluctuations in the doped region, even beyond the limits of the antiferromagnetic phase. This points out the important role of antiferromagnetic fluctuations in the compounds with high-temperature superconductivity.

In HTSCs, the gap is present in the absence of the phase coherence, i.e. in nonsuperconducting specimens. This gap is called a pseudogap. A pseudogap is shown in Fig. 2.6. It appears at temperatures less than some characteristic temperature T^* which depends on the doping. Its nature has still not been completely explained. The study of a pseudogap in the electron spectrum of HTSCs was carried out in many works.[48]

Metals become superconductors if their free electrons are bound in Cooper's pairs. Moreover, the pairs are formed in such a way that their wave functions have the same phase. The phase coherence is responsible for the change of the resistance on the cooling below the critical temperature T_c. The presence of coupled pairs in a superconductor causes the appearance of a gap in the spectrum of excitations. In standard superconductors, the phase coherence of pairs appears simultaneously with the appearance of pairs. From one viewpoint, a pseudogap is related to the appearance of coupled pairs, which is not related to the phase coherence.

Another viewpoint consists the following. The pseudogap arises in HTSCs in connection with the formation of magnetic states which compete with superconducting states. The efforts of experimenters aimed at the resolution of this dilemma are complicated by a strong anisotropy of the superconductor gap. Some physicists believe that the most probable situation is related to the creation of the superconducting state with paired electrons at a certain doping which coexists with antiferromagnetism. It is possible that this is just the "new state of matter" which has been widely discussed in the last few years in connection with HTSCs.

2.3.1.1 *Antiferromagnetism of HTSCs*

An interesting peculiarity of copper-oxide compounds which has a universal character is the presence of the antiferromagnetic ordering of spins of Cu in the CuO_2 planes. The sufficiently strong indirect exchange interaction of spins of Cu induces the 3D long-range antiferromagnetic order with the relatively high Néel temperatures $T_N = 300$–$500\,\mathrm{K}$.[49] Though the long-range order disappears in the metallic (and superconducting) phase, strong fluctuations with a wide spectrum of excitations are conserved. This allows one to advance a number of hypotheses on the possibility of electron pairing in copper-oxide compounds through the magnetic degrees of freedom.

Therefore, the study of the antiferromagnetic properties of HTSCs is of importance for the verification of the hypotheses on the magnetic mechanism of superconductivity. The interaction of spins of Cu in a plane has a 2D character, and their small values, $S = 1/2$, lead to significant quantum fluctuations.

The first indications of the existence of antiferromagnetism in the copper-oxide compounds were obtained on the basis of macroscopic measurements of susceptibility. The detailed investigation of both the magnetic structure

and spin correlations in the metallic phase became possible only with the help of the neutron scattering.

2.4 Mechanisms of Pairing of HTSCs

To explain high-temperature superconductivity, a lot of models and mechanisms of this unique phenomenon have been proposed. The key question is the nature of the mechanism of pairing of carriers. There are many different models of superconductivity available, among which we mention the following: the magnon model, exciton model, model of resonant valence bonds, bipolaronic model, bisoliton model, anharmonic model, model of local pairs and plasmon model. We give a classification of the mechanisms of pairing of HTSCs, which is shown in Fig. 2.7, according to Ref. 50.

This classification demonstrates the diverse physical patterns of HTSCs. Apart from the ordinary BCS mechanism based on the electron–phonon interaction, there exist many other mechanisms, as was mentioned above. All these models use the concept of pairing with a subsequent formation of a Bose condensate at temperatures T_c irrespective of the nature of the resulting attraction.

2.4.1 *Specific mechanisms of pairing in superconductivity*

Consider the models most popular at present. Along with the ordinary BCS mechanism based on the electron–phonon interaction, we turn to the magnetic, exciton, plasmon and bipolaronic mechanisms of pairing. All these models apply the concept of pairing with the subsequent formation of a Bose condensate (at certain temperatures T_c) regardless of the reasons for the attraction.

The BCS theory presents the formula for the critical temperature T_c in the case of the weak electron–phonon interaction:

$$T_c = 1.14\Theta \exp\left(\frac{-1}{N_0 V}\right), \tag{2.1}$$

where $\Theta = \hbar\Omega_D/k_B$, $\hbar\Omega_D$ is the Debye energy, N_0 is the density of states of the Fermi level and V is the attractive pairing potential acting between electrons.

The maximum value of the critical temperature given by the BCS theory is 40 K. Thus, there arises the question about the other mechanisms of pairing. The interaction of electrons is repulsive, i.e. one needs to seek a

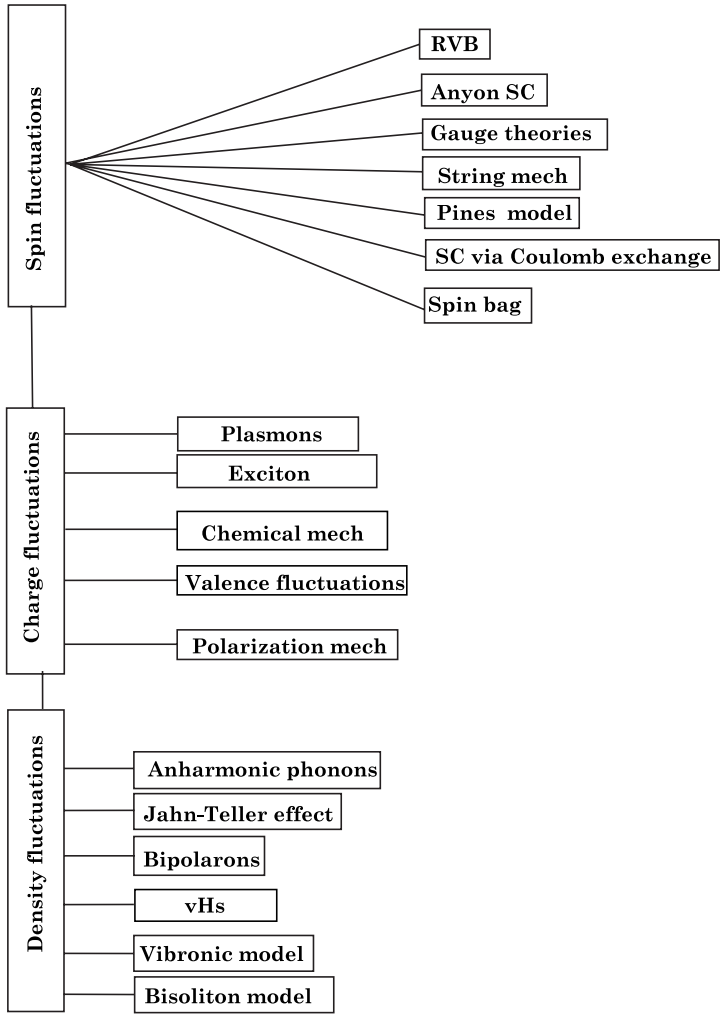

Fig. 2.7 Classification of the mechanisms of pairing of HTSCs.

"transfer system" in metals which is distinct from the phonon system. The general scheme for the interaction of electrons via a transfer system X can be presented as

$$\begin{cases} e_1 + X \to e_1^1 + X^*, \\ e_2 + X^* \to e_2^1 + X, \end{cases} \tag{2.2}$$

where e_i corresponds to an electron with momentum p_i, X is the ground state and X^* is the excited state of the transfer system.

As a result of this reaction, the system returns to the initial state, and the electrons make an exchange by momenta.

It can be shown that such an interaction leads to the attraction, and the critical temperature is given by the formula

$$T_c \sim \Delta E \exp\left(\frac{-1}{\lambda}\right),$$

where ΔE is the difference in energies of the states X and X^*, and λ depends on the interaction of electrons with the system X.[51]

2.4.2 *Magnetic mechanism of pairing*

The magnetic mechanism of pairing of HTSCs was examined by many researchers. These studies used the assumption that the pairing is realized due to the exchange by spin excitations — magnons, i.e. the transfer system is the system of spins in a magnetic metal. Magnon is a quasiparticle which is the quantum synonym of a spin wave of excitation in a magnetically ordered system. Great attention was attracted to the pioneering work by A. I. Akhiezer and I. Ya. Pomeranchuk.[52,53] They considered the interaction between conduction electrons caused by both the exchange by acoustic phonons and an additional interaction related to the exchange by spin waves (magnons). It was shown that superconductivity and ferromagnetism can coexist in the same spatial regions. At sufficiently low concentrations of the ferromagnetic component, an increase in its concentration leads to an increase of T_c in the case of the triplet pairing. Within the phonon mechanism, the pairing occurs in a singlet state; then an increase in the concentration of the ferromagnetic component induces a decrease of T_c. It is known that ferromagnetism competes with superconductivity. The different situation is characteristic of antiferromagnetism. HTSCs are antiferromagnetic dielectrics. As was mentioned above, they reveal strong magnetic fluctuations in the region of doping, which can be responsible for the pairing. In this chapter, we will consider the spin-fluctuation model of pairing.

After the discovery of HTSCs, a lot of relevant works dealt with the problem of the evolution of a system of Cu ions under the transition from the dielectric antiferromagnetic state to the metallic one.

It is also worth noting the model of resonance valence bonds (RVBs), which was advanced by Nobel Prize winner P. Anderson in 1987,[5] who made an attempt to explain the Cooper pairing in HTSCs by the participation of magnetic excitations. The Anderson model is based on the concept of magnetic ordering. The RVB mechanism ensures the joining of carriers in pairs with compensated spin — the so-called spinons. On

the doping of HTSC compounds, there arise holes which can form the complexes with spinons — holons. Superconductivity is explained by the pairing of holons, i.e. by the creation of spinless bosons with a double charge. That is to say, the pairing of carriers in the RVB model is realized due to the exchange by magnons. At low temperatures, the paired holons form a superconducting condensate. The RVB model has played a positive role, by attracting the attention of researchers to the study of antiferromagnetism in HTSCs, though spinons and holons have not been experimentally identified.

2.4.3 *Exciton mechanism of pairing*

According to the general principle concerning the "transfer system" in superconductors, the electron–phonon interaction should not be obligatorily realized. Some other interaction ensuring the pairing of electrons can be suitable. In principle, the mechanism of superconductivity can be switched on by bound electrons which interact with conduction electrons. The first exciton model, in which the pairing is realized due to electron excitations, was proposed by W. A. Little[54] for organic superconductors, and by V. L. Ginzburg and D. A. Kirzhnitz[40] for layered systems. In the construction of this model, it was necessary to assume the existence of two groups of electrons: one of them is related to the conduction band, where the superconducting pairing occurs due to the exchange by excitons which are excitations in the second group of almost-localized electrons. In view of the many-band character of the electron spectrum, layered structure and other peculiarities of the electron subsystem in HTSCs, such a distribution of electron states is quite possible. This underlies the development of a lot of exciton models. The search for superconductivity in organic materials was stimulated to a significant degree by the idea of Little about the possibility of high-temperature superconductivity due to the excitonic mechanism of the Cooper pairing of electrons in long conducting polymeric chains containing lateral molecular branches–polarizers. Since the mass M of such excitonic excitations is small, one would expect to observe a high value of the temperature, $T_c \sim M^{-1/2}$. But this model was not practically realized, since high-energy intramolecular excitonic excitations cannot ensure the binding of electrons in pairs.

At present, a number of quasi-one-dimensional organic superconductors with metallic conductance have been synthesized. They pass to the superconducting state at $T = 10\,\mathrm{K}$. Crystals of similar organic superconductors

consist of, as a rule, planar molecules packed in zigzag-like stacks which form chains. The good overlapping of electron wave functions of neighboring molecules in a stack ensures the metallic conductance along a chain. The overlapping of electron wave functions of neighboring chains is small, which leads to the quasi-one-dimensional character of the electron spectrum and to a strong anisotropy of electronic properties of a crystal. Up to now, no experimental proofs of the manifestation of the excitonic mechanism is such systems are available.

As an example of a laminar system, we mention a quasi-two-dimensional structure of the "sandwich" type (dielectric–metal–dielectric). In such a structure, the Cooper pairing of electrons in a metal film occurs due to the attraction caused by their interaction with excitons in the dielectric plates.

2.4.4 *Anharmonic model and superconductivity*

It is known that the appearance of superconductivity is often preceded by structural transformations in a crystal. These are usually explained within the anharmonic model. In the opinion of some researchers,[45] such structural transformations arising before the start of superconductivity decrease significantly the frequencies of phonons and subsequently increase the parameter of electron–phonon interaction. The softening of the phonon spectrum is caused by the great amplitudes of displacements of ions in the two-well potential which models the structural transformations. In some works,[49] the effect of a structural transformation on superconductivity in the limiting case of a weak pairing interaction and the isotropic gap was studied. The properties of high-temperature superconductivity were also studied within the model, where the superconductivity is enhanced due to the singularity of the density of electron states which appears at structural or antiferromagnetic phase transitions. The weak point of the models relating the superconductivity to structural phase transitions is due to a significant temperature interval between the known structural transitions and the temperature T_c. The works, where nonphonon pairing mechanisms are introduced, include the studies[49] which use the Hubbard Hamiltonian in systems, where only the interaction of the repulsive type is present. It is considered that the effect of pairing is caused by the kinematic interaction at a noncomplete occupation of Hubbard subbands. Unfortunately, no clear comprehension of the nature of the arising attraction has been attained in this case. It is possible that the bound state of quasiparticles is virtual, i.e. it decays. The search for new mechanisms of superconductivity caused by a strong correlation of

electrons in cuprate superconductors with quasi-two-dimensional electron structure has been reduced to a search for new, nonstandard ground states. We mention the polaron mechanism of pairing, which is related to the Jahn–Teller effect, well known in the quantum chemistry of complex compounds. The essence of the Jahn–Teller effect is that a nonlinear system in the presence of the electron degeneration deforms spontaneously its structure so that this degeneration disappears or decreases. The Jahn–Teller effect leads to rearrangement of the atomic orbitals of copper under conditions of the octahedral oxygen surroundings. A displacement of oxygen ions inside of an elementary cell which is caused by the appearance of a quasiparticle induces the displacement of equilibrium positions in the neighboring cells. In such a way, there arises the strong electron–phonon interaction of a quasiparticle with a local deformation.

2.4.5 *Van Hove singularities*

A van Hove singularity (vHs) in the density of states (DOS) $N(E)$ was proposed as a T_c-enhancement mechanism for intermetallic superconductors two decades ago. All cuprate superconductors possess two-dimensional elements of their structures. In the construction of the microscopic theory of high-temperature superconductivity, it is important to clarify the specific features of the dispersion $E(k)$ and the behavior of the DOS $N(E)$. For a two-dimensional problem ($n = 2; 2\mathrm{D}$), the DOS is independent of the energy, $N(E) = \text{const}$, and the band is dispersionless. The photoemission experiments indicate the existence of an almost-flat band near the Fermi surface for cuprate superconductors. The presence of a flat band and an isoenergetic surface in the form of an elongated saddle leads to the existence of vHs's in the DOS near the Fermi surface. In this model, in the calculations of T_c by the BCS formula, $N(E)$ is replaced by $N(E_F)$. The formula for T_c looks like

$$T_c = 1.14\Theta \exp\left(\frac{-1}{\lambda}\right), \tag{2.3}$$

where $\lambda = VN(E)$.

If the function $N(E)$ has the corresponding singularity at $E = E_F$, it will be related to the vHs. In the two-dimensional case, the presence of a logarithmic singularity of the DOS on the Brillouin zone boundary is possible:

$$N(E) \sim \ln\left|\frac{D}{E - E_F}\right|, \tag{2.4}$$

where D is the characteristic energy cutoff. Then T_c has the form

$$T_c \sim D \exp\left(\frac{-1}{\sqrt{\lambda}}\right). \tag{2.5}$$

We note that, in connection with the quasi-two-dimensionality of lattices of HTSCs, the hypothesis of anyonic superconductivity is of certain interest (Fig. 2.7). Anyons are quasiparticles with intermediate statistics (between the Bose and Fermi statistics) which can exist just in two-dimensional structures. The term "anyon" was introduced by F. Wilczek in the framework of the concept of supersymmetry.

2.4.6 *Plasmon mechanism of pairing*

Many works have been devoted to attempts at explaining high-temperature superconductivity on the basis of the idea of the pairing as a result of the exchange by quanta of longitudinal plasma waves — plasmons.

Longitudinal plasma waves are formed in solids in the region of frequencies, at which the dielectric permeability of the medium becomes zero. The characteristic frequency of plasma waves in 3D crystals is defined by the formula

$$\tilde{\omega}_p = \frac{4\pi e^2 N}{m}, \tag{2.6}$$

where N is the concentration of electrons, and e and m are their charge and mass, respectively. At the electron density $N \sim 1\text{–}3 \times 10^{22}\,\mathrm{cm}^{-3}$, the plasma frequency $\tilde{\omega}_p \sim 10^{15}\text{–}10^{16}$. We might assume that the exchange by plasmons, rather than by phonons, would induce an increase of the pre-exponential factor in the formula deduced in the BCS theory,

$$T_c = \Theta \exp\left(\frac{1}{\lambda - \mu^*}\right), \tag{2.7}$$

by 2–3 orders, if $\Theta = \hbar\tilde{\omega}_p/k_B$. However, such an increase does not cause a significant growth of T_c, because the plasmons at the frequency $\tilde{\omega}_p$, which is close to the frequency of electrons, $E_F/\hbar$, cannot cause the superconducting pairing and their role is important only for the dielectric properties of crystals.[44]

2.4.7 *Bipolaronic mechanism of superconductivity*

One of the attempts to explain the phenomenon of high-temperature superconductivity is called the bipolaronic theory. Bipolarons are Bose particles like the ordinary Cooper pairs.

In the theory of bipolarons, the superconductivity is caused by the superfluidity of the Bose condensate of bipolarons.

The ideas of polarons and bipolarons were used by A. S. Aleksandrov and J. Ranninger[55] to clarify high-temperature superconductivity.

The idea of a polaron is based on the assumption about the autolocalization of an electron in the ion crystal due to its interaction with longitudinal optical vibrations under the local polarization, which is caused by the electron itself. The electron is confined to the local-polarization-induced potential well and conserves it by its own field. The idea of autolocalization of electrons in ion crystals was intensively developed by S. I. Pekar.[56]

The efficiency of the interaction of an electron with mass m and charge e with long-wave longitudinal optical vibrations with frequency Ω in the medium is characterized by the dimensionless parameter

$$g = \frac{e^2}{\tilde{\varepsilon}} \sqrt{\frac{m}{2\Omega\hbar^2}}, \tag{2.8}$$

introduced by H. Fröhlich. Here, $\tilde{\varepsilon}$ is the dielectric permeability of the inertial polarization. The interaction is assumed to be small if $g < 1$. Due to a high frequency, Ω, the deformation field is a faster subsystem. Therefore, it has time to follow the movement of an electron. This field accompanies the movement of the electron in the form of a weak cloud of phonons. The energy of interaction of the field and the electron is proportional to the first degree of g.

In the BCS theory, the pairing of conduction electrons is realized due to the interaction with acoustic phonons and is characterized by the dimensionless constant of interaction

$$\lambda = VN(E_F), \tag{2.9}$$

where $N(E_F)$ is the density of energy states of electrons on the Fermi surface, and the quantity V is inversely proportional to the coefficient of elasticity of a crystal.

In the bipolaronic model, we have the parameter

$$\lambda^* = \frac{2\lambda^2\hbar\Omega z - V_c}{D}, \tag{2.10}$$

where λ is defined by the relation (2.9), z is the number of nearest neighbors and D is the width of the conduction band of free quasiparticles.

A bipolaron, like a Cooper pair, has charge $2e$, and its effective mass is determined by the formula

$$\tilde{m} \approx m\frac{\triangle}{D}\exp(\lambda^2). \tag{2.11}$$

The effective mass $\tilde{m}$ can be very high and can exceed the mass of a free quasiparticle in the conduction band by several orders.

To calculate the superconducting transition temperature T_c which corresponds to the Bose condensation, the authors applied the formula for the ideal Bose gas:

$$k_B T_c = \frac{3.31\hbar^2 N^{2/3}}{\tilde{m}}. \tag{2.12}$$

At $\tilde{m} = 100$ and $N = 10^{21}\,\mathrm{cm}^{-3}$, this formula yields $T_c \sim 28$ K.

Analogously to the bipolaronic model, the bisoliton mechanism of high-temperature superconductivity was proposed in Ref. 45 and 46.

2.5 Symmetry of Pairing in Cuprate Superconductors

Of great importance for HTSCs is the pairing symmetry or the symmetry of the order parameter. This question was considered at many conferences and seminars all over the world. Several NATO seminars and conferences on this trend were held in Ukraine in the town of Yalta, organized by one of the authors of this book.[57–60]

The development of the microscopic theory of superconductivity was followed by interest in the question about the nontrivial superconductivity corresponding to the Cooper pairing with nonzero orbital moment.

The system, in which the nontrivial pairing was first discovered, is He^3. To explain this phenomenon, it was necessary to introduce a supplementary mechanism of pairing due to spin fluctuations.

2.5.1 *The superconductor's order parameter*

Most physical properties depend on the properties of the symmetry of a superconductor's order parameter, which is defined by the formula

$$\Delta_{\alpha\beta}(\mathbf{k}) = \langle a_{\alpha\mathbf{k}} a_{\beta-\mathbf{k}\alpha} \rangle. \tag{2.13}$$

The problem of pairing symmetry is a problem of the pairing of charged fermions into states with the final orbital moment.

As usual, both the standard pairing called the s pairing and the non-standard d pairing are considered. They differ by the orbital moment of the pair: in the first and second cases, the moments are $L = 0$ and $L = 2$, respectively.

We also note that the continuous symmetry group in crystals is broken, and it is necessary to speak not about the orbital moment, but about the irreducible representations, by which the order parameter is classified. We will consider this question in the following subsection.

Usually, the standard pairing and the nonstandard pairing are distinguished. For the nonstandard pairing, the symmetry of the order parameter is lower than that of a crystal.

For a two-dimensional tetragonal crystal (square lattices), the possible symmetries of the superconductor's order parameter were enumerated by M. Sigrist and T. M. Rice[61] on the basis of the theory of group representations. The basis functions of relevant irreducible representations define the possible dependence of the order parameter on the wave vector.

It is worth noting that the anisotropic pairing with the orbital moment $L = 2$, i.e. $d_{x^2-y^2}$, has the following functional form in the k space:

$$\Delta(\mathbf{k}) = \mathbf{\Delta}_o[\cos(\mathbf{k_x a}) - \cos(\mathbf{k_y a})], \tag{2.14}$$

where Δ_o is the maximum value of the gap, and a is the lattice constant. The gap is strongly anisotropic along the direction (110) in the k space. In this case, the order parameter sign is changed in the directions along k_x and k_y.

Apart from the d symmetry, it is worth considering also the s symmetry, for which we can choose two collections of basis functions:

$$\Delta(\mathbf{k}) = \mathbf{\Delta_o}. \tag{2.15}$$

The anisotropic s pairing is considered as well. This form of pairing is analyzed in works by P. W. Anderson[5] and coworkers who have studied the mechanism of pairing on the basis of the tunneling of electrons between layers. In these states, the order parameter sign is invariable, and its amplitude is varied along the direction (110):

$$[\text{anisotropic } s]\Delta(k) = \Delta_o[\cos(k_x a) - \cos(k_y a)]^4 + \Delta_1, \tag{2.16}$$

where Δ_1 corresponds to the minimum along the direction (110).

It follows from the symmetry-based reasoning that the mixed states with various symmetries can be realized. We mention the states which are mostly in use. The "extended" s-coupled states were considered in works by D. J. Scalapino.[63] A possible functional form of these states is as follows:

$$[\text{extended } s \text{ wave}]\,\Delta(k) = \Delta_o\{(1+\gamma^2)[\cos(k_x a) - \cos(k_y a)]^2 - \gamma^2\}. \tag{2.17}$$

They have eight parts with alternating signs, and eight nodes which are split by $\pm\gamma\pi/2$ along the direction (110). G. Kotliar and coworkers used mixed $s + id$ states[63]:

$$[s + id]\,\Delta(k) = \Delta_o[\varepsilon + i(1-\varepsilon)[\cos(k_x a) - \cos(k_y a)]]. \tag{2.18}$$

R. B. Laughlin[62] analyzed the mixed states $d_{x^2+y^2} + id_{xy}$ on the basis of the anyonic mechanism of pairing:

$$\begin{aligned}[d + id]\,\Delta(k) = \Delta_o[&(1-\varepsilon)[\cos(k_x a) - \cos(k_y a)] \\ &+ i\varepsilon[2\sin(k_x a)\sin(k_y a)]],\end{aligned} \tag{2.19}$$

where ε is the share of s or d_{xy} states mixed with the $d_{x^2+y^2}$ states, and $\varepsilon\Delta_o$ is the minimum value of the energy gap. These mixed states are of interest because they are not invariant with respect to the inversion in the time. The value and phase of the superconductor's order parameter, as functions of the direction in cuprate planes CuO_2, are given in Fig. 2.8 for various kinds of pairing symmetry.

2.5.2 *Classification of the superconductor's order parameter by the representations of symmetry groups*

It should be noted that there is no classification of states by the orbital moment for crystals. The general theory of nonstandard pairing has been developed on the basis of the analysis of point symmetry groups.

J. Annett was one of the first to classify superconducting states by the irreducible representations of groups for HTSCs.[64] As for superconductors with heavy fermions, the group analysis was carried out in Ref. 65.

Of importance is the question whether the symmetry of the order parameter in HTSCs is lower than the symmetry of the crystal lattice.

The order parameter can be represented as a linear combination:

$$\Delta_k = \sum \eta_{\Gamma_i}\ f_{\Gamma_i}(k), \tag{2.20}$$

where η_{Γ_i} is the irreducible representation of groups, by which the order parameter is transformed, $f_{\Gamma_i}(k)$ is the basis function of the irreducible representation; A_{1g} corresponds to the anisotropic s symmetry; and B_{1g} corresponds to the d pairing.

An analogous decomposition of the superconducting order parameter was performed for a superconductor with heavy fermions:

$$UPt_3.$$

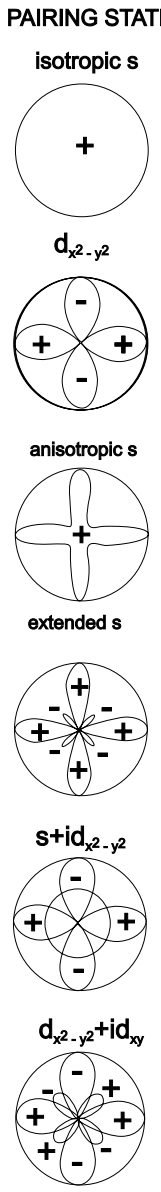

Fig. 2.8 Types of pairing symmetries which are considered for HTSCs.

The symmetric states of the system can be presented by the indication of all possible subgroups of the full group, relative to which the order parameter is invariant.[66] The full symmetry group of a crystal includes a point symmetry group G, operations of inversion of the time R, and the group of calibration

transformations $U(1)$. That is to say, we have the following partition into subgroups:

$$G \times R \times U(1). \tag{2.21}$$

The La- and Y-based superconductors which have the tetragonal symmetry of crystal lattices, i.e. $G = D_{4h} = D_4 \times I$,[58] are most-studied. In the Y-based compounds, one observes small orthorhombic distortions of a crystal lattice.

Group D_{4h} includes the operations of rotations C_n, around the z axis by angles of $\pi n/2$, and rotations U_n by angles of π:

$$x \cos\left(\frac{\pi n}{2}\right) + y \cos\left(\frac{\pi n}{2}\right), \tag{2.22}$$

where $n = 0, 1, 2, 3$ have five reducible representations: four one-dimensional $(\mathrm{A}_{1g}, \mathrm{A}_{2g}, \mathrm{B}_{1g}, \mathrm{B}_{2g})$ and one two-dimensional (E).

2.6 Experimental Studies of the Symmetry of the Superconducting Order Parameter

At present, the results of three groups of experiments, in which the symmetry of the order parameter is revealed, are available.

The first group joins different low-temperature characteristics of superconductors, such as the Knight shift, the rate of relaxation in NMR, the temperature dependence of the heat capacity, and the penetration depth.

If the superconductor's order parameter has zeros on different areas of the Fermi surface (as in the case of the $d_{x^2-y^2}$ symmetry), the mentioned quantities will have the power temperature dependence, rather than the exponential one.

The second group of experiments is based on the direct measurement of the phase of the order parameter with the help of interference phenomena on Josephson junctions in a magnetic field.

The third group deals with the direct measurements of a value of the gap by means of spectroscopic experiments. Here, the most interesting results are presented by photoemission spectroscopy with angle resolution, as well as Raman and neutron spectroscopies.

2.6.1 *Measurements of the Josephson tunnel current*

The most definite information about a symmetry of the superconducting order parameter can be obtained from the studies of the phase of the order

parameter, in which the critical current in Josephson junctions positioned in a magnetic field is measured. The critical current for a rectangular Josephson junction oscillates with the field by the Fraunhofer diffraction law:

$$I_c(\Phi) = J_0 A \frac{\sin(\pi\Phi/\Phi_0)}{\pi\Phi/\Phi_0}, \tag{2.23}$$

where Φ is the magnetic flux through the junction, Φ_0 is the quantum flux, J_0 is the density of the critical current in the zero field, and A is the junction area. A diffraction pattern is shown in Fig. 2.9(a). Let us consider the superconductor YBCO, which possesses the tetragonal symmetry. Let its axis be oriented normally to the plane of the figure, and its edges to be perpendicular to the axes $\mathcal{A}$ and $\mathcal{B}$ of the base plane. In the tunnel junction with corner geometry, another superconductor is applied to both edges which are perpendicular to $\mathcal{A}$ and $\mathcal{B}$ and, are joined with each other [Figs. 2.9(b) and 2.9(c)].

This experiment can be compared to that involving a two-junction SQUID, in which there occurs a superposition of tunnel currents produced by electrons with wave vectors k_x and k_y, so that the resulting diffraction pattern depends on the symmetry of the order parameter of a superconductor under study. For the s symmetry, the order parameter on both edges of the corner junction is the same, and the resulting diffraction pattern will be similar to the case of the standard junction. But, in the case of d symmetry, the order parameter on the corner junction edges has different signs, and this changes the diffraction pattern.

The total current is illustrated in Fig. 2.10(c). In the zero field, the critical current turns out to be zero due to the mutual compensation of its two components.

In the symmetric contact, the dependence on the field is determined by the formula[67]

$$I_c(\Phi) = J_0 A \frac{\sin^2(\pi\Phi/2\Phi_0)}{\pi\Phi/2\Phi_0}, \tag{2.24}$$

corresponding to the pattern in Fig. 2.10(c).

Thus, by the difference of a diffraction pattern from both the standard one and that corresponding to the corner Josephson junction, we can predict the symmetry of the order parameter. In Ref. 67, a similar experiment was carried out on the tunnel junction YBCO–Au–Pb. The results presented in Fig. 2.10 testify to the d symmetry of the order parameter in superconducting YBCO.

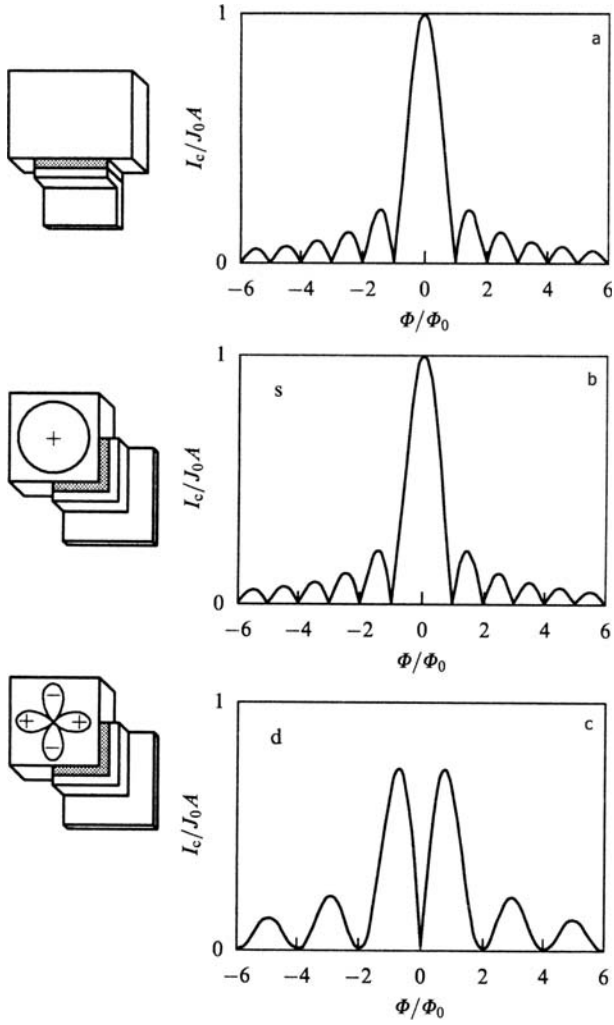

Fig. 2.9 Critical current in a Josephson junction vs the applied magnetic field: (a) standard tunnel contact, (b) corner tunnel junction for a superconductor with the *s* symmetry of the order parameter, (c) corner tunnel junction for a superconductor with the *d* symmetry of the order parameter.[67]

All the above-mentioned experiments with Josephson junctions were performed with a single crystal $YBa_2Cu_3O_6$.

2.6.2 *Measurements of the quantization of a flow by the technique of the three-crystal unit*

Another type of experiment on the determination of a symmetry of the order parameter is based on the measurement of a flow quantum in a

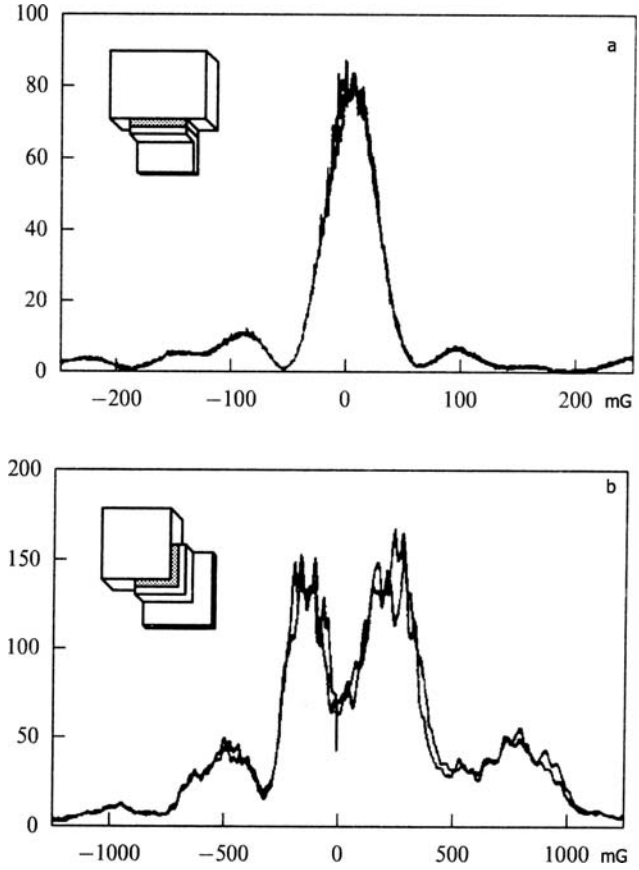

Fig. 2.10 Critical current as a function of the magnetic field in a Josephson junction YBCO-Au-Pb in two geometries: (a) standard and (b) corner.[67]

superconducting ring fabricated from three superconducting single crystals of yttrium with different orientations.

The idea of such an experiment is based on the theoretical result obtained by M. Sigrist and T. M. Rice[61]: for superconductors with the d symmetry, the tunnel current between two superconducting crystals separated by a thin boundary depends on the orientation of the order parameter with respect to the interface. The current between the superconductors with numbers ij is given by the formula

$$I_s^{ij} = (A^{ij} \cos 2\theta_i \cos 2\theta_j) \sin \Delta\Phi_{ij}. \tag{2.25}$$

Here, A^{ij} is the constant which characterizes the junction of ij; θ_i and θ_j are the angles of the crystallographic axes with the boundary plane; and Φ_{ij} is the difference of phases of the order parameters on both sides

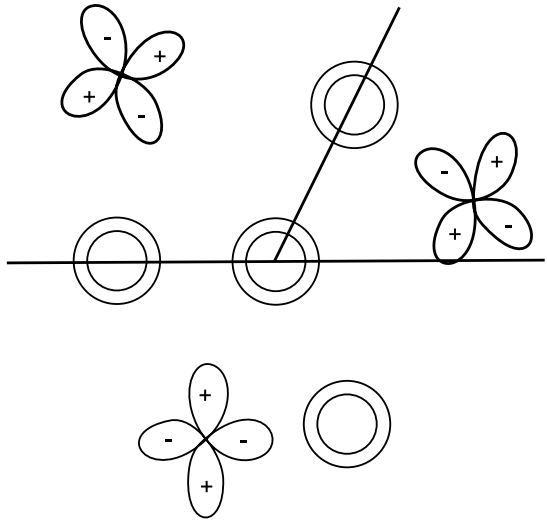

Fig. 2.11 Scheme of the experiment on the measurement of a half-integer number of quanta of the flow captured by a superconducting ring with three Josephson junctions with the d symmetry of the order parameter.[34]

of the boundary. It was shown that a spontaneous magnetization, which corresponds to the flow equal to a half of Φ_0, appears in a superconducting ring with a single Josephson junction with the phase difference π. If the ring has an odd number of π junctions, the result is the same. The direct measurement of a half-quantum of the flow through such a ring would testify to the d symmetry of the order parameter. The direct measurement of a half-quantum of the flow was realized in Ref. 68. A scheme of the experiment is shown in Fig. 2.11.

2.7 Thermodynamics of the *d* Pairing in Cuprate Superconductors

2.7.1 *Introduction*

The basic question of the theory of superconductivity concerns the mechanism ensuring the pairing of electrons. In the BCS theory, it is the electron–phonon interaction. Some recent theoretical models postulate the mechanism of antiferromagnetic spin fluctuations,[69–75] so that the electron scattering on them can be the reason for the pairing of electrons. Spin fluctuations play an important role in superconductors with heavy fermions.[72,73] The authors of Refs. 64 and 65 performed calculations of a value of the

superconductor gap, the critical temperature, the temperature dependence of the resistance, and many other quantities, but the thermodynamics was not considered. For this reason, it is of interest to calculate the thermodynamics of antiferromagnetic spin fluctuations, namely the temperature dependence of the heat capacity, its jump near T_c, and the parameter $R = \Delta C/\gamma T_c$ equal to 1.42 by the BCS theory.

The purpose of this section is the calculation of the thermodynamics of antiferromagnetic spin fluctuations, namely the electron heat capacity and the jump of the heat capacity.

The thermodynamics of superconductors at low temperatures is determined by the excitation of two quasiparticles. In the traditional superconductors with pairing of the BCS type, the energy gap is isotropic (s pairing), and the temperature dependence of the heat capacity has the exponential form $\sim \exp^{-\Delta/k_B T}$, where Δ is the superconductor's gap. In the superconductors with anisotropic pairing, the temperature dependence of the heat capacity has a power character, namely T^n. The appearance of such temperature dependences is related to the fact that the superconductor's gap has zeros on the Fermi surface.

As was noted above, the anisotropic pairing with the orbital moment $L = 2$, i.e. with the $d_{x^2-y^2}$ symmetry, has the following functional form in the k space:

$$\Delta(\mathbf{k}) = \mathbf{\Delta_o}[\cos(\mathbf{k_x a}) - \cos(\mathbf{k_y a})], \tag{2.26}$$

where Δ_o is the maximum value of the gap and a is the lattice constant.

The gap is strongly anisotropic in the direction (110) in the k space, and the sign of the order parameter is changed along the directions k_x and k_y.

The main results of this section have been published in Refs. 78–81.

2.7.2 *Antiferromagnetic spin fluctuations in HTSCs*

For the first time, the idea of the possibility of electron pairing through spin fluctuations was advanced by A. I. Akhiezer and I. Ya. Pomeranchuk.[81] They showed that the indirect interaction of electrons through spin waves in a ferromagnetic metal has the character of attraction in the triplet state and hence, can lead to triplet pairing. Consider some experiments and facts on antiferromagnetic spin fluctuations.

The basis for the hypothesis on the spin-fluctuation mechanism of pairing consists in the fact that the stoichiometric compounds La_2CuO_4 and

$YBa_2Cu_3O_6$ are antiferromagnetic dielectrics. The doping of superconductors leads to the appearance of the metallic state and superconductivity. The closeness of HTSCs to the antiferromagnetic transition with the wave vector $Q = (\pi/a, \pi/a)$ defines the important role of spin fluctuations, interaction with which forms the quasiparticle spectrum of electrons and can simultaneously result in the Cooper pairing.

HTSCs are referred to the class of strongly correlated systems which are theoretically studied in the frame of the Hubbard model. This model describes the hops of electrons in the lattice with the matrix element t for the nearest neighbors with regard to the Coulomb repulsion U, when the electrons are positioned at the same site. The model is set by the Hamiltonian

$$H = -t \sum_{i,j,\sigma} C^{\dagger}_{i\sigma} C_{j\sigma} + U \sum_{i,} n_{i\uparrow} n_{i\downarrow}, \tag{2.27}$$

where $C^{\dagger}_{i\sigma}(C_{j\sigma})$ is the operator of creation (annihilation) of an electron at the site i with spin σ, and $n_{i\uparrow} = C^{\dagger}_{i\sigma} C_{j\sigma}$ is the number of electrons at the site. In the given region of the parameters t, U and n (the electron concentration), the appearance of magnetically ordered phases is possible. Near the boundary of the existence of such a phase from the side of the paramagnetic region, strong fluctuations of the magnetic order parameter, i.e. paramagnons, must be manifested.

In the two-dimensional system of CuO layers in cuprate superconductors, the electron spectrum is presented by the formula

$$\varepsilon(t) = -2t \cos k_x a + \cos k_y a), \tag{2.28}$$

and the chemical potential μ is determined by the given electron concentration n. On the half-filling ($n = 1$), this spectrum has the nesting at the wave vector $q = Q$, which induces a sharp peak in the spin susceptibility near this point. This means an instability of the system relative to the formation of the antiferromagnetic state with the wave vector Q and the intensification of spin fluctuations near the point of the magnetic phase transition.

Near the half-filling, when the system is really antiferromagnetically unstable, the numerical calculations indicate that the superconducting order parameter has d symmetry, i.e. the gap depends on the wave vector by the relation (2.26).

The gap (2.26) is an alternating function of the wave vector (Fig. 2.12) and has zero values on the diagonals.

Figure 2.12 shows that the wave function of a Cooper pair is equal to zero just on the diagonals of the square. Therefore, the repulsive interaction on these diagonals does not act on the pair, and a Cooper pair with the

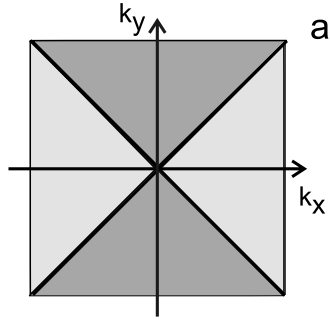

Fig. 2.12 Distribution of signs of the gap function in the limits of the Brillouin first band.

d symmetry survives even at large values of U. The superconductors with the d pairing should have a number of particular properties which can be observed in experiments. Many of these peculiarities are related to the zeros of the order parameter. The quasiparticle spectrum at low temperatures must give the power contribution to the thermodynamic properties, such as the heat capacity, parameters of NMR, and the penetration depth of a magnetic field, rather than the exponential one as in ordinary isotropic superconductors.

The observation of such power contributions will indicate the presence of a nontrivial order parameter with zeros on the Fermi surface. The totality of experimental data for various HTSCs indicates the certain realization of the anisotropic order parameter in them and, with a high probability, with the d symmetry. The last circumstances present the important argument in favor of the spin-fluctuation mechanisms of HTSCs. One of them was intensively developed by Pines and his coworkers,[69,71] who used a phenomenological form of the magnetic susceptibility with the parameters determined from the experiments on cuprates.

Let us consider this model in more detail. We introduce a Hamiltonian which involves antiferromagnetic spin fluctuations, as was done in works by Pines[69,70]:

$$H = H_0 + H_{\text{int}}, \tag{2.29}$$

where H_0 is the Hamiltonian of free electrons. The interaction is described by the Hamiltonian

$$H_{\text{int}} = \frac{1}{\Omega} \sum_q g(q) s(q) S(-q), \tag{2.30}$$

where Ω is the cell volume and $g(q)$ the interaction constant;

$$s(q) = \frac{1}{2} \sum_{\alpha,\beta,k} \Psi^{+}_{k+q} \sigma_{\alpha\beta} \Psi_{k\beta} \tag{2.31}$$

where $s(q)$ is the operator of spin density, $\sigma_{\alpha\beta}$ is the Pauli matrix, $\Psi^{+}_{k+q,\alpha}$ is the operator of creation of an electron with the momentum $k+q$ and the spin projection α, $\Psi_{k\beta}$ is the operator of creation of a hole with the momentum k and the spin projection β, and $S(-q)$ is the operator of spin fluctuations, whose properties are set by the correlator $\chi(q,\omega)$[69,70];

$\chi_{ij}(\mathbf{n},\mathbf{m})$ the spin susceptibility which is modeled by

$$\chi(q,\omega) = \frac{\chi_Q}{1 + \xi^2 (q-Q)^2 - i\omega/\omega_{\mathrm{SF}}}, \tag{2.32}$$
$$q_x > 0, \quad q_y > 0,$$

where χ_Q is the static spin susceptibility with the wave vector $Q = (\pi/a, \pi/a)$, ξ is the temperature-dependent antiferromagnetic correlation length, and ω_{SF} is the characteristic frequency of spin fluctuations of the paramagnon energy. All parameters are taken from experiments, including the data from NMR studies.[69] In this case, the interaction constant is a free parameter of the theory. It can be determined by calculating some quantity with the help of the Hamiltonian and by comparing the result with experiments.

We now define the quantities χ_Q and ω_{SF} as

$$\chi_Q = \chi_0 \left(\frac{\xi}{a}\right)^2 \beta^{1/2}, \tag{2.33}$$

$$\omega_{\mathrm{SF}} = \frac{\Gamma}{(\pi(\xi/a)^2 \beta^{1/2})}, \tag{2.34}$$

where χ_0 is the experimentally measured long-wave limit of the spin susceptibility, $\beta = \pi^2$, and Γ is the energy constant. The NMR data for the compounds yield $\xi(T_c) = 2.3a$, $\omega_{\mathrm{SF}} = 8\,\mathrm{meV}$, $\Gamma = 0.4\,\mathrm{meV}$.

It is foreseen that the phenomenological Hamiltonian will give a self-consistent description of the spin dynamics of the system in the sense that the spin susceptibility calculated with its help (through the characteristics of a quasiparticle spectrum, which themselves depend on the susceptibility) will agree with values determined by the formula (2.32).

2.7.3 *Continual model of antiferromagnetic spin fluctuations*

The authors of Refs. 78–81 proposed a continual model for the spin-fluctuation mechanism of pairing which allows one to efficiently solve the problem of thermodynamics for this mechanism.

Let us consider this model in more detail. We calculate the thermodynamics which is set by the Pines spin-fluctuation Hamiltonian. We write the Hamiltonian in the lattice representation

$$H = H_0 + H_{\text{int}}, \tag{2.35}$$

$$H = -t\sum_{\mathbf{n},\mathbf{p}} \psi_\alpha^+(\mathbf{n})\psi_\alpha(\mathbf{n}+\mathbf{p}) + \frac{1}{2}\sum_{\mathbf{n},\mathbf{m}} S_i(\mathbf{n})\chi_{ij}^{-1}(\mathbf{n},\mathbf{m})S_j(\mathbf{m}) + g\sum_{\mathbf{n}} \psi_\alpha^+(\mathbf{n})\left(\frac{\sigma_i}{2}\right)_{\alpha\beta}\psi_\beta(\mathbf{n})S_i(\mathbf{n}), \tag{2.36}$$

$$H_0 = -t\sum_{\mathbf{n},\mathbf{p}} \psi_\alpha^+(\mathbf{n})\psi_\alpha(\mathbf{n}+\mathbf{p}) + \frac{1}{2}\sum_{\mathbf{n},\mathbf{m}} S_i(\mathbf{n})\chi_{ij}^{-1}(\mathbf{n},\mathbf{m})S_j(\mathbf{m}), \tag{2.37}$$

$$H_{\text{int}} = g\sum_{\mathbf{n}} \psi_\alpha^+(\mathbf{n})\left(\frac{\sigma_i}{2}\right)_{\alpha\beta}\psi_\beta(\mathbf{n})S_i(\mathbf{n}), \tag{2.38}$$

where the sum is taken over all the sites of the infinite lattice (the lattice constant is equal to a), $\boldsymbol{\rho}$ is the unit vector joining the neighboring sites, S_i is the spin operator, $N = \sum_{\mathbf{n}} \psi_\alpha^+(\mathbf{n})\psi_\alpha(\mathbf{n})$ is the operator of the number of particles, t is the half-width of the conduction band[69,70] and $\chi_{ij}(\mathbf{n},\mathbf{m})$ is the spin correlation function.

It is necessary to calculate the grand partition function:

$$\exp\{-\beta\Omega(\mu,\beta,g)\} \equiv \operatorname{Tr}\exp\{-\beta(H-\mu N)\}, \tag{2.39}$$

$$\beta = \frac{1}{kT},$$

where μ is the chemical potential, g is the coupling constant and $\Omega(\mu,\beta,q)$ is the thermodynamic potential.

It is convenient to use the formalism of continual integration for a system of Fermi particles. The method of functional integration, i.e. the integration in the space of functions, was proposed by N. Wiener in 1925, but the physicists paid no attention to this method. Continual integrals were introduced into physics by R. Feynman[4] in the 1940s and were used for the reformulation of quantum mechanics. Continual integration is one of the most powerful methods of contemporary theoretical physics, allowing one to simplify, accelerate and clarify the process of analytic calculations. The

application of this method to a system with an infinite number of degrees of freedom enables one to develop, in such a way, the diagram theory of perturbations.

The grand partition function can be written in the form of a continual integral[83]:

$$\exp -\beta\Omega = N \int \prod_{\mathbf{n}} dS_i(n) d\psi_\alpha^+(n,\tau) d\psi_\alpha(n,\tau) \exp\left\{ - \int_0^\beta d\tau L(\tau) \right\}, \quad (2.40)$$

with

$$\begin{aligned} L(\tau) = & \sum_{\mathbf{n}} \psi_\alpha^+(\mathbf{n},\tau) \left(\frac{\partial}{\partial\tau} - \mu \right) \psi_\alpha(\mathbf{n},\tau) - t \sum_{\mathbf{n},\mathbf{p}} \psi_\alpha^+(\mathbf{n},\tau)\psi_\alpha(\mathbf{n}+\mathbf{p},\tau) \\ & + g \sum_{\mathbf{n}} \psi_\alpha^+(\mathbf{n},\tau) \left(\frac{\sigma_i}{2} \right)_{\alpha,\beta} \psi_\beta(\mathbf{n},\tau) S_i(\mathbf{n},\tau) \\ & + \frac{1}{2} \sum_{\mathbf{n},\mathbf{m}} S_i(\mathbf{n},\tau) \chi_{ij}^{-1}(\mathbf{n},\mathbf{m},\tau) S_j(m,\tau), \end{aligned} \quad (2.41)$$

where $L(\tau)$ is the Lagrangian of the system, and N is the normalizing factor:

$$N^{-1} = \int \prod_{\mathbf{n}} dS_i(n)\, d\psi_\alpha^+(n,\tau)\, d\psi_\alpha(n,\tau) \exp\left\{ - \int_0^\beta d\tau L(\tau, \mu = g = 0) \right\}. \quad (2.42)$$

We will use the matrix formalism to construct the theory of perturbations for the Green functions. It is convenient to introduce a four-component bispinor (Majorana):

$$\Psi = \begin{pmatrix} \psi \\ -\sigma_2 \psi^* \end{pmatrix}, \quad (2.43)$$

$$\psi = \begin{pmatrix} \psi_1 \\ \psi_2 \end{pmatrix},$$

where σ_1 are the Pauli spin matrices. The Majorana spinor is a Weyl spinor written in the four-component form.

Now, we can write L in the form

$$\begin{aligned} L = & \frac{1}{2} \sum_{\mathbf{n},\mathbf{p}} \mathbf{\Psi}(\mathbf{n},\tau) \left[\left(\Gamma^0 \frac{\partial}{\partial\tau} - \Gamma^0\Gamma_5\mu \right) \hat{\delta} - t(\tau - \hat{\delta}) \Gamma^0\Gamma_5 \right] \quad (2.44) \\ & \times \psi(\mathbf{n}+\mathbf{p},\tau) + \frac{g}{4} \sum_{\mathbf{n}} \mathbf{\Psi}(\mathbf{n},\tau) \Gamma^i \Gamma_5 \Psi(\mathbf{n},\tau) S^i(\mathbf{n},\tau) \\ & + \frac{1}{2} \sum_{\mathbf{n},\mathbf{m}} S_i(\mathbf{n},\tau) \chi_{ij}^{-1}(\mathbf{n},\mathbf{m},\tau) S_j(\mathbf{m},\tau), \end{aligned} \quad (2.45)$$

with

$$\Gamma^0 = \begin{pmatrix} 0 & I \\ I & 0 \end{pmatrix}, \tag{2.46}$$

$$\Gamma^i = \begin{pmatrix} 0 & -\sigma_i \\ \sigma_i & 0 \end{pmatrix},$$

$$I = \begin{pmatrix} 1 & 0 \\ 0 & 1 \end{pmatrix},$$

where Γ^i are the Dirac gamma matrices, $\bar{\Psi} \equiv \Psi^+\Gamma^0$, $\widehat{\delta} = \delta_{\mathbf{n},\mathbf{n}+\mathbf{p}}$, and Γ^i are given in the chiral representation.

There exists a connection between Ψ and $\bar{\Psi} : \Psi = C\bar{\Psi}^T$, where C is the matrix of charge conjugation, $C = \Gamma^0\Gamma^2$, $C^T = -C$. In terms of Ψ, the partition function takes the form

$$e^{-\beta\Omega} = N \int \prod n\, dS_i(n,\tau)\, d\Psi(n,\tau) e^{-\int_0^\beta d\tau L(\tau)}. \tag{2.47}$$

We now use the method of bilocal operators[84] to calculate the grand partition function. In this way, we obtain the Schwinger–Dyson equation and the equation of free energy. The details of calculations can be found in Refs. 78–81.

In order to calculate Ω, we introduce a source of the bilocal operator[84]:

$$e^{-\beta\Omega(J)} = N \int dS\, d\Psi e - \int_0^\beta d\tau \Bigg[L(\tau) \tag{2.48}$$

$$+ \frac{1}{2} \sum_{\mathbf{n},\mathbf{m}} \int_0^\beta \bar{\Psi}(\mathbf{n},\tau) J(\mathbf{m},\mathbf{n},\tau,\tau') \Psi(\mathbf{m},\tau') \Bigg].$$

The full Green fermion function is determined by the formula

$$G_{nm}(J) = e^{\beta\Omega(J)} \int dS\, d\Psi\, \Psi(n,\tau)\bar{\Psi}(m,\tau') \exp\{\cdots\} \tag{2.49}$$

$$= \langle 0|T\Psi(n,\tau)\bar{\Psi}(m,\tau')|0\rangle.$$

Let us write the Schwinger–Dyson equation for the Green function G, by using the method of the bilocal operator[81]:

$$\frac{\delta F}{\delta G} = 0, \tag{2.50}$$

$$F(G) = \beta\Omega(J = 0). \tag{2.51}$$

First, we consider the case of a free system. By integrating over the fermion fields in the functional integral, we obtain

$$F_0 = \beta\Omega(J) = -\frac{1}{2}\mathrm{Tr}\,\mathrm{Ln}(G_0^{-1} - \Gamma^0\Gamma_5\mu + J) + \frac{1}{2}\mathrm{Tr}\,\mathrm{Ln}\,G_0^{-1}, \quad (2.52)$$

$$G_0 = \left[\Gamma^0\frac{\partial}{\partial\tau} - t(1-\hat{\delta})\Gamma^0\Gamma_5\right]^{-1}. \quad (2.53)$$

For the interacting system, the free energy takes the form

$$F = F_0 + F_{\mathrm{int}}. \quad (2.54)$$

We represent F_{int} as a series in g: $F_{\mathrm{int}} = \sum_{n=1}(g^2)F_n$. In the lowest order in g, we get the relation

$$F_1 = -\frac{g^2}{32}\mathrm{Tr}\{\Gamma^i G\,Tr\Gamma^j G - 2G\Gamma^i G\Gamma^j\}\chi_{ij}, \quad (2.55)$$

where the Green function for fermions and spins is as follows:

$$\langle\Psi(x,\tau)\bar{\Psi}(y,\tau')\rangle = G(x,\tau;y,\tau'),$$
$$\langle S_i(x,\tau)S_j(y,\tau')\rangle = \chi_{ij}(x,\tau;y,\tau'). \quad (2.56)$$

Taking the condition $\delta F/\delta G = 0$ into account, we obtain the Schwinger–Dyson equation:

$$G^{-1} = G_0^{-1} - \Gamma^0\Gamma_5\mu + \frac{g^2}{12}\{\Gamma^i Tr\Gamma^j G\chi_{ij} - 2\Gamma^i G\Gamma^j\chi_{ij}\}, \quad (2.57)$$

where Γ_0 and Γ^i are Dirac matrices (Fig. 2.13).

Here, the straight line corresponds to the Green function for fermions G, and the wavy line to the Green function for spins $\chi_{i,j}$ $(= \delta_{ij}\chi)$. The equation for free energy

$$F_1 = -\frac{g^2}{32}\mathrm{Tr}\{\Gamma^i G\,\mathrm{Tr}\Gamma^j G - 2G\Gamma^i G\Gamma^j\}\chi_{ij}, \quad (2.58)$$

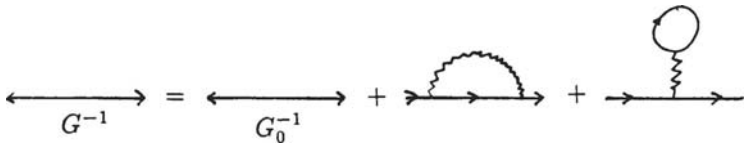

Fig. 2.13 Graphical form of Eq. (2.57).

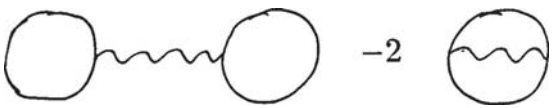

Fig. 2.14 Graphical form of the right-hand side of Eq. (2.58).

where G and χ_{ij} are, respectively, the Green fermion and spin functions, corresponds to the contribution of two vacuum diagrams (Fig. 2.14).

2.7.4 *Equation for the superconducting gap*

From Eq. (2.57), it is easy to deduce the equation for a gap, which can be found in Ref. 70. By executing the Fourier transformation

$$G(x,\tau)=\sum_{n=-\infty}^{\infty}\int_{-\pi/a}^{\pi/a}\frac{d^2k}{(2\pi)^2}G(\mathbf{k},\omega_n)e^{i\omega_n\tau-i\mathbf{k}\,\mathbf{x}}\begin{cases}\omega_n=\frac{(2n+1)\pi}{\beta} & \text{for fermions,}\\ \omega_n=\frac{2n\pi}{\beta} & \text{for bosons,}\end{cases}$$

we rewrite Eq. (2.57) in the momentum space as

$$\begin{aligned}G^{-1}(\mathbf{k},i\omega_n)=\widetilde{G_0^{-1}}(\mathbf{k},i\omega_n)+\frac{g^2}{4\beta}\sum_{m=-\infty}^{\infty}\int_{-\pi/a}^{\pi/a}\frac{d^2p}{(2\pi)^2}\\ \times[\Gamma^i\Gamma_5 Tr\Gamma^i\Gamma_5 G(\mathbf{p},i\omega_m)-2\Gamma^i\Gamma_5 G(\mathbf{p},i\omega_m)\,\Gamma^i\Gamma_5]\\ \times\chi(\mathbf{k}-\mathbf{p},i\omega_n-i\omega_m),\end{aligned}\tag{2.59}$$

where we set $\chi_{ij}=\delta_{ij}\chi$,

$$\begin{aligned}G_0^{-1}(\mathbf{k},i\omega_n)&=\begin{pmatrix}0 & \{i\omega_n-(\varepsilon(\mathbf{k})-\mu)\}I\\ \{i\omega_n+\varepsilon(\mathbf{k})-\mu\}I & 0\end{pmatrix}\\ &\equiv\Gamma^0 i\omega_n-\Gamma^0\Gamma_5(\varepsilon(\mathbf{k})-\mu),\end{aligned}\tag{2.60}$$

$$\varepsilon(\mathbf{k})=-2t[\cos k_x a+\cos k_y a].\tag{2.61}$$

In accordance with the standard relation of the diagram technique, we denote the free energy by $\Sigma(\mathbf{k},i\omega_n)$. Then we have

$$G^{-1}(\mathbf{k},i\omega_n)=\widetilde{G_0^{-1}}(\mathbf{k},i\omega_n)-\Sigma(\mathbf{k},i\omega_n),\tag{2.62}$$

and Eq. (2.57) is the equation for Σ. We write the solution for Σ in the form

$$\Sigma=\Gamma^0 A+\Gamma^0\Gamma_5 B+\Delta+\Gamma^0\Gamma_5\Gamma^i\Delta_i,\tag{2.63}$$

where A, B, Δ and Δ_i are functions of $\mathbf{k}$ and $i\omega_n$.

By determining the matrix which is inverse to (2.62), we get

$$G(\mathbf{k},i\omega_n)=\frac{\Gamma^0(\omega_n-A)-\Gamma^0\Gamma_5(\varepsilon(\mathbf{k})-\mu+B)+\Delta+\Gamma^0\Gamma_5}{(\omega_n-A)^2-(\varepsilon(\mathbf{k})-\mu+B)^2-\Delta^2-\Delta_i^2}.\tag{2.64}$$

Substituting (2.64) and (2.63) in (2.63), we obtain the system of equations for the functions A, B, Δ and Δ_i:

$$A(\mathbf{k}, i\omega_n) = \frac{3g^2}{4\beta} \sum_m \int \frac{d^2p}{(2\pi)^2} \frac{i\omega_n - A(\mathbf{p}, i\omega_m)}{D(i\omega_m, \mathbf{p})} \times \chi(\mathbf{k} - \mathbf{p},\, i\omega_n - i\omega_m), \tag{2.65}$$

$$B(\mathbf{k}, i\omega_n) = \frac{3g^2}{4\beta} \sum_m \int \frac{d^2p}{(2\pi)^2} \frac{\varepsilon(\mathbf{p}) - \mu + B(\mathbf{p}, i\omega_m)}{D(i\omega_m, \mathbf{p})} \times \chi(\mathbf{k} - \mathbf{p}, i\omega_n - i\omega_m), \tag{2.66}$$

$$\Delta(\mathbf{k}, i\omega_n) = \frac{3g^2}{4\beta} \sum_m \int \frac{d^2p}{(2\pi)^2} \frac{\Delta(\mathbf{p}, i\omega_m)}{D(i\omega_m, \mathbf{p})} \times \chi(\mathbf{k} - \mathbf{p}, i\omega_n - i\omega_m), \tag{2.67}$$

$$\Delta_i(\mathbf{k}, i\omega_n) = -\frac{g^2}{4\beta} \sum_m \int \frac{d^2p}{(2\pi)^2} \frac{\Delta_i(\mathbf{p}, i\omega_m)}{D(i\omega_m, \mathbf{p})} \times \chi(\mathbf{k} - \mathbf{p}, i\omega_n - i\omega_m), \tag{2.68}$$

where

$$D(i\omega_m, \mathbf{p}) = (\omega_n - A)^2 - (\varepsilon(\mathbf{k}) - \mu + B)^2. \tag{2.69}$$

Equations (2.67) and (2.68) correspond, respectively, to the singlet and triplet pairings. Moreover, the singlet channel is characterized by the repulsion, and the triplet one by the attraction. Therefore, it is necessary to take the trivial solution, $\Delta = \mathbf{0}$, of Eq. (2.67). In the following calculations, we will neglect the contributions from the functions A and B, which leads only to the renormalization of the wave function and the chemical potential, and we will study only Eq. (2.67). By neglecting Δ^2 in the denominator, we get the linearized equations for Δ_0 which determine the critical temperature T_c.

For the correlation function $\chi(q, i\omega_n)$, we will use the dispersion relations

$$\chi(q, i\omega_n) = -\frac{1}{\pi} \int_{-\infty}^{\infty} \frac{d\omega' \,\mathrm{Im}\, \chi(q, \omega')}{i\omega_n - \omega'} = -\frac{1}{\pi} \left[\int_0^{\infty} \frac{d\omega' \,\mathrm{Im}\, \chi(q, \omega')}{i\omega_n - \omega'} + \int_0^{\infty} \frac{d\omega' \,\mathrm{Im}\, \chi(q, -\omega')}{i\omega_n + \omega'} \right]. \tag{2.70}$$

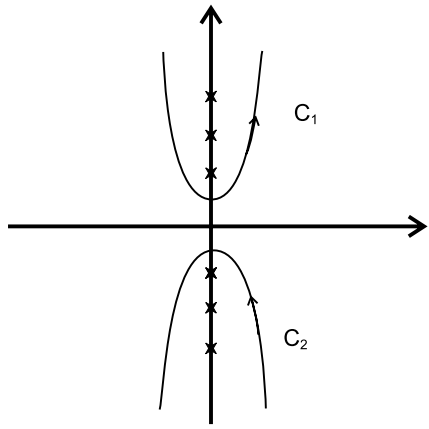

Fig. 2.15 Integration contour $C = C_1 + C_2$.

In order to sum over m in (2.70), we consider the contour $C = C_1 + C_2$ (Fig. 2.15).

The following formula for $\omega_n = \frac{(2n+1)\pi}{\beta}$ is valid:

$$\sum_{n=-\infty}^{\infty} F(i\omega_n) = -\frac{\beta}{2\pi i}\int_C \frac{F(\omega)\,d\omega}{\exp\beta\omega + 1} = -\frac{\beta}{2\pi i}\int_C \frac{F(\omega)\,d\omega}{\exp -\beta\omega + 1}, \qquad (2.71)$$

or

$$\sum_{n=-\infty}^{\infty} F(i\omega_n) = -\frac{\beta}{2\pi i}\frac{1}{2}\int_C F(\omega)\mathrm{th}\frac{\beta\omega}{2}d\omega. \qquad (2.72)$$

Taking into account that $\mathrm{Im}\,\chi(q,-\omega) = -\mathrm{Im}\,\chi(q,\omega)$, Eq. (2.70) can be reduced to

$$\chi(q, i\omega_n) = -\frac{1}{\pi}\int_0^{\infty} d\omega' \mathrm{Im}\,\chi(q,\omega')\left[\frac{1}{i\omega_n - \omega'} - \frac{1}{i\omega_n + \omega'}\right]. \qquad (2.73)$$

With the help of the formula (2.72), we can rewrite (2.67) in the form

$$\Delta(\mathbf{k}, i\omega_n) = \frac{g^2}{8\pi(2\pi i)}\int \frac{d^2p}{(2\pi)^2}\int_C d\omega F(\mathbf{p},\omega)\int_0^{\infty} d\omega' \mathrm{Im}\,\chi(\mathbf{k}-\mathbf{p},\omega')$$
$$\times\left[\frac{1}{i\omega_n - \omega - \omega'} - \frac{1}{i\omega_n - \omega + \omega'}\right]\mathrm{th}\frac{\beta\omega}{2}, \qquad (2.74)$$

where

$$F(\mathbf{p},\omega) = \frac{\Delta(\mathbf{k}, i\omega_{n)}}{\omega^2 - (\varepsilon(\mathbf{p}) - \mu)^2}.$$

After some calculations and transformations, we get the general formula for the superconducting parameter[79–81]:

$$\begin{aligned}\mathrm{Re}(\mathbf{k},\omega) = \frac{g^2}{8}\int_{-\pi/a}^{\pi/a}\frac{d^2p}{(2\pi)^2}\Bigg\{&\frac{\mathrm{th}\frac{\beta(\varepsilon(\mathbf{p})-\mu)}{2}}{2(\varepsilon(\mathbf{p})-\mu)}\\ &\times[\mathrm{Re}\,\chi(\mathbf{k}-\mathbf{p},\omega-(\varepsilon(\mathbf{p})-\mu))\\ &+\mathrm{Re}\,\chi(\mathbf{k}-\mathbf{p},\omega+(\varepsilon(\mathbf{p})-\mu))]\\ &\times\mathrm{Re}\Delta(\mathbf{p},\upsilon)-2\int_0^\infty\frac{d\upsilon}{\pi}\mathrm{cth}\frac{\beta\upsilon}{2}\mathrm{Im}\,\chi(\mathbf{k}-\mathbf{p},\upsilon)\\ &\times\Bigg[\frac{(\omega-\upsilon)^2-(\varepsilon(\mathbf{p})-\mu)^2-\delta^2}{((\omega-\upsilon)^2-(\varepsilon(\mathbf{p})-\mu)^2-\delta^2)^2+4(\omega-\upsilon)^2\delta^2}\\ &\times\mathrm{Re}\Delta(\mathbf{p},\omega-\upsilon)\\ &+\frac{(\omega+\upsilon)^2-(\varepsilon(\mathbf{p})-\mu)^2-\delta^2}{((\omega+\upsilon)^2-(\varepsilon(\mathbf{p})-\mu)^2-\delta^2)^2+4(\omega-\upsilon)^2\delta^2}\\ &\times\mathrm{Re}\Delta(\mathbf{p},\omega+\upsilon)\Bigg]\Bigg\}\end{aligned}\tag{2.75}$$

$$\mathrm{Re}\,F(\mathbf{p},\omega+i\delta)=\mathrm{Re}\Delta(\mathbf{p},\omega)\frac{\omega^2-(\varepsilon(\mathbf{p})-\mu)^2-\delta^2}{[\omega^2-(\varepsilon(\mathbf{p})-\mu)^2-\delta^2]^2+\omega^2\delta^2}.\tag{2.76}$$

If the superconducting gap depends weakly on the frequency, then $\Delta(\mathbf{k},\omega)\simeq\Delta(\mathbf{k},0)$. In this case, we set $\omega=0$ in Eq. (2.75). Considering the relation $\mathrm{Re}\chi(q,\omega)=\mathrm{Re}\,\chi(q,-\omega)$ and making the simple transformations, we obtain an equation similar to that in Ref. 70:

$$\begin{aligned}\Delta(\mathbf{k})=\frac{g^2}{8}\int_{-\pi/a}^{\pi/a}\frac{d^2p}{(2\pi)^2}\Bigg\{&\mathrm{Re}\,\chi(\mathbf{k}-\mathbf{p},\varepsilon(\mathbf{p})-\mu)\frac{\mathrm{th}\frac{\beta(\varepsilon(\mathbf{p})-\mu)}{2}}{\varepsilon(\mathbf{p})-\mu}\\ &+2\int_0^\infty\frac{d\upsilon}{\pi}\mathrm{cth}\frac{\beta\upsilon}{2}\mathrm{Im}\,\chi(\mathbf{k}-\mathbf{p},\upsilon)\\ &\times\frac{(\varepsilon(\mathbf{p})-\mu)^2-\upsilon^2+\delta^2}{[(\varepsilon(\mathbf{p})-\mu)^2-\upsilon^2+\delta^2]^2+4\upsilon^2\delta^2}\Bigg\}\Delta(\mathbf{p}).\end{aligned}\tag{2.77}$$

It is important that our method of calculations yields a more general equation for the superconducting gap than that obtained by D. Pines. Our equation coincides with the Pines equations after some simplification, which is the test for our calculations.

2.7.5 *Thermodynamic potential of antiferromagnetic spin fluctuations*

For the free energy, we have the equation

$$F(G) = \beta\Omega = -\frac{1}{2}\mathrm{Tr}[\ln G_o G^{-1} + (G_o^{-1} + \Gamma^o\Gamma_5\mu)G^{-1}] - \frac{g^2}{32}\mathrm{Tr}\{\Gamma^i G Tr \Gamma^j G\chi_{ij} - 2G\Gamma^i G\Gamma^j\chi_{ij}\}, \tag{2.78}$$

where G satisfies Eq. (2.57). We now multiply Eq. (2.58) by G and take the trace, Tr. This allows us to obtain

$$\frac{g^2}{8}\mathrm{Tr}\{\Gamma^i G Tr\Gamma^j G\chi_{ij} - 2G\Gamma^i G\Gamma^j\chi_{ij}\} = -\mathrm{Tr}\{(G_o^{-1} + \Gamma^o\Gamma_5\mu)G - 1\}. \tag{2.79}$$

Using (2.57), we can rewrite the relation (2.79) for the functional of free energy calculated with the use of solutions to the Schwinger–Dyson equation in the form

$$\beta\Omega = -\frac{1}{2}\mathrm{Tr}\left[\ln G_o\Gamma^{-1} + \frac{1}{2}(G_o^{-1} + \Gamma^o\Gamma_5\mu)G - \frac{1}{2}\right]. \tag{2.80}$$

By implementing the Fourier transformation, we get

$$\Omega = \frac{1}{2\beta}V\sum_{n=-\infty}^{\infty}\int_{-\pi/a}^{\pi/a}\frac{d^2k}{(2\pi)^2}\mathrm{Tr}\left[\ln G_o(\mathbf{k}, iw_n)G^{-1}(\mathbf{k}, iw_n) + \frac{1}{2}(G_o^{-1}(\mathbf{k}, iw_n) + \Gamma^o\Gamma_5\mu)G(\mathbf{k}, iw_n) - \frac{1}{2}\right], \tag{2.81}$$

where V is the two-dimensional volume (the area of the cuprate plane) and Tr stands for the trace of a matrix.

For the free energy functional $\Omega(\Delta)$, we have the formula

$$\Omega = -\frac{V}{2\beta}\sum_{n=-\infty}^{\infty}\int\frac{d^2k}{(2*\pi)^2}\mathrm{Tr}\left[\ln G_o(\mathbf{k}, i\omega_n)^{-1}(\mathbf{k}, i\omega_n) + \frac{1}{2}(G_o^{-1}(\mathbf{k}, i\omega_n) + r^o r_5\mu)G(\mathbf{k}, i\omega_n) - \frac{1}{2}\right], \tag{2.82}$$

where $G_o^{-1}(\mathbf{k}, i\omega_n) = r^o i\omega_n - r^o r_5\varepsilon(\mathbf{k})$, and $G(\mathbf{k}, i\omega_n)$ is given by the formula (2.57). We note that the functional $\Omega(\Delta, \mu)$ is normalized so that $\Omega(\Delta = 0, \mu = 0) = 0$.

By calculating the trace of the r matrix, we obtain the expression

$$\Omega(\Delta,\mu) = -\frac{V}{\beta}\sum_{n=-\infty}^{\infty}\int\frac{d^2k}{(2*\pi)^2}\left[\ln\frac{\omega_n^2+(\varepsilon-\mu)^2+\Delta^2}{\omega_n^2+\varepsilon^2} - \frac{\Delta^2}{\omega_n^2+(\varepsilon-\mu)^2+\Delta^2}\right]. \tag{2.83}$$

By using the formula

$$\sum_{n=-\infty}^{\infty}\ln\frac{\omega_n^2+b^2}{\omega_n^2+a^2} = \int_0^{\infty}dx\left[\frac{\beta}{2\sqrt{a^2+x}}\mathrm{th}\frac{\beta\sqrt{a^2+x}}{2} - \frac{\beta}{2\sqrt{b^2+x}}\mathrm{th}\frac{\beta\sqrt{b^2+x}}{2}\right] = 2\ln\frac{\mathrm{ch}\frac{\beta b}{2}}{\mathrm{ch}\frac{\beta a}{2}}, \tag{2.84}$$

we get the equation for the thermodynamic potential:

$$\Omega(\Delta) = V\int\frac{d^2k}{(2\pi)^2}\left\{-\frac{2}{\beta}\ln\frac{\mathrm{ch}\frac{\beta}{2}\sqrt{(\varepsilon-\mu)^2+\delta^2}}{\mathrm{ch}\frac{\beta\varepsilon}{2}} + \frac{\Delta^2}{2\sqrt{(\varepsilon-\mu)^2+\Delta^2}}\mathrm{th}\frac{\beta\sqrt{(\varepsilon-\mu)^2+\Delta^2}}{2}\right\}. \tag{2.85}$$

By making some transformations and calculating the traces of Γ matrices, we arrive at the equation

$$\Omega(\Delta)-\Omega(0) = \frac{V}{2}\int_C\frac{dw}{2\pi i}\int\frac{d^2k}{(2\pi)^2}\Delta_i^4(\mathbf{k},w) \times\frac{1}{e^{Bw}+1}\frac{1}{[w^2-(\varepsilon(\mathbf{k}-\mu)^2]^2}. \tag{2.86}$$

By expanding the contour C and calculating the contribution to the integral at poles $w=\pm(\varepsilon(\mathbf{k})-\mu)$, we get

$$\Omega(\Delta)-\Omega(0) = \frac{V}{8}\int\frac{d^2k}{(2\pi)^2}\frac{\Delta_i^4(\mathbf{k})}{[\varepsilon(\mathbf{k})-\mu]^2} \times\left\{\frac{\beta}{2}\left(1-\mathrm{th}^2\frac{\beta(\varepsilon(\mathbf{k})-\mu)}{2}\right) - \frac{1}{\varepsilon(\mathbf{k})-\mu}\mathrm{th}\frac{\varepsilon(\mathbf{k})-\mu}{2}, \right. \tag{2.87}$$

where $\varepsilon(\mathbf{k})$ describes the spectrum of two-dimensional electrons; the free energy F is connected with the thermodynamic potential Ω by the relation

$F = \beta\Omega$; $\Omega(\Delta)$ and $\Omega(0)$ are the thermodynamic potentials at $T < T_c$ and $T > T_c$, respectively, and V is the two-dimensional volume (the area of a cuprate layer).

It is easy to verify that despite the presence of the factors $[\varepsilon(\mathbf{k}) - \mu]$ in the denominator of the formula (2.87), no singularity on the Fermi surface $\varepsilon(\mathbf{k}) - \mu$ is present.

Equations (2.85) and (2.87) (at $T \sim T_c$) can be a basis for calculations of various thermodynamic quantities, including a jump of the heat capacity.

A similar method of calculations was developed by S. Weinberg.[85]

2.7.6 *Heat capacity of the d pairing*

Equation (2.85) yields the following formula for the thermodynamic potential: $\Omega(\Delta)$[79]

$$\Omega(\Delta) = V \int \frac{d^2k}{(2\pi)^2} \left\{ -\frac{2}{\beta} \ln \frac{\mathrm{ch}\frac{\beta}{2}\left(\sqrt{(\varepsilon(\mathbf{k}) - \mu)^2 + \Delta(\mathbf{k})^2}\right)}{\mathrm{ch}\frac{\beta\varepsilon}{2}} + \frac{\Delta(\mathbf{k})^2}{2\sqrt{(\varepsilon(\mathbf{k}) - \mu)^2 + \Delta(\mathbf{k})^2}} \mathrm{th} \frac{\sqrt{(\varepsilon(\mathbf{k}) - \mu)^2 + \Delta(\mathbf{k})^2}}{2} \right\}. \quad (2.88)$$

Here, V is the two-dimensional volume (the area of a cuprate layer), $\Delta(\mathbf{k})$ is the superconductor gap, $\mathbf{k}$ is the momentum of an electron, and $\varepsilon(\mathbf{k}) = -2t[\cos(k_x a) + \cos(k_y a)]$ gives the spectrum of two-dimensional electrons. The heat capacity is calculated by the formula

$$C = -T \frac{\partial^2 \Omega}{\partial T^2}. \quad (2.89)$$

The results of calculations of the heat capacity C are given in Ref. 45. We have carried out computer-based calculations of the heat capacity of the compound $YBa_2Cu_3O_{6.63}$. The equation for the superconductor gap Δ was obtained in Sec. 2.7.5. The task of solving the integral equation was reduced to that of an algebraic equation which was solved by the method of iterations.

The equation for the superconductor gap depends on the spin correlation function. For it, the necessary data were taken from Refs. 69 and 70. In calculations, we used the following values of parameters of the correlator: $\omega_{\mathrm{SF}}(T_C) \approx 7.7\,\mathrm{meV}$, $\chi_S(Q) = 44\,\mathrm{eV}$, $\xi/a \approx 2.5, \mathrm{t} = 2\,\mathrm{eV}$, $\mu = 0.25$ and $T_c = 95\,\mathrm{K}$. We chose a value of the constant g which satisfies the relation $2\Delta/kT_c = 3.4$, similar to that in Refs. 66 and 67. The results of numerical

calculations are presented in Fig. 2.15, where we can see the temperature dependence of the electron heat capacity: 1 — a curve which is an approximation of the results of computer-based calculations (crosses); 2 — a curve which describes the exponential BCS dependence. These results are in good agreement with experiments made by A. Kapitulnik and co-workers[86] at low temperatures.

The calculations indicated a square dependence of the heat capacity on the temperature in the temperature range from zero to the superconducting temperature. It was shown[45,46,79,80] that the dependence has the form

$$C = AT^2, \tag{2.90}$$

where $A = 0.126\,\mathrm{J/K^3\,mol}$.

2.7.7 *Heat capacity jump in superconductors*

In what follows, we present the results of calculations of a jump of the heat capacity near the critical temperature,

$$\Delta C = -T\frac{\partial^2 \Delta\Omega}{\partial T^2}, \quad \beta = \frac{1}{T}, \tag{2.91}$$

and evaluate the parameter $R = \Delta C/\gamma T_c$. Omitting the awkward and quite complicated details, we will give the final results.

We obtained $R = 1.6$. This value of the parameter is larger than that in the BCS theory, where $R = 1.43$. It is worth noting that the heat capacity jump is very sensitive to the doping. Figure 2.16 shows the results of recent calculations by one of the authors[81] for R as a function of the doping. It is seen that this parameter depends strongly on the doping. By using these results, it is possible to evaluate the condensation energy for HTSCs which is proportional to R^2.[82]

The calculations imply that the heat capacity depends on the temperature as T^2. Analogous results were obtained for the physics of heavy fermions.[91] It was shown in this work that d symmetry leads to a linear dependence of C/T on the temperature, whereas s symmetry is related to the exponential dependence of this quantity on the temperature. The linear dependence of C/T on the temperature was observed in the experimental works (Refs. 87–90) for YBaCuO superconductors. The experimental results are presented in Fig. 2.17. As was mentioned above, the problem of the determination of the symmetry of a gap in cuprate superconductors is

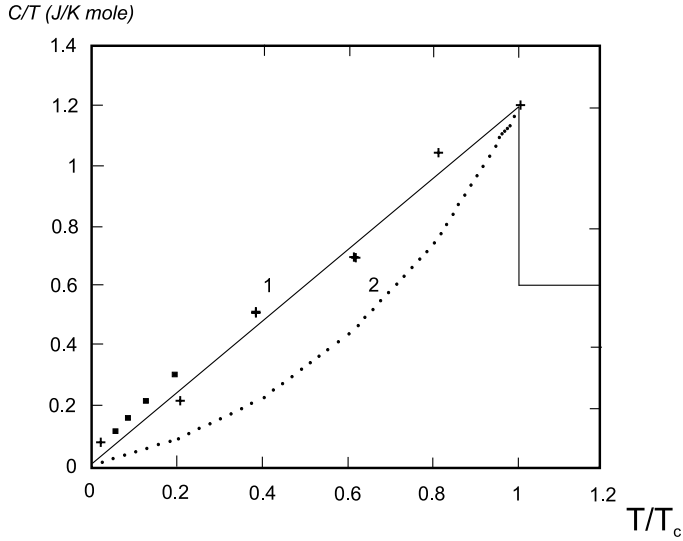

Fig. 2.16 Temperature dependence of the electron heat capacity: 1 — a curve which is an approximation of the results of computer-based calculations (crosses); 2 — a curve which describes the exponential BCS dependence, with the points giving the experimental data.[86]

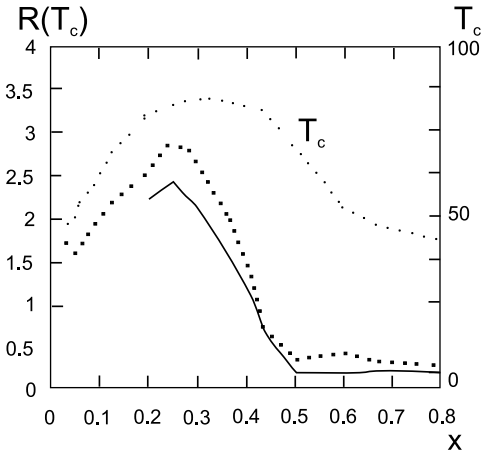

Fig. 2.17 The parameter $R(T_c)$, which characterizes the heat capacity jump as a function of the doping for $Y_{0.8}Ca_{0.2}Ba_2Cu_3O_{7-x}$. The solid curve presents the results of theoretical calculations; the points mark the experimental data.[89]

urgent at the present time. Many experiments have confirmed the d symmetry of the pairing.[67,68] In particular, we mention new experiments,[68] in which the researchers have studied the quantization of magnetic flows in a ring which includes three Josephson junctions. These works supporting the existence of d pairing in HTSCs were marked by the Barkley Prize. It was also shown that the sign of the order parameter in $YBa_2Cu_3O_{7-\delta}$ depends on the direction. This dependence corresponds to the $d_{x^2-y^2}$ symmetry.

The temperature dependence of the electron heat capacity obtained in our calculations[79,80] is related to the d pairing. These thermodynamic calculations can be a supplementary test in the determination of the pairing symmetry in HTSCs.

It should be noted that thermodynamic calculations clarifying the behavior of HTSCs have also been performed in Refs. 92–95 in the frame of the other mechanisms of pairing.

2.8 Summary

High-temperature superconductivity is a dynamical field of solid-state physics which has been intensively developed by theorists and experimenters. By summarizing the physical properties and the mechanisms of superconductivity in new HTSCs , we wish to separate the main properties and the theoretical problems arising in the studies of HTSCs.

In order to comprehend the nature of the superconducting state, it is necessary to construct a consistent microscopic theory which would be able to describe superconductive and normal properties of HTSCs. It is seen from the above-presented survey that many mechanisms of pairing in HTSCs, proposed as the explanations for this phenomenon, have been advanced. On the whole, the most probable seems to be the "synergetic" mechanism of pairing, whose constituents are the electron–phonon interaction, spin fluctuation, and other types of interaction in cuprate planes.

We believe that the known challenging properties — which are contradictory to a certain extent — of many chemical compounds in the superconducting and normal phases can be explained only by considering the interaction of all the degrees of freedom, such as lattice-, electron- and spin-related ones. In this case, it is also necessary to take into account the complicated structure of HTSCs. Further development of the theory will require not only the execution of bulky numerical calculations, but also the solution of a number of fundamental problems concerning the strong electron

correlations. It seems to us that one of the key problems in the field of superconductivity is the mechanism and the symmetry of pairing.

We have shown above that some thermodynamical problems of high-temperature superconductivity, in particular the problem of antiferromagnetic spin fluctuations, can be efficiently solved within the method of continual integrals. We conclude with the following remarks:

(1) The thermodynamic theory of antiferromagnetic spin fluctuations in HTSCs has been constructed. The method of functional integration was applied to the calculations of the superconductor gap and the thermodynamic potential. The Schwinger–Dyson equation and the equation for the free energy were deduced.
(2) From the Schwinger–Dyson equation, the equations for the superconductor gap, which are used in the numerical calculations within the thermodynamics of HTSCs, were constructed. The analytic formulas for the thermodynamic potential and its jump were obtained.
(3) Numerical calculations of the temperature dependence of the electron heat capacity were carried out, and it was shown that the electron heat capacity is proportional to the square of the temperature. It was emphasized that such a temperature dependence is related to the d pairing. It was shown that the measurement of the temperature dependence of the heat capacity can be a supplementary test in the determination of the type of pairing symmetry in HTSCs. The jump of the heat capacity of cuprate superconductors near the critical temperature was evaluated as well.

CHAPTER 3

Multiband Superconductivity

3.1 Introduction

In this chapter, we present the theory of superconductivity with regard to a complicated multiband structure of superconductors. Calculations of the band structure of cuprate superconductors indicate that several energy bands intersect one another on the Fermi surface in these compounds,[96] and the Fermi surface passes through high-symmetry points which correspond to the Lifshitz electronic topological transition. In addition, the discovery of two-gap superconductivity in two-band superconductors MgB_2 allows one to consider the possibility of using a multiband theory of superconductivity. In Sec. 3.2, we analyze the problems of multiband superconductivity and superconductivity at room temperature. In Sec. 3.3, we study the physical properties of superconductors MgB_2 and problems of two-gap superconductivity, as well as the phase diagram for superconductors MgB_2 on the basis of the renormalization group approach. In the field of superconductivity, we meet the problem-maximum — the creation of room-temperature superconductors. We consider this problem in our book and give some recommendations on the search for these superconductors. The results of this chapter were obtained by the authors and published in Refs. 96–103.

The theory of superconductivity arising from the electron–phonon interaction mechanism by Bardeen, Cooper and Schrieffer (BCS)[104] has been well established, and it is now the standard theory for superconductivity.[2,3,6,15,16,104] In Chap. 2, we have considered non-BCS mechanisms via spin fluctuations, charge fluctuations (plasmons) and electron excitations (excitons), which have attracted great interest, for example in relation to the possibility of high-T_c superconductivity. These mechanisms have the common characteristic that the electron–electron (e–e) interaction is an origin

of the superconductivity. After the discovery of the high-T_c copper oxides,[2] Anderson[6] emphasized an important role of the e–e interaction. Over the past decade, many non-BCS theories[106–111] have been proposed, but they do not converge as a unified and well-accepted theory yet. On the other hand, experimental studies on copper oxides have revealed the following characteristics:

(1) These species are antiferromagnets before doping, in accordance with the importance of the e–e interaction;
(2) The high-T_c superconductivity appears in the intermediate region of the metal–insulator transition and disappears in the metallic or overdoped region.[112–114]

Accumulated experimental results on the species and related materials suggest a guiding principle that the doping in magnetic systems, more generally charge-transfer (CT) insulators, may provide several exotic phases which are

(a) Ferromagnetic metal or insulator,
(b) Spin glass,
(c) Paramagnetic metals,
(d) Antiferromagnetic metals,
(e) Ferrimagnetic metal or insulator,
(f) Charge- or spin-mediated superconductor.

Relative stabilities of these phases should be dependent on several factors. The theoretical description of such phases and phase transitions in a systematic fashion is quite hard. Recently, the importance of multiband effects in high-T_c superconductivity has been pointed out.[3,16,104] In the framework of the two-particle Green function techniques,[98,101] it is shown that a class of new so-called coupled states arises in the electron–phonon system. The model numerical calculations have shown that the superconducting (SC) gap depends on the number of bands crossing the Fermi level, and the temperature dependence of the SC gap for high-T_c superconductors is more complicated than that predicted in the BCS approach. We have also investigated anomalous phases in a two-band model by using the Green function techniques.[101,103] The expressions for the transition temperature for several phases have been derived, and the approach has been applied to the superconductivity in molecular crystals by charge injection and field-induced superconductivity.

In this chapter, we investigate the superconductivity by using the two-band model and the two-particle Green function technique. In the framework of the two-band model, the coupled states in the electron system and the conditions under which the coupled states can appear are investigated. We apply the model to the electron–phonon mechanism within the traditional BSC method, the electron–electron interaction mechanism for high-T_c superconductivity, and the cooperative mechanism in relation to the multiband superconductivity.

3.2 Multiband Hamiltonian

In this section, we summarize the two-band model for superconductivity, introduce a two-particle Green function and investigate the spectral properties of the model.

3.2.1 *Hamiltonian*

We start from the Hamiltonian for two bands i and j:

$$H = H_0 + H_{\text{int}}, \tag{3.1}$$

with

$$H_0 = \sum_{\mathbf{k},\sigma} \big[[\varepsilon_i - \mu] a^+_{i\mathbf{k}\sigma} a_{i\mathbf{k}\sigma} + [\varepsilon_j - \mu] a^+_{j\mathbf{k}\sigma} a_{j\mathbf{k}\sigma}\big], \tag{3.2}$$

$$\begin{aligned} H_{\text{int}} = \frac{1}{4} \sum_{\delta(\mathbf{p}_1+\mathbf{p}_2,\mathbf{p}_3+\mathbf{p}_4)} \sum_{\alpha\beta\gamma\delta} \big[& \Gamma^{iiii}_{\alpha\beta\gamma\delta} a^+_{i\mathbf{p}_1\alpha} a^+_{i\mathbf{p}_2\beta} a_{i\mathbf{p}_3\gamma} a_{i\mathbf{p}_4\delta} + (i \to j) \\ & + \Gamma^{iijj}_{\alpha\beta\gamma\delta} a^+_{i\mathbf{p}_1\alpha} a^+_{i\mathbf{p}_2\beta} a_{j\mathbf{p}_3\gamma} a_{j\mathbf{p}_4\delta} + (i \to j) \\ & + \Gamma^{ijij}_{\alpha\beta\gamma\delta} a^+_{i\mathbf{p}_1\alpha} a^+_{j\mathbf{p}_2\beta} a_{i\mathbf{p}_3\gamma} a_{j\mathbf{p}_4\delta} + (i \to j)\big], \end{aligned} \tag{3.3}$$

where Γ is the bare vertex part,

$$\Gamma^{ijkl}_{\alpha\beta\gamma\delta} = \langle i\mathbf{p}_1\alpha\ j\mathbf{p}_2\beta \,|\, k\mathbf{p}_3\gamma\ l\mathbf{p}_4\delta\rangle\, \delta_{\alpha\delta}\, \delta_{\beta\gamma} - \langle i\mathbf{p}_1\alpha\ j\mathbf{p}_2\beta \,|\, l\mathbf{p}_4\delta\ k\mathbf{p}_3\gamma\rangle\, \delta_{\alpha\gamma}\, \delta_{\beta\delta}, \tag{3.4}$$

with

$$\begin{aligned} \langle i\mathbf{p}_1\alpha j\mathbf{p}_2\beta | k\mathbf{p}_3\gamma l\mathbf{p}_4\rangle = \int d\mathbf{r}_1\, d\mathbf{r}_2 \phi^*_{i\mathbf{p}_1\alpha}(\mathbf{r}_1) \phi^*_{j\mathbf{p}_2\beta}(\mathbf{r}_2) \\ \times V(\mathbf{r}_1,\mathbf{r}_2) \phi_{k\mathbf{p}_3\gamma}(\mathbf{r}_2) \phi_{l\mathbf{p}_4\delta}(\mathbf{r}_1), \end{aligned} \tag{3.5}$$

and $a^{+}_{\mathrm{ip}\sigma}$ ($a_{\mathrm{ip}\sigma}$) is the creation (annihilation) operator corresponding to the excitation of electrons (or holes) in the ith band with spin σ and momentum $\mathbf{p}$, μ is the chemical potential and $\phi^{*}_{ip\alpha}$ is a single-particle wave function. Here, we suppose that the vertex function in Eq. (3.3) consists of the effective interactions between the carriers caused by the linear vibronic coupling in several bands and the screened Coulombic interband interaction of carriers. When we use the two-band Hamiltonian (3.1) and define the order parameters for the singlet exciton, triplet exciton and singlet Cooper pair, the mean field Hamiltonian is easily derived.[96–100,115,116] Here, we focus on four-electron scattering processes:

$$g_1 = \langle ii\,|\,ii\rangle = \langle jj\,|\,jj\rangle, \tag{3.6}$$

$$g_2 = \langle ii\,|\,jj\rangle = \langle jj\,|\,ii\rangle, \tag{3.7}$$

$$g_3 = \langle ij\,|\,ij\rangle = \langle ji\,|\,ji\rangle, \tag{3.8}$$

$$g_4 = \langle ij\,|\,ji\rangle = \langle ji\,|\,ij\rangle. \tag{3.9}$$

g_1 and g_2 represent the intraband two-particle normal and umklapp scatterings respectively, g_3 is the interband two-particle umklapp process and g_4 indicates the interband two-particle interaction on different bands (see Fig. 3.1). Note that Γ's are given by

$$\begin{aligned}
\Gamma^{iiii}_{\alpha\beta\gamma\delta} &= \Gamma^{jjjj}_{\alpha\beta\gamma\delta} = g_1(\delta_{\alpha\delta}\delta_{\beta\gamma} - \delta_{\alpha\gamma}\delta_{\beta\delta}),\\
\Gamma^{iijj}_{\alpha\beta\gamma\delta} &= \Gamma^{jjii}_{\alpha\beta\gamma\delta} = g_2(\delta_{\alpha\delta}\delta_{\beta\gamma} - \delta_{\alpha\gamma}\delta_{\beta\delta}),\\
\Gamma^{ijij}_{\alpha\beta\gamma\delta} &= \Gamma^{jiji}_{\alpha\beta\gamma\delta} = g_3\delta_{\alpha\delta}\delta_{\beta\gamma} - g_4\delta_{\alpha\gamma}\delta_{\beta\delta},
\end{aligned} \tag{3.10}$$

where an antisymmetrized vertex function Γ is considered to be a constant independent of the momenta.

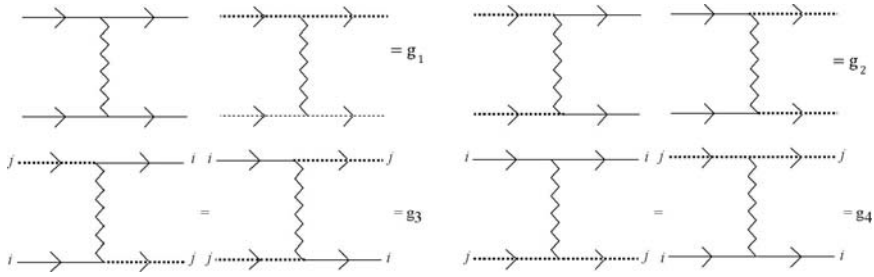

Fig. 3.1 Electron–electron interactions. Dependence of g on the direction in the momentum space is ignored in this model, $g_x(\mathbf{k}) \approx g_x(x = i, j)$. We assume that g_x is constant.

The spectrum is elucidated by the Green function method. Using Green functions which characterize the CDW (charge-density-wave), SDW (spin-density-wave) and SSC (singlet superconducting) phases, we obtain a self-consistent equation, according to the traditional procedure.[13,96,115,116] Then, we can obtain expressions for the transition temperature for some cases.

In the framework of the one-band model, the electronic phases are characterized by

$$\begin{gathered} -g_2 - 2g_3 + g_4 > 0, \text{ for CDW}, \\ g_2 + g_4 > 0, \text{ for SDW}, \\ -g_1 > 0, \text{ for SSC}. \end{gathered}$$

In the framework of the two-band model, we have already derived expressions of the transition temperature for CDW, SDW and SSC. In the previous papers,[13,96,115,116] we have investigated the dependence of T_c on the hole or electron concentration for the superconductivity of copper oxides by using the two-band model and have obtained a phase diagram of $Bi_2Sr_2Ca_{1-x}Y_xCu_2O_8$ (Bi-2212) by means of the above expressions for the transition temperature. The dependence of T_c on Δp can be reproduced in agreement with the experiment.[13,96,115,116] Recently, we have also obtained phase diagrams of copper oxides, anthracene, oligothiophene and C_{60} crystals by using the analytic solutions.[13,96,115,116]

3.2.2 *Two-particle Green function*

In this subsection, we introduce a two-particle Green function[96–98] (see also Appendix A) to investigate the physical properties of superconductivity in the two-band model. In statistical mechanics, Green functions are a convenient generalization of the notion of correlation functions. Like the latter, the former are closely related to the calculations of observables and give the well-known advantages in the construction and the solution of equations. First, let us define one-particle Green functions:

$$G_\sigma^\upsilon(\mathbf{k}, t'-t) = \left\langle -iT\left[a_{\upsilon\mathbf{k}\sigma}(t)a_{\upsilon\mathbf{k}\sigma}^+(t')\right]\right\rangle, \tag{3.11}$$

where σ and υ represent labels for a spin and a band, respectively. The equation for a Green function derived by using the two-band model (3.1) is written as

$$i\frac{\partial}{\partial t}\left\langle -iT\left[a_{\upsilon\mathbf{k}\sigma}(t)a_{\upsilon\mathbf{k}\sigma}^+(t')\right]\right\rangle = \delta(t-t') + \left\langle -iT\left[i\frac{\partial a_{\upsilon\mathbf{k}\sigma}(t)}{\partial t}a_{\upsilon\mathbf{k}\sigma}^+(t')\right]\right\rangle, \tag{3.12}$$

where

$$i\frac{\partial a_{\upsilon\mathbf{k}\sigma}(t)}{\partial t} = [a_{\upsilon\mathbf{k}\sigma}, H]. \tag{3.13}$$

The equation for the Green function (3.12) is rewritten after inserting Eq. (3.13) as

$$\begin{aligned}
&i\frac{\partial}{\partial t}\left\langle -iT\left[a_{\upsilon\mathbf{k}\sigma}(t)a^{+}_{\upsilon\mathbf{k}\sigma}(t')\right]\right\rangle \\
&\quad = \delta(t-t') + [\varepsilon_\upsilon - \mu]\left\langle -iT\left[a_{\upsilon\mathbf{k}\sigma}(t)a^{+}_{\upsilon\mathbf{k}\sigma}(t')\right]\right\rangle \\
&\qquad + \frac{1}{2}\sum_{\beta\gamma\delta}\sum_{\delta(\mathbf{k}+\mathbf{p}_2,\mathbf{p}_3+\mathbf{p}_4)} g_1(\delta_{\sigma\delta}\delta_{\beta\gamma} - \delta_{\sigma\gamma}\delta_{\beta\delta})G^{\gamma\delta\beta\sigma}_{2_{\upsilon\upsilon\upsilon\upsilon}}(\mathbf{p}_3,\mathbf{p}_4,\mathbf{p}_2,\mathbf{k};t,t') \\
&\qquad + \frac{1}{2}\sum_{\upsilon'}\sum_{\beta\gamma\delta}\sum_{\delta(\mathbf{k}+\mathbf{p}_2,\mathbf{p}_3+\mathbf{p}_4)} g_2(\delta_{\sigma\delta}\delta_{\beta\gamma} - \delta_{\sigma\gamma}\delta_{\beta\delta})G^{\gamma\delta\beta\sigma}_{2_{\upsilon'\upsilon'\upsilon\upsilon}}(\mathbf{p}_3,\mathbf{p}_4,\mathbf{p}_2,\mathbf{k};t,t') \\
&\qquad + \frac{1}{2}\sum_{\upsilon'}\sum_{\beta\gamma\delta}\sum_{\delta(\mathbf{k}+\mathbf{p}_2,\mathbf{p}_3+\mathbf{p}_4)} (g_3\delta_{\sigma\delta}\delta_{\beta\gamma} - g_4\delta_{\sigma\gamma}\delta_{\beta\delta})G^{\gamma\delta\beta\sigma}_{2_{\upsilon\upsilon'\upsilon'\upsilon}}(\mathbf{p}_3,\mathbf{p}_4,\mathbf{p}_2,\mathbf{k};t,t'),
\end{aligned} \tag{3.14}$$

where

$$G^{\gamma\delta\beta\sigma}_{2_{\upsilon\upsilon\upsilon\upsilon}}(\mathbf{p}_3,\mathbf{p}_4,\mathbf{p}_2,\mathbf{k};t,t') = \left\langle -iT\left[a_{\upsilon\mathbf{p}_3\gamma}(t)a_{\upsilon\mathbf{p}_4\delta}(t)a^{+}_{\upsilon\mathbf{p}_2\beta}(t-0)a^{+}_{\upsilon\mathbf{k}\sigma}(t')\right]\right\rangle, \tag{3.15}$$

$$G^{\gamma\delta\beta\sigma}_{2_{\upsilon'\upsilon'\upsilon\upsilon}}(\mathbf{p}_3,\mathbf{p}_4,\mathbf{p}_2,\mathbf{k};t,t') = \left\langle -iT\left[a_{\upsilon'\mathbf{p}_3\gamma}(t)a_{\upsilon'\mathbf{p}_4\delta}(t)a^{+}_{\upsilon\mathbf{p}_2\beta}(t-0)a^{+}_{\upsilon\mathbf{k}\sigma}(t')\right]\right\rangle, \tag{3.16}$$

$$G^{\gamma\delta\beta\sigma}_{2_{\upsilon\upsilon'\upsilon'\upsilon}}(\mathbf{p}_3,\mathbf{p}_4,\mathbf{p}_2,\mathbf{k};t,t') = \left\langle -iT\left[a_{\upsilon\mathbf{p}_3\gamma}(t)a_{\upsilon'\mathbf{p}_4\delta}(t)a^{+}_{\upsilon'\mathbf{p}_2\beta}(t-0)a^{+}_{\upsilon\mathbf{k}\sigma}(t')\right]\right\rangle. \tag{3.17}$$

υ' indicates a band different from υ. To calculate the density of electron states, we have to focus on the case where $t' \to t-0$. The two-particle Green functions in Eq. (3.14) is rewritten as $G_2(\mathbf{p}_3,\mathbf{p}_4,\mathbf{p}_2,\mathbf{k};t-t')$ $(t' \to t-0)$.

In this study, we investigate only the spectral properties of two-particle Green functions for the superconductivity. Therefore, we focus on the following two-particle Green function:

$$G^{\gamma\delta\beta\sigma}_{2_{\upsilon\upsilon\upsilon\upsilon}}(\mathbf{p}_3,\mathbf{p}_4,\mathbf{p}_2,\mathbf{k};t,t') = \left\langle -iT\left[a_{\upsilon\mathbf{p}_3\gamma}(t)a_{\upsilon\mathbf{p}_4\delta}(t)a^{+}_{\upsilon\mathbf{p}_2\beta}(t')a^{+}_{\upsilon\mathbf{k}\sigma}(t')\right]\right\rangle. \tag{3.18}$$

For simplicity, we consider only three cases: (i) $g_1 \neq 0$ and others $= 0$; (ii) $g_2 \neq 0$ and others $= 0$; (iii) $g_1 \neq 0$, $g_2 \neq 0$ and others $= 0$.

3.2.3 *Traditional superconductivity*

In general, in the framework of the BCS theory, the Hamiltonian is described by a single-band model. In the effective electron–electron interaction (Eq. (3.1)), we consider that $g_1 \neq 0$ and others $= 0$ and focus only on the single-band model. According to the approach[101] used for phonon systems which is based on the method of Bogoliubov and Tyablikov,[148] we can derive the equation for a two-particle electron Green function. The spectral features of the electron system in the mentioned region of energy are described by the Fourier transform of this function. For the simplest case of a one-electron zone crossing the Fermi energy level, it can be given as

$$G^{\gamma\gamma\delta\beta\sigma}_{2_{\upsilon\upsilon\upsilon\upsilon}}(\mathbf{p}_3, \mathbf{p}_4, \mathbf{p}_2, \mathbf{k}; t - t') = \frac{f(\mathbf{k}, \mathbf{k}', \omega) \sum_{\sigma,\sigma'} \phi(\sigma, \sigma')}{1 - g_1 \sum_{\mathbf{q}} K(\omega, \mathbf{k}, \mathbf{k}', \mathbf{q})}, \tag{3.19}$$

where

$$K(\omega, \mathbf{k}, \mathbf{k}', \mathbf{q}) = \frac{2 - n^{\upsilon}_{\mathbf{k}+\mathbf{q}} - n^{\upsilon}_{\mathbf{k}'-\mathbf{q}}}{2\omega - \varepsilon^{\upsilon}_{\mathbf{k}+\mathbf{q}} - \varepsilon^{\upsilon}_{\mathbf{k}'-\mathbf{q}}}. \tag{3.20}$$

n_k indicates the filling number of electrons and g_1 is the effective Fourier transform of the e–e interaction. If the e–e interaction constant renormalized by the electron–phonon interaction becomes negative, coupled states will appear in the electron system. In the previous papers,[96–98] we have presented analysis of the spectral properties of the two-particle Green function. According to the same procedure,[96–98] we obtain the equation for coupled states in the electron system:

$$1 - g_1 N(\varepsilon_f) \left[-\ln \left| 1 - \frac{\Delta}{a} \right| \right] = 0, \tag{3.21}$$

where

$$N(\varepsilon_f) = \sqrt{2}\pi m^*_{\upsilon} \sqrt{m^*_{\upsilon}\varepsilon} \left(2 - n^{\upsilon}_{\mathbf{k}+\mathbf{q}} - n^{\upsilon}_{\mathbf{k}'-\mathbf{q}}\right)\Big|_{\varepsilon=\varepsilon_f}, \tag{3.22}$$

$$n^{\upsilon}_{\mathbf{k}} = \frac{1}{\exp\left[\left(\varepsilon^{\upsilon}_{\mathbf{k}} - \varepsilon_f\right)/T\right] + 1}. \tag{3.23}$$

$a = 2(\omega - \varepsilon_f - \Delta_{\upsilon} - E)$, $E = k^2/2m$, $\varepsilon = q^2/2m$ and $m^*_{\upsilon} = m_{\upsilon}/m$. m^*_{υ} means the reduced effective mass of the electron in the crystal energy zone. m is the mass of the free electron ε_f — the Fermi level. If $g_1 < 0$, we can find solutions to Eq. (3.21) for superconductivity.

3.2.4 *Copper oxides*

In copper oxides, the effective e–e interaction g_2 is important for realizing the high-T_c superconductivity.[135,136] Therefore, we consider that $g_2 \neq 0$ and others $= 0$. The two-particle Green function (3.18) is rewritten as

$$G^{\gamma\delta\beta\sigma}_{2_{\upsilon\upsilon\upsilon\upsilon}}(\mathbf{p}_3, \mathbf{p}_4, \mathbf{p}_2, \mathbf{k}; t - t') = \frac{f(\mathbf{k}, \mathbf{k}', \omega) \sum_{\sigma,\sigma'} \phi(\sigma, \sigma')}{1 - g_2^2 \sum_{\mathbf{q},\mathbf{q}'} K_2(\omega, \mathbf{k}, \mathbf{k}', \mathbf{q}, \mathbf{q}')}, \tag{3.24}$$

where

$$K_2\big(\omega, \mathbf{k}, \mathbf{k}', \mathbf{q}, \mathbf{q}'\big) = \frac{\big(2 - n^{\upsilon'}_{\mathbf{k}+\mathbf{q}-\mathbf{q}'} - n^{\upsilon'}_{\mathbf{k}'-\mathbf{q}+\mathbf{q}'}\big)\big(2 - n^{\upsilon}_{\mathbf{k}+\mathbf{q}} - n^{\upsilon}_{\mathbf{k}'-\mathbf{q}}\big)}{\big(2\omega - \varepsilon^{\upsilon'}_{\mathbf{k}+\mathbf{q}-\mathbf{q}'} - \varepsilon^{\upsilon'}_{\mathbf{k}'-\mathbf{q}+\mathbf{q}'}\big)\big(2\omega - \varepsilon^{\upsilon}_{\mathbf{k}+\mathbf{q}} - \varepsilon^{\upsilon}_{\mathbf{k}'-\mathbf{q}}\big)}. \tag{3.25}$$

According to a similar procedure in previous papers,[96,98] we study the situation near the extremum (minimum or maximum) of the electron zone. Then we suppose that $\mathbf{k} = \mathbf{k}' = \mathbf{k}_0 + \mathbf{k}''$, and $\varepsilon^{\upsilon}_{k0} = \varepsilon^{\upsilon}$ corresponds to the extremum of the zone. We expand the energy in the momentum $\mathbf{k} \pm \mathbf{q}$ in a series up to terms of the second order and suppose that the energy extremum is located near the Fermi-level energy. Then, the sum in the denominator of Eq. (3.24) is approximately reduced to the following expression:

$$\sum_{\mathbf{q},\mathbf{q}'} K_2(\omega, \mathbf{k}, \mathbf{k}', \mathbf{q}, \mathbf{q}') \approx N\big(\varepsilon^{\upsilon}_f\big) N\big(\varepsilon^{\upsilon'}_f\big) \ln\left|\left(1 - \frac{2\Delta}{a_{\upsilon'}}\right)\left(1 - \frac{2\Delta}{a_{\upsilon}}\right)\right|. \tag{3.26}$$

Therefore, we obtain the equation for coupled states in the electron system:

$$1 - g_2^2 N\big(\varepsilon^{\upsilon}_f\big) N\big(\varepsilon^{\upsilon'}_f\big) \ln\left|\left(1 - \frac{2\Delta}{a_{\upsilon'}}\right)\left(1 - \frac{2\Delta}{a_{\upsilon}}\right)\right| = 0. \tag{3.27}$$

From Eq. (3.27), we find the possibility of the existence of a solution for the coupled states, if $g_2 \neq 0$. Thus, the effective e–e interaction g_2 with a positive value contributes to the superconductivity.

3.2.5 *Cooperative mechanism*

Here, we consider that $g_1 \neq 0$, $g_2 \neq 0$ and others $= 0$. In a similar way, the two-particle Green function (3.18) is approximately derived as

$$G^{\gamma\delta\beta\sigma}_{2_{\upsilon\upsilon\upsilon\upsilon}}(\mathbf{p}_3, \mathbf{p}_4, \mathbf{p}_2, \mathbf{k}; t - t') = \frac{f(\mathbf{k}, \mathbf{k}', \omega) \sum_{\sigma,\sigma'} \phi(\sigma, \sigma')}{[1 - (g_1 + g_2) \sum_{\mathbf{q}} K(\omega, \mathbf{k}, \mathbf{k}', \mathbf{q})][1 - (g_1 - g_2) \sum_{\mathbf{q}} K(\omega, \mathbf{k}, \mathbf{k}', \mathbf{q})]}, \tag{3.28}$$

where $K(\omega, \mathbf{k}, \mathbf{k}', \mathbf{q})$ is as given by Eq. (3.20). The summation in the denominator of Eq. (3.28) is performed in a similar way, and the equation for coupled states in the electron system is approximately derived as

$$\left[1-(g_1+g_2)N(\varepsilon_f)\ln\left|1-\frac{\Delta}{a}\right|\right]\left[1-(g_1-g_2)N(\varepsilon_f)\ln\left|1-\frac{\Delta}{a}\right|\right]=0. \tag{3.29}$$

When $g_1+g_2<0$ or $g_1-g_2<0$, we can find solutions to this equation.

3.2.6 *Room-temperature superconductors*

In the previous subsections, we have approximately calculated two-particle Green functions for three cases — traditional superconductivity, copper oxides and the cooperative mechanism — in the framework of a two-band model. From these Green functions, we have derived the equation for coupled states for each case. In the case of a single-band model, which indicates traditional superconductivity such as the BCS theory, it is necessary that the effective e–e interaction be negative ($g_1<0$) in order to realize the superconductivity. The maximal transition temperature for the superconductivity predicted by the theory is about 40 K. On the other hand, we can expect, in a two-band model for negative g_1, that the transition temperature becomes higher than that derived within a single-band model, because of the tunneling of Cooper pairs between two bands. The tunneling of Cooper pairs causes stabilization of the order parameter of the superconductivity.[119,120,129] In the framework of a two-band model, we consider that the Fermi energy level crosses with two bands. The results derived from the two-particle Green function in the previous section suggest that the superconductivity appears for $g_2<0$ or $g_2>0$. Note that g_2 contributes to SDW. From the results derived from calculations involving g_1 and g_2 (cooperative mechanism), we expect a higher T_c than that of copper oxides.

On the basis of the results obtained in this section, we present a schematic diagram for superconductivity, shown in Fig. 3.2. The mechanism of high-T_c superconductivity of materials such as copper oxides might be around the cooperative mechanism in the figure. In what follows, we calculate a two-particle Green function in the two-band model and derive an equation for coupled states. In the framework of the two-band model, the results predict that superconductivity appears even if the e–e interaction is positive. We can

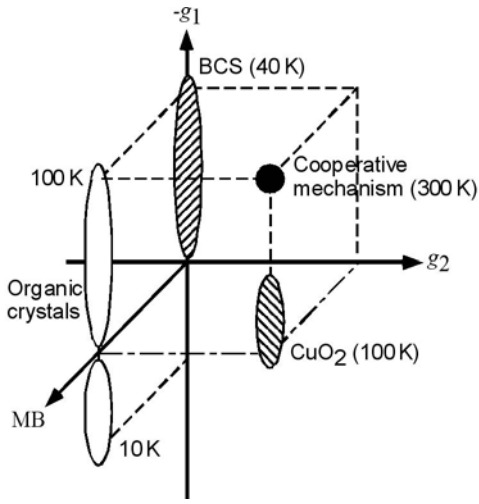

Fig. 3.2 Schematic diagram for superconductivity. MB means multiband effects.

expect that the transition temperature is higher (300 K) than that for copper oxides by the cooperative mechanism.

Let us discuss the problem of superconductors operating at room temperature (RTSCs). It is obvious that the main task in the field of superconductivity is the fabrication of materials with superconducting properties at room temperature. The study of HTSCs is only a stage on the way to the main purpose, namely to the development of RTSCs. At the present time, the highest known $T_c = 135\,\mathrm{K}$ (at the atmospheric pressure). Now there occurs a wide-scale search for such superconductors. Since none of the known physical laws allows one to exclude the possibility for RTSCs to exist, the future discovery of RTSCs seems to be without doubt. New materials are created by means of physical and chemical modifications of the known compounds, including the application of nanotechnological methods. The creation of new materials with preassigned physical properties is one of the actual problems of modern science. At present, various approaches are being developed in order to avoid the labor-consuming sorting of different chemical compounds and conditions of synthesis, i.e. to optimize the solution of this problem. One of the most efficient and promising solution is the method of structural design. In Ref. 121, the structural design was used in solving the problems related to the search for new HTSCs on the basis of complex copper oxides.

We now present the recommendations concerning the search for new HTSCs with higher critical temperatures which were advanced by the Nobel

Prize winner K. A. Müller.[122] He divided the well-known HTSCs into three classes:

(1) Layered cuprates,
(2) MgB_2,
(3) Doped fullerenes of the type K_3C_{60}.

Müller emphasizes that the discovery of cuprate superconductors was promoted by the concept of Jahn–Teller polarons. Two singlet polarons form a bipolaron. Bipolarons are able, in turn, to form metallic clusters (stripes). Müller indicated the following factors which should be taken into account in the search for new HTSCs:

(1) Superconductivity is favored by a layered (quasi-two-dimensional) crystalline structure;
(2) Oxygen ions are proposed as anions;
(3) Fluorine, chlorine and nitrogen can be considered as well.

It is worth noting that the recent discovery of FeAs superconductors eliminated the monopoly of cuprates in the physics of HTSCs. It is possible that new superconductors should be sought in the other rows and columns of the periodic table. It is necessary to concentrate efforts on the purposeful search for and the creation of new HTSCs.

3.3 Two-gap Superconductivity in MgB_2

3.3.1 *The physical properties of MgB_2*

Recently, the superconductivity of MgB_2 with $T_c = 39\,\mathrm{K}$, which is the highest temperature among two-component systems, was discovered.[124] The great interest in the study of magnesium diboride is related to the fact that MgB_2 has occupied the "intermediate" place between low- and high-temperature superconductors by the value of T_c. Therefore, modern literature calls MgB_2 a "medium-T_c superconductor" (MTSC). The low cost of this superconductor also makes it economical for use. We recall that wires made of cuprate superconductors include 70% of silver, which is expensive. An important peculiarity of MgB_2 is its quasi-two-dimensional structure of the AlB_2 type. Interestingly, AlB_2 is not superconducting. Note that MgB_2 is another example of the crucial role played by the lattice structure regarding superconductivity.[123] It is an "old" material which has been known since the early 1950s, but only recently discovered to be superconducting. MgB_2

has a hexagonal structure[118]; see Fig. 3.3.[23] The results of calculations of the temperature dependence of the specific heat of MgB_2 given in Fig. 3.5 follow the corresponding experimental data. The band structure of MgB_2 has been calculated in several works since the discovery of superconductivity.[128] The electronic properties of MgB_2 are plotted in Fig. 3.4. The band structure of MgB_2 is similar to that of graphite and is formed by the σ and π zones.

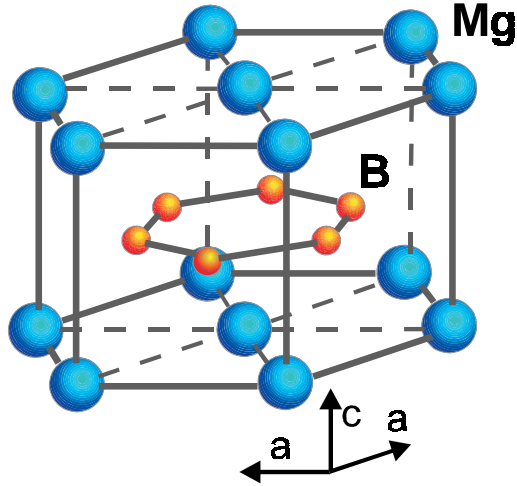

Fig. 3.3 The structure of MgB_2 containing graphite-type B layers separated by hexagonal close-packed layers of Mg.

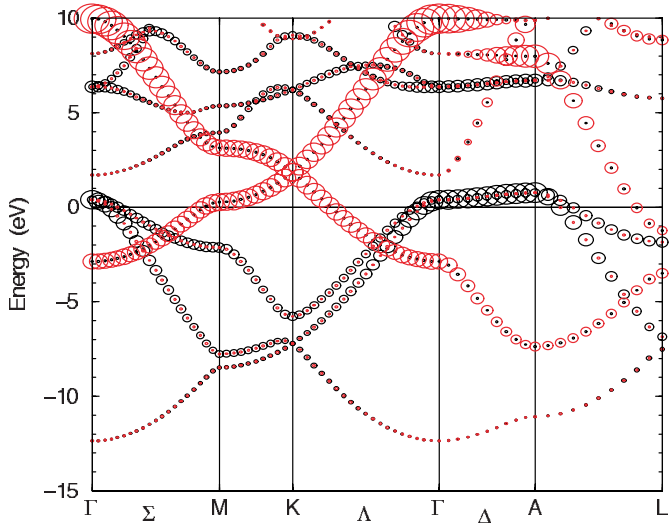

Fig. 3.4 Band structure of MgB_2.

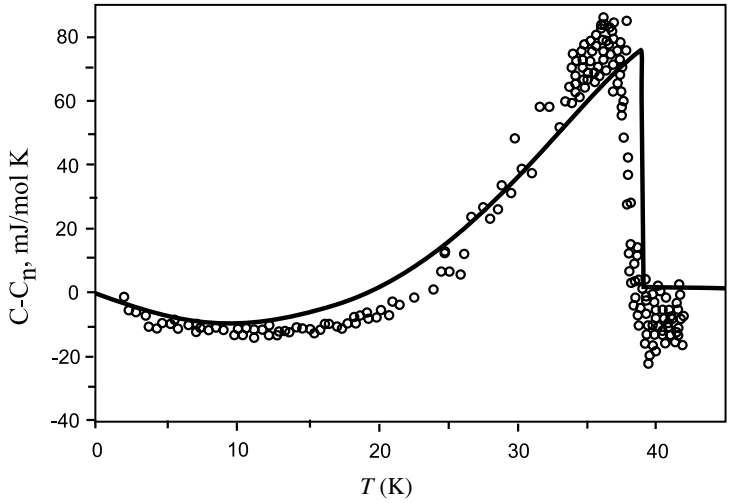

Fig. 3.5 The MgB_2 specific heat vs. temperature. The line indicates theory, and the circles represent the experimental data.

The important problem for superconductivity in MgB_2 is the mechanism of superconductivity. It can be the conventional electron–phonon (e–p) mechanism or a more exotic mechanism. The presence of an isotope effect is a strong indicator of the phonon mediation of superconductivity. The large isotope effect $\alpha_B = 0.26$[130] shows that phonons associated with B vibrations play a significant role in the MgB_2 superconductivity, whereas the magnesium isotope effect is very small: $\alpha_M = 0.02$.[130] The total isotope effect is $\alpha_B + \alpha_M = 0.3$, which supports the electron–phonon mechanism of superconductivity.

MgB_2 is a II-type superconductor.[123] The discovery of the superconductivity of MgB_2 has aroused great interest in multigap superconductivity.[125] MgB_2 has two superconducting gaps, 4 meV and 7.5 meV, due to the π and σ electron bands. The two-gap structure was established in a number of experiments.[130] The plot of the specific heat of MgB_2 vs. temperature (Fig. 3.5) demonstrates good agreement between the theoretical and experimental data. Both gaps have s symmetry and result from the highly anisotropic layer structure of MgB_2. Although multigap superconductivity was discussed theoretically[119,120,129] as early as 1958, it was only observed experimentally[126] in the 1980s. MgB_2 is the first material in which the effects of multigap superconductivity are so dominant, and its implications so thoroughly explored. Recent band calculations[127,128] of MgB_2 with the McMillan formula for the transition temperature have supported the

e–p interaction mechanism for the superconductivity. In this case, the possibility of two-band superconductivity has also been discussed in relation to two-gap functions experimentally and theoretically. Very recently, two-band or multiband superconductivity has been theoretically investigated in relation to the superconductivity arising from Coulomb repulsive interactions. The two-band model was introduced by Kondo.[129] We have also investigated anomalous phases in the two-band model by using the Green function techniques.[96–99,101,103] Recently, we have pointed out the importance of multiband effects in high-T_c superconductivity.[96–98] The expressions for the transition temperature for several phases have been derived, and the approach has been applied to the superconductivity in molecular crystals by charge injection and the field-induced superconductivity.[13] In previous papers,[96–99,101,103] we have investigated the superconductivity by using the two-band model and the two-particle Green function techniques. We have applied the model to the e–p mechanism for the traditional BCS method, the e–e interaction mechanism for high-T_c superconductivity,[2] and the cooperative mechanism. In the framework of the two-particle Green function techniques,[101] it has been shown that the temperature dependence of the superconductivity gap for high-T_c superconductors is more complicated than that predicted in the BCS approach. In Ref. 99, phase diagrams for the two-band model superconductivity have been investigated, by using the renormalization group approach. Below, we will discuss the possibility of the cooperative mechanism of two-band superconductivity in relation to high-T_c superconductivity and study the effect of the increase of T_c in MgB_2 due to the enhanced interband pairing scattering. In this section, we will investigate our two-band model for the explanation of the multigap superconductivity of MgB_2. We apply the model to the e–p mechanism for the traditional BCS method, the e–e interaction mechanism for high-T_c superconductivity, and the cooperative mechanism in relation to multiband superconductivity.

3.3.1.1 $Mg_{1-x}Al_xB_2$

Critical temperature and other superconducting properties of two-band superconductors depend on the doping level as well as the interband and intraband scattering, which can be modified by chemical substitutions. The influence of doping on the transition temperature in $Mg_{1-x}Al_xB_2$ is illustrated in Fig. 3.6. It is seen that the doping destroys the superconductivity in MgB_2. This can be understood as a result of the competition of two

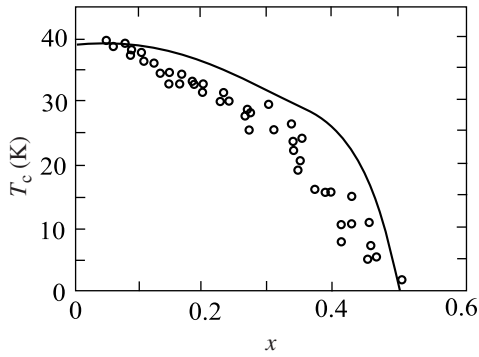

Fig. 3.6 The influence of doping on T_c in $Mg_{1-x}Al_xB_2$. The line indicates theory, and the circles represent the experimental data.

effects: the first one is a coupling effect related to the changes of the carrier concentration, and the second one depends on the introduction of new scattering centers leading to a modification of the interband and intraband scattering.

3.3.2 *Theoretical model*

In this subsection, we will use the two-band model for superconductivity. We start from the Hamiltonian for two bands i and j:

$$H = H_0 + H_{\text{int}}, \tag{3.30}$$

with

$$H_0 = \sum_{\mathbf{k},\sigma} \left[[\epsilon_i(\mathbf{k}) - \mu] a^\dagger_{i\mathbf{k}\sigma} a_{i\mathbf{k}\sigma} + [\epsilon_j(\mathbf{k}) - \mu] a^\dagger_{j\mathbf{k}\sigma} a_{j\mathbf{k}\sigma} \right], \tag{3.31}$$

$$\begin{aligned} H_{\text{int}} = \frac{1}{4} \sum_{\delta(\mathbf{p}_1+\mathbf{p}_2,\mathbf{p}_3+\mathbf{p}_4)} \sum_{\alpha,\beta,\gamma,\delta} \big[& \Gamma^{iiii}_{\alpha\beta\gamma\delta} a^\dagger_{i\mathbf{p}_1\alpha} a^\dagger_{i\mathbf{p}_2\beta} a_{i\mathbf{p}_3\gamma} a_{i\mathbf{p}_4\delta} + (i \leftrightarrow j) \\ & + \Gamma^{iijj}_{\alpha\beta\gamma\delta} a^\dagger_{i\mathbf{p}_1\alpha} a^\dagger_{i\mathbf{p}_2\beta} a_{j\mathbf{p}_3\gamma} a_{j\mathbf{p}_4\delta} + (i \leftrightarrow j) \\ & + \Gamma^{ijij}_{\alpha\beta\gamma\delta} a^\dagger_{i\mathbf{p}_1\alpha} a^\dagger_{j\mathbf{p}_2\beta} a_{i\mathbf{p}_3\gamma} a_{j\mathbf{p}_4\delta} + (i \leftrightarrow j) \big], \end{aligned} \tag{3.32}$$

where Γ is the bare vertex part,

$$\Gamma^{ijkl}_{\alpha\beta\gamma\delta} = \langle i\mathbf{p}_1\alpha j\mathbf{p}_2\beta | k\mathbf{p}_3\gamma l\mathbf{p}_4\delta \rangle \delta_{\alpha\delta}\delta_{\beta\gamma} - \langle i\mathbf{p}_1\alpha j\mathbf{p}_2\beta | l\mathbf{p}_4\delta k\mathbf{p}_3\gamma \rangle \delta_{\alpha\gamma}\delta_{\beta\delta}, \tag{3.33}$$

with

$$\langle i\mathbf{p}_1\alpha j\mathbf{p}_2\beta|k\mathbf{p}_3\beta l\mathbf{p}_4\alpha\rangle$$
$$= \int dr_1\, dr_2 \phi^*_{i\mathbf{p}_1\alpha}(r_1)\phi^*_{j\mathbf{p}_2\beta}(r_2)V(r_1,r_2)\phi_{k\mathbf{p}_3\beta}(r_2)\phi_{l\mathbf{p}_4\alpha}(r_1), \quad (3.34)$$

where $a_{i\mathbf{p}\sigma^+}$ ($a_{i\mathbf{p}\sigma}$) is the creation (annihilation) operator corresponding to the excitation of electrons (or holes) in the ith band with spin σ and momentum $\mathbf{p}$, μ is the chemical potential and ϕ is a single-particle wave function. Here, we suppose that the vertex function in Eq. (3.32) involves the effective interactions between the carriers caused by the linear vibronic coupling in several bands and the screened Coulombic interband interaction of carriers.

When we use the two-band Hamiltonian (3.1) and define the order parameters for a singlet exciton, triplet exciton and singlet Cooper pair, the mean field Hamiltonian is easily derived.[96–99,101,103] Here, we focus on three electron scattering processes contributing to the singlet superconducting phase in the Hamiltonian (3.1):

$$g_{i1} = \langle ii|ii\rangle, \quad g_{j1} = \langle jj|jj\rangle, \quad (3.35)$$
$$g_2 = \langle ii|jj\rangle = \langle jj|ii\rangle, \quad (3.36)$$
$$g_3 = \langle ij|ij\rangle = \langle ji|ji\rangle, \quad (3.37)$$
$$g_4 = \langle ij|ji\rangle = \langle ji|ij\rangle, \quad (3.38)$$

where g_{i1} and g_{j1} represent the ith and jth intraband two-particle normal scattering processes, respectively, and g_2 indicates the intraband two-particle umklapp scattering (see Fig. 3.7). For simplicity, we consider the three cases in Refs. 99 and 100: (i) $g_1 \neq 0$ and others $= 0$; (ii) $g_2 \neq 0$; and others $= 0$; (iii) g_{i1} and g_{j1}, and others $= 0$, using the two-particle Green function techniques (see Fig. 3.7).

It was shown that, possibly, the two-gap superconductivity arises in case (iii). The superconductivity arising from the e–p mechanism ($g_1 < 0$ and $g_1 < g_2$) such as for MgB_2 is in the two-gap region. On the other hand, the superconductivity of copper oxides ($g_1 > g_2$) is outside the two-gap region. These results predict that we may observe two-gap functions for MgB_2 and only a single-gap function for copper oxides.

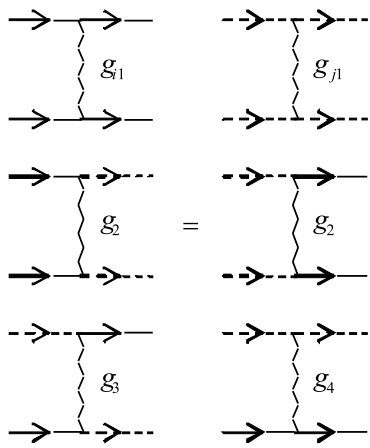

Fig. 3.7 Electron–electron interactions. Solid and dashed lines indicate π and σ bands, respectively; g_{i1}, g_{j1}, g_2, g_3 and g_4 contribute to superconductivity.

3.3.3 *Superconductivity in MgB_2*

Using case (iii) for g_{i1} and g_{j1}, $g_2 \neq 0$ and others $= 0$ to describe the superconductivity in MgB_2. We now have a reduced Hamiltonian:

$$H = H_0 + H_{\text{int}}, \tag{3.39}$$

where

$$H_0 = \sum_{\mathbf{k},\sigma} \left[[\epsilon_i - \mu] a^\dagger_{i\mathbf{k}\sigma} a_{i\mathbf{k}\sigma} + [\epsilon_j - \mu] a^\dagger_{j\mathbf{k}\sigma} a_{j\mathbf{k}\sigma} \right], \tag{3.40}$$

$$H_{\text{int}} = \sum g_{1i} a^\dagger_{i\mathbf{k}} a^\dagger_{i-\mathbf{k}} a_{i-\mathbf{k}} a_{i\mathbf{k}} + \sum i \to j + \sum g_2 a^\dagger_{i\mathbf{k}} a^\dagger_{i-\mathbf{k}} a_{j-\mathbf{k}} a_{j\mathbf{k}}. \tag{3.41}$$

We now define the order parameters which are helpful in constructing the mean-field Hamiltonian:

$$\Delta_i = \sum_p \left\langle a^\dagger_{ip\uparrow} a^\dagger_{i-p\downarrow} \right\rangle, \tag{3.42}$$

$$\Delta_j = \sum_p \left\langle a^\dagger_{jp\uparrow} a^\dagger_{j-p\downarrow} \right\rangle. \tag{3.43}$$

The relation between two superconducting gaps of the system is as follows:

$$\Delta_j = \frac{1 - g_{i1}\rho_i f_i}{g_2 \rho_j f_j} \Delta_i, \tag{3.44}$$

where

$$f_i = \int_{\mu}^{\mu - E_c} \frac{d\xi}{(\xi^2 + \Delta_i^2)^{1/2}} \tan \mathrm{h} \frac{(\xi^2 + \Delta_i^2)^{1/2}}{2T},$$
$$f_j = \int_{\mu - E_c}^{\mu - E_j} \frac{d\xi}{(\xi^2 + \Delta_j^2)^{1/2}} \tan \mathrm{h} \frac{(\xi^2 + \Delta_j^2)^{1/2}}{2T}, \tag{3.45}$$

with the coupled gap equation

$$(1 - g_{i1}\rho_i f_i)(1 - g_{j1}\rho_j f_j) = g_2^2 f_i f_j. \tag{3.46}$$

We have tried to estimate the coupling constant of the pair electron scattering process between the π and σ bands of MgB_2 and have calculated the parameters by using a rough numerical approximation. We focus on one π band and σ band of MgB_2 and consider electrons near Fermi surfaces. We found that the parameter $g_1 = -0.4\,\mathrm{eV}$, by using the transfer integral between the π and σ bands. We estimate the coupling parameter g_2 of the pair electron scattering process by the expression

$$g_2 = \sum_{k1,k2} V_{k1,k2}^{1,2}, \tag{3.47}$$

$$V_{k1,k2}^{1,2} = \sum_{r,s,t,u} u_{1,r}^*(k1) u_{1,s}^*(k1) v_{rs} u_{2,t}(k2) u_{2,u}(k2), \tag{3.48}$$

where the labels 1 and 2 are the π band and the σ band, respectively, $u_{i,r}(\xi)$ is the LCAO coefficient for the ith band and ξ is the moment.[115,116] The indices $k1$ and $k2$ are summed over each Fermi surface. However, it is difficult to perform the sum exactly. In this case, we used a few points near the Fermi surface. The coupling constant of the pair electron scattering between the π band and the σ band is $g_2 = 0.025\,\mathrm{eV}$. From numerical calculations of Eqs. (3.44)–(3.46), we can also obtain the temperature dependence of the two-gap parameters (see Fig. 3.8). We have used the density of states of the π and σ bands ($\rho_i = 0.2\,\mathrm{eV}^{-1}$; $\rho_j = 0.14\,\mathrm{eV}^{-1}$), chemical potential $\mu = -2.0$, the top energy of the σ band $E_j = -1.0$ and the fitting parameters ($g_{i1} = -0.4\,\mathrm{eV}$; $g_{j1} = -0.6\,\mathrm{eV}$; $g_2 = 0.02\,\mathrm{eV}$). These calculations have qualitative agreement with experiments.[118,130,131] The expression for the transition temperature of superconductivity derived in a simple approximation is:

$$T_{c_+} = 1.13(\zeta - E_j) \cdot \exp\left(\frac{-1}{g_+ \rho}\right), \tag{3.49}$$

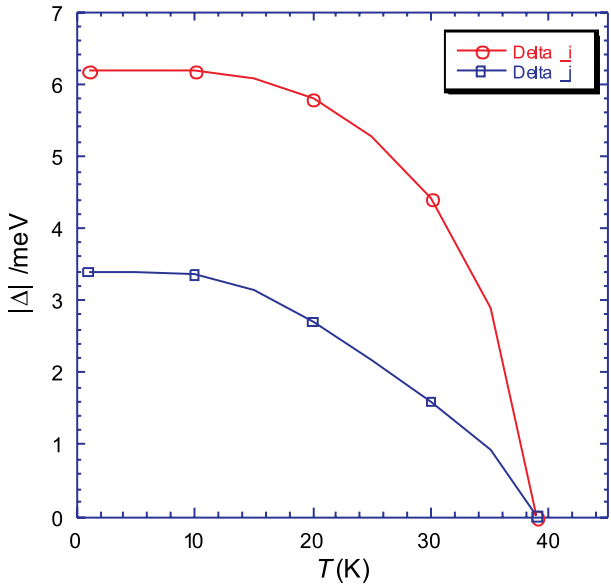

Fig. 3.8 Temperature dependence of two superconducting gaps.

where

$$g_+ = \frac{1}{24}(B + \sqrt{B^2 - 4A}) \tag{3.50}$$

and

$$A = g_{1i}g_{1j} - g_2^2, \tag{3.51}$$

$$B = g_{1i} + g_{1j}, \tag{3.52}$$

$$\zeta = -\mu. \tag{3.53}$$

From the expressions for T_{c+}, we can see the effect of increase of T_{c+} due to the enhanced interband pairing scattering (g_2).

Figure 3.9 shows a schematic diagram of the mechanism of pairing for two gaps. The scenario is as follows. Electrons from the π and σ bands make up the subsystems. For g_2, we have two independent subsystems with the different transition temperatures of superconductivity $T_{c\pi}$ and $T_{c\sigma}$ and two independent superconducting gaps. In our model, we have two coupled superconducting gaps with the relation (3.44) and one transition temperature of superconductivity T_{c+}, which is in agreement with experiments. In this model, we have two channels of superconductivity: conventional channel (intraband g_1) and unconventional channel (interband g_2). Two gaps appear simultaneously in different bands which are like BCS gaps. The gap

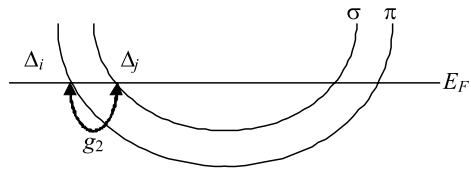

Fig. 3.9 Schematic diagram of the mechanism of pairing for two gaps.

in the π band is bigger than that for the σ band, because the density of state is 0.25 eV in the π band and 0.14 eV in the σ band. The current of Cooper pairs flows from the π band into the σ band, because the density of Cooper pairs in the π band is much higher. The tunneling of Cooper pairs also stabilizes the order parameter in the σ band. In this way, we can predict the physical properties of the multigap superconductivity if we have the superconductors with a multiband structure, as shown in Fig. 3.9.

Thus, we have presented our two-band model with the intraband two-particle scattering and interband pairing scattering processes to describe two-gap superconductivity in MgB_2. We defined the parameters of our model and made numerical calculations of the temperature dependence of two gaps in qualitative agreement with experiments. We have proposed a two-channel scenario of superconductivity: the conventional channel (intraband g_1), which is connected with the BCS mechanism in different bands; and the unconventional channel (interband g_2), which describes the tunneling of Cooper pairs between two bands. The tunneling of Cooper pairs also stabilizes the order parameters of superconductivity and increases the critical temperature of superconductivity.

3.4 Theoretical Studies of Multiband Effects in Superconductivity by Using the Renormalization Group Approach

We present the renormalization equations using the two-band model and construct phase diagrams for the two-band superconductivity. In the framework of the two-band model, the given results predict that superconductivity appears, even if the e–e interaction is positive. We discuss the possibility of a cooperative mechanism in the two-band superconductivity in relation to high-T_c superconductivity. The recent discovery of superconductivity in MgB_2[124] has also attracted great interest to the elucidation of its mechanism from both the experimental and theoretical viewpoints. A crucial

role of the e–p interaction has been pointed out for the superconductivity of MgB_2. Recent band calculations of the transition temperature for MgB_2[127,128] with the McMillan formula[132] have supported the e–p interaction mechanism for the superconductivity. In this case, the possibility of the two-band superconductivity in relation to two-gap functions has also been considered experimentally and theoretically. Very recently, the two-band or multiband superconductivity has been theoretically investigated in relation to the superconductivity arising from Coulomb repulsive interactions.[129] The two-band model was introduced by Kondo.[129] Recently, we have pointed out the importance of multiband effects in high-T_c superconductivity.[99,138] We have also investigated anomalous phases in the two-band model by using the Green function techniques.[101,136] The expressions of the transition temperature for several phases have been derived, and the approach has been applied to the superconductivity in several crystals by charge injection and the field-induced superconductivity.[136,139] In the previous section, we have investigated superconductivity by using the two-band model and the two-particle Green function techniques.[99,101] We have applied the model to the e–p mechanism for the traditional BSC method, the e–e interaction mechanism for high-T_c superconductivity and the cooperative mechanism. In the framework of the two-particle Green function techniques,[103] it has been shown that, in the e–p system, a class of new so-called coupled states arises. In this section, we investigate two- or multiband effects in superconductivity by using the two-band model within the renormalization group approach. Renormalization equations for the two-band superconductivity are derived from the response function and the vertex correction of the model. Phase diagrams numerically obtained from the renormalization equations are presented. We also discuss the superconductivity arising from the e–e repulsive interaction in relation to the two-band superconductivity.

3.4.1 *Theoretical model*

In this subsection, we summarize the two-band model for the superconductivity and introduce the renormalization group approach.[142,144]

We consider a Hamiltonian for two bands i and j, written as

$$H = H_0 + H_{\rm int}, \tag{3.54}$$

with

$$H_0 = \sum_{\mathrm{k},\sigma} \left[[\epsilon_i(\mathrm{k}) - \mu] a^\dagger_{i\mathrm{k}\sigma} a_{i\mathrm{k}\sigma} + [\epsilon_j(\mathrm{k}) - \mu] a^\dagger_{j\mathrm{k}\sigma} a_{j\mathrm{k}\sigma} \right], \tag{3.55}$$

$$H_{\rm int} = \frac{1}{4} \sum_{\delta(\mathrm{p}_1+\mathrm{p}_2,\mathrm{p}_3+\mathrm{p}_4)} \sum_{\alpha,\beta,\gamma,\delta} \big[\Gamma^{iiii}_{\alpha\beta\gamma\delta} a^\dagger_{i\mathrm{p}_1\alpha} a^\dagger_{i\mathrm{p}_2\beta} a_{i\mathrm{p}_3\gamma} a_{i\mathrm{p}_4\delta} + (i \leftrightarrow j)$$
$$+ \Gamma^{iijj}_{\alpha\beta\gamma\delta} a^\dagger_{i\mathrm{p}_1\alpha} a^\dagger_{i\mathrm{p}_2\beta} a_{j\mathrm{p}_3\gamma} a_{j\mathrm{p}_4\delta} + (i \leftrightarrow j)$$
$$+ \Gamma^{ijij}_{\alpha\beta\gamma\delta} a^\dagger_{i\mathrm{p}_1\alpha} a^\dagger_{j\mathrm{p}_2\beta} a_{i\mathrm{p}_3\gamma} a_{j\mathrm{p}_4\delta} + (i \leftrightarrow j) \big], \tag{3.56}$$

where Γ is the bare vertex part,

$$\Gamma^{ijkl}_{\alpha\beta\gamma\delta} = \langle i\mathrm{p}_1\alpha j\mathrm{p}_2\beta | k\mathrm{p}_3\gamma l\mathrm{p}_4\delta \rangle \, \delta_{\alpha\delta} \, \delta_{\beta\gamma} - \langle i\mathrm{p}_1\alpha j\mathrm{p}_2\beta | l\mathrm{p}_4\delta k\mathrm{p}_3\gamma \rangle \, \delta_{\alpha\gamma}\delta_{\beta\delta}, \tag{3.57}$$

with

$$\langle i\mathrm{p}_1\alpha j\mathrm{p}_2\beta | k\mathrm{p}_3\beta l\mathrm{p}_4\alpha \rangle$$
$$= \int dr_1 dr_2 \phi^*_{i\mathrm{p}_1\alpha}(r_1) \phi^*_{j\mathrm{p}_2\beta}(r_2) V(r_1, r_2) \phi_{k\mathrm{p}_3\beta}(r_2) \phi_{l\mathrm{p}_4\alpha}(r_1), \tag{3.58}$$

where $a^\dagger_{i\mathrm{p}\sigma}$ ($a_{i\mathrm{p}\sigma}$) is the creation (annihilation) operator corresponding to the excitation of electrons (or holes) in the ith band with spin σ and momentum p, μ is the chemical potential and $\phi^*_{i\alpha\mathrm{p}_1}$ is a single-particle wave function. Here, we suppose that the vertex function in Eq. (3.56) involves the effective interactions between carriers caused by the linear vibronic coupling in several bands and the screened Coulombic interband interaction of carriers.

We focus on three electron scattering processes contributing to the singlet superconducting phase in the Hamiltonian (3.56), as shown in Fig. 3.10:

$$g_{i1} = \langle ii|ii \rangle, \tag{3.59}$$
$$g_{j1} = \langle jj|jj \rangle, \tag{3.60}$$
$$g_2 = \langle ii|jj \rangle = \langle jj|ii \rangle, \tag{3.61}$$

where g_{i1} and g_{j1} represent the ith and jth intraband two-particle normal scattering processes, respectively, and g_2 indicates the intraband two-particle umklapp scattering. Note that the Γ's are given by

$$\Gamma^{iiii}_{\alpha\beta\gamma\delta} = g_{i1}(\delta_{\alpha\delta}\delta_{\beta\gamma} - \delta_{\alpha\gamma}\delta_{\beta\delta}),$$
$$\Gamma^{jjjj}_{\alpha\beta\gamma\delta} = g_{j1}(\delta_{\alpha\delta}\delta_{\beta\gamma} - \delta_{\alpha\gamma}\delta_{\beta\delta}),$$
$$\Gamma^{iijj}_{\alpha\beta\gamma\delta} = \Gamma^{jjii}_{\alpha\beta\gamma\delta} = g_2(\delta_{\alpha\delta}\delta_{\beta\gamma} - \delta_{\alpha\gamma}\delta_{\beta\delta}), \tag{3.62}$$

where we assume that an antisymmetrized vertex function Γ is a constant independent of the momenta.

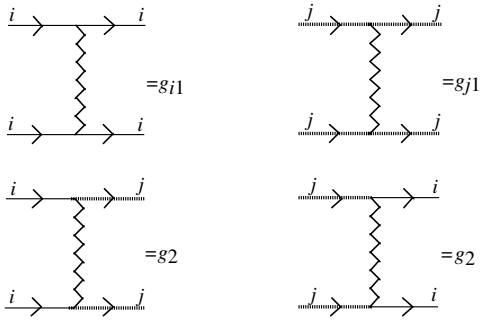

Fig. 3.10 Electron–electron interactions. Dependence of g on the direction in the momentum space is ignored in this model [$g_x(\mathrm{k}) \approx g_x$ $(x = i, j)$]. We assume that g_x is constant.

The spectrum is elucidated by the Green function method. Using Green functions which characterize the CDW, SDW and SSC phases, we obtain a self-consistent equation according to the traditional procedure.[115,136,138,145–147] Then we can obtain expressions for the transition temperature in some cases. Electronic phases of a one-dimensional system have been investigated by using a similar approximation in the framework of the one-band model.[144–147] In the framework of the mean-field approximation within the two-band model, we have already derived expressions for the transition temperature for CDW, SDW and SSC. In Refs. 136 and 138, we have investigated the dependence of T_c on the hole or electron concentration for the superconductivity of copper oxides by using the two-band model and have obtained a phase diagram of $Bi_2Sr_2Ca_{1-x}Y_xCu_2O_8$ (Bi-2212) by means of the above expressions for the transition temperature.

3.4.2 *Renormalization-group approach*

The Dyson equation is invariant under a multiple renormalization of Green function and coupling parameters g. From this invariance for a scaling procedure, we obtain differential equations for the coupling parameters and the external vertex of a Cooper pair:

$$y\frac{\partial}{\partial y}\tilde{g}_i(y,u,g) = \frac{\partial}{\partial \xi}\tilde{g}_i\left(\xi, \frac{u}{y}, \tilde{g}(t,u,g)\right)|_{\xi=1}, \tag{3.63}$$

$$y\frac{\partial}{\partial y}\ln\Lambda(y,u,g) = \frac{\partial}{\partial \xi}\ln\Lambda\left(\xi, \frac{u}{y}, \tilde{g}(t,u,g)\right)|_{\xi=1}, \tag{3.64}$$

where y and u are parameters with the dimension of energy, g is the set of original couplings and Λ is the external vertex.

3.4.3 *Vertex correction and response function for Cooper pairs*

To solve Eqs. (3.63) and (3.64), we estimate the right-hand side of Eq. (3.63) by using the perturbation theory. We consider the lowest-order correction to the vertex for a Cooper pair, as shown in Fig. 3.11. From these diagrams, we obtain

$$\begin{pmatrix} \tilde{g}_{i1} \\ \tilde{g}_{j1} \end{pmatrix} = \begin{pmatrix} g_{i1} \\ g_{j1} \end{pmatrix} + \begin{pmatrix} -g_{i1}^2 & -g_2^2 \\ -g_{j1}^2 & -g_2^2 \end{pmatrix} \begin{pmatrix} L_i \\ L_j \end{pmatrix}, \tag{3.65}$$

$$\begin{pmatrix} \tilde{g}_2 \\ \tilde{g}_2 \end{pmatrix} = \begin{pmatrix} g_2 \\ g_2 \end{pmatrix} + \begin{pmatrix} -g_{i1}g_2 & -g_2 g_{j1} \\ -g_{j1}g_2 & -g_2 g_{i1} \end{pmatrix} \begin{pmatrix} L_i \\ L_j \end{pmatrix}, \tag{3.66}$$

with

$$\begin{aligned} L_i = \Pi_i(\mathrm{k}, \omega) &= \frac{T}{N} \sum_{\mathrm{q},\omega'} G_i(\mathrm{q}, \omega') G_i(\mathrm{k} - \mathrm{q}, \omega - \omega'), \\ L_j = \Pi_j(\mathrm{k}, \omega) &= \frac{T}{N} \sum_{\mathrm{q},\omega'} G_j(\mathrm{q}, \omega') G_j(\mathrm{k} - \mathrm{q}, \omega - \omega'), \end{aligned} \tag{3.67}$$

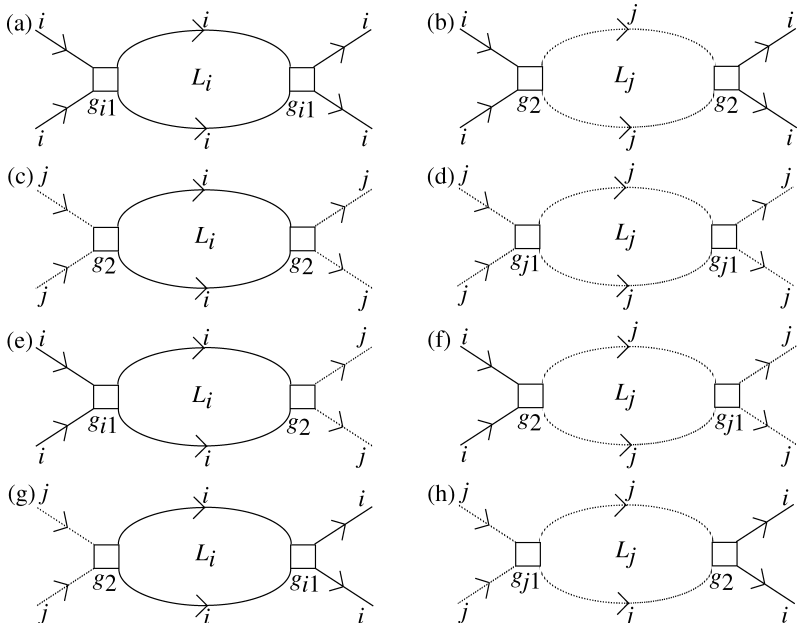

Fig. 3.11 Diagrams of the first-order vertex correction. (a) and (b) contribute to $\tilde{g}_{i1}$, (c) and (d) are diagrams for $\tilde{g}_{j1}$, and (e)–(h) for $\tilde{g}_2$.

where G and T are the temperature Green function and temperature, respectively. For the special case $\omega = 0$, $\mathrm{k} = 0$, the functions L_i and L_j become

$$L_i = -\left[\tan\mathrm{h}\left(\frac{u_i/y}{2\xi}\right) + \tan\mathrm{h}\left(\frac{u_i'/y}{2\xi}\right)\right]\ln\xi - 2A, \tag{3.68}$$

$$L_j = -\left[\tan\mathrm{h}\left(\frac{u_j/y}{2\xi}\right) + \tan\mathrm{h}\left(\frac{u_j'/y}{2\xi}\right)\right]\ln\xi - 2A, \tag{3.69}$$

where

$$A = \int dx \ln x \,\mathrm{sech}^2\mathrm{x}, \tag{3.70}$$

u_i (u_j) and u_i' (u_j') are dimensionless functions expressed by the chemical potential, the cutoff energy, the top energy of the jth band, and the density of state for the ith (jth) band.

Next, we consider a first-order response function for a singlet Cooper pair, as shown in Fig. 3.12. Then the first-order vertex function Λ for the ith and jth bands can be written as

$$\begin{pmatrix}\Lambda_i + \Lambda_j \\ \Lambda_i - \Lambda_j\end{pmatrix} = \begin{pmatrix}2 \\ 0\end{pmatrix} + \begin{pmatrix}-g_1 & -g_2 \\ -g_1 & g_2\end{pmatrix}\begin{pmatrix}L_i + L_j \\ L_i - L_j\end{pmatrix}. \tag{3.71}$$

3.4.4 *Renormalization equation*

For simplicity, we hereafter assume that $g_{i1} = g_{j1}$. From Eqs. (3.63), (3.65) and (3.66), we obtain the differential equations written as

$$\frac{\partial}{\partial x}\tilde{g}_1 = -\left(\tilde{g}_1^2 + \tilde{g}_2^2\right), \tag{3.72}$$

$$\frac{\partial}{\partial x}\tilde{g}_2 = -2\tilde{g}_1\tilde{g}_2. \tag{3.73}$$

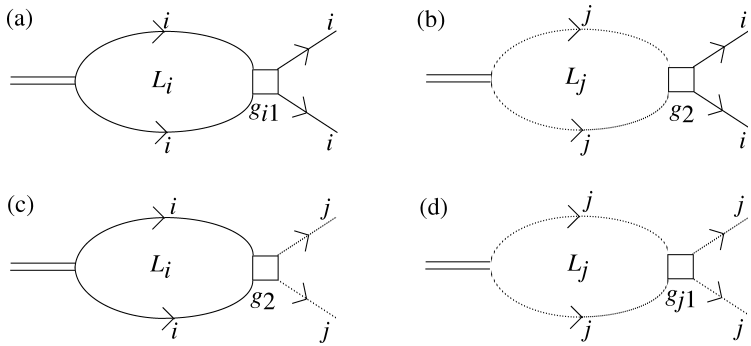

Fig. 3.12 Diagrams of the first-order response function. (a) and (b) contribute to Λ_i, and (c) and (d) show diagrams for Λ_j.

In a similar way, using Eqs. (3.64) and (3.71), we obtain the differential equations written as

$$\frac{\partial}{\partial x}\ln\Lambda_+ = -\tilde{g}_1 - \tilde{g}_2, \tag{3.74}$$

$$\frac{\partial}{\partial x}\ln\Lambda_- = -\tilde{g}_1 + \tilde{g}_2, \tag{3.75}$$

where $\Lambda_+ = \Lambda_i + \Lambda_j$ and $\Lambda_- = \Lambda_i - \Lambda_j$.

3.4.5 *Phase diagrams*

In the previous subsection, we have derived the basic equations (3.72)–(3.75) to find the low-temperature phases. For the special case of $g_2 = 0$, we obtain an analytic solution:

$$\tilde{g}_1 = \frac{1}{x + g_1^{-1}}, \tag{3.76}$$

$$\tilde{g}_2 = 0, \tag{3.77}$$

$$\Lambda_i = \Lambda_j = \frac{1}{g_1 x + 1}. \tag{3.78}$$

From these solutions, we find that the superconducting phase appears only when the intraband interaction g_1 is negative. In the case of the traditional superconductivity described by the BCS theory, it is necessary that the effective e–e interaction be negative ($g_1 < 0$) in order to realize the superconductivity. The present result agrees with that of the traditional theory for superconductivity expressed by the one-band model. For the case of $g_2 \neq 0$, the phase diagrams numerically obtained from the above renormalization equations are shown in Fig. 3.13. Figure 3.13(a) shows the phase diagram for the sum of contributions to the superconductivity from the ith and jth bands. Thus, this phase implies that the signs of the superconducting state for the ith and jth bands are the same. From this diagram, we find the superconductivity only for $-g_1 - g_2 > 0$, with negative g_2. On the other hand, the phase diagram for the difference between the superconducting states for the ith and jth bands is shown in Fig. 3.13(b). In this case, this phase means that the sign of the superconductivity for the ith band is different from that of the jth band. We can see that the superconductivity appears only for $-g_1 + g_2 > 0$ with positive g_2 from Fig. 3.13(b). Thus, the present results suggest that the two-band superconductivity appears when the intraband umklapp repulsive scattering g_2 is larger than the normal repulsive scattering g_1. In the region of $g_2 > g_1$ with $g_2 < 0$ and

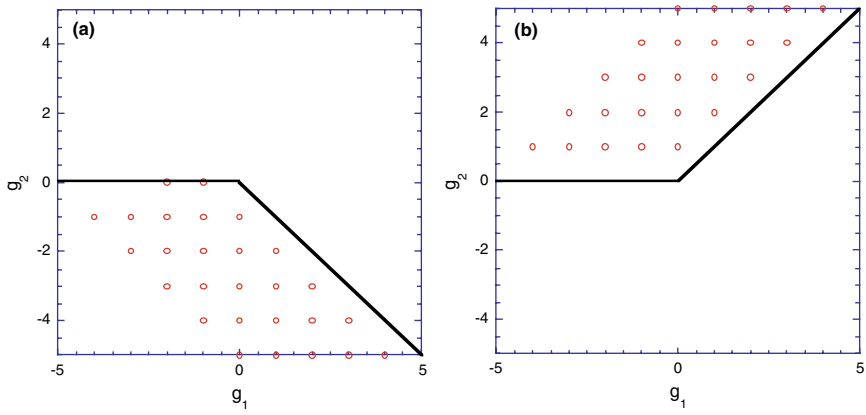

Fig. 3.13 Phase diagrams for superconductivity: (a) $\Lambda_i + \Lambda_j$, (b) $\Lambda_i - \Lambda_j$.

$g_2 < -g_1$ with $g_2 > 0$ (two-gap region), we can expect that two-gap functions are observed. In the former region, those superconducting gaps may be expressed by $|\Lambda_+| > |\Lambda_-|$, and the latter may be $|\Lambda_+| < |\Lambda_-|$. On the other hand, we expect only a single-gap function in the other region. These results agree with the previous solutions[96,99] derived by using the two-particle Green function techniques. The superconductivity arising from the e–p mechanism ($g_1 < 0$ and $|g_2| < |g_1|$) such as that in MgB_2 is in the two-gap region. On the other hand, the superconductivity such as in copper oxides ($|g_2| > |g_1|$) is outside the two-gap region. These results predict that we may observe two-gap functions for MgB_2 and only a single-gap function for copper oxides. In the two-band model for negative g_1 with transferring or tunneling of Cooper pairs between two bands, we can expect that the transition temperature becomes higher than that derived from the single-band model. The tunneling of Cooper pairs causes stabilization of the order parameter of superconductivity.[119,120,129] We can also expect higher T_c of the superconductivity than that for copper oxides in two regions ($g_1 < 0$, $g_2 < 0$ and $g_1 < 0$, $g_2 > 0$) by the cooperative mechanism. Phase diagrams for CDW, SDW, and singlet superconductivity derived from a more general Hamiltonian will be presented elsewhere.

Thus, we have derived the renormalization equations and presented the phase diagrams for the two-band superconductivity. In the framework of the two-band model, the present results predict that superconductivity appears even if the e–e interaction is positive. We can expect that the transition temperature becomes higher than that of copper oxides by the cooperative mechanism.

CHAPTER 4

Mesoscopic Superconductivity

4.1 Introduction

Recent advances in nanoscience have demonstrated that fundamentally new physical phenomena are found when systems are reduced in size to dimensions which become comparable to the fundamental microscopic lengths of the investigated material. Superconductivity is a macroscopic quantum phenomenon, and it is therefore especially interesting to see how this quantum state is influenced when the samples are reduced to nanometer sizes. Recent developments in nanotechnologies and measurement techniques allow experimental investigation of the magnetic and thermodynamic superconducting properties of mesoscopic samples in this regime.

In this book, we develop some theoretical models for describing such nanoscale superconducting systems and explore possible new experimental phenomena which we can predict based upon these models. In bulk samples, the standard BCS theory gives a good description of the phenomenon of superconductivity.[104] However, it was noticed by Anderson in 1959 that, as the size of a superconductor becomes smaller, and the quantum energy level spacing of the electrons in the sample approaches the superconducting gap, the BCS theory will fail.[6] The exact solution to the reduced BCS Hamiltonian for finite-size systems was developed by Richardson in the context of nuclear physics a long time ago.[149] This shows that, while the grand canonical BCS wave function gives a very accurate solution to the BCS Hamiltonian in the limit where the number of electrons is very large $N \gg 1$, for small values of N one has to use exact analytical methods to obtain reliable results. The recent experimental advances in fabricating and measuring superconductivity in ultrasmall mesoscopic and nanoscale grains has renewed theoretical interest in the Richardson solution.[150–153] In this book,

we propose to develop theoretical models for nanoscale superconducting systems and to apply these models to a variety of systems of current experimental interest. The Richardson solution depends on the electron energy level spacings near to the Fermi level, and so these different geometric shapes will lead to different size dependences of the thermodynamic and electronic properties. Experiments have recently demonstrated superconductivity in one-dimensional nanowires of lead[154] and carbon.[155] Our theoretical predictions will include the even–odd parity effects in tunneling spectra, which have already been observed on the nanometer scale in Al grains, (Fig. 4.1),[150] but which could also be observed in nanotube superconductors. In Figs. 4.1 and 4.2, we can see the ensemble of small metallic grains which can be in the normal or superconducting state. For such systems, the important parameters are the l-granular size, the electron coherence length, and the penetration depth.[123] In grains, there appears the quantum size effect (discretization of the electron energy spectrum). In Fig. 4.2, we show the size effect in grains. We note that the level spacing depends on many parameters, such as the electron coherence length and the penetration depth. Carbon nanotubes were first observed in 1991 by Iijima in Japan, (Fig. 4.3).

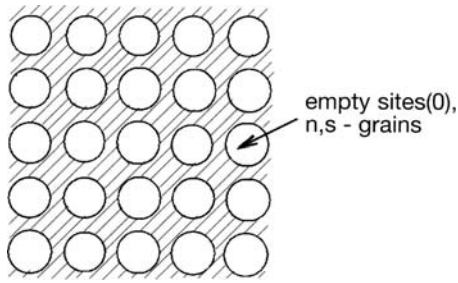

Fig. 4.1 Illustration of superconductor grains.

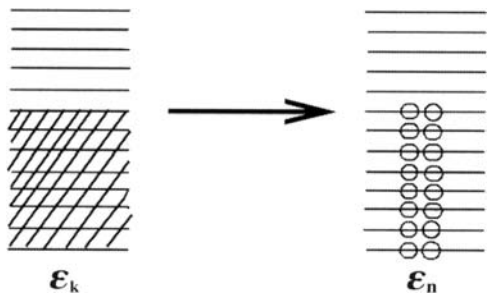

Fig. 4.2 Size effect in superconductor grains.

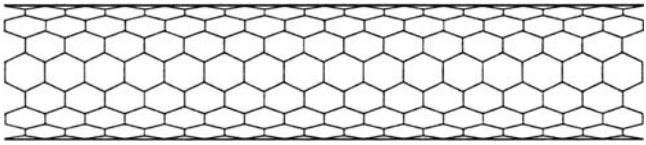

Fig. 4.3 Carbon nanotube revealing superconductivity.

In this chapter, we investigate properties of nanosize two-gap superconductivity by using a two-sublevel model in the framework of the mean-field approximation. A model corresponding to nanosize two-gap superconductivity is presented, and the partition function of the nanosize system is analytically derived by using the path-integral approach. A definition of the critical level spacing of the two-gap superconductivity is also presented, and we discuss the condensation energy and the parity gap of the two-gap superconductivity in relation to the size dependence of those properties with two bulk gaps and the effective pair scattering process between two sublevels. We present the theory of interactions between two nanoscale ferromagnetic particles embedded in a superconductor and spin orientation phase transitions in such a system. We also consider the ideas of quantum computing and quantum information in mesoscopic circuits. The theory of the Josephson effect is presented, and its applications in quantum computing are analyzed. The results of this chapter were obtained by the authors and published in Refs. 123, 156–158.

4.2 Nanosize Two-Gap Superconductivity

Multiband superconductivity has been theoretically investigated in relation to MgB_2 superconductivity in Chap. 3.

Recent experiments[160,164] by Black *et al.* have also generated high interest in the size dependence of the superconductivity. Properties of ultrasmall superconducting grains have been theoretically investigated by many groups.[161,162,165–169] In such ultrasmall grains, the old but fundamental theoretical question was noticed by Anderson.[6] The standard BCS theory gives a good description of the phenomenon of superconductivity in large samples. However, as the size of a superconductor becomes small, the BCS theory fails. In ultrasmall Al grains, the bulk gap has been discussed in relation to physical properties in ultrasmall grains such as the parity gap,[169] condensation energy[167] and electron correlation,[162] with the size dependence of the level spacing[161] of samples.

In nanosize grains of a superconductor, the quantum level spacing approaches the superconducting gap. In the case of a two-gap superconductor, we can consider a model with two sublevels corresponding to two independent bands. In this section, we present a model for nanosize two-gap superconductivity and an expression for the partition function of the system.

4.2.1 *Hamiltonian for nanosize grains*

We consider a pairing Hamiltonian with two sublevels corresponding to two bands 1 and 2 written as

$$H = H_0 + H_{\text{int}}, \tag{4.1}$$

where

$$H_0 = \sum_{j,\sigma}[\varepsilon_{1j} - \mu]a^\dagger_{j\sigma}a_{j\sigma} + \sum_{k,\sigma}[\varepsilon_{2k} - \mu]b^\dagger_{k\sigma}b_{k\sigma}, \tag{4.2}$$

$$\begin{aligned} H_{\text{int}} = &-g_1 \sum_{j,j'\in I} a^\dagger_{j\uparrow}a^\dagger_{j\downarrow}a_{j'\downarrow}a_{j'\uparrow} - g_2 \sum_{k,k'\in J} b^\dagger_{k\uparrow}b^\dagger_{k\downarrow}b_{k'\downarrow}b_{k'\uparrow} \\ &+ g_{12} \sum_{j\in I,k\in J} a^\dagger_{j\uparrow}a^\dagger_{j\downarrow}b_{k\downarrow}b_{k\uparrow} + g_{12} \sum_{j\in I,k\in J} b^\dagger_{k\uparrow}b^\dagger_{k\downarrow}a_{j\downarrow}a_{j\uparrow}. \end{aligned} \tag{4.3}$$

Here, $a^\dagger_{j\sigma}(a_{j\sigma})$ and $b^\dagger_{j,\sigma}(b_{j,\sigma})$ are the creation (annihilation) operator in sublevels 1 and 2 with spin σ and energies ε_{1j} and ε_{2j}, respectively, the operators for each sublevel satisfy the anticommutation relations, and the operators between sublevels are independent, μ is the chemical potential, the second term of Eq. (4.1) is the interaction Hamiltonian, g_1 and g_2 are the effective interaction constant for sublevels 1 and 2, and g_{12} is an effective interaction constant which corresponds to the pair scattering process between two bands. The sums of j and k in Eq. (4.3) are over the set I of N_{1I} states which correspond to the half-filled band 1 with fixed width $2\omega_{1D}$ and the set J of N_{2J} states for band 2, respectively.

In this study, we assume that the Debye energies for two sublevels are the same: $\omega_{1D} = \omega_{2D} = \omega_D$. Within this assumption, N_{1I} and N_{2J} are relatively estimated by the density of state (DOS) for two bands as $N_{1I}/N_{2J} = \rho_1/\rho_2$, where ρ_1 and ρ_2 are the DOS for two bands. The interaction constants g_1 and g_2 can be written as $d_1\lambda_1$ and $d_2\lambda_2$, respectively. $d_1 = 2\omega_D/N_{1I}$ and $d_2 = 2\omega_D/N_{2J}$ are the mean energy level spacings, and λ_1 and λ_2 are the dimensionless parameters for two sublevels. We take the intersublevel

interaction constant $g_{12} = \sqrt{d_1 d_2}\lambda_{12}$. We then obtain the relation $\rho_1/\rho_2 = N_{1I}/N_{2J} = d_2/d_1$.

4.2.2 *Path-integral approach*

It is convenient to introduce a path-integral approach for the treatment of fluctuations of the order parameters. This approach gives an exact expression for the grand partition function of a superconductor.

$$Z(\mu, T) = \mathrm{Tr}\, \exp\left[-\frac{H - \mu N}{T}\right], \tag{4.4}$$

where T is the temperature and N is the number operator in the grain. The idea of the path-integral approach is to replace the description of a system under study in terms of electronic operators by an equivalent description in terms of the superconducting order parameter.

By the path-integral approach, we obtain an expression for the grand partition function for the Hamiltonian (4.1):

$$Z(\mu, T) = \int D\Delta_1 D\Delta_1^* D\Delta_2 D\Delta_2^* e^{-S[\Delta_1, \Delta_2]}. \tag{4.5}$$

Here, the action $S[\Delta_1, \Delta_2]$ is defined as

$$\begin{aligned} S[\Delta_1, \Delta_2] = &- \sum_j \left[\mathrm{Tr} \ln G_{1j}^{-1} - \frac{\xi_{1j}}{T}\right] - \sum_k \left[\mathrm{Tr} \ln G_{2k}^{-1} - \frac{\xi_{2k}}{T}\right] \\ &+ \int_0^{1/T} d\tau \frac{1}{g_1 g_2 - g_{12}^2} [g_2 |\Delta_1(\tau)|^2 + g_1 |\Delta_2(\tau)|^2 \\ &+ g_{12}(\Delta_1(\tau)\, \Delta_2(\tau)^* + \Delta_1(\tau)^* \Delta_2(\tau))]. \end{aligned} \tag{4.6}$$

Δ_1 and Δ_2 are bulk gaps for sublevels 1 and 2, respectively, $\xi_{1j} = \varepsilon_{1j} - \mu$ and $\xi_{2k} = \varepsilon_{2k} - \mu$, and the inverse Green functions

$$G_{1j}^{-1}(\tau, \tau') = \left[-\frac{d}{d\tau} - \xi_{1j}\sigma^z - \Delta_1(\tau)\sigma^+ - \Delta_1^*(\tau)\sigma^-\right] \delta(\tau - \tau'), \tag{4.7}$$

$$G_{2k}^{-1}(\tau, \tau') = \left[-\frac{d}{d\tau} - \xi_{2k}\sigma^z - \Delta_2(\tau)\sigma^+ - \Delta_2^*(\tau)\sigma^-\right] \delta(\tau - \tau'), \tag{4.8}$$

where $\sigma^{\pm} = \sigma^x \pm i\sigma^y$, and $\sigma^{x,y,z}$ are the Pauli matrices. G_1^{-1} and G_2^{-1} satisfy antiperiodic boundary conditions.

In the case of a stronger interaction, $\Delta_1 \gg d_1$ and $\Delta_2 \gg d_2$, we consider the mean-field approximation for the order parameters in the path-integral approach. Substituting the time-independent order parameters into

the action (4.6), we have

$$\Omega(\mu) = \sum_j (\xi_{1j} - \epsilon_{1j}) + \sum_k (\xi_{2k} - \epsilon_{2k}) + \frac{1}{g_1 g_2 - g_{12}^2}[g_2\,\Delta_1^2 + g_1\,\Delta_2^2 + g_{12}(\Delta_1^*\,\Delta_2 + \Delta_1\,\Delta_2^*)], \quad (4.9)$$

where $\epsilon_{1j} = (\xi_{1j}^2 + \Delta_1^2)^{1/2}$ and $\epsilon_{2k} = (\xi_{2k}^2 + \Delta_2^2)^{1/2}$. In Eq. (4.9), the values of Δ_1 and Δ_2 must be chosen in such a way as to minimize Ω. From the minimization of Ω, we obtain a coupled gap equation at zero temperature for the two-gap system:

$$\begin{pmatrix} \Delta_1 \\ \Delta_2 \end{pmatrix} = \begin{pmatrix} g_1 \sum_j \frac{1}{2\epsilon_{1j}} & -g_{12} \sum_k \frac{1}{2\epsilon_{2k}} \\ -g_{12} \sum_j \frac{1}{2\epsilon_{1j}} & g_2 \sum_k \frac{1}{2\epsilon_{2k}} \end{pmatrix} \begin{pmatrix} \Delta_1 \\ \Delta_2 \end{pmatrix}. \quad (4.10)$$

From the coupled gap equation (4.10), we formally obtain an expression for the bulk gap for two-gap superconductivity at zero temperature:

$$\tilde{\Delta}_1 = \omega \sinh^{-1}\left(\frac{1}{\eta_1}\right), \quad (4.11)$$

$$\tilde{\Delta}_2 = \omega \sinh^{-1}\left(\frac{1}{\eta_2}\right), \quad (4.12)$$

where

$$\frac{1}{\eta_1} = \frac{\lambda_2 + \alpha_\pm[\eta_1, \eta_2]\lambda_{12}}{\lambda_1\lambda_2 - \lambda_{12}^2}, \quad (4.13)$$

$$\frac{1}{\eta_2} = \frac{\lambda_1 + \alpha_\pm^{-1}[\eta_1, \eta_2]\lambda_{12}}{\lambda_1\lambda_2 - \lambda_{12}^2}, \quad (4.14)$$

with

$$\alpha_\pm[\eta_1, \eta_2] = \pm\frac{\sinh\left(\frac{1}{\eta_1}\right)}{\sinh\left(\frac{1}{\eta_2}\right)}. \quad (4.15)$$

For the two-band superconductivity, we can consider two cases for the phase of the gaps: $\mathrm{sgn}(\tilde{\Delta}_1) = \mathrm{sgn}(\tilde{\Delta}_2)$ and $\mathrm{sgn}(\tilde{\Delta}_1) = -\mathrm{sgn}(\tilde{\Delta}_2)$. For the same phase, α_+ is used in Eqs. (4.13) and (4.14), and we use α_- for the opposite phase. Note that $\tilde{\Delta}_1 = -\tilde{\Delta}_2$ in the limit of strong intersublevel coupling λ_{12}, i.e. the opposite phase. For $\lambda_{12} = 0$, we find the same results for two bulk gaps derived from the conventional BCS theory for two independent sublevels.

4.2.3 *Condensation energy*

In this subsection, we discuss properties such as condensation energy, critical level spacing and the parity gap of nanosize two-gap superconductivity by using the partition function derived in the previous subsection.

In nanosize superconductivity, the condensation energy can be defined as $E^C_{N,b}(\lambda) = E^G_{N,b}(0) - E^G_{N,b}(\lambda) - n\lambda d$, where $E^G_{N,b}$ is the ground state energy of the N-electron system in the interaction band, b is the number of electrons on single occupied levels, and λ and n are the dimensionless coupling parameter and the number of pair-occupied levels, respectively. In the case of a nanosize two-band system, the condensation energy can be written as

$$E^C_{N_1,b_1;N_2,b_2}(\lambda_1,\lambda_2,\lambda_{12}) = E^G_{N_1,b_1;N_2,b_2}(0,0,0) - E^G_{N_1,b_1;N_2,b_2}(\lambda_1,\lambda_2,\lambda_{12}) - n_1\lambda_1 d_1 - n_2\lambda_2 d_2, \tag{4.16}$$

where $E^G_{N_1,b_1;N_2,b_2}(\lambda_1,\lambda_2,\lambda_{12})$ is the ground state energy of the (N_1+N_2)-electron system. From Eqs. (4.4) and (4.9), the condensation energy of the two-sublevel system can be expressed by the condensation energy of independent single-level systems:

$$E^C_{N_1,b_1;N_2,b_2}(\lambda_1,\lambda_2,\lambda_{12}) = E^C_{N_1,b_1}(\lambda_1) + E^C_{N_2,b_2}(\lambda_2) - \frac{\lambda_{12}^2}{\lambda_1\lambda_2 - \lambda_{12}^2} \times \left(\frac{\Delta_1^2}{d_1\lambda_1} + \frac{\Delta_2^2}{d_2\lambda_2} + \frac{2(\Delta_1^*\Delta_2 + \Delta_1\Delta_2^*)}{\sqrt{d_1 d_2}\lambda_{12}}\right), \tag{4.17}$$

where $E^C_{N_1,b_1}(\lambda_1)$ and $E^C_{N_2,b_2}(\lambda_2)$ correspond to the condensation energy for the single-band case. In the same phases of Δ_1 and Δ_2, the condensation energy (4.17) decreases, i.e. there appears the instability by the coupling constant λ_{12}. On the other hand, in the opposite phases, the condensation energy becomes larger, because $\Delta_1^*\,\Delta_2 + \Delta_1\,\Delta_2^* < 0$. We can expect that the condensation energy for two-gap superconductivity results in a higher stability than that of two independent systems, due to the intersublevel coupling λ_{12} and the opposite phases.

4.2.4 *Critical level spacing*

To discuss the critical level spacing for a two-gap system, we start from the coupled gap equation (4.10). For the case of the critical level spacing of the

two-gap system, we have

$$1 = \lambda_1 \sum_j \frac{1}{2|\tilde{\xi}_{1j}|} + \lambda_2 \sum_k \frac{1}{2|\tilde{\xi}_{2k}|} - (\lambda_1\lambda_2 - \lambda_{12}^2) \sum_j \frac{1}{2|\tilde{\xi}_{1j}|} \sum_k \frac{1}{2|\tilde{\xi}_{2k}|}, \tag{4.18}$$

where $\tilde{\xi}_i = \xi_i/d_i$ for sublevel $i = 1, 2$. For the odd or even cases, Eq. (4.18) can be approximately solved by using the digamma function: for the odd case, the critical level spacing becomes

$$d_{1c}^o = \omega_D e^\gamma \exp\left[-\frac{1}{\lambda}\right], \quad d_{2c}^o = \frac{d_2}{d_1} d_{1c}^o, \tag{4.19}$$

and, for the even case,

$$d_{1c}^e = 4\omega_D e^\gamma \exp\left[-\frac{1}{\lambda}\right], \quad d_{2c}^e = \frac{d_2}{d_1} d_{1c}^e. \tag{4.20}$$

Here, we use

$$\frac{1}{\lambda} = \frac{1}{2x}\left[\lambda_1 + \lambda_2 - ax + \sqrt{(\lambda_1 - \lambda_2 - ax)^2 + 4\lambda_{12}^2}\right], \tag{4.21}$$

with

$$x = \lambda_1\lambda_2 - \lambda_{12}^2, \tag{4.22}$$

$$a = \log \frac{d_1}{d_2}. \tag{4.23}$$

From these expressions, we find some relations:

$$d_{1c}^e = 4d_{1c}^o, \quad d_{2c}^e = 4d_{2c}^o, \tag{4.24}$$

$$d_{1/2c}^o \approx \frac{e^\gamma}{2} \exp\left[\frac{1}{\eta_{1/2}} - \frac{1}{\lambda}\right] \tilde{\Delta}_{1/2}. \tag{4.25}$$

In the case of $|\lambda_1 - \lambda_2| \gg \lambda_{12}$, Eq. (4.25) can be approximately rewritten as

$$d_{1/2c}^o \approx \frac{e^\gamma}{2} \exp\left[\frac{\lambda_2 - \lambda_1 + 2\alpha\lambda_{12}}{\lambda_1\lambda_2 - \lambda_{12}^2}\right] \tilde{\Delta}_{1/2}. \tag{4.26}$$

On the other hand, in the limit of $|\lambda_1 - \lambda_2| \ll \lambda_{12}$, we have

$$d_{1/2c}^o \approx \frac{e^\gamma}{2} \exp\left[\frac{(1+\alpha)\lambda_{12}}{\lambda_1\lambda_2 - \lambda_{12}^2}\right] \tilde{\Delta}_{1/2}. \tag{4.27}$$

For the case of $\lambda_{12} = 0$, Eq. (4.25) can be rewritten as $d_{1/2c}^o \approx \exp[\gamma]/2 \exp[1/\lambda_1 - 1/\lambda_2]\, \tilde{\Delta}_{1/2}$. Therefore, when the coupling constants λ_1 and λ_2 take the same value, we have a relation similar to that for a single-level system: $d_{1/2c}^o \approx 0.89\, \tilde{\Delta}_{1/2}$. These results suggest that the critical level spacing strongly depends upon λ_{12} and the difference between the effective interaction constants for sublevels. The relation in Eq. (4.24) is the same relation in the conventional nanosize BCS theory.

4.2.5 *Parity gap*

In this subsection, we consider a parity gap in the case of two-gap superconductivity in ultrasmall grains. In the case of two sublevel spacings, the chemical potential lies halfway between the highest occupied and the lowest unoccupied levels of a smaller level spacing in the half-filled case, as shown in Fig. 4.4(a). We assume that $d_1 < d_2$ and that the numbers of occupied levels corresponding to each sublevel are n_1 and n_2, respectively. Then, the total number of electrons becomes $N = 2n_1 + 2n_2$. When we consider $N = 2n_1 + 2n_2 + 1$, the chemical potential lies on the level ε_{1n_1+1}, as shown in Fig. 4.4(b). Figure 4.4(c) indicates the position of the chemical potential in the case of $N = 2n_1 + 2n_2 + 2$. The parity gap of nanosize two-gap superconductivity is written as

$$\Delta_p^1 = E^G_{2n_1+1+2n_2,1} - \frac{1}{2}\left(E^G_{2n_1+2n_2,0} + E^G_{2(n_1+1)+2n_2,0}\right). \tag{4.28}$$

From Eq. (4.9) and for the ground state energy $E^G_{N,b} = \Omega_{\mu_N} + \mu_N N$, we obtain

$$\Delta_p^1 = \Delta_1 - \frac{d_1}{4}\left(\frac{\rho_1}{\rho_2} - 1\right). \tag{4.29}$$

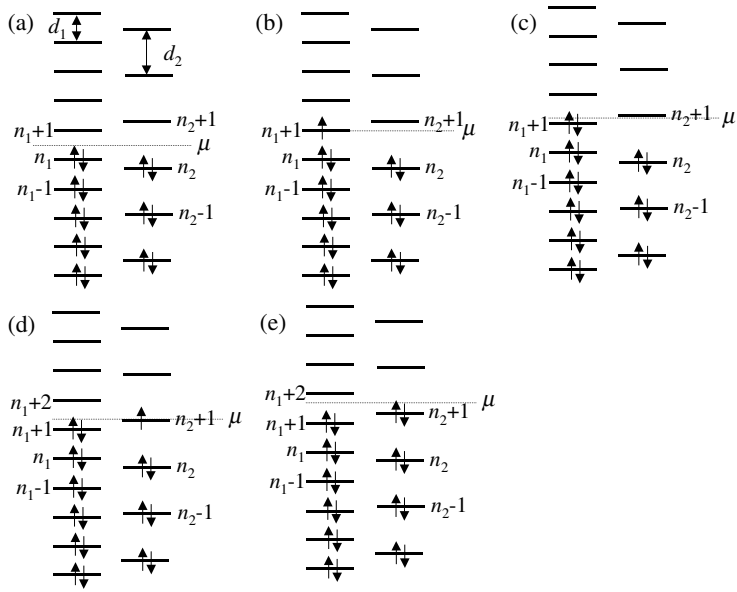

Fig. 4.4 Position of the chemical potential relative the electronic energy levels in a two-gap superconducting grain. Solid and dotted lines mean two sublevels. (a) Half-filled system with $2n_1+2n_2$ electrons; (b) $(2n_1+1+2n_2)$-electron system; (c) $[2(n_1+1)+2n_2]$-electron system; (d) $[2(n_1+1)+2n_2+1]$-electron system; (e) $[2(n_1+1)+2(n_2+1)]$-electron system.

From Figs. 4.4(c)–4.4(e), we can define another parity gap:

$$\Delta_p^2 = E^G_{2(n_1+1)+2n_2+1,1} - \frac{1}{2}\left(E^G_{2(n_1+1)+2n_2,0} + E^G_{2(n_1+1)+2(n_2+1),0}\right). \quad (4.30)$$

From the latter definition of Eq. (4.30), we have

$$\Delta_p^2 = \Delta_2 - \frac{d_2}{4}\left(\frac{3\rho_2}{\rho_1} - 1\right). \quad (4.31)$$

The present results suggest two kinds of the dependence of the parity gap on the level spacing. The parity gap does not depend on the effective interaction λ_{12}. The structure around the Fermi level plays an important role in the contribution to the size dependence of the parity gap. We have investigated the properties of nanosize two-gap superconductivity by using a two-sublevel model in the framework of the mean-field approximation. From the discussion of the condensation energy in nanosize two-gap superconductivity, the phases of the gaps are very important for stabilizing the superconductivity. In the same phases, the two-gap superconductivity is unstable by the coupling constant λ_{12}. On the other hand, in the opposite phases, the superconductivity becomes stable. We can expect that, due to the condensation energy, the two-gap superconductivity becomes more stable than that for two independent systems due to the intersublevel coupling λ_{12} and the opposite phases.

We have also discussed the critical level spacing for two-gap superconductivity in ultrasmall grains. These results suggest that the critical level spacing strongly depends on λ_{12} and the difference between the effective interaction constants for sublevels. Moreover, the relation between the critical level spacing and the bulk gaps is modified as compared with the result obtained for ultrasmall superconducting Al grains.

For the parity gap in two-gap superconductivity, the present results suggest two kinds of the dependence of the parity gap on the level spacing and that the structure around the Fermi level plays an important role by contributing to the size dependence on the parity gap. The parity gap does not depend on the effective interaction λ_{12}.

In the case of a cluster system, we have to apply a more accurate approach beyond the mean-field approximation presented in this study by investigating the physical properties, and we also have to consider the contribution of the surface of samples to the level structure around the Fermi level. We will present these problems in the next section. On the basis of the presented results, we might expect the possibility of a new multigap superconductivity arising in the nanosize region with a higher critical transition temperature.

In summary, a model corresponding to nanosize two-gap superconductivity has been presented, and an expression for the partition function of the nanosize system has been analytically derived by using the path-integral approach. A definition of the critical level spacing of the two-gap superconductivity has also been presented, and we discussed the condensation energy and the parity gap of the two-gap superconductivity in relation to the size dependence of those properties with two bulk gaps, as well as the effective pair scattering process between two sublevels.

4.3 Exact Solution of Two-Band Superconductivity in Ultrasmall Grains

Many groups have theoretically investigated the physical properties such as critical level spacing, condensation energy and parity gap in ultrasmall grains with the conventional superconductivity.[161,162,165–169] The question concerning such nanosize superconducting grains has been discussed by Anderson.[6] The standard BCS theory becomes false when the level spacing approaches the superconducting gap. To investigate the properties in such nanosize systems, it is necessary to perform a more accurate treatment. Braun and von Delft[165,166,173] have reintroduced the exact solution for the reduced BCS Hamiltonian developed by Richardson.[170–172] It is noteworthy that Richardson's solution is applicable at distributions of single-electron energy levels. V. N. Gladilin *et al.*[167] have investigated the pairing characteristics such as the condensation energy, spectroscopic gap and parity gap, by using Richardson's exact solution for the reduced BCS Hamiltonian.

The recent discovery of the superconductivity of MgB_2[124] with $T_c = 39\,\mathrm{K}$ has also attracted great interest, aimed at the elucidation of its mechanism from both the experimental and theoretical viewpoints. Since this discovery, the possibility of two-band superconductivity has also been discussed in relation to the two-gap functions experimentally and theoretically.

In this section, we investigate the two-band superconductivity in ultrasmall grains. Richardson's exact solution is extended to two-band systems, and a new coupled equation is derived according to the procedure of Richardson's works. The parity gap and the condensation energy of an ultrasmall two-band superconducting grain are numerically given by solving the coupled equation. We discuss these properties of ultrasmall grains in relation to the correlation, interband interaction and size dependence.

4.3.1 *Exact solution for two-band superconductivity*

In this subsection, we derive an exact solution of the two-band superconductivity for a reduced BCS Hamiltonian.

4.3.2 *Hamiltonian*

We consider a Hamiltonian for two bands 1 and 2 written as

$$H = H_1 + H_2 + H_{\text{int}}, \tag{4.32}$$

where

$$H_1 = \sum_{j\sigma} \varepsilon_{1j} a^\dagger_{j\sigma} a_{j\sigma} - g_1 \sum_{jk} a^\dagger_{j\uparrow} a^\dagger_{j\downarrow} a_{k\downarrow} a_{k\uparrow}, \tag{4.33}$$

$$H_2 = \sum_{j\sigma} \varepsilon_{2j} b^\dagger_{j\sigma} b_{j\sigma} - g_2 \sum_{jk} b^\dagger_{j\uparrow} b^\dagger_{j\downarrow} b_{k\downarrow} b_{k\uparrow}, \tag{4.34}$$

$$H_{\text{int}} = g_{12} \sum_{jk} a^\dagger_{j\uparrow} a^\dagger_{j\downarrow} b_{k\downarrow} b_{k\uparrow} + g_{12} \sum_{jk} b^\dagger_{j\uparrow} b^\dagger_{j\downarrow} a_{k\downarrow} a_{k\uparrow}. \tag{4.35}$$

The first and second terms of Eq. (4.32) correspond to the reduced BCS Hamiltonian for bands 1 and 2, respectively. The third term means a coupling between them and corresponds to the pair scattering process between these two bands (see Fig. 4.5). $a^\dagger_{j\sigma}$ ($a_{j\sigma}$) and $b^\dagger_{j\sigma}$ ($b_{j\sigma}$) are the creation (annihilation) operator in bands 1 and 2 with spin σ and the single-particle levels ε_{1j} and ε_{2j}, respectively. The sums of j and k are taken over a set of

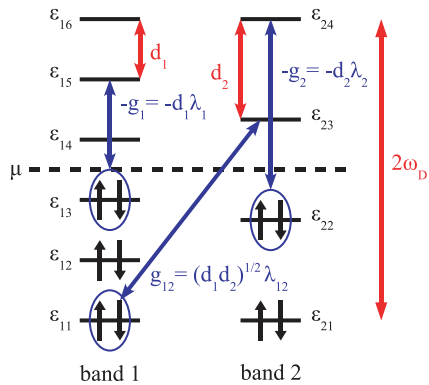

Fig. 4.5 Two-band system. The dotted line means the chemical potential; ε_{nj} is the single-particle energy for band n and level j; $-g_1$ and $-g_2$ are the intraband pair interaction coupling constants and g_{12} are the interband pair interaction coupling constant.

N_1 states for band 1 with fixed width $2\hbar\omega_{1D}$ and a set of N_2 states for band 2 with fixed width $2\hbar\omega_{2D}$, respectively.

In this study, we assume that the Debye energies for two bands coincide, i.e.

$$\omega_{1D} = \omega_{2D} = \omega_D. \tag{4.36}$$

Within this assumption, N_1 and N_2 are relatively estimated by the DOS for two bands as

$$\frac{N_1}{N_2} = \frac{\rho_1}{\rho_2}, \tag{4.37}$$

where ρ_1 and ρ_2 are the DOS for two bands, respectively. The interaction constants g_1 and g_2 can be written as

$$g_1 = d_1\lambda_1, \quad g_2 = d_2\lambda_2, \tag{4.38}$$

where d_1 and d_2 are the mean single-particle level spacings,

$$d_1 = \frac{2\hbar\omega_D}{N_1 - 1}, \qquad d_2 = \frac{2\hbar\omega_D}{N_2 - 1}, \tag{4.39}$$

and λ_1 and λ_2 are the dimensionality interaction parameters for two bands. We define the interband interaction constant as

$$g_{12} = \sqrt{d_1 d_2}\ \lambda_{12}. \tag{4.40}$$

In summary, we obtain the relation

$$\frac{\rho_1}{\rho_2} \approx \frac{N_1 - 1}{N_2 - 1} = \frac{d_2}{d_1}. \tag{4.41}$$

The system we are considering consists of two half-filled bands, each of which has equally spaced N_n single-particle levels and $M_n(= N_n/2)$ doubly occupied pair levels $(n = 1, 2)$. We take the single-particle level spacing as our energy unity. Thus, the single-particle spectrum is given by

$$\varepsilon_{nj} = d_n j - \omega_D, \quad j = 1, 2, \ldots, N_n \quad (n = 1, 2). \tag{4.42}$$

Richardson has obtained his solution within the single-band model for an arbitrary set of single-particle levels. For simplicity, we assume that there are no singly occupied single-particle levels. As can be seen from Eqs. (4.33)–(4.35), these levels are decoupled from the rest of the system. They are said to be blocked and contribute to the total energy with their single-particle energies. The above simplification implies that every single-particle level j is either empty (i.e. $|\text{vac}\rangle$) or occupied by a pair of electrons (i.e. $a^\dagger_{j\uparrow}a^\dagger_{j\downarrow}|\text{vac}\rangle$ and $b^\dagger_{j\uparrow}b^\dagger_{j\downarrow}|\text{vac}\rangle$). These are called the unblocked level.

4.3.3 *Exact solution*

In order to extend Richardson's solution to a two-band system, we define two kinds of hard-core boson operators as

$$c_j = a_{j\downarrow}a_{j\uparrow}, \quad c_j^\dagger = a_{j\uparrow}^\dagger a_{j\downarrow}^\dagger, \tag{4.43}$$

$$d_j = b_{j\downarrow}b_{j\uparrow}, \quad d_j^\dagger = b_{j\uparrow}^\dagger b_{j\downarrow}^\dagger, \tag{4.44}$$

which satisfy the commutation relations

$$c_j^{\dagger 2} = 0, \quad [c_j, c_k^\dagger] = \delta_{jk}(1 - 2c_j^\dagger c_j), \quad [c_j^\dagger c_j, c_k^\dagger] = \delta_{jk}c_j^\dagger, \tag{4.45}$$

$$d_j^{\dagger 2} = 0, \quad [d_j, d_k^\dagger] = \delta_{jk}(1 - 2d_j^\dagger d_j), \quad [d_j^\dagger d_j, d_k^\dagger] = \delta_{jk}d_j^\dagger, \tag{4.46}$$

which reflects the Pauli principle for the fermions they were constructed from.

The Hamiltonian (4.32) for the unblocked levels can then be written as

$$H_U = 2\sum_j^{N_1} \varepsilon_{1j} c_j^\dagger c_j - g_1 \sum_{jk}^{N_1} c_j^\dagger c_k + 2\sum_j^{N_2} \varepsilon_{2j} d_j^\dagger d_j - g_2 \sum_{jk}^{N_2} d_j^\dagger d_k$$
$$+ g_{12} \sum_j^{N_1}\sum_k^{N_2} c_j^\dagger d_k + g_{12} \sum_j^{N_2}\sum_k^{N_1} d_j^\dagger c_k. \tag{4.47}$$

We find the eigenstates $|M_1; M_2\rangle$ of this Hamiltonian with $M_1 + M_2$ pairs in the form

$$H_U|M_1; M_2\rangle_U = E(M_1; M_2)|M_1; M_2\rangle_U$$
$$= \left(\sum_{J=1}^{M_1} E_{1J} + \sum_{K=1}^{M_2} E_{2K}\right)|M_1; M_2\rangle_U, \tag{4.48}$$

where $E(M_1; M_2)$ is the eigenvalue and

$$|M_1; M_2\rangle_U = \prod_{J=1}^{M_1} C_J^\dagger \prod_{K=1}^{M_2} D_K^\dagger |\text{vac}\rangle, \tag{4.49}$$

with

$$C_J^\dagger = \sum_j^{N_1} \frac{c_j^\dagger}{2\varepsilon_{1j} - E_{1J}}, \quad D_J^\dagger = \sum_j^{N_2} \frac{d_j^\dagger}{2\varepsilon_{2j} - E_{2J}}. \tag{4.50}$$

Now, we define $C_0^\dagger$ and $D_0^\dagger$ as

$$C_0^\dagger = \sum_j^{N_1} c_j^\dagger, \quad D_0^\dagger = \sum_j^{N_2} d_j^\dagger. \tag{4.51}$$

Then we can rewrite Eq. (4.47) as

$$H_U = 2\sum_j^{N_1} \varepsilon_{1j} c_j^\dagger c_j - g_1 C_0^\dagger C_0 + 2\sum_j^{N_2} \varepsilon_{2j} d_j^\dagger d_j - g_2 D_0^\dagger D_0 + g_{12} C_0^\dagger D_0 + g_{12} D_0^\dagger C_0. \tag{4.52}$$

The commutation relations for new operators are given as

$$[c_j^\dagger c_j, C_J^\dagger] = \frac{c_j^\dagger}{2\varepsilon_{1j} - E_{1J}}, \quad [d_j^\dagger d_j, D_J^\dagger] = \frac{d_j^\dagger}{2\varepsilon_{2j} - E_{2J}}, \tag{4.53}$$

$$[C_0, C_J^\dagger] = \sum_j^{N_1} \frac{1 - c_j^\dagger c_j}{2\varepsilon_{1j} - E_{1J}}, \quad [D_0, D_J^\dagger] = \sum_j^{N_2} \frac{1 - d_j^\dagger d_j}{2\varepsilon_{2j} - E_{2J}}, \tag{4.54}$$

$$[H_U, C_J^\dagger] = E_{1J} C_J^\dagger + C_0^\dagger + g_1 C_0^\dagger \sum_j^{N_1} \frac{1 - c_j^\dagger c_j}{2\varepsilon_{1j} - E_{1J}} + g_{12} D_0^\dagger \sum_j^{N_1} \frac{1 - c_j^\dagger c_j}{2\varepsilon_{1j} - E_{1J}}, \tag{4.55}$$

$$[H_U, D_J^\dagger] = E_{2J} D_J^\dagger + D_0^\dagger + g_1 D_0^\dagger \sum_j^{N_2} \frac{1 - d_j^\dagger d_j}{2\varepsilon_{2j} - E_{2J}} + g_{12} C_0^\dagger \sum_j^{N_2} \frac{1 - d_j^\dagger d_j}{2\varepsilon_{2j} - E_{2J}}. \tag{4.56}$$

Using the above-presented commutation relations, we find that

$$H_U |M_1; M_2\rangle_U = \left(\sum_{J=1}^{M_1} E_{1J} + \sum_{K=1}^{M_2} E_{2K} \right) |M_1; M_2\rangle_U + C_0^\dagger \sum_{J=1}^{M_1} \left(1 - \sum_j^{N_1} \frac{g_1}{2\varepsilon_{1j} - E_{1J}} + \sum_{J' \neq J}^{M_1} \frac{2g_1}{E_{1J'} - E_{1J}} \right) |M_1(J); M_2\rangle_U + D_0^\dagger \sum_{J=1}^{M_1} \left(\sum_j^{N_1} \frac{g_{12}}{2\varepsilon_{1j} - E_{1J}} - \sum_{J' \neq J}^{M_1} \frac{2g_{12}}{E_{1J'} - E_{1J}} \right) |M_1(J); M_2\rangle_U$$

$$+C_0^\dagger \sum_{K=1}^{M_2} \left(\sum_j^{N_2} \frac{g_{12}}{2\varepsilon_{2j} - E_{2K}} - \sum_{K' \neq K}^{M_2} \frac{2g_{12}}{E_{2K'} - E_{2K}} \right) |M_1; M_2(K)\rangle_U$$

$$+D_0^\dagger \sum_{K=1}^{M_2} \left(1 - \sum_j^{N_2} \frac{g_2}{2\varepsilon_{2j} - E_{2K}} + \sum_{K' \neq K}^{M_2} \frac{2g_2}{E_{2K'} - E_{2K}} \right) |M_1; M_2(K)\rangle_U, \tag{4.57}$$

where

$$|M_1(L); M_2\rangle_U = \prod_{J=1}^{L-1} C_J^\dagger \prod_{J'=L+1}^{M_1} C_{J'}^\dagger \prod_{K=1}^{M_2} D_K^\dagger |\text{vac}\rangle, \tag{4.58}$$

$$|M_1; M_2(L)\rangle_U = \prod_{J=1}^{M_1} C_J^\dagger \prod_{K=1}^{L-1} D_K^\dagger \prod_{K'=L+1}^{M_2} D_{K'}^\dagger |\text{vac}\rangle. \tag{4.59}$$

Comparing Eq. (4.57) with Eq. (4.48), we obtain, for arbitrary J and K,

$$\begin{pmatrix} C_0^\dagger & D_0^\dagger \end{pmatrix} \begin{pmatrix} 1 + g_1 A_{1J} & -g_{12} A_{2K} \\ -g_{12} A_{1J} & 1 + g_2 A_{2K} \end{pmatrix} \begin{pmatrix} |M_1(J); M_2\rangle_U \\ |M_1; M_2(K)\rangle_U \end{pmatrix} = 0, \tag{4.60}$$

where

$$A_{nL} = -\sum_j^{N_n} \frac{1}{2\varepsilon_{nj} - E_{nL}} + \sum_{L' \neq L}^{M_n} \frac{2}{E_{nL'} - E_{nL}}. \tag{4.61}$$

A nontrivial solution to Eq. (4.60) is derived from the determinantal equation

$$F_{JK} = (1 + g_1 A_{1J})(1 + g_2 A_{2K}) - g_{12}^2 A_{1J} A_{2K} = 0. \tag{4.62}$$

This constitutes a set of $M_1 + M_2$ coupled equations for $M_1 + M_2$ parameters E_{1J} and E_{2K} ($J = 1, 2, \ldots, M_1; K = 1, 2, \ldots, M_2$), which may be thought of as self-consistently determined pair energies. Equation (4.62) is the exact eigenvalue equation for a two-band superconducting system and can be regarded as a generalization of Richardson's original eigenvalue equation.

4.3.4 *Preprocessing for numerical calculations*

To remove the divergences from the second term of A_{nL} in Eq. (4.61), we make changes of the energy variables:

$$\begin{aligned} E_{n2\lambda} &= \xi_{n\lambda} + i\eta_{n\lambda}, \\ E_{n2\lambda-1} &= \xi_{n\lambda} - i\eta_{n\lambda}, \\ \lambda &= 1, 2, \ldots, M_n/2, \end{aligned} \tag{4.63}$$

where we assume that the number of pairs is even. Since the complex pair energies appear in complex conjugate pairs, the total energy will be expressed as the real component.

A further transformation is necessary in order to remove the divergences from the first term of A_{nL}. We define new variables $x_{n\lambda}$ and $y_{n\lambda}$ as

$$\xi_{n\lambda} = \varepsilon_{n2\lambda} + \varepsilon_{n2\lambda-1} + d_n x_{n\lambda} \quad (x_{n\lambda} \le 0), \tag{4.64}$$

$$\eta^2_{n\lambda} = -(\Delta\varepsilon^2_{n2\lambda} - d_n^2 x^2_{n\lambda}) y_{n\lambda} \quad (y_{n\lambda} \ge 0), \tag{4.65}$$

where

$$\Delta\varepsilon_{n2\lambda} = \varepsilon_{n2\lambda} - \varepsilon_{n2\lambda-1}. \tag{4.66}$$

Considering the sign of $y_{n\lambda}$, we can express $\eta_{n\lambda}$ as

$$\begin{aligned} \eta_{n\lambda} &= |\eta_{n\lambda}| \mathrm{e}^{-i\phi_{n\lambda}}, \\ \phi_{n\lambda} &= \begin{cases} 0 & \text{for} \quad \Delta\varepsilon^2_{n2\lambda} - d_n^2 x^2_{n\lambda} \le 0, \\ \frac{\pi}{2} & \text{for} \quad \Delta\varepsilon^2_{n2\lambda} - d_n^2 x^2_{n\lambda} > 0. \end{cases} \end{aligned} \tag{4.67}$$

Then we can rewrite F_{JK}, by using the new variables, and define the result as $F_{\alpha\beta}$. We extract the real and imaginary parts of $F_{\alpha\beta}$ as

$$\begin{aligned} F^+_{\alpha\beta} = \frac{1}{2}(F_{\alpha\beta} + F^*_{\alpha\beta}) &= 1 + g_1 R_{1\alpha} + g_2 R_{2\beta} + (g_1 g_2 - g_{12}^2) R_{1\alpha} R_{2\beta} \\ &- (g_1 g_2 - g_{12}^2) I_{1\alpha} I_{2\beta} \cos(\phi_{1\alpha} + \phi_{2\beta}) \\ &- \{g_1 + (g_1 g_2 - g_{12}^2) R_{2\beta}\} I_{1\alpha} \sin\phi_{1\alpha} \\ &- \{g_2 + (g_1 g_2 - g_{12}^2) R_{1\alpha}\} I_{2\beta} \sin\phi_{2\beta}, \end{aligned} \tag{4.68}$$

$$\begin{aligned} F^-_{\alpha\beta} = \frac{1}{2i}(F_{\alpha\beta} - F^*_{\alpha\beta}) &= -(g_1 g_2 - g_{12}^2) I_{1\alpha} I_{2\beta} \sin(\phi_{1\alpha} + \phi_{2\beta}) \\ &+ \{g_1 + (g_1 g_2 - g_{12}^2) R_{2\beta}\} I_{1\alpha} \cos\phi_{1\alpha} \\ &+ \{g_2 + (g_1 g_2 - g_{12}^2) R_{1\alpha}\} I_{2\beta} \cos\phi_{2\beta}, \end{aligned} \tag{4.69}$$

where

$$R_{n\lambda} = -\frac{2d_n x_{n\lambda}(1+y_{n\lambda})}{(1-y_{n\lambda})^2\Delta\varepsilon_{n2\lambda}^2 - (1+y_{n\lambda})^2\, d_n^2 x_{n\lambda}^2} + 4\sum_{\mu\neq\lambda}^{M_n} \frac{\xi_{n\mu\lambda}(\xi_{n\mu\lambda}^2 + \eta_{n\mu}^2 + \eta_{n\lambda}^2)}{(\xi_{n\mu\lambda}^2 + \eta_{n\mu}^2 + \eta_{n\lambda}^2)^2 - 4\eta_{n\mu}^2\eta_{n\lambda}^2} - \sum_{j\neq 2\lambda-1,2\lambda}^{N_n} \frac{2\varepsilon_{n\lambda} - \xi_{n\lambda}}{(2\varepsilon_{n\lambda} - \xi_{n\lambda})^2 + \eta_{n\lambda}^2}, \tag{4.70}$$

$$I_{n\lambda} = \left\{ \frac{1-y_{n\lambda}^2}{(1-y_{n\lambda})^2\,\Delta\varepsilon_{n2\lambda}^2 - (1+y_{n\lambda})^2\, d_n^2 x_{n\lambda}^2} - 4y_{n\lambda}\sum_{\mu\neq\lambda}^{M_n} \frac{\xi_{n\mu\lambda}^2 - \eta_{n\mu}^2 + \eta_{n\lambda}^2}{(\xi_{n\mu\lambda}^2 + \eta_{n\mu}^2 + \eta_{n\lambda}^2)^2 - 4\eta_{n\mu}^2\eta_{n\lambda}^2} + y_{n\lambda}\sum_{n\neq 2\lambda-1,2\lambda}^{N_n} \frac{1}{(2\varepsilon_{n\lambda} - \xi_{n\lambda})^2 + \eta_{n\lambda}^2} \right\} \times \sqrt{\left| \frac{\Delta\varepsilon_{n2\lambda}^2 - d_n^2 x_{n\lambda}^2}{y_{n\lambda}} \right|}, \tag{4.71}$$

with

$$\xi_{n\mu\lambda} = \xi_{n\mu} - \xi_{n\lambda}. \tag{4.72}$$

Thus, for an arbitrary combination of α and β, we must solve the following equations:

$$\begin{aligned} F_{\alpha\beta}^{+} &= 0, \\ F_{\alpha\beta}^{-} &= 0 \quad (\alpha = 1, 2, \ldots, M_1/2; \beta = 1, 2, \ldots, M_2/2). \end{aligned} \tag{4.73}$$

4.3.5 *Results and discussion*

We now apply the exact solution for a two-band system to discuss the properties of the two-band superconductivity in ultrasmall grains. The single-particle level patterns of the $(2M_1 + m) + 2M_2$ electron system ($m = 0, 1, 2$) under consideration are represented in Figs. 4.6(a), 4.6(b) and 4.6(c), respectively. The dotted lines represent the chemical potential, and d_1 and d_2 ($d_1 < d_2$) are the mean level spacings. As seen in these figures, the additional electrons first occupy band 1 and then band 2.

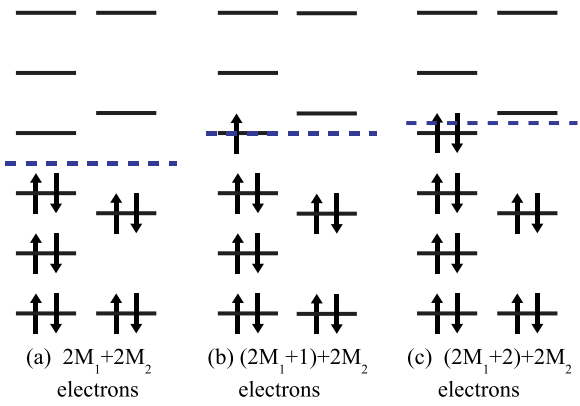

Fig. 4.6 Single-particle levels near the Fermi level in the case of two-band superconductivity. The dotted lines represent the chemical potential. The left and right bands are band 1 and band 2, respectively. d_1 and d_2 are the mean level spacings. (a) $2M_1 + 2M_2$ electron system, where M_n is the number of pair levels; (b) $(2M_1 + 1) + 2M_2$ electron system; (c) $(2M_1 + 2) + 2M_2$ electron system.

Numerical calculations are carried out under the condition that N_1:N_2 = 3:2, $\hbar\omega_D = 50$ and $\lambda_1 = \lambda_2 = \lambda$.

4.3.6 *Pair energy level*

By minimizing the sum of squares of Eqs. (4.69) and (4.70),

$$F = \sum_{\alpha=1}^{M_1/2} \sum_{\beta=1}^{M_2/2} \left(F_{\alpha\beta}^{+2} + F_{\alpha\beta}^{-2} \right), \tag{4.74}$$

for various interaction parameters, we obtain a behavior of pair energy levels E_{nJ} of two bands, as shown in Fig. 4.7, in which the solid and broken lines correspond to the pair energy levels of band 1 and band 2, respectively. The parameters used in this calculation are $N_1 = 12$, $N_2 = 8$, $M_1 = 6$, $M_2 = 4$, $0 \leq \lambda \leq 1.0$ and $0 \leq \lambda_{12} \leq 0.2$.

As seen in the figures, band 2 condenses into degenerate levels, but band 1 does not. In general, we can expect that the single-particle levels in a band, whose mean level spacing d is larger than that of the other band, degenerate faster. The behavior of the condensing band is qualitatively the same as that in the case of calculations for the single band.[166] The coexistence of the normal band and the condensed one may be reflected in the opposite phase of the gaps of these bands.[156]

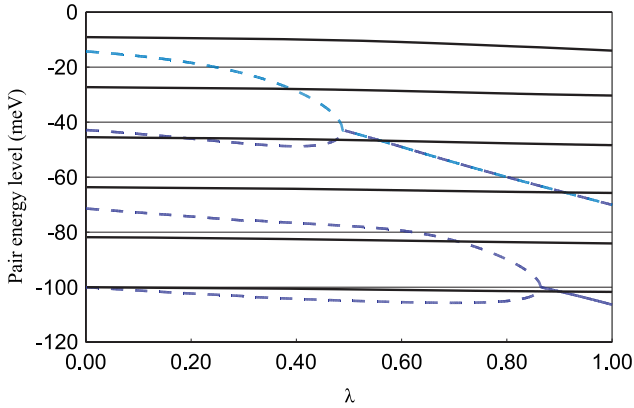

Fig. 4.7 Typical behavior of pair energy levels of two bands for the ground state. The parameters used in calculation are $N_1 = 12$, $N_2 = 8$, $M_1 = 6$, $M_2 = 4$, $\hbar\omega_D = 50$, $0 \leq \lambda_1 = \lambda_2 \leq 1.5$ and $0 \leq \lambda_{12} \leq 0.3$. The solid and broken lines correspond to the pair energy levels of band 1 and band 2, respectively.

4.3.7 *Condensation energy*

The condensation energy of band n for the $(2M_1+m)+2M_2$ electron system can be defined as

$$E_n^C(2M_1+m, 2M_2) = E_n(2M_1+m, 2M_2) + \left(M_n + \frac{m}{2}\right) g_n - E_n^0(2M_1+m, 2M_2), \tag{4.75}$$

where $E_n(2M_1+m, 2M_2)$ and $E_n^0(2M_1+m, 2M_2)$ are the ground-state energies and the sum of the single-particle energies, respectively.

We calculate the condensation energies and show them in Figs. 4.8(a) and 4.8(b). The parameters used in this calculation are $\lambda = 0.5$, and $\lambda_{12} = 0.01$ for (a) and $\lambda_{12} = 0.1$ for (b). Values are normalized by the bulk gap, $\Delta = \omega_D \sinh^{-1}\left(\frac{\lambda}{\lambda^2 - \lambda_{12}^2}\right)$. The solid and broken lines correspond to the condensation energy for band 1 and band 2, respectively. The lines plotted with squares, triangles and circles are for the $2M_1 + 2M_2$ electron system, $(2M_1 + 1) + 2M_2$ electron system and $(2M_1 + 2) + 2M_2$ electron system, respectively.

As seen in the figures, we can understand that band 2 condenses, but band 1 does not because of the sign of values. This difference of signs may also be reflected in the opposite phases of the gaps of these bands. The behavior of the results for the condensed band (band 2) is qualitatively the same as in the case of the single-band calculations. The condensation energy

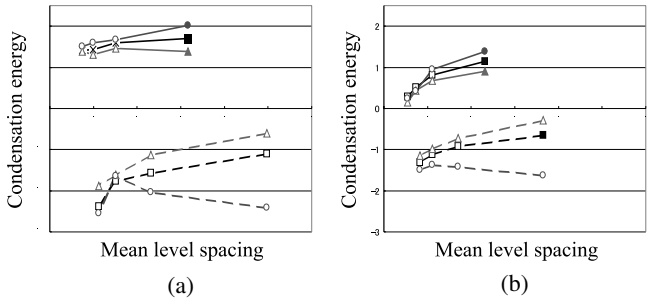

Fig. 4.8 Condensation energy. The parameters used in calculation are $\hbar\omega_D = 50$ and $\lambda_1 = \lambda_2 = 0.5$. Values are normalized by the bulk gap, $\Delta_1 = \omega_D \sinh^{-1}\left(\frac{\lambda_2}{\lambda_1\lambda_2 - \lambda_{12}^2}\right)$ or $\Delta_2 = \omega_D \sinh^{-1}\left(\frac{\lambda_1}{\lambda_1\lambda_2 - \lambda_{12}^2}\right)$. The solid and broken lines correspond to the condensation energy for band 1 and band 2, respectively. The lines plotted with squares, triangles and circles are for the $2M_1 + 2M_2$ electron system, $(2M_1 + 1) + 2M_2$ electron system and $(2M_1 + 2) + 2M_2$ electron system, respectively. (a) The condensation energy for the interband coupling parameter $\lambda_{12} = 0.01$; (b) the condensation energy for $\lambda_{12} = 0.1$.

of band 2 for the $(2M_1+2)+2M_2$ electron system is, however, different from the others. We can also see that the condensation energy is affected by the interband interaction λ_{12}. This was mentioned in our previous work.[156]

4.3.8 *Parity gap*

The parity gap of band n is defined as

$$\Delta_n^p = E_n(2M_1 + 1, 2M_2) - \frac{1}{2}\{E_n(2M_1, 2M_2) + E_n(2M_1 + 2, 2M_2)\}, \tag{4.76}$$

which was introduced by Matveev and Larkin and characterizes the difference of even–odd ground-state energies.[169]

We have also calculated the parity gaps shown in Fig. 4.9. The solid and broken lines correspond to the parity gap for band 1 and band 2, respectively. The lines plotted with triangles and squares are for the interband coupling parameter $\lambda_{12} = 0.01$ and $\lambda_{12} = 0.1$, respectively. Other parameters used in this calculation are the same as for the calculation of the condensation energy. Values are normalized by the bulk gap.

For the condensed band, we obtain qualitatively the same result as in the case of the single-band calculations, i.e. there is a minimal point and a tendency towards 1 for $d \to 0$. The mean level spacing giving the minimal

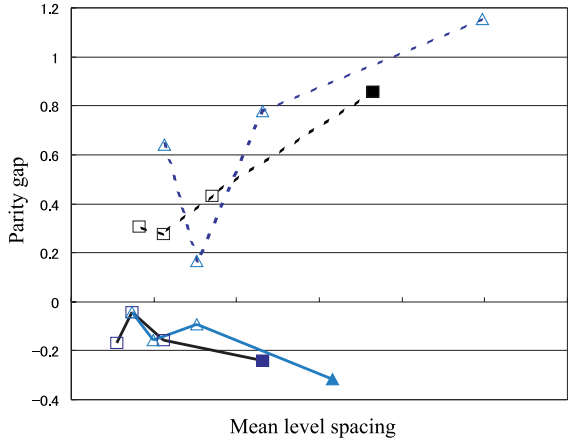

Fig. 4.9 Parity gap. The parameters used in calculation are $\hbar\omega_D = 50$ and $\lambda_1 = \lambda_2 = 0.5$. The solid and broken lines correspond to the parity gap for band 1 and band 2, respectively. The lines plotted with triangles and squares are for the interband coupling parameter $\lambda_{12} = 0.01$ and $\lambda_{12} = 0.1$, respectively. Values are normalized by the bulk gap.

point is, however, much less than that for the case of calculations for the single band. The parity gap is almost independent of the interband interaction λ_{12}. This was also mentioned in our previous work.[156]

We have extended Richardson's exact solution to the two-band system, and have derived a new coupled equation. To investigate the properties of the two-band superconductivity, we have solved the equation numerically and determined the behavior of pair energy levels, the condensation energy and the parity gap.

The band whose mean level spacing is larger than that of the other band degenerates and condenses faster. The behavior of the condensing band is qualitatively the same as that in the case of calculations for the single band. The coexistence of the normal band and the condensed one may be reflected in the opposite phases of the gaps of these bands. This phase character appears in all the results of numerical calculations. Therefore, the phase of a gap is important for stabilizing the two-band superconductivity.

We have also calculated the condensation energy and the parity gap for two-band superconductivity. The results suggest that the interband interaction λ_{12} affects the condensation energy, but not the parity gap.

In summary, the expression of Richardson's exact solution for two-band superconductivity has been presented, by solving numerically a new coupled equation. Then, the behaviors of pair energy levels, the condensation

energy and the parity gap have been determined. The results for the condensed band are almost qualitatively the same as those for the single-band calculation, and the coexistence of the normal band and the condensed one may have originated from the opposite phases of the gaps of these bands.

4.4 Kondo Effect Coupled to Superconductivity

The Kondo effect has attracted great interest, while considering the properties of semiconductor quantum dots. It can be understood as the magnetic exchange interaction between a localized impurity spin and free conduction electrons.[174] To minimize the exchange energy, the conduction electrons tend to screen the spin of the magnetic impurity, and the ensemble forms a spin singlet. In a quantum dot, some exotic properties of the Kondo effect have been observed.[175,176] Recently, Sasaki *et al.* have found a significant Kondo effect in quantum dots with an even number of electrons.[177] The spacing of discrete levels in such quantum dots is comparable with the strength of the e–e Coulomb interaction. The Kondo effect in multilevel quantum dots has been investigated theoretically by several groups.[178–180] They have shown that the contribution from many levels enhances the Kondo effect in normal metals. There are some investigations into the Kondo effect in quantum dots revealing ferromagnetism,[181] noncollinear magnetism,[182] superconductivity[183] and so on.[184,185]

Properties of ultrasmall superconducting grains have also been theoretically investigated by many groups.[160–162,164,165,167–169,186] Black *et al.* have revealed the presence of a parity-dependent spectroscopic gap in the tunneling spectra of nanosize Al grains.[160,164] For such ultrasmall superconducting grains, the bulk gap has been discussed in relation to physical properties such as the parity gap,[169] condensation energy[165] and electron correlation[166] with the size dependence of the level spacing of samples.[167] In the previous works,[156] we have also discussed physical properties such as condensation energy, the parity gap, and electron correlation of two-gap superconductivity in relation to the size dependence and the effective pair scattering process. In addition, the possibility of new two-gap superconductivity has been discussed by many groups.[14,97,119,129,133,135,137,140,187,188]

In a standard *s*-wave superconductor, the electrons form pairs with antialigned spins and are in a singlet state as well. When the superconductivity and the Kondo effect are present simultaneously, they are usually expected to be competing physical phenomena. The local magnetic

moments from the impurities tend to align the spins of the electron pairs in the superconductor, which often results in a strongly reduced transition temperature. Buitelaar *et al.* have experimentally investigated the Kondo effect in a carbon nanotube quantum dot coupled to superconducting Au/Al leads.[183] They found that the superconductivity of the leads does not destroy the Kondo correlations in the quantum dot at the Kondo temperature. A more subtle interplay has been proposed for exotic and not well-understood materials such as heavy-fermion superconductors, in which the two effects might actually coexist.[189]

In this paper, we investigate the Kondo effect and the superconductivity in ultrasmall grains by using a model which consists of the *sd* and reduced BCS Hamiltonians with the introduction of a pseudofermion. The mean-field approximation for the model is introduced, and we calculate physical properties of the critical level spacing and the condensation energy. These physical properties are discussed in relation to the coexistence of the superconductivity and the Kondo regime. Finally, we derive the exact equation for the Kondo regime in a nanosystem and discuss the condensation energy from the viewpoint of the correlation energy.

4.4.1 *Kondo regime coupled to superconductivity*

In nanosize superconducting grains, the quantum level spacing approaches the superconducting gap. It is necessary to treat the discretized energy levels of a small-size system. For ultrasmall superconducting grains, we can consider the pairing-force Hamiltonian to describe the electronic structure of the system[172] and can determine the critical level spacing in the case where the superconducting gap function vanishes at a quantum level spacing.[167] In this section, we present a model for a system in the Kondo regime coupled to the superconductivity and discuss the physical properties such as critical level spacing and condensation energy by using the mean-field approximation in relation to the gap function, spin singlet order as the Kondo effect, coexistence and so on.

4.4.2 *Model*

We consider a model coupled to the superconductivity for quantum dots to investigate the Kondo effect in normal metals, which can be expressed by the effective low-energy Hamiltonian obtained by the Schrieffer–Wolff

transformation[190]:

$$H = H_0 + H_1 + H_2, \tag{4.77}$$

where

$$H_0 = \sum_{k,\sigma} \varepsilon_k a^\dagger_{k\sigma} a_{k\sigma} + \sum_{\sigma} E_\sigma d^\dagger_\sigma d_\sigma, \tag{4.78}$$

$$H_1 = J \sum_{k,k'} \Big[S_+ a^\dagger_{k'\downarrow} a_{k\uparrow} + S_- a^\dagger_{k'\uparrow} a_{k\downarrow} + S_z \big(a^\dagger_{k'\uparrow} a_{k\uparrow} - a^\dagger_{k'\downarrow} a_{k\downarrow} \big) \Big], \tag{4.79}$$

$$H_2 = -g \sum_{k,k'} a^\dagger_{k\uparrow} a^\dagger_{k\downarrow} a_{k'\downarrow} a_{k'\uparrow}. \tag{4.80}$$

$a^\dagger_{k\sigma}$ ($a_{k\sigma}$) and $d^\dagger_\sigma$ (d_σ) are the creation (annihilation) operator corresponding to conduction electrons and the effective magnetic particle as an impurity, respectively. In this study, we assume that the magnetic particle is a fermion with $S = 1/2$, for simplicity. E represents an extraction energy given by $E_{\uparrow,\downarrow} = -E_0 \pm E_z$, including the Zeeman effect. The second term of Eq. (4.77) is the interaction between conduction electrons and the spin in a quantum dot. S is the spin operator as $S_+ = d^\dagger_\uparrow d_\downarrow$, $S_- = d^\dagger_\downarrow d_\uparrow$ and $S_z = (d^\dagger_\uparrow d_\uparrow - d^\dagger_\downarrow d_\downarrow)/2$. The third term corresponds to the interaction between conduction electrons included in the pairing-force Hamiltonian.

Here, we introduce a pseudofermion for the magnetic particle operator[191] as

$$\begin{aligned} d^\dagger_\uparrow &= f_\downarrow, \quad d_\uparrow = f^\dagger_\downarrow, \\ d^\dagger_\downarrow &= -f_\uparrow, \quad d_\downarrow = -f^\dagger_\uparrow. \end{aligned} \tag{4.81}$$

For this transformation, we have the condition

$$f^\dagger_\uparrow f_\uparrow + f^\dagger_\downarrow f_\downarrow = 1, \tag{4.82}$$

and we have $|\sigma\rangle = f^\dagger_\sigma |0\rangle$. The spin operator S can be presented as $S_+ = f^\dagger_\uparrow f_\downarrow$, $S_- = f^\dagger_\downarrow f_\uparrow$ and $S_z = (f^\dagger_\uparrow f_\uparrow - f^\dagger_\downarrow f_\downarrow)/2$. The Hamiltonian can be rewritten as

$$H_0 = \sum_{k,\sigma} \tilde{\varepsilon}_k c^\dagger_{k\sigma} c_{k\sigma} + \sum_{\sigma} E f^\dagger_\sigma f_\sigma, \tag{4.83}$$

$$H_1 = J \sum_{k,k',\sigma,\sigma'} f^\dagger_\sigma f_{\sigma'} c^\dagger_{k'\sigma'} c_{k\sigma}, \tag{4.84}$$

$$H_2 = -g \sum_{k,k'} c^\dagger_{k\uparrow} c^\dagger_{k\downarrow} c_{k'\downarrow} c_{k'\uparrow}, \tag{4.85}$$

where $c_{k\sigma} = \sum_i U_{ik} a_{i\sigma}$ and $\tilde{\varepsilon}_k = \sum_{i,j} U^\dagger_{ki} [\varepsilon_i \delta_{ij} - J/2] U_{jk}$. For the sake of simplicity, we focus only on $E_z = 0$ without an external magnetic field: $E = E_0$.

4.4.3 *Mean-field approximation*

In this subsection, we introduce the mean-field approximation for the present Hamiltonian (4.77). Eto *et al.* have presented the mean-field approximation for the Kondo effect in quantum dots.[192]

In the mean-field approximation, we can introduce the spin singlet order parameter

$$\Xi = \frac{1}{\sqrt{2}} \sum_{k,\sigma} \langle f^\dagger_\sigma c_{k\sigma} \rangle. \tag{4.86}$$

This order parameter describes the spin couplings between the dot states and conduction electrons. The superconducting gap function can be expressed as

$$\Delta = \sum_k \langle c_{k\downarrow} c_{k\uparrow} \rangle. \tag{4.87}$$

Using these order parameters in Eqs. (4.84) and (4.85), we obtain the mean-field Hamiltonian

$$\begin{aligned} H_{\mathrm{MF}} = & \sum_{k,\sigma} \tilde{\varepsilon}_k c^\dagger_{k\sigma} c_{k\sigma} + \sum_\sigma \tilde{E} f^\dagger_\sigma f_\sigma + \sqrt{2} J \sum_{k,\sigma} [\Xi f_\sigma c^\dagger_{k\sigma} + \Xi^* c_{k\sigma} f^\dagger_\sigma] \\ & - g \sum_k [\Delta^* c_{k\downarrow} c_{k\uparrow} + \Delta c^\dagger_{k\uparrow} c^\dagger_{k\downarrow}]. \end{aligned} \tag{4.88}$$

The constraint (4.82) is taken into account by the second term with a Lagrange multiplier λ. In this study, we assume a constant DOS with the energy region of the Debye energy, and the coupling constants can be expressed as $J = d\tilde{J}$ and $g = d\lambda$.

4.4.4 *Critical level spacing in the Kondo effect*

By minimizing the expectation value of H_{MF} in Eq. (4.88), the order parameters can be determined self-consistently. First, we show the Kondo effect without the pairing-force part ($g = 0$) in the framework of the mean-field

approximation. Next, the Kondo effect in the presence of the superconductivity is discussed in relation to the critical level spacing and the condensation energy. Finally, we derive the exact equation for the Kondo effect in ultrasmall grains coupled to normal metals and discuss properties such as the condensation energy in relation to Richardson's exact equation for the superconductivity.

For ultrasmall superconducting grains, the critical level spacing d_c^{BCS} can be expressed as $d_c^{\mathrm{BCS}} = 4\omega_D e^{\gamma} \exp(-1/\lambda)$ for an even number of electrons, where ω_D means the Debye energy. This result suggests that the gap function of a nanosize system with the level spacing d vanishes when the coupling parameter λ_c is less than the value $(\ln 4\omega_D/d + \gamma)^{-1}$. The bulk gap function Δ_c with λ_c can be expressed as $\Delta_c = \omega_D \mathrm{sh}^{-1}(1/\lambda_c)$.

Figure 4.10(a) shows the gap function of a nanosize system in the framework of the standard BCS theory. We can find the region where the gap function vanishes when the coupling becomes less than λ_c. This means that the level spacing is larger than the gap function in this region.

Here, we drive the critical level spacing for only the Kondo regime ($\lambda = 0$). The equation determining the singlet order parameter can be

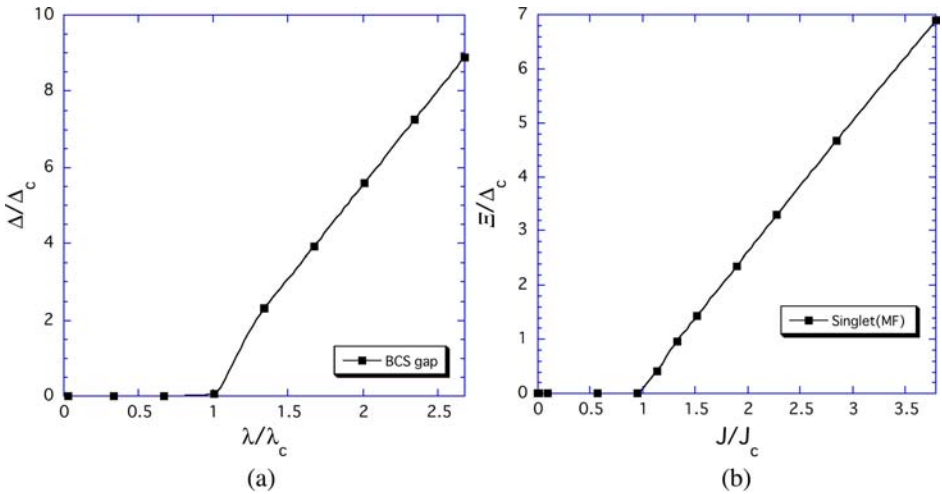

Fig. 4.10 Gap function and spin-singlet order. (a) The gap function. This vanishes in the region of λ values less than λ_c. (b) Spin singlet order parameter. In the case of $\tilde{J} < \tilde{J}_c$, the singlet order vanishes. The system consists of eight energy levels and eight electrons with the level spacing $d = 1.0$ and $\omega_D = 1.0$.

expressed as

$$\Xi = \sum_k \frac{\Xi(\xi_k - x)}{(\xi_k - x)^2 + \Xi^2}, \tag{4.89}$$

where $\xi_k = \tilde{\varepsilon}_k - \mu$, $x = \left[\tilde{\varepsilon}_k + \tilde{E} \pm \sqrt{(\tilde{\varepsilon}_k - \tilde{E})^2 + 4\Xi^2}\right]/2$ and μ is the chemical potential. For the case of the critical level spacing, the solution shows that the spin singlet order parameter vanishes. From Eq. (4.89), we can find the critical level spacing $d_c^{\rm Kondo}$ for the Kondo regime.

$$d_c^{\rm Kondo} = 4\omega_D e^{\gamma} \exp\left[-\frac{1}{2\sqrt{2}\tilde{J}}\right]. \tag{4.90}$$

When the coupling parameter $\tilde{J}$ is smaller than $\tilde{J}_c = [2\sqrt{2}(\ln(4\omega_D/d) + \gamma)]^{-1}$, the spin singlet order parameter vanishes.

Figure 4.10(b) presents the spin singlet order parameter given by Eq. (4.86) in the case $g = 0$. In the region of $\tilde{J} < \tilde{J}_c$, the order parameter vanishes. This result suggests the critical level spacing in the Kondo effect.

4.4.5 *Kondo effect coupled to superconductivity*

Here, we consider a simple system which consists of eight energy levels and eight electrons, and investigate the critical level spacing and the condensation energy of the coupled system between the superconductivity and the Kondo regime in the framework of the mean-field approximation of Eq. (4.88).

Figure 4.11(a) shows the spin singlet order parameter and the gap function for several cases. We can find the critical level spacings for the gap function and for the spin singlet order parameter. When $\lambda < \lambda_c$ and $\tilde{J} > \tilde{J}_c$, we can find only the spin singlet order parameters. In the region of λ/λ_c from 1.4 to 1.7 with $\tilde{J}/\tilde{J}_c = 0.189$, we can find the coexistence of the gap function and the spin singlet order parameter. For λ/λ_c larger than 1.7, only the gap function still exists, and the spin singlet order parameter vanishes. At $\tilde{J}/\tilde{J}_c = 0.284$, we can find the coexistence in the region $\lambda/\lambda_c = 1.7 - 2.3$. These results suggest that strong local magnetic moments from the impurities reduce the transition temperature for superconductivity. However, the weak couplings λ of the superconductivity do not destroy the spin singlet order parameter at all. These results are in good agreement with the experimental results.[183] We can find that there is a coexistence region for the superconductivity and the Kondo regime.

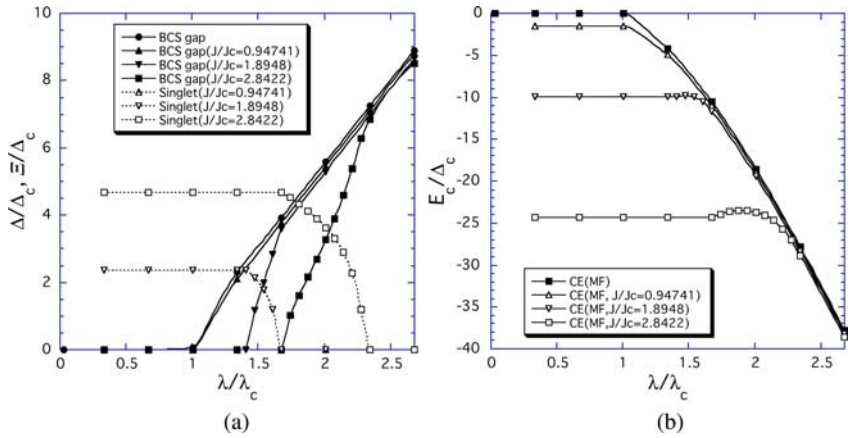

Fig. 4.11 Physical properties in a coupled system. (a) Gap function and spin singlet order parameter. (b) Condensation energy. $\tilde{J}/\tilde{J}_c = 0$, 0.94741, 1.8948, 2.8422. Other parameters are the same.

Figure 4.11(b) shows the condensation energy for several λ and $\tilde{J}$ values. We have found that the condensation energy of the coupled system between the superconductivity and the Kondo regime becomes lower than that for the pure superconductivity. In the coexistence region, the highest value of the condensation energy appears in all cases.

4.4.6 *Exact solution for the Kondo regime*

The standard BCS theory gives a good description of the phenomenon of superconductivity in large samples. However, when the size of a superconductor becomes small, the theory fails. To investigate the physical properties such as the condensation energy, and the parity gap, it is necessary to perform a more accurate treatment. For the superconductivity in ultrasmall grains, the exact solution to the reduced BCS Hamiltonian presented by Richardson[172] has been applied to investigate the above-mentioned physical properties.[168]

By using the wave function describing all pair electron excitations, we can derive the exact solution for the pairing-force (reduced) Hamiltonian:

$$2 - \sum_{k=1}^{N} \frac{\lambda}{\tilde{\varepsilon}_k - E_i} + \sum_{l=1, l\neq i}^{n} \frac{2\lambda}{E_l - E_i} = 0, \tag{4.91}$$

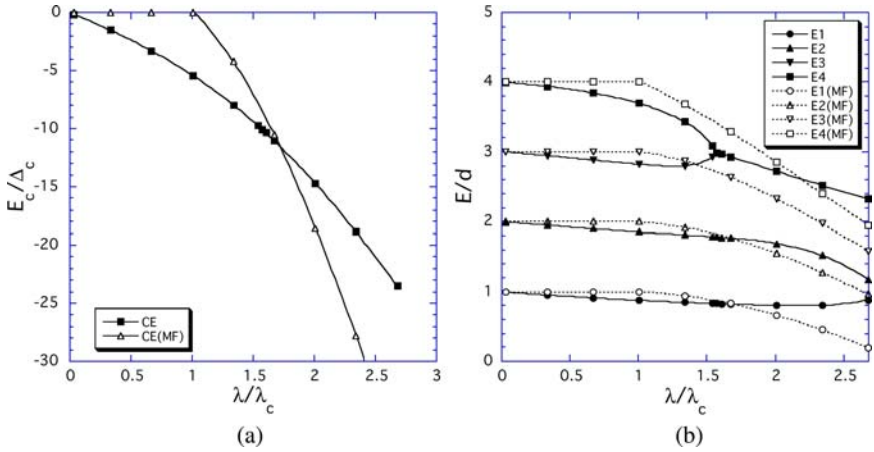

Fig. 4.12 Exact solution for the superconductivity. (a) Condensation energy of the exact solution and that obtained in the mean-field approximation. (b) Pairing energy level with energy level obtained in the mean-field approximation. Eight energy levels, eight electrons, $d = 1.0$, $\omega_D = 4.0$.

where N and n are the number of orbitals and the number of the occupied orbitals, respectively, and E_i corresponds to the exact orbital. Figure 4.12 shows the condensation energy and the pairing energy level for the nanosize superconductivity. Note that the physical properties obtained in the mean-field approximation give a good description of the high DOS ($d \to \infty$). We have found the different behavior of the condensation energy from that obtained in the mean-field approximation, as shown in Fig. 4.12(a). Figure 4.12(b) presents the qualitative behavior of the pairing energy level in the ground state. At λ about 1.6, more than two energy levels in Fig. 4.12(b) are completely paired. The pairing behavior has already been reported by many groups.[138, 172]

Let us derive the exact equation for the Kondo regime in ultrasmall grains. We can consider the Hamiltonian $H = H_0 + H_1$ in Eq. (4.77). We introduce a creation operator describing all excited states at the spin singlet coupling between a conduction electron and a pseudofermion:

$$B_j^\dagger = \sum_{k,\sigma} \frac{c_{k\sigma}^\dagger f_\sigma}{\tilde{\varepsilon}_k - E_j}, \tag{4.92}$$

where E_j represents the exact eigenenergies in the Kondo regime. The exact eigenstate $|\Psi_n\rangle$ for the Kondo regime can be written as $|\Psi_n\rangle = \Pi_{\upsilon=1}^n B_\upsilon^\dagger |0\rangle$. Other electrons, which are not related to the spin singlet order, contribute $E_{\text{single}} = \sum_{k=1}^n \tilde{\varepsilon}_k$ to the eigenenergy. The ground-state energy E_{GS} can be written as $E_{\text{GS}} = \sum_{k=1}^n [E_k + \tilde{\varepsilon}_k]$.

By operating the Hamiltonian to the exact eigenstate, we obtain the condition

$$1 + \sum_{k=1}^{N} \frac{\tilde{J}}{\tilde{\varepsilon}_k - E_j} = 0. \tag{4.93}$$

This equation gives the exact solution for the Kondo regime. Note that the creation operator (4.92) might be a true boson one compared with the case of the reduced BCS model.

Figure 4.13 shows the condensation energy of the exact solution in the Kondo regime with that obtained in the mean-field approximation. We can find the different behavior of the condensation energy from that obtained in the mean-field approximation. However, the behavior is similar to that in the case of the superconductivity in nanosize systems.

We have investigated properties of the Kondo regime coupled to the superconductivity in ultrasmall grains by using the mean-field approximation. In the framework of the mean-field approximation, we have found the critical level spacing for the Kondo regime. The result suggests that the Kondo effect vanishes when the level spacing becomes larger than the critical level spacing.

We have calculated physical properties of the critical level spacing and the condensation energy of the coupled system by using the mean-field

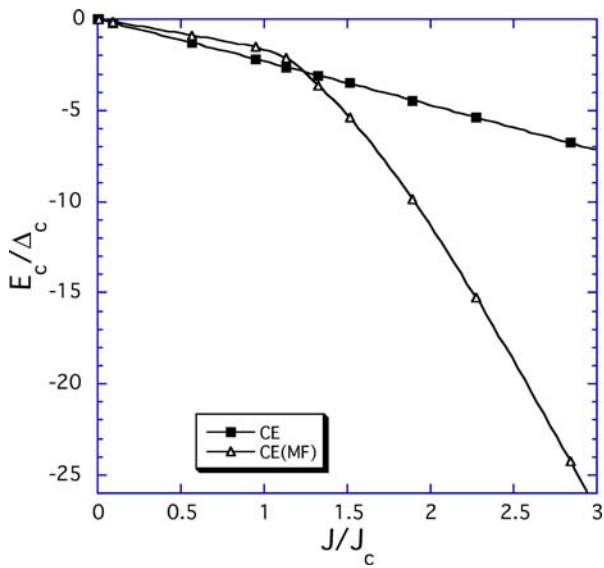

Fig. 4.13 Condensation energy for the Kondo regime: all parameters used in the system are as follows: eight energy levels, eight electrons, $d = 1.0$ and $\omega_D = 4.0$.

approximation. From the results, we have found that strong local magnetic moments from the impurities reduce the transition temperature for superconductivity. However, weak couplings λ of the superconductivity do not destroy the spin singlet order parameter at all. These results are in good agreement with the experimental results.[183] We have found that there is a coexistence region for the superconductivity and the Kondo regime.

Finally, we have derived the exact equation for the Kondo regime in a nanosystem, which was not an easy task, and have discussed the condensation energy from the viewpoint of energy levels. Further study of the properties in the Kondo regime with the use of the exact equation will be presented elsewhere.

In summary, we have investigated the Kondo effect and the superconductivity in ultrasmall grains by using a model which involves the *sd* and reduced BCS Hamiltonians with the introduction of a pseudofermion. The mean-field approximation for the model has been introduced, and we have calculated physical properties of the critical level spacing and the condensation energy. These physical properties have been discussed in relation to the coexistence of the superconductivity and the Kondo regime. Finally, we have derived the exact equation for the Kondo regime in a nanosystem and discussed the condensation energy from the viewpoint of energy levels.

4.5 Interaction of Nanoscale Ferromagnetic Granules in London Superconductors

Recent experiments have fabricated structured arrays of ferromagnetic nanoparticles in proximity to a bulk superconductor. We consider the theory of interactions between two nanoscale ferromagnetic particles embedded in a superconductor. In the London limit approximation, we will show that the interactions between ferromagnetic particles can lead to either parallel or antiparallel spin alignment. The crossover between these is dependent on the ratio of the interparticle spacing and the London penetration depth. We show that a phase transition between spin orientations can occur under variation of the temperature. Finally, we comment on the extension of these results to arrays of nanoparticles in different geometries.

Magnetism and superconductivity are two competing collective ordered states in metals. In the case of ferromagnetism, the exchange interactions lead to parallel alignment of electronic spins, while e–p interactions in the BCS superconductivity lead to spin singlet pairing of electrons. Clearly,

these two types of order are in general mutually incompatible. In bulk systems, the frustration between the electron singlet pairing and the spin ordering is resolved by the FFLO (Fulde–Ferrell,[193] Larkin–Ovchinnikov[194]) state. However, this has proven to be elusive experimentally, and few examples are known. In particular, the FFLO state appears to be highly sensitive to disorder.

In recent years, however, there has been a great increase of interest in the interactions between ferromagnetism and superconductivity in artificially structured systems. Advances in nanotechnology and microfabrication have made it possible to build hybrid structures containing both ferromagnetic and superconducting components which interact magnetically or via the proximity effect.[195,204] Superconductor–ferromagnet–superconductor planar structures have been found to show the π-junction Josephson behavior.[196–198] Ferromagnet–superconductor–ferromagnet spin valve structures have also been fabricated,[199] with potential applications to spintronics. In addition, more complex types of structures have been produced; for example, Moschalkov *et al.* fabricated arrays of ferromagnetic nanoscale dots on superconducting substrates.[200,201] A description of such structures based upon the G–L theory was developed by Peeters.[202]

In this section, we consider the interaction between magnetic nanoparticles embedded in a superconductor, as shown in Fig. 4.14. Theoretical studies of such systems can be carried out exactly in two limiting cases, depending on the relative magnitudes of the London penetration depth, λ, and the coherence length, ξ. If we consider the nanoparticles to be essentially pointlike on the scale of both these characteristic lengths, then they correspond to effective pointlike magnetic moments of the form

$$\mathbf{M}(\mathbf{r}) = \sum_i \mathbf{m}_i \delta(\mathbf{r} - \mathbf{r}_i), \tag{4.94}$$

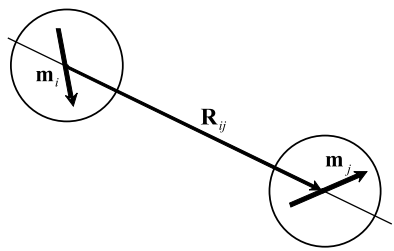

Fig. 4.14 Schematic diagram of a nanocomposite superconductor containing ferromagnetic granules.

where the particle at r_i has magnetic moment m_i. Interactions between these isolated moments arise directly from magnetic dipole–dipole forces modified by the screening of the bulk supercurrents. A second source of the interaction between the moments is the RKKY interaction modified by the presence of the BCS energy gap Δ. It is clear that the range of the dipolar forces is determined by the penetration depth λ, while the usual oscillatory power-law RKKY interaction is truncated exponentially on a length scale of the order of ξ_m. Therefore, the dipolar forces dominate for superconductors in the London limit $r_0 \ll \lambda$, while the RKKY interactions are more important in the Pippard case $r_0 \gg l$, where $r_0^{-1} = \xi_m^{-1} + l^{-1}$, and l is the mean free path.[15] Here, we consider the London limit and neglect RKKY interactions. Magnetic impurities interacting via RKKY interactions were considered by Larkin.[203] In the London limit, we first derive general expressions for the configuration of magnetic fields and the interaction energy of an ensemble of ferromagnetic granules. Then we consider the case of two interacting nanoparticles. It is found that, as a function of the temperature, an orientational phase transition can take place. The conditions for such a phase transition to occur are derived for a chain of ferromagnetic granules. Finally, we comment on the application of these results to the determination of the equilibrium configurations of more general lattices of ferromagnetic particles.

4.5.1 *Magnetic field of ferromagnetic inclusions in a London superconductor*

We determine the magnetic configurations in superconducting nanocomposite systems by means of Maxwell's equations. The total current, $\mathbf{j}$, includes both normal and superconducting parts:

$$\mathbf{j} = \mathbf{j}_s + \mathbf{j}_n. \tag{4.95}$$

The role of the normal currents in a superconductor is negligible, since the superconductor exhibits weak magnetic characteristics in the normal state. However, a normal current will be present within the ferromagnetic inclusions. This normal-state current can be written in the traditional form

$$\mathbf{j}_n = \nabla \times \mathbf{M}, \tag{4.96}$$

where $\mathbf{M}$ is the magnetization of a material. The supercurrent obeys the usual London equation

$$\nabla \times \mathbf{j}_s = -\frac{n_s e^2}{m}\mathbf{B} \tag{4.97}$$

in SI units,[64] where $\mathbf{B}$ is the magnetic field, n_s is the superfluid density, and m and e are the electron mass and charge, respectively.

Combining the relations (4.95)–(4.97) with the Maxwell equation $\nabla \times \mathbf{B} = \mu_0 \mathbf{j}$, the magnetic field can be found in the form

$$\nabla \times (\nabla \times \mathrm{B}) + \lambda^{-2}\mathrm{B} = \mu_0 \nabla \times (\nabla \times \mathbf{M}), \tag{4.98}$$

where λ is the London penetration depth of the field in the superconductor. Since $\operatorname{div} \mathrm{B} = 0$, Eq. (4.98) can be rewritten as

$$-\nabla^2 \mathrm{B} + \lambda^{-2}\mathrm{B} = \mu_0 \nabla \times (\nabla \times \mathbf{M}). \tag{4.99}$$

For the boundary conditions, we assume that the magnetic field in the superconductor vanishes far from the region of the ferromagnetic inclusions. According to these boundary conditions, the solution Eq. (4.99) can be expressed as follows:

$$\mathrm{B}(\mathbf{r}) = \frac{\mu_0}{4\pi} \int d^3 r' \, G(|\mathbf{r} - \mathbf{r}'|) \, \nabla \times (\nabla \times \mathbf{M}(\mathbf{r}')), \tag{4.100}$$

where the Green function is given by

$$G(|\mathbf{r} - \mathbf{r}'|) = \frac{\exp(-|\mathbf{r} - \mathbf{r}'|/\lambda)}{|\mathbf{r} - \mathbf{r}'|}. \tag{4.101}$$

After the double integration by parts from manipulation (see App. B), this expression can be rewritten in the general form

$$\begin{aligned} \mathrm{B}(\mathbf{r}) = \frac{\mu_0}{4\pi} \int d^3 r' \exp\left(-\frac{R}{\lambda}\right) \cdot \left\{ \left(\frac{3\mathbf{R}(\mathbf{R} \cdot \mathbf{M}(\mathbf{r}'))}{R^5} - \frac{\mathbf{M}(\mathbf{r}')}{R^3} \right) \right. \\ \left. \times \left(1 + \frac{R}{\lambda} + \frac{R^2}{\lambda^2}\right) - \frac{2\mathbf{R}(\mathbf{R} \cdot \mathbf{M}(\mathbf{r}'))}{\lambda^2 \cdot R^3} \right\}, \end{aligned} \tag{4.102}$$

where $\mathbf{R} = \mathbf{r} - \mathbf{r}'$ and $R = |\mathbf{r} - \mathbf{r}'|$.

The expression (4.102) determines the magnetic field outside of the ferromagnetic inclusions. Since the magnetization of the system $\mathbf{M}(\mathbf{r})$ is defined by (4.96), we find in (4.101) that $\mathbf{M}(\mathbf{r}) = 0$ outside of the volume of ferromagnetic granules.

4.5.2 *Magnetic field of ferromagnetic quantum dots in a superconducting nanocomposite material*

Assuming that the sizes of the ferromagnetic inclusions are on the nanometer length scale, they will appear essentially pointlike on the scale of the penetration depth λ. In this case, we can approximate the magnetization

as a sum of point magnetic moments, as shown in Eq. (4.94). Using this approximation in the general expression (4.102), we find the result (see App. B)

$$\mathrm{B}(\mathbf{r}) = \frac{\mu_0}{4\pi}\sum_i \exp\left(-\frac{R_i}{\lambda}\right)\cdot\left\{\left(\frac{3\mathbf{R_i}(\mathbf{R_i}\cdot\mathbf{m_i})}{R_i^5} - \frac{\mathbf{m_i}}{R_i^3}\right)\right.$$
$$\left.\times\left(1+\frac{R_i}{\lambda}+\frac{R_i^2}{\lambda^2}\right) - \frac{2\mathbf{R_i}(\mathbf{R_i}\cdot\mathbf{m_i})}{\lambda^2\cdot R_i^3}\right\}, \tag{4.103}$$

where $\mathbf{R}_i = \mathbf{r} - \mathbf{r}_i$ and $R_i = |\mathbf{r} - \mathbf{r}_i|$.

It is apparent from Eq. (4.103) that if the temperature of a superconductor approaches T_c, and the penetration depth $\lambda \to \infty$, then the expression (4.103) tends to the limit

$$\mathrm{B}(\mathbf{r}) = \frac{\mu_0}{4\pi}\sum_i\left(\frac{3\mathbf{R}_i(\mathbf{R}_i\cdot\mathbf{m}_i)}{R_i^5} - \frac{\mathbf{m}_i}{R_i^3}\right), \tag{4.104}$$

which describes the usual magnetic field of isolated dipoles in the normal-state medium.

In the other limiting case, if the distance between granules is greater than the depth penetration, we have

$$\mathrm{B}(\mathbf{r}) = \frac{\mu_0}{4\pi}\sum_i \frac{\exp(-R_i/\lambda)}{R_i\cdot\lambda^2}\cdot\left(\frac{\mathbf{R}_i(\mathbf{R}_i\cdot\mathbf{m}_i)}{R_i^2} - \mathbf{m}_i\right). \tag{4.105}$$

4.5.3 *Interaction energy of quantum dots in a superconducting nanocomposite material*

To determine the collective states of the magnetic moments in superconducting nanocomposite materials in the London limit, we make use of the expression for the free energy F of the system[205]:

$$F = \frac{1}{2\mu_0}\int d^3r\{\mathrm{B}^2 + \lambda^2(\nabla\times\mathrm{B})^2\}. \tag{4.106}$$

Integrating by parts and using the Gauss theorem, we transform Eq. (4.106) into

$$F = \frac{1}{2\mu_0}\int d^3r\,\mathrm{B}\{\mathrm{B} + \lambda^2\nabla\times(\nabla\times\mathrm{B})\} = -2\pi\lambda^2\int d^3r\,\mathrm{B}\cdot\nabla\times(\nabla\times\mathbf{M}). \tag{4.107}$$

Integrating by parts and using the Gauss theorem again, we transform Eq. (4.107) into

$$F = -2\pi\lambda^2\int d^3r\,\mathbf{M}\cdot\nabla\times(\nabla\times\mathrm{B}). \tag{4.108}$$

Then, using the London equation (4.98) and omitting the magnetostatic self-energy from consideration, we find the interaction energy of magnetic

moments. The obtained expression can be used to determine the collective state of magnetization of an ensemble of granules:

$$U = \frac{\mu_0}{8\pi} \sum_i \sum_j \exp\left(-\frac{R_{ij}}{\lambda}\right) \cdot \left\{ \left(\frac{3(\mathbf{R_{ij}} \cdot \mathbf{m_j})(\mathbf{R_{ij}} \cdot \mathbf{m_i})}{R_{ij}^5} - \frac{\mathbf{m_i} \cdot \mathbf{m_j}}{R_{ij}^3} \right) \times \left(1 + \frac{R_{ji}}{\lambda} + \frac{R_{ij}^2}{\lambda^2} \right) - \frac{2(\mathbf{R_{ij}} \cdot \mathbf{m_j})(\mathbf{R_{ij}} \cdot \mathbf{m_i})}{\lambda^2 \cdot R_{ij}^3} \right\}, \tag{4.109}$$

where $\mathbf{R}_{ij} = \mathbf{r}_j - \mathbf{r}_i$, $R_{ij} = |\mathbf{r}_j - \mathbf{r}_i|$, $i \neq j$.

4.5.4 *Spin-orientation phase transitions in a nanocomposite material with arrays of ferromagnetic quantum dots*

We begin by studying the magnetic configuration of an isolated pair of magnetic moments. The interaction energy of such a pair can be written as

$$U = -\frac{\mu_0}{4\pi} \exp\left(-\frac{R_{12}}{\lambda}\right) \cdot \left\{ \left(\frac{3(\mathbf{R_{12}} \cdot \mathbf{m_1})(\mathbf{R_{12}} \cdot \mathbf{m_2})}{R_{12}^5} - \frac{\mathbf{m_2} \cdot \mathbf{m_1}}{R_{12}^3} \right) \times \left(1 + \frac{R_{12}}{\lambda} + \frac{R_{12}^2}{\lambda^2} \right) - \frac{2(\mathbf{R_{12}} \cdot \mathbf{m_1})(\mathbf{R_{12}} \cdot \mathbf{m_2})}{\lambda^2 \cdot R_{12}^3} \right\}. \tag{4.110}$$

Let us introduce a coordinate system with the origin at the first magnetic moment $\mathbf{m}_1$ and the polar axis along the line connecting magnetic moments. In this coordinate system, the magnetic moments have the components $\mathbf{m}_i = m_i(\cos\varphi_i \sin\theta_i, \sin\varphi_i \sin\theta_i, \cos\theta_i)$, and their interaction energy (4.110) is written in the form

$$U = \frac{\mu_0}{4\pi} m_1 m_2 \cdot \frac{\exp(-R_{12}/\lambda)}{R_{12}^3} \cdot f(\theta_i, \varphi_i, R_{12}/\lambda), \tag{4.111}$$

where

$$f(\theta_i, \varphi_i, x) = -2(1+x)\cos\theta_1 \cos\theta_2 + (1 + x + x^2)\sin\theta_1 \sin\theta_2 \cos\varphi \tag{4.112}$$

and $\varphi = \varphi_2 - \varphi_1$.

Differentiating the function $f(\theta_i, \varphi_i, x)$ with respect to angular variables and equating the results to zero, we find that there are four possible stable

energy configurations:

$$\theta_1 = \theta_2 = 0, \quad \theta_1 = \theta_2 = \pi, \quad 0 \le \varphi < 2\pi, \tag{4.113}$$

$$\theta_1 = \theta_2 = \frac{\pi}{2}, \quad \varphi = \pi, \tag{4.114}$$

$$\theta_1 = \theta_2 = \frac{\pi}{2}, \quad \varphi = 0, \tag{4.115}$$

$$\theta_1 = 0, \quad \theta_2 = \pi, \quad 0 \le \varphi < 2\pi, \tag{4.116}$$

which are illustrated in Fig. 4.15.

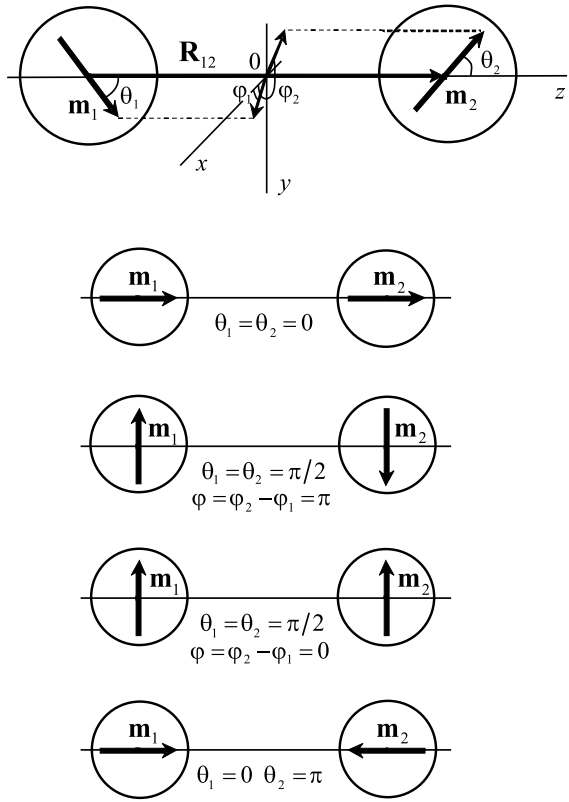

Fig. 4.15 Four energy saddle points of a pair of ferromagnetic quantum dots, as defined in Eq. (4.113). Of the four, 1 and 2 correspond to the ground state, depending on the condition (4.118). States 3 and 4 are never stable.

Further analysis shows that configurations (4.115) and (4.116) are saddle points, not energy minima. Evaluating the second derivatives of (4.112), we obtain the stability condition of the configuration (4.113):

$$\left(\frac{R}{\lambda}\right)^2 - \frac{R}{\lambda} - 1 \leq 0. \tag{4.117}$$

This implies that the ferromagnetic ordering of the pair of magnetic moments is possible if

$$\frac{R}{\lambda} \leq \frac{1}{2}(1 + \sqrt{5}). \tag{4.118}$$

It turns out that if the condition (4.118) is violated, then the alternative configuration (4.114) is a stable energy minimum. We can conclude that if the temperature changes, and the penetration depth parameter $\lambda(T)$ varies in such a way that the condition (4.118) is not satisfied, then the ground-state orientation will change from (4.113) to (4.114).

This result is readily generalized to ordered arrays of ferromagnetic granules, and so we conclude that orientational phase transitions are possible in systems of quantum dots in a superconducting matrix. For example, it is clear that the condition (4.118) can be applied to linear chains of quantum dots. On the other hand, the results for square or cubic lattices remain to be determined.

We have considered the interactions between nanoscale magnetic dots embedded in a bulk superconducting material. Our approach is valid for materials which are well described in the London limit $r_0 \ll \lambda$, since RKKY interactions are negligible. We have shown that, depending on the dimensionless parameter R/λ, different stable ground states occur. So, as the temperature varies, orientational phase transitions will take place for periodic arrays of such quantum dots. Of course, our calculation does not include all types of interactions which define the orientation of magnetic moments in space. In particular, we neglect the energy of a magnetic anisotropy of granules which is determined by the shape of granules or the type of their crystal lattice. However, when the shape of granules is close to the spherical one and the lattice of a ferromagnet has the cubic symmetry, then Eq. (4.109) will essentially be exact.

In the experimental systems studied by V. V. Moshchalkov,[201] a square of Pt/Co magnetic nanodots was deposited on the surface on the Pb superconductor, which is of type $I(k = 0.48)$. The dots were about 0.26 μm in diameter, and they were deposited on the grid with a spacing of 0.6 μm. For Pb, the penetration depth is 39 nm at low temperatures. So, this array

was in the limit $R > \lambda$ and the dot–dot interaction would be expected to correspond to the antiferromagnetic alignment shown in the second state in Fig. 4.15. With increase in the temperature, the transition to the ferromagnetic alignment would occur according to Eq. (4.118) at $\lambda = 0.36R$, i.e. 219 nm.

According to the Casimir formula $\lambda(T) = \lambda(0)(1 - t^4)^{-1/2}$, with $t = T/T_c$, this would occur at $T = 7.14\,\mathrm{K}$, compared with $T_c = 7.2\,\mathrm{K}$. Therefore, the experimental conditions for the transition to be observed are certainly feasible. Of course, for an exact comparison with theory in this case, our theory should be generalized to deal with magnetic particles near the surface rather than with those embedded in the bulk of a superconductor.

Of course, it would be interesting in the future to generalize our results to superconductors in the Pippard limit, where the RKKY interactions between quantum dots will dominate over dipolar forces.[203]

The expression (4.110) can be used to study, by means of numerical methods, the magnet configurations and the orientational phase transitions in an ensemble of nanogranules. It is possible to determine the conditions of orientational transformations in the analytic form for the ordered structures (a chain of granules, plane and volume lattices). Inasmuch as the state of the magnetic subsystem of a specimen at phase transitions is changed, this phenomenon can be experimentally observed under the change in the magnetic susceptibility in the region of low fields.

4.6 Spin-Orientation Phase Transitions in a Two-Dimensional Lattice of Ferromagnetic Granules in a London-Type Superconductor

In order to determine the collective state of magnetic moments in nanocomposite materials with the matrix made of a London-type superconductor, we use the formula (4.103) for the energy of magnetic interaction.

First of all, we note that the realization of one or other magnetic configuration is defined by both the competition of diamagnetic effects from the side of the superconducting matrix and the magnetostatic interaction in the system of ferromagnetic granules. At lower temperatures eliminating the thermal disordering of the system, the magnetostatic interaction leads to a correlation of magnetic moments. As the main conditions for the formation of magnetic configurations, we take the equivalence of all sites and the zero value of the net magnetic moment of the lattice. The planar

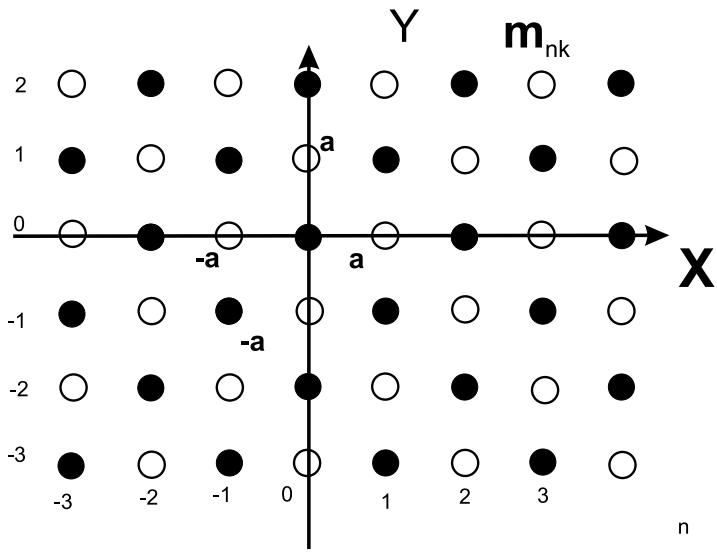

Fig. 4.16 Two-dimensional lattice of magnetic points. Magnetic moments (black) are directed up or down (white); a is the lattice constant.

lattice of granules by itself sets a preferred direction in space. Therefore, we will separate two configurations from the whole manifold of spatial orientations of magnetic moments. The first configuration is presented in Fig. 4.16. It is characterized by the orientation of the magnetization of granules which is orthogonal to the base plane. The alternation of the magnetization of neighboring granules decreases, to a certain extent, the energy of magnetic interaction. In addition, such a distribution of magnetic moments favors a decrease in the amplitude of a magnetic field in the superconducting matrix, which is also advantageous from the energy viewpoint. Thus, the given configuration can be considered as a version of the magnetic order.

A configuration of the second type is shown in Fig. 4.17. It is characterized by the distribution of magnetic moments in the base plane of the lattice such that the magnetic moments are aligned as magnetic chains with alternating directions of the magnetization. Here, like the configuration presented in Fig. 4.16, the main requirement, i.e. the equivalence of the states of magnetic points, is satisfied. A similar distribution also decreases the energy of magnetostatic interaction, and favors a decrease in the amplitude of a magnetic field in a superconductor. At the same time, the planar orientation of magnetic moments has the basic distinction from the orthogonal one. For example, by means of

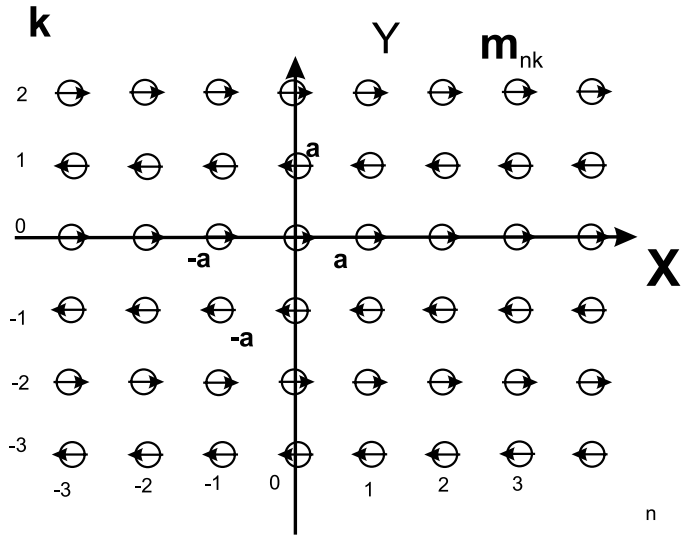

Fig. 4.17 Two-dimensional lattice of magnetic points. Magnetic moments are aligned in the plane in the form of chains; a is the lattice constant.

a continuous deformation of the magnetization in the base plane, the configuration in Fig. 4.16 can be transferred into the structure shown in Fig. 4.17.

Such a system is characterized by a coherent rotation of magnetic moments by an angle $\pm\varphi$ relative to the principal direction of the lattice. In this case, there occur both the modulation of the direction of moments at sites of the lattice and some increase in the energy of magnetic chains, but these processes are accompanied by the formation of magnetic vortices in cells, which promotes a decrease in the energy of magnetic interaction. The states of separate magnetic points in the lattice remain equivalent at the zero total magnetization. Thus, the following questions arise: How does the energy of the array of magnetic moments in the base plane shown in Fig. 4.18 depend on the angle $\pm\varphi$, and to which value is it equal in the equilibrium state? To answer these questions, we consider the relation (4.110) for the interaction energy and reduce it to a single sum by virtue of the fact that the states of magnetic points are equivalent. In this case, in order to calculate the energy of the lattice, it is sufficient to determine the energy of a single magnetic point, e.g. $m_{0,0}$, located at the origin of the coordinate system, and then multiply the result by the total number of magnetic points N. The relation (4.110) becomes significantly

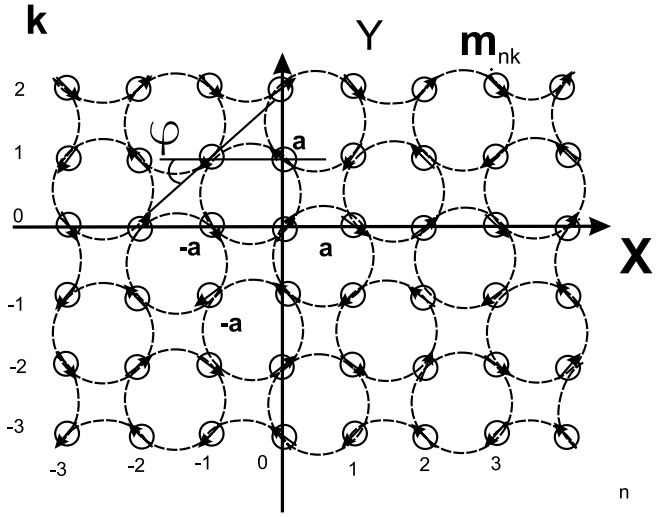

Fig. 4.18 Part of the lattice with a modulated planar distribution of the magnetization; a is the lattice constant. Circles represent magnetic points, and the arrows on them indicate the directions of magnetic moments $m_n k$ in the base plane (n and k are the spatial indices of magnetic points). The angle φ defines the deviation of the moments of magnetic points from the principal direction of the lattice. The states of all points in the given configuration are equivalent. The net magnetic moment is zero. The separated circles schematically denote magnetic vortices. The dotted lines are tangents to the directions of magnetic moments at sites of the lattice.

simpler:

$$U = -\frac{\mu_0}{4\pi}\frac{N}{2}\left\{3\left(1-\frac{\partial}{\partial\alpha}\right)+\frac{\partial^2}{\partial\alpha^2}\right\}\sum_i^N \exp\left(-\frac{\alpha\cdot r_i}{\delta}\right)\frac{(\mathbf{r}_i\cdot\mathbf{m}_i)(\mathbf{r}_i\cdot\mathbf{m}_{0,0})}{r_i^5}$$

$$+\frac{N}{2}\left\{1-\frac{\partial}{\partial\alpha}+\frac{\partial^2}{\partial\alpha^2}\right\}\sum_i^N \exp\left(-\frac{\alpha\cdot r_i}{\delta}\right)\frac{\mathbf{m}_i\cdot\mathbf{m}_{0,0}}{r_i^3}. \qquad (4.119)$$

By writing the formula (4.119), we used the method of differentiation with respect to the parameter α, which should be set equal to 1 after the calculations. The index i stands for the summation over all sites of the lattice, δ — the penetration depth for 2D case. Performing the summation in the relation (4.119), it is convenient to introduce the pair of indices (n,k) defining the position of a site in the lattice (Fig. 4.18) instead of the running index of magnetic points i. It is easy to see that the system represented in Fig. 4.18 *possesses* the translational invariance with a period of $2a$ so that

$$\mathbf{m}_{n,k} = \mathbf{m}_{n+2l,\,k+2p},$$
$$l,p = \pm1,\pm2,\ldots. \qquad (4.120)$$

The lattice has only four types of magnetic points differ which from one another by a spatial orientation of magnetic moments. Their vector components depend on the angle φ in the following manner:

$$\mathbf{m}_{n,k} = \mathbf{m}_{n+2l,k+2p}, \quad \mathbf{m}_{2l,2p} = \mathbf{m}_{0,0} = m\begin{pmatrix}\cos\varphi\\ \sin\varphi\\ 0\end{pmatrix},$$

$$\mathbf{m}_{2l+1,2p} = \mathbf{m}_{1,0} = m\begin{pmatrix}\cos\varphi\\ -\sin\varphi\\ 0\end{pmatrix},$$

$$\mathbf{m}_{2l,2p+1} = \mathbf{m}_{0,1} = m\begin{pmatrix}-\cos\varphi\\ \sin\varphi\\ 0\end{pmatrix},$$

$$\mathbf{m}_{2l+1,2p+1} = \mathbf{m}_{1,1} = m\begin{pmatrix}-\cos\varphi\\ -\sin\varphi\\ 0\end{pmatrix},$$

$$l, p = \pm 1, \pm 2, \ldots,$$

$$l, p = \pm 1, \pm 2, \ldots, \tag{4.121}$$

where m is the modulus of the magnetic moment of a site.

After the substitution of Eq. (4.121) in Eq. (4.119) and the summation over sites of the unbounded lattice, we get the following interesting result. It turned out that the interaction energy of the system of magnetic points (see Fig. 4.18) does not depend on the angle φ and is determined by the relation

$$\frac{U_{\|}}{N} = \frac{\mu_0}{4\pi}\frac{m^2}{\mathrm{a}^3}\cdot F\,(\mathrm{a}/\delta), \tag{4.122}$$

where N is the number of sites of the lattice, m is the magnetic moment of a granule and $F(\mathrm{a}/\delta)$ is the energy characteristic of a magnetic state which is a universal function of a single parameter and determines the dependence of the energy on both the period and the field penetration depth in the case where the magnetic moments are distributed in the base plane of the lattice. It can be represented in the form of a sum:

$$F(\mathrm{a}/\delta) = \frac{\mu_0}{4\pi}\left(-1 + \frac{\partial}{\partial\alpha} + \frac{\partial^2}{\partial\alpha^2}\right)\cdot\frac{1}{8}\sum_{l=1}^{\infty}\sum_{p=0}^{\infty}\frac{\exp(-2\alpha(\mathrm{a}/\delta)\sqrt{l^2+p^2})}{(l^2+p^2)^{3/2}}$$

$$-\left(-1 + \frac{\partial}{\partial\alpha} + \frac{\partial^2}{\partial\alpha^2}\right)\cdot\frac{1}{4}\sum_{l=-\infty}^{\infty}\sum_{p=-\infty}^{\infty}$$

$$\times \frac{\exp(-\alpha(a/\delta)\sqrt{(2l+1)^2+(2p+1)^2})}{((2l+1)^2+(2p+1)^2)^{3/2}}$$
$$- \left(3 - 3\frac{\partial}{\partial\alpha} + \frac{\partial^2}{\partial\alpha^2}\right) \cdot \frac{1}{2} \sum_{l=-\infty}^{\infty} \sum_{p=-\infty}^{\infty}$$
$$\times \frac{((2l+1)^2-(2p)^2) \cdot \exp(-\alpha(a/\delta)\sqrt{(2l+1)^2+(2p)^2})}{((2l+1)^2+(2p)^2)^{5/2}}. \tag{4.123}$$

Thus, there occurs the degeneration of the state in the parameter φ in the presence of a tough correlation of the mutual orientations of moments of the ensemble of magnetic points. The energies of the configuration shown in Fig. 4.17(1b) and the ensemble with a modulated distribution of the magnetization (see Fig. 4.18) coincide. In turn, the determination of the energy of magnetic interaction for the configuration possessing the orthogonal orientation of magnetic moments (Fig. 4.16) requires a smaller number of calculations, because the first sum in the formula (4.119) vanishes. The result of calculations can be represented in the form

$$\frac{U_\perp}{N} = \frac{\mu_0}{4\pi}\frac{m^2}{a^3} \cdot \Phi\,(a/\delta), \tag{4.124}$$

where $\Phi(a/\delta)$ is the energy characteristic of the magnetic state which is a universal function of the single parameter and determines the dependence of the energy on both the period and the field penetration depth under the distribution of magnetic moments normally to the base plane of the lattice. This function can be represented in the form

$$\Phi(a/\delta) = \frac{\mu_0}{4\pi}\left(1 - \frac{\partial}{\partial\alpha} + \frac{\partial^2}{\partial\alpha^2}\right) \cdot \frac{1}{2}$$
$$\times \left\{ \sum_{l=1}^{\infty} \sum_{p=0}^{\infty} \frac{4 \cdot \exp\left(-\alpha \cdot (a/\delta) \cdot \sqrt{2 \cdot l^2 + 2 \cdot p^2}\right)}{\left(2 \cdot l^2 + 2 \cdot p^2\right)^{3/2}} - \sum_{l=-\infty}^{\infty} \sum_{p=-\infty}^{\infty} \right.$$
$$\left. \times \frac{\exp\left(-\alpha \cdot (a/\delta) \cdot \sqrt{2 \cdot (l+1/2)^2 + 2 \cdot (p+1/2)^2}\right)}{\left(2 \cdot (l+1/2)^2 + 2 \cdot (p+1/2)^2\right)^{3/2}} \right\}. \tag{4.125}$$

The calculation of the functions $F(a/\delta)$ and $\Phi(a/\delta)$ on the basis of the relations (4.123) and (4.125) is not a difficult task and can be realized with

any mathematical software. The results are presented in graphical form in Fig. 4.19.

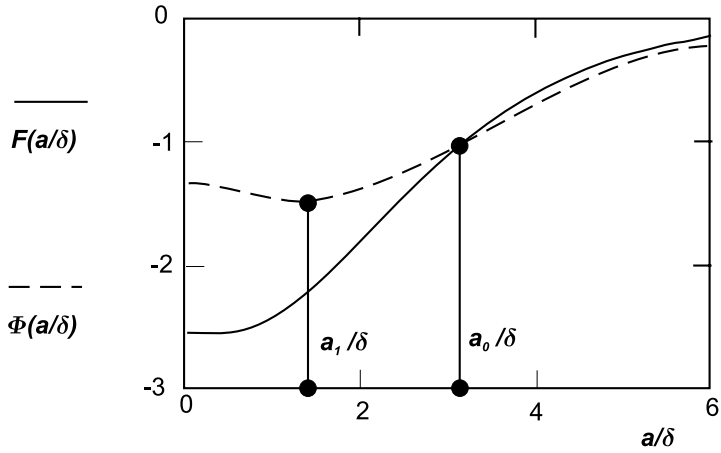

Fig. 4.19 Plots of the energy characteristics $F(\mathrm{a}/\delta)$ and $\Phi(\mathrm{a}/\delta)$ of states of the lattice with normal and planar orientations of magnetic moments, respectively. Values of $F(0)$ and $\Phi(0)$ correspond to the transition of the superconducting matrix to the normal state.

In Fig. 4.19, we represent the plots of the energy characteristics of two different states of a magnetic lattice versus the ratio of the parameter of a cell and the penetration depth of the magnetic field, a/δ. The limit $\mathrm{a}/\delta \to 0$ corresponds to the transition of the matrix to the normal state. It is obvious that a lattice with planar orientation of magnetic moments (Figs. 4.17 and 4.18) possesses the lower energy in the normal state at $a/\delta = 0$. Therefore, the state with the perpendicular direction of moments (Fig. 4.16) cannot be realized at all in the absence of a superconductor. As the temperature decreases and the penetration depth diminishes gradually, the parameter a/δ begins to grow. When this parameter attains the value $a_0/\delta \approx 3.3$, the configuration with the orthogonal orientation of magnetic moments (Fig. 4.16) becomes more advantageous in energy, and the orientation phase transition occurs in the system. Upon at a decrease in the temperature, a similar scenario of events completely corresponds to a reorientation of the magnetic moments of an isolated pair of magnetic points, which was considered in the previous work.[205]

In conclusion, we note that an analogous phase transition can be expected to occur in a planar lattice with a rectangular cell. The only difference

will consist in the elimination of the degeneration relative to the directions of magnetic moments in the base plane. Of course, the direct observation of a phase transition will be hampered, because the problem involves the magnetic lattice surrounded by a superconductor. However, a similar orientation transformation must happen in a lattice applied on the surface of a massive superconductor, though values of the parameter a_0/δ will be different in this case.

4.7 Quantum Computer on Superconducting Qubits

4.7.1 *Principle of quantum computers*

Silicon microprocessors, being the main element of modern computers, have reached the limit of development. The miniaturization, i.e. the aspiration to place as many components as possible on a smaller and smaller area of a chip, has approached the boundary of physical possibilities. Further, it will be impossible to conserve the stability of the operation of computers. Many researchers believe that silicon processors will begin to go into the past in at most five years, and the production of chips will be based on the other material — carbon nanotubes. It is worth noting that the computational processes are accompanied by the release of heat. Feynman said: "Any classical computation is a physical process running with the release of heat." As is known, the calculations lead to an increase in the entropy and, hence, to the release of heat. The idea of the creation of quantum computers arose several decades ago, when it was proposed to reject the application of electric circuits in the processing of information and to pass to the use of quantum mechanics. Classical computers are processing the information only on the basis of ideas of one bit of information (it corresponds to the transition from state 0 to state 1 or conversely). Quantum computers can process the information by basing on ideas of a quantum bit (qubit), which allows one to realize simultaneously four logical operations $(0+0=0; 0+1=1; 1+0=1; 1+1=2)$.

The qubit is an abridged notation for the quantum bit and represents the unity of information coded in a quantum system which can be in the states $|0\rangle$ and $|1\rangle$, and in any superposition of these states.

Let the state of a qubit be described by the state $|f\rangle$, which can be represented as a superposition of the states $|0\rangle$ and $|1\rangle$:

$$|f\rangle = a|0\rangle + b|1\rangle,$$

where

$$a^2 + b^2 = 1. \tag{4.126}$$

Since the devices can register only classical quantities, the measurement of a quantum bit will give the states $|0\rangle$ or $|1\rangle$ with probabilities determined by the squares of the coefficients a and b.

The use of the principle of superposition allows one to increase the informational space exponentially with linear growth of the size of a physical system, because the register including n qubits can be in a superposition of at once 2^n states. In addition, quantum mechanics admits the existence of the so-called entangled states possessing no analogs in classical physics. An ensemble of qubits is a collection of qubits in different but given states.

It is worth noting that, even on the level of mathematics, a quantum computer operates in a basically different way than a classical computer. Input data are coded in "quantum cells of memory." In this case, the collection of qubits becomes a single quantum system. This system undergoes the sequence of elementary quantum operations. Quantum computations are a realization of the most astonishing idea of applying the principles of quantum mechanics to the world of computers. Ordinary computers, despite their complexity, use classical laws of mechanics. In recent years, the theory of classical computations has been developed on the basis of works by A. Turing. With the appearance of quantum computations, new possibilities have arisen, and the situation has been radically changed. Quantum methods can be successfully used in the solution of mathematical problems, though the time consumed for the solution of mathematical problems increases exponentially with the complexity of the problem.

For the theory of quantum calculations, the physical nature of qubits is not of crucial importance; the basically important point is that the system in the course of calculations obeys the laws of quantum mechanics.

4.7.2 *Superconducting qubits*

The realization of a quantum computer requires the availability of systems with a doubly degenerate ground state. For this reason, great attention is paid to systems with two-level wells which can be fabricated by facilities of solid-state electronics. The modern technology allows one to produce circuits containing millions of transistors and Josephson junctions.

By observing the operation of electrical circuits at temperatures close to absolute zero, researchers found a new proof of the fact that the laws of quantum mechanics are suitable not only for the microscopic objects

(atoms and electrons) but also for large electronic schemes, which include superconducting bits (qubits).

Many years ago, attempts to construct a Josephson computer on the basis of the Josephson tunnel logic failed hopelessly. The principal reason for the failure was the huge technological dispersion of parameters of tunnel junctions, which did not allow one to produce large microcircuits. A Josephson computer can be created only on the way, having nothing in common with that based on semiconductors; namely, it can be just a quantum computer.

The hope is related to two circumstances. First, the fabrication of superconducting qubits is quite possible in the framework of up-to-date technology. Second, the presence of a gap in the spectrum of excitations of a superconductor allows one to expect the suppression of generation in a system.

Let us consider the first steps on the way toward construction of a superconducting quantum computer. First, we consider, in brief, the Josephson effect.

4.7.3 *Josephson effect*

The Josephson effect is certainly one of the most interesting phenomena in superconductivity. It is the passing of a superconducting current through a thin dielectric layer separating two superconductors (the so-called Josephson junction).

It was predicted by an English physicist, B. Josephson, on the basis of superconductivity theory (in 1962; Nobel awarded the Prize in 1973), and discovered experimentally in 1963. Conduction electrons pass through a dielectric (a film of copper oxide $\sim$10 Å in thickness) due to the tunneling effect.[209, 210]

In Fig. 4.20, we present a scheme of the Josephson tunneling between two superconductors. The Josephson stationary effect considers the fact that the

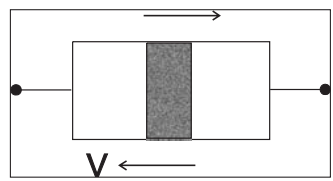

Fig. 4.20 Scheme of the Josephson tunneling between two superconductors.

superconducting current

$$J_c = J_0 \sin \varphi, \tag{4.127}$$

$$\frac{d\varphi}{dt} = \frac{2eV}{\hbar}, \tag{4.128}$$

where φ is the phase difference on the interface of superconductors, V the applied voltage, and J_0 the critical current through the junction.

The Josephson effect indicates the existence of the electron ordering in superconductors, namely the phase coherence: in the ground state, all electron pairs have the same phase φ which characterizes their wave function $\Psi_1 = \sqrt{n_{s1}} e^{i\varphi_1}$. According to quantum mechanics, the presence of a phase difference must cause a current through the junction. The discovery of such a current in experiment proves the existence of macroscopic phenomena in nature which are directly determined by the phase of a wave function:

$$\Psi = \sqrt{n} e^{i\psi}. \tag{4.129}$$

4.7.3.1 *Current passing through two series-connected Josephson junctions*

The Josephson current in the scheme drawn in Fig. 4.21 can be easily determined with the help of the elementary Feynman approach to a Josephson junction as a two-level quantum-mechanical system.[4] By introducing an intermediate object, some island, with the wave function Ψ_0 into the two-level system characterized by the wave functions $\Psi_1 = \sqrt{n_{s1}/2} e^{i\varphi_1}$ and $\Psi_2 = \sqrt{n_{s2}/2} e^{i\varphi_2}$, we write the Schrödinger equation in the form

$$i\hbar \frac{d\Psi_1}{dt} = \frac{eV}{2}\Psi_1 + K\Psi_0, \tag{4.130}$$

$$i\hbar \frac{d\Psi_0}{dt} = K\Psi_1 + K\Psi_2 + E_0\Psi_0, \tag{4.131}$$

$$i\hbar \frac{d\Psi_2}{dt} = K\Psi_0 - \frac{eV}{2}\Psi_2. \tag{4.132}$$

The formula for a constant current running through two series-connected Josephson junctions at the zero external potential difference takes the form

$$J = \hbar \frac{\partial \sqrt{n_{S1}}}{\partial t} = -\frac{K^2}{E_0}\sqrt{n_{S2}} \sin(\varphi_2 - \varphi_1). \tag{4.133}$$

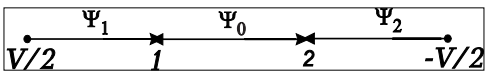

Fig. 4.21 Current passing through two series-connected Josephson junctions.

This relation can be rewritten as follows:

$$J_c = J_0 \sin(\varphi), \tag{4.134}$$

where $\varphi = \varphi_2 - \varphi_1$ is the phase difference. The relation obtained is called the Josephson formula (the Josephson stationary effect) and determines the current of superconductive electron pairs due to the tunneling transition.

The Josephson coupling energy is an important parameter of the Josephson junction. From (4.127), we have

$$E = \int JV\, dt = \frac{hJ_0}{2} \int_0^{\pi} \sin\varphi\, d\varphi = -\frac{hJ_0}{2e} \cos\varphi. \tag{4.135}$$

The Josephson effect is still one of the phenomena that make superconductors such a fascinating area of study. Despite more than 40 years of intensive studies and numerous applications, it remains an important field of research in connection with the use of small superconducting grains.

4.7.3.2 *SQUIDs*

The Josephson effect allowed one to construct superconducting interferometers, called SQUIDs (superconducting quantum interference devices), which contain parallel weak connections between superconductors.[206] In Fig. 4.22, we present a scheme with Josephson junctions. The total current running from 1 to 2 is equal to

$$I = I_0 d[\sin(\Delta\varphi_1) + \sin(\Delta\varphi_2)], \tag{4.136}$$

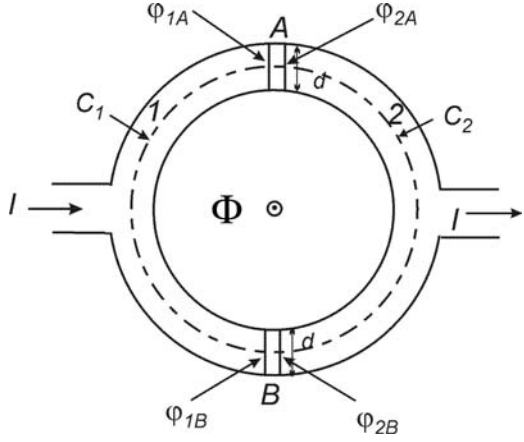

Fig. 4.22 Basic diagram of a quantum interferometer.

where

$$\Delta\varphi_1 = \varphi_{2A} - \varphi_{1A},$$

$$\Delta\varphi_2 = \varphi_{2B} - \varphi_{1B}$$

are the phase differences on the first and second Josephson junctions. There occurs a distinctive interference of the superconducting currents running through these connections.

Inside the superconductor, the current is zero: $\vec{j} \equiv 0$. We will use the following formula for the current j:

$$\mathbf{j} \sim h\nabla\varphi - \frac{2e}{c}\mathbf{A}. \tag{4.137}$$

We can write

$$\varphi_{1B} - \varphi_{1A} = \frac{2e}{hc}\int_{C_1} \mathbf{A}\cdot\mathbf{dl}, \tag{4.138}$$

$$\varphi_{2B} - \varphi_{2A} = \frac{2e}{hc}\int_{C_2} \mathbf{A}\cdot\mathbf{dl}. \tag{4.139}$$

Summing up these two equations, we get

$$\varphi_{1B} - \varphi_{2B} + \varphi_{2A} - \varphi_{1A} = \frac{2e}{hc}\oint \mathbf{A}\cdot\mathbf{dl} = 2\pi\frac{\Phi}{\Phi_0}. \tag{4.140}$$

Thus, we have

$$\Delta\varphi_1 - \Delta\varphi_2 = 2\pi\frac{\Phi}{\Phi_0}, \tag{4.141}$$

where Φ is the total quantum flux.

The flux quantum is defined as

$$\Phi_0 = \frac{h}{2e}. \tag{4.142}$$

For a balance SQUID ring system, we can write

$$\Delta\varphi_1 = \varphi_0 + \pi\frac{\Phi}{\Phi_0},$$

$$\Delta\varphi_2 = \varphi_0 - \pi\frac{\Phi}{\Phi_0}. \tag{4.143}$$

The total current in the SQUID is

$$\begin{aligned} I &= I_0\sin(\Delta\varphi_1) + I_0\sin(\Delta\varphi_2) \\ &= I_0\sin\left(\varphi_0 + \pi\frac{\Phi}{\Phi_0}\right) + I_0\sin\left(\varphi_0 - \pi\frac{\Phi}{\Phi_0}\right) \\ &= 2I_0\sin(\varphi_0)\cos\left(\pi\frac{\Phi}{\Phi_0}\right) = I_{\max}\left|\cos\left(\pi\frac{\Phi}{\Phi_0}\right)\right|, \end{aligned} \tag{4.144}$$

with $I_{\max} = 2I_0\sin(\varphi_0)$.

In this case, the critical current turns out to be periodically dependent on the flow of an external magnetic field, which allows one to use such a unit for exact measurement of the magnetic field.

4.7.3.3 *Flux qubit*

Let us consider the first steps on the way towards creation of a superconducting computer. The simplest superconducting system demonstrating the coherence is the SQUID, which is a superconducting ring including a Josephson junction at one point. The energy of this system contains two terms, the Josephson transition energy ($\cos\Phi$) and the energy related to the ring L:

$$H = -E_J \cos\left(2\pi\frac{\Phi}{\Phi_0}\right) + \frac{(\Phi - \Phi_x)^2}{2L}. \tag{4.145}$$

Here, Φ is the difference of superconductive phases at the junction. The superconductive phase in the ring is proportional to a magnetic flow applied to the ring (quantization of the magnetic flow). If Φ_x is equal exactly to a half of the magnetic flow, the potential of a SQUID becomes doubly degenerate.

Two minima of the well correspond to the currents in the ring passing in the clockwise and counterclockwise directions, respectively.[208]

A superposition of these states in SQUIDs, was observed experimentally in Refs. 208, 211. These experiments demonstrated clearly the possibility of creating a superposition of states in a system with a macroscopic number of particles. In the given case, the circular current including 10^{13} electrons was registered in a loop. The states participating in a superposition were macroscopically distinguishable, by differing from one another by the currents, whose difference was several microamperes. Recently, an important notion has been introduced in the course of studies of structures with Josephson junctions. It is the notion of macroscopic quantum coherence. In such systems, the Josephson energy can have two almost-degenerate minima at values of the phase which are separated by a potential barrier (see Fig. 4.23). It is possible that the phase passes from one minimum to another due to the quantum-mechanical tunneling, and the eigenstates of the system are superpositions of the states localized in the first and second minima.

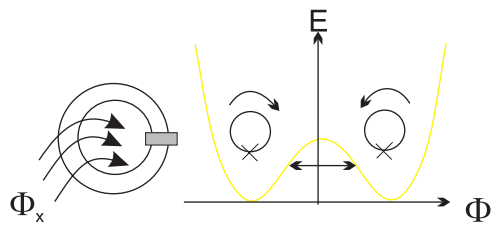

Fig. 4.23 Scheme of the Josephson tunneling between two superconductors.

The operation of a superconducting computer requires low temperatures, which are needed, in particular, to suppress heat-induced excitations destroying the quantum-mechanical state of a system.

It is worth noting that the best condition for the observation of these current states is defined by the size of the superconducting ring. If the ring size is taken to be 1 cm, there appear the effects of decoherence which will destroy the current states. But if the ring is taken to be much smaller (say, 5 μm), then it is possible to observe these states. These states were discovered in experiments with Rabi oscillations.[211]

4.7.3.4 *Charge qubit*

The second type of superconducting bit can be realized in the "Cooper-pair box" system, which is characterized by two charge states: without an excess Cooper pair $|0\rangle$ and with a single Cooper pair $|1\rangle$. A Cooper-pair box is a nanotransistor that has Coulomb blockage with controlling voltage V_g, as shown in Fig. 4.24. It is represented by an aluminum superconducting film of the order of 1 mm in size, with a working temperature of about several millikelvins, which is significantly lower than the superconducting temperature T_c. Its quantum state can be characterized by the number of Cooper pairs. According to the BCS theory, the ground state of a superconductor is a superposition of states with different numbers of Cooper pairs. The excited — i.e. unpaired — states in an ordinary superconductor are separated from the ground state by the energy gap. Therefore, as the number of electrons varies by 1, i.e. $N \to N \pm 1$, the ground-state energy must be changed by $\pm\delta$. The sign (plus or minus) depends on wherever the initial number of electrons N is even or odd. The effects of parity of the number of electrons which are considered in this chapter in connection with

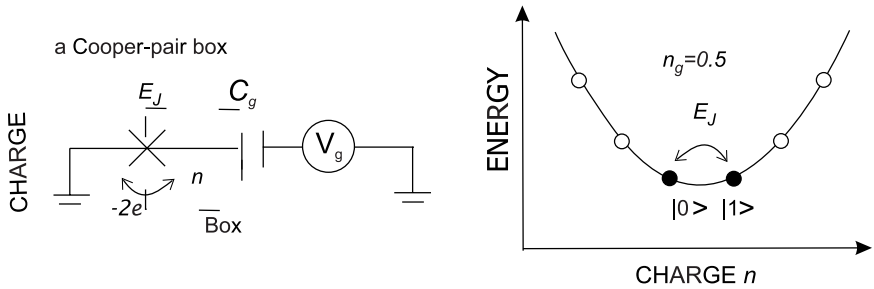

Fig. 4.24 Cooper-pair box [× denotes a Josephson junction (JJ)]. C_g and V_g are the capacitor and the controlling voltage.

mesoscopic superconductivity were successfully measured on nanotransistors with Coulomb blockage.

The Hamiltonian of such a system can be written as

$$H = E_c(n - n_g)^2 + E_j \cos \varphi, \tag{4.146}$$

where E_c and E_j are the charging and Josephson energies, and φ is the phase change. In the charging mode where $E_c \gg E_j$, only two lower-charged states are of importance. The controlling voltage V_g induces a charge in the box:

$$n_g = C_g \frac{V_g}{2e}, \tag{4.147}$$

where $2e$ is the charge of each Cooper pair and C_g is the gate capacitance. At $n_g = 1/2$, such a system operates as a two-level atomic system, in which the states $|0\rangle$ and $|1\rangle$ can be realized. The control is realized by a voltage V_g. On the basis of such a qubit, a system of two qubits was realized,[208,209] and the formation of entangled states was demonstrated. The effects of parity of the number of electrons which are considered in this chapter in connection with mesoscopic superconductivity were successfully measured on nanotransistors with Coulomb blockage.

4.7.3.5 *Phase qubit*

There exists one more possibility of realizing SQUIDs with the use of HTSCs possessing lattice, d pairing (π-loop ones).[210]

The physics of d pairing was considered in Chap. 2. Quantum processors on the base of these SQUIDs are being developed at the Canadian company D-wave.

We note also that, in addition to superconducting qubits, quantum computers use qubits possessing other physical properties. Scientists at Yale University used a very fine aluminum plate in the fabrication of a quantum chip. A single qubit consists of one billion aluminum atoms, which nevertheless behaves as a single unit that can be in two energy states, denoted as 0 and 1. Such quantum-mechanical states of a qubit cannot be long-term — their lifetime is about one microsecond. But it is sufficient for a chip to solve the so-called algorithm. We have considered the technologies of superconducting computers which represent a new type of quantum computers. These computers are based on the other mechanism obeying the laws of quantum mechanics. We recall that, till recently, the principle of devices was invariable, and the archetype of such devices is mechanical clocks. In such devices, all stages of their relative motion can be observed; therefore, it is quite simple to understand their structure. On the contrary, the principle

of operation of quantum computers involves the specific features of quantum mechanics which are difficult to understand. Nevertheless, by possessing the quantum resources, we can solve the very difficult complicated problems. In particular, the most important potential field of application of quantum computers is the problem of the exact calculation of properties of quantum systems.

Summary and Conclusions

In this book we have concentrated our attention on the most urgent problems of superconductivity, such as the nature of high-temperature superconductivity, mechanisms and symmetry of pairing, two-gap superconductivity in magnesium diborades, mesoscopic superconductivity and the problems of room-temperature superconductivity.

We considered some questions concerning the application of quantum field theory to the problems of superconductivity. Quantum field theory provides the original and powerful means for the solution of certain problems of superconductivity. In the field of superconductivity, we meet the problem-maximum — it consists the creation of room-temperature superconductors. We considered this problem in our book, gave some recommendations on the search for these superconductors and analyzed the possibility of the fabrication of artificial materials possessing the property of superconductivity at room temperature.

We also touched on the questions of the application of superconducting qubits to quantum computers. It was shown that the description of superconducting qubits is based on the laws of quantum mechanics.

It is worth noting that HTSCs have been investigated for more than two decades with great efforts but the whole pattern of the phenomenon is not yet available. We are sure that the comprehension of HTSCs will be attained when our knowledge of HTSCs reaches the critical level which will be sufficient for understanding the huge amount of experimental data from a single viewpoint. The study is in progress. In particular, we mention the

recent discovery of Cu-less superconductors with a high critical temperature which contain layers of FeAs.

The theoretical and experimental investigations into superconductivity and its practical applications at present constitute this wide, uncommon and interesting branch of science.

APPENDIX A

Two-particle Green Function for Multiband Superconductors

In this appendix, we will solve the problem of determining a two-particle Green function for multiband superconductors. In Chap. 3 we considered multiband superconductivity using a two-particle Green function.

We will calculate a two-particle Green function for multi-band superconductors. The Hamiltonian describing the systems of interacting electrons and phonons of a crystal is written in the form

$$H = \sum_{k,a,\upsilon} \varepsilon_k^{\upsilon} a_{k\sigma}^{+\upsilon} a_{k\sigma}^{\upsilon} + \frac{1}{N} \sum_{q,k_1,\sigma_1,\upsilon_1,k_2,\sigma_2,\upsilon_2} V_q a_{k_1\sigma_1}^{+\upsilon_1} a_{k_2\sigma_2}^{\upsilon_2} a_{k_2+q,\sigma_2}^{\upsilon_2} a_{k_1-q,\sigma_1}^{\upsilon_1}$$
$$+ \frac{1}{\sqrt{N}} \sum_{k,\sigma,\upsilon,q,s} \chi_q^s a_{k,\sigma}^{+\upsilon} a_{k-q,\sigma}^{\upsilon} Q_q^s + \sum_{q,s} \Omega_{qs} b_q^{+s} b_q^s, \tag{A.1}$$

where $a_{k\sigma}^{+v}$ are creation operators for the electron with the momentum k in band υ, $a_{k\sigma}^{v}$ are annihilation operators for the electron with the momentum k in band υ, b_q^{+s} and b_q^s are creation and annihilation operators for the phonons with the momentum q, ε_k^v is the energy of the electron with the impulse k, Ω_{qs} is the energy of the phonons, $Q_q^s = b_q^{+s} + b_q^s$, s is the number of phonon branches, $V-q = V_q, X_q^{*s} = X_q^s$ are the Fourier components of the Coulomb interactions of the electron and their coupling constant with the lattice phonons, respectively. We can see that both constants are independent of the spin index of an electron. Let us introduce new operators for electron and phonon systems by the rules

$$a_k^v = e^S A_{k,v} e^{-S}, \quad b_q^s = e^S \beta_{s,q} e^{-S}, \tag{A.2}$$

where S is the anti-Hermitian operator ($S^+ = -S$).

In the following unitary transformation it will be more convenient to rewrite the term $H_{\mathrm{e-p}}$ in the form

$$H_{\mathrm{e-p}} = \sum_{k,q,s,v,\mu} \chi^{v,\mu}_{s,q} a^{+v}_{k} a^{\mu}_{k-q} Q^{s}_{q} \quad (\chi^{\mathrm{v},\mu}_{\mathrm{s},q} = \chi^{\mathrm{s}}_{q}\delta_{\mathrm{v},\mu}) \tag{A.3}$$

where we have united two indices and so $\upsilon = (\upsilon, \sigma)$ and $\mu = (\mu, \sigma')$ are the complex indices which characterize the number of crystals in the electron zone and the spin of the electron. The Hamiltonian describing the system of interacting electrons and phonons of the crystal after transformation by a unitary operator is written in the form[98–102]

$$\begin{aligned} H = &\sum_{k,v} \left(\varepsilon^{v}_{k} - \frac{1}{N} \sum_{s,q} \frac{\left|\chi^{s}_{q}\right|^{2}}{\Omega_{s,q}} \right) A^{+}_{k,v} A_{k,v} \\ &+ \frac{1}{2N} \sum_{q,k,v,k',v'} \left(V_{q} - 2 \sum_{s} \frac{\left|\chi^{s}_{q}\right|^{2}}{\Omega_{s,q}} \right) A^{+}_{k,v} A^{+}_{k',v'} A_{k'-q,v'} A_{k-q,v} \\ &+ \sum_{s,q} \Omega_{s,q} \beta^{+}_{s,q} \beta_{s,q} + \text{higher-order term.} \end{aligned} \tag{A.4}$$

The unitary transformation gives rise to renormalization of the electron energy (first term) and renormalization of the Fourier component of the Coulomb electron–electron interaction. To calculate the density of electron states we have to study the Green function for the case with the approximation $t' \to t - 0$. The two-particle Green function can be written as follows:

$$\begin{aligned} &G_{2}\left(\begin{matrix} k_{2}, v_{2}; k, v \\ k+q, v; k_{2}-q, v_{2} \end{matrix} \middle| t - t' \right) \\ &\quad = \left\langle -iT A_{k+q,v}(t) A_{k_{2}-q,v_{2}}(t) A^{+}_{k_{2},v_{2}}(t-0) A^{+}_{k,v}(t') \right\rangle \quad (t' \to t - 0). \end{aligned} \tag{A.5}$$

The equation for the Green function can be found from the equation of motion:

$$i \frac{\partial}{\partial t} \left\langle -iT A_{k,v}(t) A^{+}_{k,v}(t') \right\rangle = \delta(t - t') + \left\langle -iT \left(\frac{\partial}{\partial t} A_{k,v}(t) \right) A^{+}_{k,v}(t') \right\rangle, \tag{A.6}$$

where

$$
\begin{aligned}
i\frac{\partial A_{k,v}}{\partial t} &= [A_{k,v}\cdot H] = \left\langle -iTA_{k,v}(t)A^{+}_{k,v}(t')\right\rangle = \left\langle -iTA_{k,v}(t)A^{+}_{k,v}(t')\right\rangle \\
&= \tilde{\varepsilon}^{v}_{k}A_{k,v} + \frac{1}{N}\sum_{q,k_2,v_2}\tilde{V}_q A^{+}_{k_2,v_2}A_{k_2+q,v_2}A_{k-q,v} \\
&= \tilde{\varepsilon}_{k,v}A_{k,v} - \frac{1}{N}\sum_{q,k_2,v_2}\tilde{V}_q A_{k+q,v}A_{k_2-q,v_2}A^{+}_{k_2,v_2},
\end{aligned}
\tag{A.7}
$$

with

$$
\tilde{\varepsilon}^{v}_{k} = \varepsilon^{v}_{k} - \frac{1}{N}\sum_{s,q}\frac{\left|\chi^{s}_{q}\right|^2}{\Omega_{s,q}}, \tag{A.8}
$$

$$
\tilde{\varepsilon}_{k,v} = \tilde{\varepsilon}^{v}_{k} + \sum_{v_2}\left(\tilde{V}_{q=0} - n\frac{1}{N}\sum_{q}\tilde{V}_q\right). \tag{A.9}
$$

Therefore, the equation for the Green function (A.6) is changed, after we insert (A.7):

$$
\begin{aligned}
&i\frac{\partial}{\partial t}\left\langle -iTA_{k,v}(t)A^{+}_{k,v}(t')\right\rangle \\
&\quad = \delta(t-t') + \tilde{\varepsilon}_{k,v}\left\langle -iTA_{k,v}(t)A^{+}_{k,v}(t')\right\rangle \\
&\qquad - \frac{1}{N}\sum_{q,k_2,v_2}\tilde{V}_q\left\langle -iTA_{k+q,v}(t)A_{k_2-q,v_2}(t)A^{+}_{k_2,v_2}(t-0)A^{+}_{k,v}(t')\right\rangle.
\end{aligned}
\tag{A.10}
$$

Such a two-particle Green function satisfies an equation of the Bethe–Salpeter type (we do not split this function into two one-particle Green functions of the Gorkov type). The solution of this equation according to the Bogoliubov–Tyablikov method gives rise to the following expression for the Fourier component of the two-particle Green function:

$$
G_2\left(\begin{matrix}k_2,\upsilon;k_1,\mu\\ k_1+q,\mu;k_2-q,\upsilon\end{matrix}\middle|\omega\right) \sim \frac{f(k_1,\mu;k_2,\upsilon;\omega)\sum_{\sigma,\sigma'}\varphi(\mu,\upsilon;\sigma,\sigma')}{1-VK(k_1,\mu;k_2,\upsilon;\omega)}, \tag{A.11}
$$

with

$$
K(k_1,\mu;k_2,\upsilon;\omega) = \frac{1}{N}\sum_{q}\frac{1-n^{\mu}_{k_1+q}-n^{\upsilon}_{k_2+q}}{\omega-\varepsilon_{k_1+q,\mu}-\varepsilon_{k_2+q,\upsilon}}, \tag{A.12}
$$

where V is the Fourier component of the Coulomb interactions of the electron, $\varphi(\mu, \upsilon; \sigma, \sigma')$ is some function depending on the frequency ω, and the momenta k_1 and k_2 of interacting electrons, $f(k_1, \mu; k_2, \upsilon; \omega)$ is expressed in terms of functions, $n^{\mu}_{k_1+q}$ and $\varepsilon_{k_1+q,\mu}$ are the number of filling and energy of electrons respectively,

$$\varphi(\mu, \upsilon; \sigma, \sigma') = \delta_{\sigma\sigma}\delta_{\sigma'\sigma'} - \delta_{\mu\upsilon}\delta_{\sigma\sigma'}\delta_{\sigma\sigma'}, \tag{A.13}$$

and σ and σ' are the spins of the first (σ) and second (σ') electrons. The superconducting gaps are given by the zeros of the denominator of (A.11).[99,102] Let us study the particular case where $k_1 = k_2 = k_0 + k$ and $\varepsilon_{k0,\mu} = \varepsilon_{\mu}$ corresponds to the extremum of the zone. Then, expanding the energy by momentum $k \pm q$ in series up to terms of the second order, we can obtain

$$\varepsilon_{k\pm q,\mu} = \varepsilon_{\mu} + \frac{(k \pm q)^2}{2m_{\mu}} = \varepsilon_f + \Delta_{\mu} + \frac{(k \pm q)^2}{2m_{\mu}} \quad (\mu = 1, 2, \ldots), \tag{A.14}$$

where m_{μ} is the effective mass of electron in the μ energy band of the crystal, $\Delta\mu$ is a parameter which indicates the position of the exremum of the μ band relative to the Fermi level, and $\varepsilon_{k\pm q,\mu}$ is the energy of electrons. The sum in the denominator (A.11) is reduced to the following expression (we consider only one zone):

$$\begin{aligned} K(k, k', \omega) &= \frac{1}{N}\sum_{q}\frac{1 - n_{k+q} - n_{k-q}}{\omega - \varepsilon_{k+q} - \varepsilon_{k-q}} \\ &= 2N(\varepsilon_f)\int_0^{\Delta}\frac{d\varepsilon}{\omega - 2(\varepsilon_f + \Delta_1) - 2E - 2\varepsilon} \\ &= 2N(\varepsilon_f)\left(-\ln\left|1 - \frac{\Delta}{a}\right|\right), \end{aligned} \tag{A.15}$$

where such assignments have been used: $\varepsilon = q^2/2m$; $E = k^2/2m$; $a = \omega - 2(\varepsilon_f + \Delta_1) - 2E$; $m_1^* = m_1/m$ and m are the reduced effective mass of electron in the crystal energy zone and the mass of free electrons, respectively.

$$N(\varepsilon_f) = \sqrt{2}\pi\, m_1^*\sqrt{m_1^*\varepsilon}\,(1 - n_{k+q} - n_{k-q})\,\big|_{\varepsilon_f}, \tag{A.16}$$

$$n_k = \left[\exp\left(\frac{\varepsilon_k - \varepsilon_f}{T}\right) + 1\right]^{-1}. \tag{A.17}$$

The equation for the superconducting gap has the following form:

$$1 - VN(\varepsilon_f)\left(-\ln\left|1 - \frac{\Delta}{a}\right|\right) = 0. \tag{A.18}$$

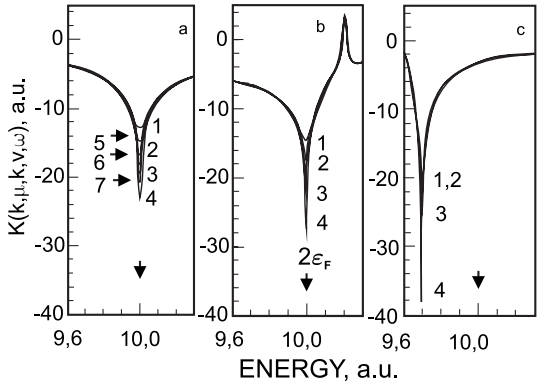

Fig. A.1 The effect of temperature on the $K(k,\mu;k,\upsilon;\omega)$ function ($E = k^2/2m = 0$) for different structures of the energy zones: (a) $\Delta_1 = -1$, $m_1^* = 1$; (b) $\Delta_2 = 0.2$, $m_2^* = -2$; (c) $\Delta_1 = -1$, $m_1^* = 1$, $\Delta_2 = 0.2$, $m_2^* = -2$; curves 4, $T = 2\,\mathrm{K}$; curves 3, $T = 10\,\mathrm{K}$; curves 2, $T = 50\,\mathrm{K}$; curves 1, $T = 100\,\mathrm{K}$; arrows 5–7 correspond to different $1/V$ values (arrow 5, $V = -0.07$; arrow 6, $V = -0.06$; arrow 7, $V = -0.05$). All energy values are taken as arbitrary values, i.e. $V = V/M$, where M is a scale factor ($M = 1\,\mathrm{eV}$, for convenience; $m_i^* = \frac{m_i}{m}$, where m is the free electron mass).

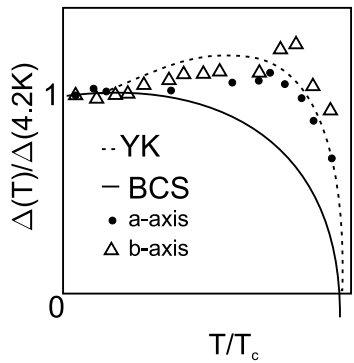

Fig. A.2 The temperature dependence of the superconducting gap. Dashed line — theory; continuous line — BCS; *a* axis, *b* axis — experiment.

The results of some numerical calculations are given in Fig. A.1. We will study theoretically the situation close to the $Ba_2Sr_2CaCu_2O_8$ crystal because it has a high T_c. The results of some numerical calculations of the temperature dependence of superconductivity are given in Fig. A.2. For illustration, the experimental dependences of the superconducting gap obtained for the $Ba_2Sr_2CaCu_2O_8$ crystal are presented in Fig. A.2 together with theoretical curves of the BCS type and our calculation. The obtained dependences are not similar to the standard BCS ones. It is clearly seen that

our calculation predicting the maximum in the T dependence of the superconducting gap gives the curve which is closer to the experimental results. In our approach we take into account that all electron bands (the numerical calculations show that only bands located near the Fermi are important) contribute to the superconductivity.

Bibliography

1. Parks, R. D. (ed.) (1969). *Superconductivity* (Marcel Dekker, New York).
2. Bednorz, J. G. and Müller, K. A. (1986). Possible high-T_c superconductivity in the Ba–La–Cu–O system, *Z. Phys. B* **64**, pp. 189–193.
3. Schrieffer, J. R. (1983). *Theory of Superconductivty* (Benjamin, New York).
4. Feynman, R. P. (1982). *Statistical Mechanics* (Addison–Wesley, Redwood City).
5. Anderson, P. W. (1987). The resonating valence bond state in LaCuO and superconductivity, *Science* **4**, pp. 1196–1198.
6. Anderson, P. W. (1959). Theory of dirty superconductivity, *J. Phys. Chem. Solids* **11**, pp. 26–30.
7. London, F. and London, H. (1935). The electromagnetic equations of the supraconductor, *Proc. R. Soc. London A* **147**, p. 71.
8. Ryder, L. H. (1996). *Quantum Field Theory*, 2nd edn. (Cambridge University Press).
9. Ginzburg, V. L. and Landau, L. D. (1950). On the theory of superconductivity, *Zh. Eksp. Theor. Fiz.* **20**, p. 11064.
10. Tinkam, M. (1975). *Introduction to Superconductivity* (McGraw-Hill, New York).
11. Nambu, Y. (1960). Quasi-particles and gauge invariance in the theory of superconductivity, *Phys. Rev.* **117**, p. 648.
12. Takahashi, Y. (1976). *Field Theory for Solid State Physics* (in Japanese) (Baifuhkan).
13. Nagao, H., Nishino, H., Shigeta, Y. and Yamaguchi, K. (2000). Theoretical studies on anomalous phases of photodoped systems in two-band model, *J. Chem. Phys.* **113**, pp. 11237–1244.
14. Kondo, J. (2002). Theory of multiband superconductivity, *J. Phys. Soc. Jpn.* **71**, p. 1353.
15. Fetter, L. A. and Walecka, J. D. (1987). *Quantum Theory of Many-Particle Systems* (McGraw-Hill).
16. Abrikosov, A. A., Gorkov, L. P. and Dzyaloshinski, I. E. (1975). *Methods of Quantum Field Theory in Statistical Physics* (Dover).
17. Aono, S. (2003). Molecular orbital theory: spinor representation, *J. Phys. Soc. Jpn.* **72**, pp. 3097–3105.
18. Kimura, M., Kawabe, H., Nishikawa, K. and Aono, S. (1986). EPR observations of trivalent titanium in orthophosphate single crystals, *J. Chem. Phys.* **85**, pp. 1–6.
19. Salem, L. and Longuet-Higgins, H. C. (1959). The alternation of bond lengths in long conjugated chain molecules, *Proc. R. Soc. London A* **255**, p. 172.
20. Peierls, R. E. (1955). *Quantum Theory of Solids* (Oxford University Press).

21. Kimura, M., Kawabe, H., Nakajima, A., Nishikawa, K. and Aono, S. (1988). Possibility of superconducting and other phases in organic high polymers of polyacene carbon skeletons, *Bull. Chem. Soc. Jpn.* **61**, pp. 4239–4224.
22. Kubo, R. and Tomita, J. (1954). A general theory of magnetic resonance absorption, *Phys. Soc. Jpn.* **9**, pp. 888–919.
23. Doi, Y. and Aono, S. (1974). Theory of line shape in nuclear magnetic resonance, *Prog. Theor. Phys.* **51**, pp. 1019–1029.
24. Hebel, L. C. and Slichter, C. P. (1959). Nuclear spin relaxation in normal and superconducting aluminum, *Phys. Rev.* **113**, pp. 1504–1519.
25. Fibich, M. (1965). Phonon effects on nuclear spin relaxation in superconductors, *Phys. Rev. Lett.* **14**, pp. 561–564.
26. Maki, K. (1967). *Gapless Superconductors in Superconductivity*, ed. Parks, R. D. (Marcel Dekker, New York).
27. Uchino, K., Maeda, A. and Terasaki, I. (1959). *Nature of the High Temperature Superconductor* (in Japanese) (Baifuukann).
28. Aono, S. (1998). Superconductivity as symmetry breaking classical treatment, *Bull. Chem. Soc. Jpn.* **71**, pp. 49–56.
29. Scalapino, D. J. (1995). The case for $d_{x^2-y^2}$ pairing in the cuprate superconductors, *Phys. Rep.* **250**, pp. 329–360.
30. Gorkov, L. P. (1959). Microscopic derivation of the Ginzburg–Landau equations in the theory of superconductivity, *Sov. Phys. JETP* **9**, pp. 1364–1375.
31. Negele, J. W. and Orland, H. (1987). *Quantum Many-Particle Systems* (Addison-Wesley, Reading, Masscchusetts).
32. Kawabe, H., Nishikawa, K. and Aono, S. (1994). Path integral approach to correlation energy, *Int. J. Quantum Chem.* **51**, pp. 265–283.
33. Feynman, R. P. (1948). Space–time approach to non-relativistic quantum mechanics, *Rev. Mod. Phys.* **20**, pp. 367–387.
34. Hubbard, J. (1959). Calculation of partition functions, *Phys. Rev. Lett.* **3**, pp. 77–78.
35. Das, A. (2006). *Field Theory: A Path Integral Approach* (World Scientific, Singapore).
36. DeWitt, B. (1984) *Supermanifolds* (Cambridge University Press).
37. Ferraz, A. and Nguyen, A. V. (1995). Supersymmetry and electron–hole excitations in semiconductors, *Phys. Rev. B* **51**, pp. 10548–10555.
38. Yang, C. N. (1962). Concept of off-diagonal long-range order and the quantum phases of liquid He and of superconductors, *Rev. Mod. Phys.* **34**, pp. 694–704.
39. Dunne, L. J., Murrell, J. N. and Brändas, E. J. (1997). Off-diagonal long-range order, eta-pairing, and Friedel oscillations in high T_c cuprate superconductors and the ground state of the extended Hubbard model, *Int. J. Quantum Chem.* **63**, pp. 675–684.
40. Ginzburg, V. L. and Kirzhnitz, D. A. (1982) (eds). *High-Temperature Superconductivity* (Consultants Bureau, New York).
41. Fröhlich H. (1954). On the theory of superconductivity, *Proc. R. Soc. London A* **223**, p. 296–305.
42. Bogolyubov, N. N. (1958). A new method in the theory of superconductivity, *Zh. Eksp. Teor. Fiz.* **34**, pp. 58–65.
43. Josephson, B. D. (1974). The discovery of tunneling superconductivity, *Rev. Mod. Phys.* **1074**, pp. 251–254.
44. Maroushkine, A. (2004). *Room-Temperature Superconductivity* (Cambridge International Science, Cambridge).

45. Davydov, A. S. (1990). *High-Temperature Superconductivity* (Naukova Dumka, Kiev).
46. Davydov, A. S. and Kruchinin, S. P. (1991). Interlayer effects in the newest high-T superconductors, *Phys. C* **179**, pp. 461–468.
47. Davydov, A. S. and Kruchinin, S. P. (1991). Dependence of the superconducting transition temperature on the number of cuprate layers in a unit cell of high-temperature superconductors, *Sov. J. Low Temp. Phys.* **17**, 10, pp. 634–635.
48. Timusk, T. and Statt, B. (1999). The pseudogap in high-temperature superconductors: an experimental survey, *Rep. Prog. Phys.* **62**, pp. 61–122.
49. Plakida, N. M. (1995). *High-T_c Superconductivity: Experiment and Theory* (Springer), p. 306.
50. Brusov, P. (1999). *Mechanisms of High Temperature Superconductivity* (Rostov State University Publishing), p. 685.
51. Abrikosov, A. A. (1998). *Fundamentals of the Theory of Metals* (North-Holland, Amsterdam), p. 380.
52. Akhiezer, A. I. and Pomeranchuk, I. Ya. (1959). On the interaction between conductivity electrons in ferromagnetics, *Zh. Eksp. Teor. Fiz.* **36**, p. 819.
53. Akhiezer, A. I., Bar'yakhtar, V. G. and Peletminskii, S. V. (1968). *Spin Waves* (North-Holland, Amsterdam), p. 369.
54. Little, W. A. (1964). Possibility of synthesizing on organic superconductivity, *Phys. Rev.* **134**, p. 1416.
55. Alexandrov, A. S. and Ranninger, J. (1981). Bipolaronic superconductivity, *Phys. Rev.* **23**, 4, pp. 1796–1801.
56. Pekar, S. I. (1951). *Studies on the Electron Theory of Crystals* (Gostekhizdat, Moscow), p. 168.
57. Brusov, P. (1999). *Mechanisms of High Temperature Superconductivity* (Rostov State University), p. 685.
58. Ausloos, M. and Kruchinin, S. (eds.) (1999). *Symmetry and Pairing in Superconductors: Proc. NATO ARW* (Kluwer, Dordrecht), p. 410.
59. Annett, J. and Kruchinin, S. (eds.) (2002). *New Trends in Superconductivity: Proc. NATO ARW* (Kluwer, Dordrecht), p. 435.
60. Kruchinin, S. (eds.) (2003). *Modern Problems of Superconductivity: Proc. Yalta Conference*; *Mod. Phys. Lett. B* **17**, 10–12, p. 393–724.
61. Sigrist, M. and Rice, T. M. (1995). Unusual paramagnetic phenomena in granular high-temperature superconductors — a consequence of d-wave pairing, *Rev. Mod. Phys.* **67**(2) pp. 503–513.
62. Laughlin, R. B. (1998). Magnetic induction of $d_{x^2+y^2} + id_{xy}$ order in high-T_c superconductors, *Phys. Rev. Lett.* **80**, p. 5188.
63. Scalapino, D. J. (1999). The case for d pairing in the cuprate superconductors, *Phys. Rep.* **250**, pp. 331–370.
64. Annet, J. F. (2003). *Superconductivity, Superfluids and Condensates* (University of Bristol, Oxford University Press), p. 183.
65. Volovik, G. E. and Gorkov, L. P. (1985). Superconducting classes in heavy-fermion systems, *Sov. Phys. JETP* **61**, p. 843.
66. Mineev, V. P. and Samokhin, K. V. (1998). *Introduction to the Theory of Unconventional Superconductivity* (Moscow Fiz.-Tekh. Inst. Press, Moscow), p. 141.
67. Van Harligen, D. J. (1995). Phase-sensitive test of the symmetry of pairing state in the high-temperature superconductors — evidence for D symmetry, *Rev. Mod. Phys.* **67**, 2, pp. 515–535.

68. Tsuei, C. C. and Kirtley, J. R. (2000). Pairing symmetry in cuprate superconductors, *Rev. Mod. Phys.* **72**, 4, pp. 969–1015.
69. Pines, D. (1991). Spin fluctuations and high temperature superconductivity in the antiferromagnetically correlated oxides: YBaCuO, LaSrCuO, *Physica C* **185–189**, pp. 120–129.
70. Monthoux, P., Balatsky A. V. and Pines, D. (1991). Toward a theory of high-temperature superconductivity in the antiferromagnetically correlated cuprates oxides, *Phys. Rev. Lett.* **67**, 24, p. 3448.
71. Balatsky, A. V., Vekhter, I. V. and Zhu, J. X. (2008). Impurity-induced state in conventional and unconventional superconductors, *Rev. Mod. Phys.* **78**, pp. 373–433.
72. Izyumov, Yu. A. (1999). Spin-fluctuation mechanism in high-T_c superconductivity and symmetry of order parameter, *Usp. Phys.* **169**, 3, p. 215.
73. Morya, T. and Ueda, K. (2000). Spin fluctuations and high-temperature superconductivity, *Adv. Phys.* **49**, 5, pp. 556–605.
74. Levi, B. G. (1993). In high-T_c superconductors, is d-wave the new wave? *Phys. Today* **5**, pp. 17–20.
75. Manske, D. (2004). *Theory of Unconventional Superconductors* (Heidelberg, Springer).
76. Maple, M. B. (1986). New type superconductivity in f-electron system, *Phys. Today* **4**, p. 72.
77. Miyake, K. and Schmitt-Rink, S. (1986). Spin fluctuation mediated even party pairing in heavy fermion superconductors, *Phys. Rev. B* **34**, 9, pp. 6554–6556.
78. Kruchinin, S. P. (1995). Functional integral of antiferromagnetic spin fluctuations in high-temperature superconductors, *Mod. Phys. Lett. B* **9**, pp. 205–215.
79. Kruchinin, S. P. and Patapis, S. K. (1996). Thermodynamics of d-wave pairing in cuprate superconductors, *J. Low Temp. Phys.* **105**, pp. 717–721.
80. Kruchinin, S. P. and Patapis, S. K. (1997). Specific heat of antiferromagnetic spin fluctuations in cuprate superconductors, *Physica C* **282–285**, pp. 1397–1398.
81. Kruchinin, S. P. (2000). The pseudogap of antiferromagnetic spin fluctuations in cuprate superconductors, *Physica C* **341–348**, pp. 901–902.
82. Kruchinin, S. P. (2005). Condensation energy for spin fluctuation mechanism of pairing in high-T_c superconductors, in *Proc. NATO Advanced Research Workshop "New Challenges in Superconductivity: Experimental Advances and Emerging Theories"*, ed. Ashkenazi, J. (Kluwer, Dordrecht), pp. 145–150.
83. Popov, Y. N. (1987). *Functional Integrals and Collective Excitations* (Cambridge University Press), p. 216.
84. Conwall, J., Jackiw, R. and Tomhoulis, E. (1974). Effective action for composite operators, *Phys. Rev. D* **10**, 8, pp. 2428–2444.
85. Weinberg, S. (1993). Effective action and renormalization group flow of anisotropic superconductors [preprint UTTG 18], pp. 1–17.
86. Shen, Z. X., Dessan, D. S., Wells, B. O., King, D. M., Spicer, W. E., Arko, A. J., Marshall, D., Lombarolo, L. W., Kapitulnik, A., Dickinson, P., Doniach, S., Carko, J. Di, Loesser, A. G. and Park, C. H. (1993). Anomalously large gap anisotropy in the a–b plane of $Bi_2Sr_2CaCu_2O_{8+\gamma}$, *Phys. Rev. Lett.* **70**, p. 1553.
87. Moler, M. B., Barr, D. I., Urbach, J. S., Hardy, W. H. and Kapitulnik, A. (1994). *Magnetic field dependence of the density of states of YBaCuO as determined from the specific heat*, *Phys. Rev. Lett.* **73**, p. 2744.
88. Momono, N., Ido, M., Nakano, T. and Oda, M. (1994). Low-temperature electronic specific heat in LaSrCuZnO, *Physica C* **235–240**, pp. 1739–1740.

89. Loram, J. W., Mirza, K. A., Cooper, J. R. and Tallon, J. L. (1998). Specific heat evidence on the normal state pseudogap, *J. Phys. Chem. Solids* **59**, 10–12, pp. 2091–2094.
90. Revaz, B., Genond, J. Y., Junod, A., Naumdier, K., Erb, A. and Walker. E. (1998). d-wave scaling relations in the mixed-state specific heat $YBa_2Cu_3O_7$, *Phys. Rev. Lett.* **80**, 15, pp. 3364–3367.
91. Hasselbach, K., Kirtley, J. R. and Flouquet, J. (1994). Symmetry of the gap in superconducting UReSi, *Phys. Rev. B* **47**, pp. 509–512.
92. Muhrer, G. and Schachinger, E. (2000). Free energy of a d-wave superconductor in the nearly antiferromagnetic Fermi liquid model, *J. Low Temp. Phys.* **88–120**, 1–2, pp. 65–88.
93. Dorbolo, S., Ausloos, M. and Houssa, M. (1998). Electronic specific heat of superconductors with van Hove singularities: effects of a magnetic field and thermal fluctuations, *Phys. Rev. B* **57**, pp. 5401–5411.
94. Dobrosavljevic-Crujic, L. and Miranovic, P. (2003). Low temperature specific heat in anisotropic superconductors, *Physica C* **397**, pp. 117–122.
95. Bogolyubov, Jr., N. N. and Kruchinin, S. P. (2003). Modern approach to the calculation of the correlation function for superconductivity model, *Mod. Phys. Lett. B* **17**, 10–12, pp. 709–724.
96. Nagao, H., Kruchinin, S. P., Yaremko, A. M. and Yamaguchi, K. (2002) Multiband superconductivity, *Int. J. Mod. Phys. B* **16**, pp. 3419–3428.
97. Kruchinin, S. P. and Nagao, H. (2005) Two-gap superconductivity in MgB, *Phys. Particles Nuclei* **36**, Suppl. 1, pp. 127–130.
98. Kruchinin, S. P. and Yaremko, A. M. (1998). Many zone effect in cuprate superconductors, *Supercond. Sci. Technol.* **11**, pp. 4–8.
99. Nagao, H., Kawabe, H., Kruchinin, S. P., Manske, D. and Yamaguchi, K. (2003). Theoretical studies on many band effects superconductivity by using renormalization group approach, *Mod. Phys. Lett. B* **17**, 10–12, pp. 423–431.
100. Nagao, H., Kawabe, H., Kruchinin, S. P. and Yamaguchi, K. (2003). Superconductivity in two-band model by renormalization group approach, *Int. J. Mod. Phys. B* **17**, pp. 3373–3376.
101. Yaremko, A. M., Mozdor, E. V. and Kruchinin, S. P. (1996). Coupled states of electron–phonon system, superconductivity and HTSC of crystals, *Int. J. Mod. Phys. B* **10**, pp. 2665–2674.
102. Kruchinin, S. P. and Nagao, H. (2006). Multi-gap superconductivity in MgB_2, in *Proc. NATO Advanced Research Workshop* "*Symmetry and Heterogeneity in High-T_c Superconductors*", ed. Bianconi, A. (Kluwer, Dorderecht), pp. 43–53.
103. Nagao, H., Yaremko, A., Kruchinin, S. P. and Yamaguchi, K. (2002). Many band effects in superconductivity, in *Proc. NATO Advanced Research Workshop* "*New Trends in Superconductivity*", (eds.) Annett, J. and Kruchinin, S. P. (Kluwer, Dordrecht), pp. 155–167.
104. Bardeen, J., Cooper, L. N. and Schrieffer, J. R. (1957). Microscopic theory of superconductivity, *Phys. Rev.* **108**, pp. 1175.
105. Anderson, P. W. and Zou, Z. (1988). "Normal" tunneling and "normal" transport: diagnostics for the resonating-valence-bond state, *Phys. Rev. Lett.* **60**, p. 132.
106. Kampf, A. P. (1994). Magnetic correlations in high temperature superconductivity, *Phys. Rep.* **249**, p. 219.
107. Emery, V. J. (1987). Theory of high-T_c superconductivity in oxides, *Phys. Rev. Lett.* **58**, p. 2794.

108. Hirsch, J. E. (1985). Attractive interaction and pairing in fermion systems with strong on-site repulsion, *Phys. Rev. Lett.* **25**, p. 1317.
109. Zhang, F. C. and Rice, T. M. (1988). Effective Hamiltonian for the superconducting Cu oxides, *Phys. Rev. B* **37**, p. 3759.
110. Fradkin, E. (1991). *Field Theories of Condensed Matter Systems* (Addison Wesley).
111. Nagaosa, N. and Lee, P. A. (1990). Normal-state properties of the uniform resonating-valence-bond state, *Phys. Rev. Lett.* **64**, p. 2450.
112. Baskaran, G., Zou, Z. and Anderson, P. W. (1987). The resonating valence bond state and high-T_c superconductivity — a mean field theory, *Solid State Commun.* **63**, p. 973.
113. Fukuyama, H. and Yoshida, K. (1987). Critical temperature of superconductivity caused by strong correlation, *Jpn. J. Appl. Phys.* **26**, pp. 371–373.
114. Yamamoto, S., Yamaguchi, K. and Nasu, K. (1990). *Ab initio* molecular-orbital study on electron correlation effects in CuO_6 clusters relating to high-T_c superconductivity, *Phys. Rev. B* **42**, pp. 266–272.
115. Nagao, H., Kitagawa, Y., Kawakami, T., Yoshimoto, T., Saito, H. and Yamaguchi, K. (2001). Theoretical studies on field-induced superconductivity in molecular crystals, *Int. J. Quantum Chem.* **85**, pp. 608–618.
116. Kimura, M., Kawabe, H., Nakajima, A., Nishikawa, K. and Aono, S. (1988). Possibility of superconducting and other phases in organic high polymers polyacene carbon skeletons, *Bull. Chem. Soc. Jpn.* **61**, p. 4239.
117. Torrance, J. B., Bezinge, A., Nazzal, A. I. and Parkin, S. S. (1989). Disappearance of high temperature superconductivity induced by high carrier concentrations, *Physica C* **162**–**164**, p. 291.
118. Ord, T., Kristoffel, N. and Rago, K. (2003). MgB_2 superconductivity properties in a two-gap model, *Mod. Phys. Lett. B* **17**, pp. 667–673.
119. Suhl H., Matthias, B. T. and Walker, R. (1959). Bardeen–Cooper–Schrieffer theory of superconductivity in the case of overlapping bands, *Phys. Rev. Lett.* **3**, p. 552.
120. Moskalenko, V. A. (1959). Superconductivity metals with overlapping energetic bands, *Fiz. Metalloved* **8**, p. 503.
121. Antipov, E. and Abakumov, A. (2008). Structural design of superconductors based on complex copper oxides, *Phys. Usp.* **51**, p. 180.
122. Müller, K. A. (2006). The search for new high temperature superconductors, *Supercond. Sci. Technol.* **58**, pp. 1–3.
123. Bennemann, K. H. and Ketterson, J. B. (2008). *Superconductivity* (Springer, Heidelberg), vol. 1.
124. Nagamatsu, J., Nakamura, N., Muranaka, T., Zentani, Y. and Akimitsu, J. (2001). Superconductivity at 39 K in magnezium deboride, *Nature* **410**, p. 63.
125. Canfield, J. P. C., Bud'ko, S. L. and Finnemore, D. K. (2003). An overview of the basic physical properties of MgB_2, *Physica C* **385**, 1–2, pp. 1–3.
126. Binnig, G., Baratoff, A., Hoenig, H. E. and Bednorz, J. G. (1980). Two-band superconductivity in Nb-doped $SrTiO_3$, *Phys. Rev. Lett.* **45**, p. 1352.
127. An, J. M. and Picket, W. E. (2001). Superconductivity of MgB_2: covalent bonds driven metallic, *Phys. Rev. Lett.* **86**, p. 4366.
128. Kortus, J., Mazin, I. I., Belashenko, K. D., Antropov, V. P. and Boyer, I. L. (2001). Superconductivity of metallic boron in MgB_2, *Phys. Rev. Lett.* **86**, p. 4656.
129. Kondo, J. (1963). Superconductivity in transition metals, *Prog. Theor. Phys.* **29**, p. 1.
130. Kristoffel, N., Ord, T. and Rago, K. (2003). MgB_2 two-gap superconductivity with intra- and interband couplings, *Europhys. Lett.* **61**, pp. 109–115.

131. Szabo, P., Samuely, P., Klein, T., Marcus, J., Fruchart, D., Miraglia, S., Marcenat C. and Jansen, A. (2001). Evidence for two superconducting energy gaps in MgB_2 by point-contact spectroscopy, *Phys. Rev. Lett.* **87**, p. 137005.
132. McMillan, W. L. (1968). Transition temperature of strong-coupled superconductors, *Phys. Rev.* **167**, p. 331.
133. Konsin, P., Kristoffel, N. and Örd, T. (1988). The interband interaction as a possible cause of high-temperature superconductivity, *Phys. Lett. A* **129**, pp. 339–342.
134. Combescot, R. and Leyronas, X. (1995). Coupling between planes and chains in $YBa_2Cu_3O_7$: a possible solution for the order parameter controversy, *Phys. Rev. Lett.* **75**, pp. 3732–3735.
135. Konsin, P. and Sorkin, B. (1998). *Electric field effects in high-T_c cuprates*, *Phys. Rev. B* **58**, pp. 5795–5802.
136. Nagao, H., Nishino, M., Shigeta, Y., Yoshioka, Y. and Yamaguchi, K. (2000). Theoretical studies on superconducting and other phases: triplet superconductivity, ferromagnetism, and ferromagnetic metal, *J. Chem. Phys.* **113**, pp. 721–732.
137. Kondo, J. (2001). Superconductivity of the two-dimensional Hubbard models with a small U., *J. Phys. Soc. Jpn.* **70**, p. 808.
138. Nagao, H., Mitani, M., Nishino, M., Shigeta, Y., Yoshioka, Y. and Yamaguchi, K. (1999). Theoretical studies on anomalous phases in molecular systems with external field: possibility of photo-induced superconductivity, *Int. J. Quantum Chem.* **75**, pp. 549–561.
139. Nagao, H., Nishino, M., Mitani, M., Yoshioka, Y. and Yamaguchi, K. (1997). Possibilities of charge- and/or spin-mediated superconductors and photo-induced superconductors in the intermediate region of metal-insulator transitions, *Int. J. Quantum Chem.* **65**, pp. 947–957.
140. Nagao, H., Mitani, M., Nishino, M., Shigeta, Y., Yoshioka, Y. and Yamaguchi, K. (1988). Possibility of charge-mediated superconductors in the intermediate region of metal–insulator transitions, *Int. J. Quantum Chem.* **70**, pp. 1075–1084.
141. Bogoliubov, N. N. and Bogoliubov, N. N., Jr. (1986). *An Introduction to Quantum Statistical Mechanics* (Nauka, Moscow) (transl. into English 1994).
142. Bogoliubov, N. N. and Shirkov, D. V. (1959). *Introduction to the Theory of Quantized Field* (Interscience, New York).
143. Mattuck, R. D. (1976). *A Guide to Feynman Diagrams in the Many-Body Problem* 2nd edn. (McGraw-Hill, New York).
144. Kimura, M., Kawabe, H., Nishikawa, K. and S. Aono (1988). Possibility of superconducting and other phases in organic high polymers of polyacene carbon skeletons II: screened electron–electron interaction, *Bull. Chem. Soc. Jpn.* **61**, pp. 4245–4252.
145. Kimura, M., Kawabe, H., Nishikawa, K. and Aono, S. (1986). Superconducting and other phases in organic high polymers of polyacenic carbon skeletons I: the method of sum of divergent perturbation series, *J. Chem. Phys.* **85**, pp. 3090–3096.
146. Kimura, M., Kawabe, H., Nishikawa, K. and Aono, S. (1985). Superconducting and other phases in organic high polymers of polyacenic carbon skeletons II: the mean field method, *J. Chem. Phys.* **85**, pp. 3097–3100.
147. Kimura, M., Kawabe, H., Nakajima, A., Nishikawa, K. and Aono, S. (1988). Possibility of superconducting and other phases in organic high polymers of polyacene carbon skeletons II: screened electron-electron interaction. *Bull. Chem. Soc. Jpn.* **61**, pp. 4239–4244.
148. Bogoliubov, N. N. and Tyablikov, S. (1959). Retarded and advanced Green functions in statistical physics, *Dokl. Acad. Sci. USSR* **126**, p. 53; *Sov. Phys. Dokl.* **4**, p. 589.

149. Richarson, R. W. (1963). A restricted class of exact eigenstates of the pairing-force Hamiltonian, *Phys. Lett.* **3**, pp. 277–279.
150. Matveev, K. A. and Larkin, A. I. (1997). Parity effect in ground state energies of ultrasmall superconducting grains, *Phys. Rev. Lett.* **78**, pp. 3749–3752.
151. Ralph, D. C., Black, C. T. and Tinkham, M. (1997). Gate-voltage studies of discrete electronic staes in aluminum nanoparticles, *Phys. Rev. Lett.* **78**, p. 4087.
152. Schechter, M., Imry, Y., Levinson, Y. and von Delft, J. (2001). Thermodynamic properties of a small superconducting grain, *Phys. Rev. B* **63**, pp. 214518–214534.
153. Sierra, G. (2000). Conformal field theory and the exact solution of the BCS Hamiltonian, *Nucl. Phys. B* **572**, pp. 517–527.
154. Stenuit, G., Michotte, S., Govaerts, J. and Piraux, L. P. (2003). Vortex matter in lead nanowires, *Eur. Phys. J. B* **33**, pp. 103–110.
155. Kasumov, A. Yu., *et al.* (1999). Supercurrents through single-walled carbon nanotubes, *Science* **284**, pp. 1508–1511.
156. Nagao, H., Kawabe, H. and Kruchinin, S. (2006). Nanosize two-gap superconductivity, in *Proc. NATO ARW* "*Electron Correlation in New Materials and Nanosystems*", eds. Scharnberg, K. and Kruchinin, S. (Springer), pp. 117–127.
157. Kawabe, H., Nagao, H. and Kruchinin, S. (2006). Exact solution of two-band superconductivity, in *Proc. NATO ARW* "*Electron Correlation in New Materials and Nanosystems*", eds. Scharnberg, K. and Kruchinin, S. (Springer), pp. 129–139.
158. Nagao, H. and Kruchinin, S. P. (2008). Kondo effect coupled to superconductivity ultrasmall grains, in *Proc. NATO ARW Electron Transport in Nanosystems eds. Bonca, J. and Kruchinin, S.* (Springer), pp. 105–115.
159. Kruchinin, S. P., Dzezherya, Yu. and Annett, J. (2009). Imteractions of nanoscale ferromagnetic granules in a London superconductor, *Supercond. Sci. Technol.* **19**, pp. 381–384.
160. Ralph, D. C., Black, C. T. and Tinkham, M. (1995). Spectroscopic measurements of discrete electronic states in single metal particles, *Phys. Rev. Lett.* **74**, p. 3241.
161. Smith, R. A. and Ambegaokar, V. (1996). Effect of level statistics on superconductivity in ultrasmall metallic grains, *Phys. Rev. Lett.* **77**, p. 4962.
162. von Delft, J., Zaikin, A. D., Golubev, D. S. and Tichy, W. (1996). Parity-affected superconductivity in ultrasmall metallic grains, *Phys. Rev. Lett.* **77**, pp. 3189–3192.
163. Yamaji, K. and Shimoi, Y. (1994). Superconducting transition of the two-chain Hubbard model indicated by diagonalization calculations, *Physica C* **222**, pp. 349–360.
164. Black, C. T., Ralph, D. C. and Tinkham, M. (1996). Spectroscopy of the superconducting gap in individual nanometer-scale aluminum particles, *Phys. Rev. Lett.* **76**, pp. 688–611.
165. Braun, F. and von Delft, J. (1998). Fixed-N superconductivity: the crossover from the bulk to the few-electron limit, *Phys. Rev. Lett.* **81**, pp. 4712–4715.
166. von Delft, J. and Braun, F. (1999). Superconductivity in ultrasmall metallic grains, *Phys. Rev. B* **59**, pp. 9527–9544.
167. Gladilin, V. N., Fomin, V. M. and Devreese, J. T. (2002). Shape of nanosize superconducting grains: does it influence pairing characteristics?, *Solid State Commun.* **121**, pp. 519–523.
168. Jankó, B., Smith, A. and Ambegaokar, V. (1994). BCS superconductivity with fixed number parity, *Phys. Rev. B* **50**, pp. 1152–1161.

169. Matveev, K. A. and Larkin, A. L. (1997). Parity effect in ground state energies of ultrasmall superconducting grains, *Phys. Rev. Lett.* **78**, pp. 3749–3752.
170. Richardson, R. W. and Sherman, N. (1964). Pairing models of Pb206, Pb204 and Pb202, *Nucl. Phys.* **523**, pp. 253–268.
171. Richardson, R. W. (1977). Pairing in the limit of a large number of particles, *J. Math. Phys.* **6**, pp. 1802–1811.
172. Richardson, R. W. (1966). Numerical study of the 8–32-particle eigenstate of the pairing Hamiltonian, *Phys. Rev.* **141**, pp. 949–955.
173. Sierra, G., Dukelsky, J., Dussel, G. G., von Delft, J. and Braun, F. (2000). Exact study of the effect of level statistics in ultrasmall superconducting grains, *Phys. Rev. B* **61**, pp. 11890–11893.
174. Kouwenhoven, L. and Glazman, L. (2001). The revival of the Kondo effect, *Phys. World* **14**, 1, pp. 33–38.
175. van der Wiel, G., De Franceschi, S., Fujisawa, T., Elzerman, J. M., Tarucha, S. and Kouwenhoven, L. P. (2000). The Kondo effect in the unitary limit, *Science* **289**, pp. 2105–2108.
176. Inoshita, T. (1998). Kondo effect in quantum dots, *Science* **281**, pp. 526–527.
177. Sasaki, S., De Franceschi, S., Elzerman, J. M., van der Wiel, W. G., Eto, M., Tarucha, S. and Kouwenhoven, L. P. (2000). Kondo effect in an integer-spin quantum dot, *Nature* (*London*) **405**, pp. 764–767.
178. Inoshita, T., Shimizu, A., Kuramoto, Y. and Sakaki, H. (1993). Correlated electron transport through a quantum dot: the multiple-level effect, *Phys. Rev. B* **48**, pp. 114725–114728.
179. Izumida, W., Sakai, O. and Shimizu, Y. (1998). Kondo effect in single quantum dot systems study with numerical renormalization group method, *J. Phys. Soc. Jpn.* **67**, p. 2444.
180. Yeyati, A. L., Flores, F. and Martin-Rodero, A. (1999). Transport in multilevel quantum dots: from the Kondo effect to the Coulomb blockade regime, *Phys. Rev. Lett.* **83**, pp. 600–603.
181. Pasupathy, A. N., Bialczak, R. C., Martinek, J., Grose, J. E., Donev, L. A. K., McEuen, P. L. and Ralph, D. C. (2004). The Kondo effect in the presence of ferromagnetism, *Science* **306**, pp. 86–90.
182. Matsubayashi, D. and Eto, M. (2007). Spin splitting and Kondo effect in quantum dots coupled to noncollinear ferromagnetic leads, *Phys. Rev. B* **75**, p. 165319.
183. Buitelaar, M. R., Nussbaumer, T. and Schönenberger, C. (2002). Quantum dot in the Kondo regime coupled to superconductors, *Phys. Rev. Lett.* **89**, p. 256801.
184. Ueda, A. and Eto, M. (2006). Resonant tunneling and Fano resonance in quantum dots with electron–phonon interaction, *Phys. Rev. B* **73**, pp. 235353–235365.
185. Eto, M. and Nazarov, Y. V. (2000). Enhancement of Kondo effect in quantum dots with an even number of electrons, *Phys. Rev. Lett.* **85**, pp. 1306–1309.
186. Reich, S., Leitus, G., Popovitz-Biro, R. and Schechter, M. (2003). Magnetization of small lead particles, *Phys. Rev. Lett.* **91**, p. 147001.
187. Yamaji, K. and Shimoi, Y. (1994). Superconducting transition of the two-chain Hubbard model indicated by diagonalization calculations, *Physica C* **222**, pp. 349–360.
188. Combescot, R. and Leyronas, X. (1995). Coupling between planes and chains in $YBa_2Cu_3O_7$: a possible solution for the order parameter controversy, *Phys. Rev. Lett.* **75**, pp. 3732–3735.

189. Cox, D. L. and Maple, M. B. (1995). Electronic pairing in exotic superconductors, *Phys. Today* **48**, 2, p. 32.
190. Hewson, A. C. (1993). The Kondo Problem to Heavy Fermion (Cambridge, University Press).
191. Yoshimori, A. and Sakurai, A. (1970). Functional integral approach to the bound state due to the *s–d* exchange Interaction, *Suppl. Prog. Theor. Phys.* **46**, pp. 162–181.
192. Eto, M. and Nazarov, Y. V. (2001). Mean field theory of the Kondo effect in quantum dots with an even number of electrons, *Phys. Rev. B* **64**, p. 85322.
193. Fulde, P. and Ferrell, A. (1964). Superconductivity in a strong spin-exchange field, *Phys. Rev.* **135**, pp. A550–A563.
194. Larkin, A. and Ovchinnikov, Y. (1965). Inhomogeneous state of superconductors, *Sov. Phys. JETP* **20**, p. 762.
195. Lyuksyutov, I. F. and Pokrovsky, V. L. (2005). Ferromagnet superconductor hybrids, *Adv. Phys.* **54**, pp. 67–136.
196. Ryazanov, V. V., Oboznov, V. A., Rusanov, A. V., Veretennikov, A. V., Golubov, A. A. and Aarts, J. (2001). Coupling of two superconductors through a ferromagnet: evidence for a π-junction, *Phys. Rev. Lett.* **86**, pp. 2427–2430.
197. Frolov, S. M., Van Harlingen, D. J., Oboznov, V. A., Bolginov, V. V. and Ryazanov, V. V. (2004). Measurement of the current-phase relation of superconductor/ferromagnet/superconductor Josephson junctions, *Phys. Rev. B* **70**, p. 144505.
198. Bell, C., Loloee, R., Burnell, G. and Blamire, M. G. (2005). Characteristics of strong ferromagnetic Josephson junctions with epitaxial barriers, *Phys. Rev. B* **71**, p. 180501.
199. Ruotolo, A., Pepe, G. P., Bell, C. Leung, C. W. and Blamire, M. G. (2005). Modulation of the dc Josephson current in pseudo-spin-valve Josephson multilayers, *Supercond. Sci. Technol.* **18**, pp. 921–926.
200. Lange, M., Van Bael, M. J., Van Look, L., Raedts, S., Moschalkov, V. V. and Bruynseraede, Y. (2002). Nanostructured superconductor ferromagnet bilayers, in *New Trends in Superconductivity*, eds. Annett, J. F. and Kruchinin, S., *NATO Science Series II: Mathematics, Physics and Chemistry* **67**, pp. 365–373 (Kluwer, Dordrecht).
201. Aladyshkin, A. Yu., Silhanek, A. V., Gillijns, W. and Moshchalkov, V. V. (2009). Nucleation of superconductivity and vortex matter in superconductor–ferromagnet hybrids, *Supercond. Sci. Technol.* **22**, pp. 1–48.
202. Milosovec, M. V. and Peeters, F. M. (2005). Field-enhanced critical parameters in magnetically nanostructured superconductors, *Europhys. Lett.* **70**, pp. 670–676.
203. Fetter, V. M. and Larkin, A. I. (2002). Spin glass versus superconductivity, *Phys. Rev. B* **66**, p. 64526.
204. Andreev, A. F. (1998). Superfluidity, superconductivity and magnetism in mesoscopics, *Usp. Phys.* **168**, 6, pp. 656–663.
205. Milosevic, M. V., Yampolskii, S. V., Peeters, F. M. (2002). Magnetic pinning of vortices in a superconducting film: the (anti)vortex–magnetic dipole interaction energy in the London approximation, *Phys. Rev. B* **66**, p. 174519.
206. de Gennes, P.-G. (1966). *Superconductivity of Metals and Alloys* (Addision-Wesley, Advanced Book Programme).
207. Van der Wal, C. (2000). Quantum superposition of macroscopic persistent-current states, *Science* **290**, p. 773.
208. You, J. Q. and Nori, F. (2005). Superconducting circuits and quantum information, *Phys. Today* **12**, pp. 42–45.

209. Nakamura, Y., Pashkin, Y. A. and Tsai, J. S. (1999). Quantum oscillations in two coupled charge qubits, *Nature* **398**, pp. 786–788.
210. Makhlin, Y., Schon, G. and Shnirman, A. (2001). Quantum-state engineering with Josephson-junction devices, *Rev. Mod. Phys.* **73**, pp. 357–400.
211. Chiorescu, I., Nakamura, Y., Harmans, C. J. P. M. and Mooij, J. E. (2003). Coherent quantum dynamics of a superconducting flux qubit, *Science* **299**, pp. 1869–1871.

INDEX